Magnetostriction of Gd-Tb alloys

Ahmad Ali Joraide

MAGNETOSTRICTION OF Gd-Tb ALLOYS

by

AHMAD ALI JORAIDE

B.Sc. (Riyadh University)

M.Sc. (Durham University)

Grey College

PRESENTED IN CANDIDATURE FOR THE DEGREE OF DOCTOR OF PHILOSPHY

IN THE UNIVERSITY OF DURHAM

MARCH 1980

TO MY SON, NADER

C O N T E N T S

ABSTRACT

The work described in this thesis is directed towards study of the magnetostriction in the Gd-Tb alloy system using resistive strain gauge technique. The experiments were carried out at various ranges of temperatures between 4.5 K and 250 K, and magnetic fields up to 13 Tesla were available.

High quality single crystals of $Gd_{0.95}Tb_{0.05}$, $Gd_{0.80}Tb_{0.20}$, $Gd_{0.50}Tb_{0.50}$, and $Gd_{0.25}Tb_{0.75}$ were used to measure the four magnetostriction coefficients $\lambda^{\gamma,2}$, $\lambda_2^{\alpha,2}$, $\lambda_1^{\alpha,2}$ and $\lambda^{\varepsilon,2}$

The temperature dependences of the magnetostriction coefficients were fitted with both single-ion mechanism and a theory containing a term representing a two-ion interaction. Only the values of the magnetostriction coefficients for the samples containing high concentration of Terbium obey the single-ion $\hat{I}_{5/2}\,[\,\mathcal{L}^{-1}(m_n)]$ law. However, the experimental results were better fitted using the other theory, but in most cases the fit was less close than could have been desired.

An anomalous behaviour was observed for the samples containing 5% and 20% of Terbium in the magnetostriction curves along the c-axis, 45° to c-axis, and b-axes in the b-c plane. These anomalies disappeared by raising the field and temperature above 70 K. Another anomaly was observed in the temperature dependence of $\lambda_2^{\alpha,2}$ for the sample containing 20% of Terbium where a very sharp peak was obtained for this coefficient at 60 K.

The variation of the coefficients $\lambda^{\gamma,2}$, $\lambda_2^{\alpha,2}$, and $\lambda^{\varepsilon,2}$ with alloy composition were able to be represented using an exponential relation, while a linear relation was found for the coefficient $\lambda_1^{\alpha,2}$. The values of the coefficients extrapolated well to the values of the pure metals given by previous workers.

The ratio $\lambda^{\varepsilon,2}_{(0)} / \lambda^{\gamma,2}_{(0)}$ was found to have anomalously large values compared with that expected for the heavy rare earth metals and increase with increasing Terbium concentration in the alloy.

LIST OF FIGURES

CAPTIONS FOR TABLES

ACKNOWLEDGEMENTS

I would like to take this opportunity to give thanks to persons and organizations who offered aid, encouragement and advice as this work progressed. Firstly, to Professor B.H. Bransden for the provision of facilities for research in the Physics Department, Durham University.

I am particularly grateful to my supervisor Dr. W. D. Corner for suggesting the project and agreeing to supervise my work, for his encouragement, patience and constant advice.

I am also indebted to some members of the solid state group and in particular to Dr. B. K. Tanner for his enthusiasm, Mr. K.G. Moulson for help with the construction of the apparatus and advice on technical matters, and Mr. R. D. Hawkins for his assistance on running the experiments at Nottingham. Also I would like to thank Mr. W. Leslie and the staff of the main workshop for their help in the construction of the apparatus.

My sincere thanks are due to the Physics Department of the University of Nottingham for allowing me to use their superconducting magnet, in particular to Dr. K. Maxwell and Mr. J. Dennis for their help in running the magnet.

I would like to thank Dr. J. Welford for assistance with the writing of the computer program and in running it.

I am obligated to S.R.C. for financial assistance which made possible the use of the Nottingham magnet and also to Sunderland Polytechnic for allowing me to use their electrospark erosion machine to cut some of the samples.

I am indeed grateful to my wife Najat and son Nader, to whom this thesis is dedicated, for their support, bearing my absence from home, and their patience especially when I was away at Nottingham. Also to my family, in particular my parents at Saudi Arabia for their encouragement

and backing. Miss C. Plummer is thanked for taking the task of typing this thesis.

Finally, I would like to thank the institution who awarded me an academic scholarship without which this work would not be completed, the King Abdulaziz Military College.

CHAPTER 1

GENERAL INTRODUCTION

1.1 Introduction

A small coil carrying a current behaves like a magnetic dipole of moment,

$$M = I A \qquad \ldots\ldots\ldots(1.1),$$

where I is the current, and A is the area of the loop.
This suggests a possible origin for magnetic properties of atoms. There are two possible types of charge circulation that could give rise to an atomic magnetic moment, the orbital motion of the electron around the nucleus and the rotation of the electron about its own axis,a motion referred to as spin. The magnetic moment associated with this orbital and spin motion is,

$$M = -\frac{g\mu_o e}{2m} P \qquad \ldots\ldots\ldots(1.2),$$

where g is the gyro magnetic ratio, g = 1 for orbital motion and g = 2 for spin, e the electron charge and m is the electron mass. $\mu_o = 4\pi \times 10^{-7}$ Hm^{-1} is the permeability of free space and P is the angular momentum of the electron.
For a many electron atom the total orbital angular momentum of electrons (i = 1,2,....,n) is given as

$$L = \sum_{i=1}^{n} l_i \qquad \ldots\ldots\ldots(1.3)$$

Similarly the spin vectors s_i of individual electrons (i = 1,2,....,n) are coupled through the spin-spin interaction to give the total spin angular momentum as

$$S = \sum_{i=1}^{n} s_i \qquad \ldots\ldots\ldots(1.4)$$

Then L and S are coupled with each other via the spin-orbit interaction to give the total angular momentum J as

$$J = L + S \qquad \ldots\ldots\ldots(1.5)$$

This sort of coupling is referred to as Russell-Saunders coupling, Chikazumi (1964).

This exists in addition to the Coulomb interaction between the electrons and the nucleus and interactions between the electrons themselves. In order to determine the most stable spin and orbital configuration we follow Hund's rules realising that the vector L and S no longer remain constant while J remains constant, Omar (1975, p. 438). In general one can show that the average total moment is

$$\mu_{avg.} = g \left(\frac{-e}{2m}\right) J \qquad \ldots\ldots\ldots(1.6),$$

where

$$g = 1 + \frac{J(J+1) + S(S+1) - L(L+1)}{2J(J+1)} \qquad \ldots\ldots\ldots(1.7)$$

This is the g-factor; when S = 0, J = L, and g = 1, while for L = 0, J = S and g = 2 which agree with the values quoted on page one. If the atom lies in a magnetic field of induction B we may write the potential energy of the orbital component as

$$E_l = \mu_B B m_l \qquad \ldots\ldots\ldots(1.8),$$

where

$$\mu_B = \frac{\hbar e}{2m} \qquad \ldots\ldots\ldots(1.9)$$

μ_B is the Bohr magneton and has the numerical value 1.165×10^{-29} Wbm, m_l is an integer which takes the values $-l, -l+1, \ldots\ldots, l-1, l$ where l is the orbital quantum number for the angular momentum of the electron. For the spin moment

$$E_S = 2 \mu_B B m_S \qquad \ldots\ldots\ldots(1.10)$$

m_S is $\mp \frac{1}{2}$ the allowed values for the spin quantum number. These apply if L and S are uncoupled. If they are coupled we could also have

$$E_J = g \mu_B B m_J \qquad \ldots\ldots\ldots(1.11)$$

where m_J is an integer which takes the values $-J, -J+1, \ldots, J-1, J$. The relation between the magnetic induction or magnetic flux density B and the magnetic field intensity H is related in vacuum as, Omar (1975 p. 429)

$$\underline{B} = \mu_o \underline{H} \qquad \ldots\ldots\ldots(1.12)$$

The magnetic induction inside a material medium is related to the magnetic field as

$$\underline{B} = \mu_o (\underline{H} + \underline{M}) \qquad \ldots\ldots\ldots(1.13),$$

where M is the magnetization vector.

The relation between the intensity of magnetization M and magnetic field H can be expressed by

$$\underline{M} = \kappa \underline{H} \qquad \ldots\ldots\ldots(1.14),$$

where κ is the magnetic susceptibility. Thus κ is dimensionless and

$$\underline{B} = \mu_o (\underline{H} + \kappa \underline{H}) = \mu_r \mu_o \underline{H} \qquad \ldots\ldots\ldots(1.15),$$

where μ_r is the relative permeability which is also dimensionless. The susceptibility has values which range from 10^{-5} for very weak magnetism to 10^6 for very strong magnetism and may even be negative in sign. From this point of view materials may be grouped into various kinds of magnetic classes depending on the sign and magnitude of the susceptibility.

1.2 Classification of Various Kinds of Magnetism

1.2.1 Diamagnetism

This is a weak magnetism with a negative susceptibility of magnitude about 10^{-5} and independent of temperature, Craik (1971, p. 32). The diamagnetic materials have electrons or ions with complete shells or saturated molecules and their magnetism is due to the precession of electron orbitals about the nuclei under the influence of an external field.

The diamagnetic susceptibility per unit volume can be calculated by employing the Larmor theorem, Kittel (1971, p. 500), and is given by

$$\kappa = -\frac{\mu_o N Z e^2}{6 m} \langle r^2 \rangle \qquad \ldots\ldots\ldots(1.16),$$

where N is the number of atoms per unit volume, Z is the number of electrons per atom, e and m are the electron charge and mass respectively and $\langle r^2 \rangle$ is the mean square distance of the electrons from the nucleus. The mean is calculated for all the occupied orbitals in the atom.

1.2.2 Paramagnetism

This is also a weak magnetism with a positive susceptibility of magnitude 10^{-3} to 10^{-5}. The paramagnetism arises when atoms or ions have resultant moments. These can be aligned by an applied field, but the process is opposed by thermal agitation which may result in only a very small magnetization parallel to the magnetic field. A full calculation of the component of magnetization parallel to a field yields a Brillouin function, but for small fields it can be shown that for a system containing N atomic moments per unit volume the magnetization is given by, Omar (1975, p. 435).

$$M = \frac{N \mu^2 B}{3 k T} = \frac{C}{T} B \qquad \ldots\ldots\ldots(1.18)$$

Thus the susceptibility is given by

$$\kappa = \frac{N \mu_o \mu^2}{3 k T} \qquad \ldots\ldots\ldots(1.19),$$

where N is the atomic concentration, μ is the atomic magnetic moment, and k is Boltzmann's constant. C in eq. (1.18) is the Curie constant and equal to $\frac{N \mu^2}{3k}$. Quantum-mechanical calculations give the paramagnetic susceptibility as

$$\kappa = \frac{N g^2 \mu_B^2 J(J+1)}{3 k T} = \frac{C}{T}$$

1.2.3. Ferromagnetism

This is a very strong form of magnetism and ferromagnetic materials possess a positive susceptibility of order 10^4 to 10^5. This high value is due to a spontaneous magnetization produced by an effective internal magnetic field which was first suggested by Weiss (1907). We assume B_{int} to be the flux density of the internal field. If the field is due to interaction with other moments we may consider it to be proportional to the magnetization, Bleaney and Bleaney (1976)

$$\underline{B_{int}} = \lambda \underline{M} \qquad \ldots\ldots\ldots(1.21),$$

where λ is a constant independent of temperature, sometimes called the Weiss constant.

Then the total field acting on an ion is $B_o + B_{int} = B_o + \lambda M$, where B_o is the flux density of the external field. If we assume that Curie's law $\frac{\mu_o M}{B_o} = \frac{C}{T}$ still holds and if we replace B_o by $B_o + \lambda M$ we find

$$M = \frac{C B_o}{T \mu_o} = \frac{C}{\mu_o T} (B_o + \lambda M) \qquad \ldots\ldots\ldots(1.22),$$

and hence the Curie-Weiss law given as

$$\kappa = \frac{C}{(T - \lambda C/\mu_o)} = \frac{C}{(T - \theta)} \qquad \ldots\ldots\ldots(1.23),$$

where $\theta = \frac{\lambda C}{\mu_o}$ is called the paramagnetic Curie temperature. Such materials are paramagnetic at $T > \theta$ and ferromagnetic at $T < \theta$. The Curie-Weiss law is given from quantum-mechanics as

$$\kappa = \frac{J(J + 1) N g^2 \mu_B^2}{3 k (T - \theta)} \qquad \ldots\ldots\ldots(1.24)$$

The neighbouring atoms interact with eacn other, and the interaction is spin-dependent, Omar (1975, p. 448). The interaction energy between two atoms having spin S_i and S_j is given by

$$U_{ij} = -2J' \underline{S}_i \cdot \underline{S}_j \qquad \text{.....(1.25),}$$

where J' is called the exchange integral. This type of interaction was first presented by Heisenberg (1928).

1.2.4. Antiferromagnetism

Néel (1936) suggested that in many substances a large negative exchange interaction occurs resulting in an ordered state where neighbouring dipoles are aligned in an antiparallel arrangement. This means that there are effectively two sublattices whose magnetizations cancel each other. This kind of magnetism is called antiferromagnetism. It is a weak magnetism with a positive susceptibility of order 10^{-3} which increases with decreasing temperature up to a certain temperature where a maximum occurs. Below this so-called Néel temperature, the susceptibility decreases with a decrease in temperature. It is possible to express the susceptibility above the Néel temperature with the Curie-Weiss law, but the paramagnetic Curie temperature is in this case negative in contrast to the positive sign found in ferromagnetism. More complicated types of antiferromagnetic ordering are now known.

1.2.5. Ferrimagnetism

In antiferromagnetism the magnetization of the two sublattices cancels each other exactly. If one of these magnetizations is stronger than the other it would be expected that the difference will give fairly strong resultant magnetization. This type of magnetism is called ferrimagnetism. The first theoretical treatment was suggested by Néel (1948). His theory considered that the ferrimagnetic materials contain two sublattices A and B. Ferrimagnetism can arrise from a number of arrangements. In the simplest arrangement all the dipoles are equal in magnitude, but there are more on one sublattice than on the other

FIG. 1.1 SOME POSSIBLE ARRANGEMENT OF ELECTRON SPINS.

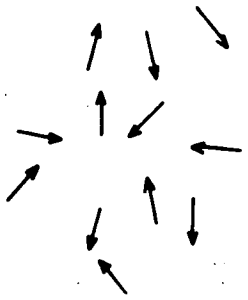

(a)

PARAMAGNETISM, WEEK INTERACTION BETWEEN EQUAL MOMENTS, RANDOM SPIN VECTORS.

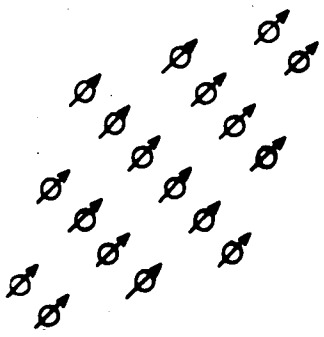

(b)

FERROMAGNETISM, POSITIVE INTERACTION BETWEEN EQUAL MOMENTS, PARALLEL SPIN VECTORS.

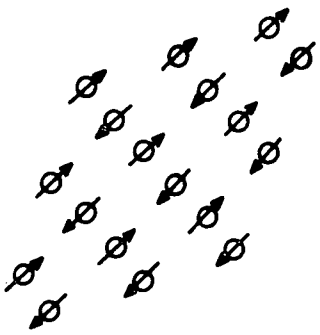

(c)

ANTI-FERROMAGNETISM, NEGATIVE INTERACTION BETWEEN EQUAL MOMENTS, ANTI-PARALLEL SPIN VECTORS ON TWO SITES.

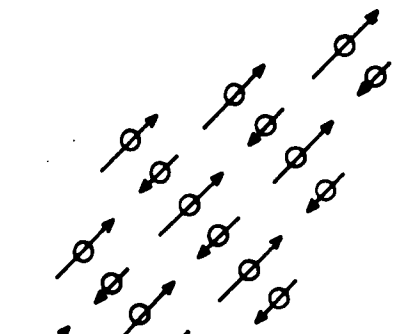

(d)

FERRIMAGNETISM, NEGATIVE INTERACTION BETWEEN UNEQUAL MOMENTS, ANTI-PARALLEL SPIN VECTORS ON TWO SITES.

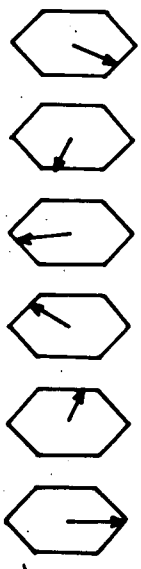

(e) HELICAL SPIN ARRAY

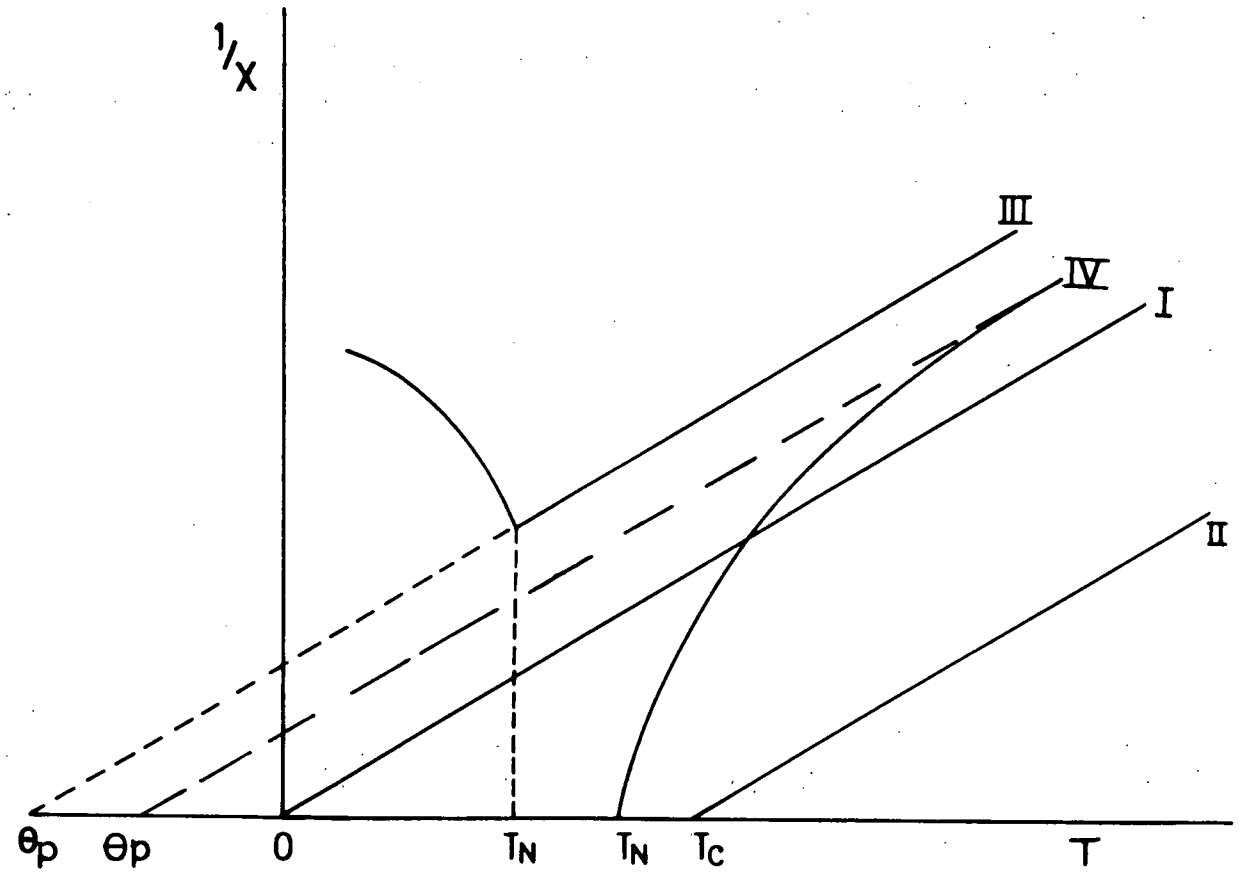

FIG 1·2 THE RECIPROCAL OF SUSCEPTIBILITY VERSUS TEMPERATURE. I. SIMPLE PARAMAGNETIC II. CURIE -WEISS PARAMAGNETIC WITH POSITIVE INTERACTION TERM T_C (CURIE TEMPERATURE) INDICATING FERROMAGNETIC ORDERING BELOW T_C III ANTIFERROMAGNETIC WITH NEGATIVE INTERACTION AND CURIE TEMPERATURE BUT MAGNETIC ORDERING BELOW NÉEL TEMPERATURE, T_N. IV FERRIMAGNETIC, ORDERING APPEARING BELOW T_N.

such as in yttrium iron garnet. In the ferrites the two sublattices have different numbers of positive ion sites and two different dipole moments are usually involved.

1.3 Triangular and Helical Spin Configuration

Yafet and Kittel (1952) suggested the first theoretical treatment of a triangular arrangement of spins to explain an anomalous small value of spontaneous magnetization in some ferrites. Yoshimori (1959) proposed a helical spin configuration to explain the antiferromagnetic spin structure of MnO_2 and a similar suggestion was made by Villain (1959) for $MnAu_2$. To show how this helical arrangement can arise, consider a single row of spins. The spins change their direction with displacement along the z-axis while remaining parallel to one another in each xy plane as shown in Fig. (1.3). The exchange energy stored in a unit volume is given by Chikazumi (1964 p. 445).

$$E_{ex} = - 2 N S^2 (J_1 \cos \theta + J_2 \cos 2 \theta) \qquad .....(1.26),$$

where N is the number of magnetic atoms in a unit volume, J_1 is the exchange integral between adjacent spins and J_2 that between next nearest neighbours. The stable configuration occurs when we have

$$\cos \theta = \left| \frac{J_1}{4 J_2} \right| \qquad .....(1.27)$$

Helical and related spin structures have been deeply investigated for rare earth metals and their alloys which will be discussed in the next chapter.

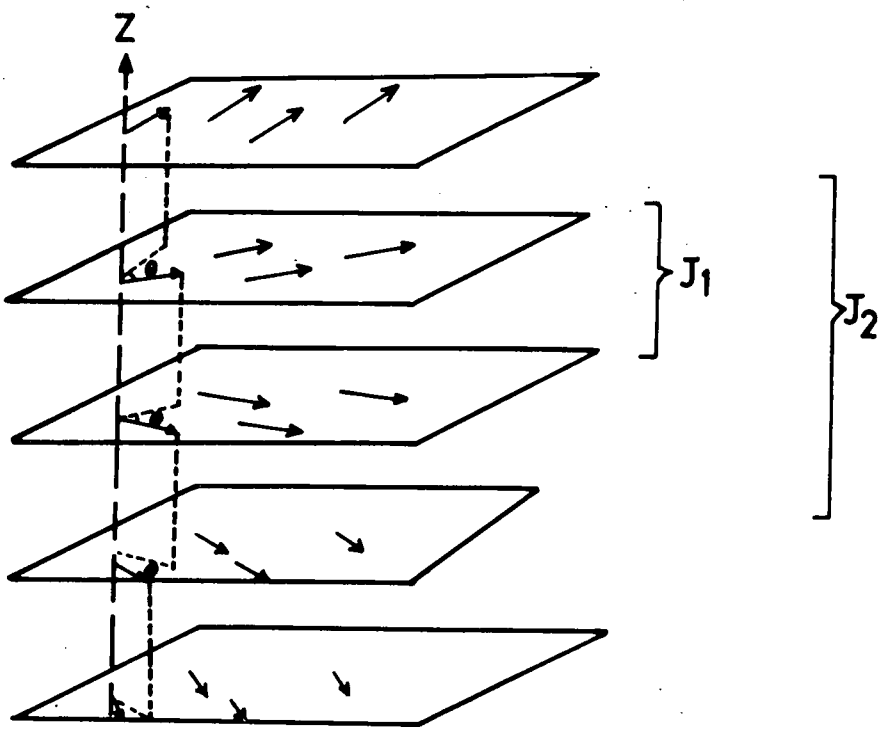

FIG 1.3 EXCHANGE INTERACTION IN HELICAL SPIN CONFIGURATION

CHAPTER 2

SOME PROPERTIES OF RARE EARTH METALS

2.1 Crystal Structure of Rare Earth Metals

The rare earth elements are the fifteen elements which are usually arranged outside the periodical table of the elements from Lanthanum (La) of atomic number 57 to Lutetium (Lu) of atomic number 71. This group is sometimes referred to as the lanthanides and these are classified into two groups, the lighter elements before gadolinium and the heavier from gadolinium to lutetium. The heavier rare earth elements all have hexagonal close packed (hcp) structures. The light lanthanides have double hexagonal close packed (dhcp) structures, with the exception of Samarium (Sm) which has rhombohedral (so called Sm-type) structure, Taylor and Darby (1972). Temperature, pressure and alloying all affect the crystal structures. Some basic information about the crystal structures of the rare earth metals at room temperature is given in Table (2.1). The heavy rare earths Gd-Lu except Ytterbium (Yb) have the usual hexagonal close packed structure at room temperature. As we can see from Fig. (2.1 b) this structure has a stacking sequence of the layers ABAB. . . The system which is usually used to define the axes of the heavy rare earths is shown in Fig. (2.1 e). There are two ways in which the axes may be set up: either we can have three axes a, b, and c, the a-axis in the basal plane passing through one corner of the hexagon, the b-axis in the basal plane and perpendicular to the a-axis, and the c-axis perpendicular to the hexagonal basal plane, or we can recognize four axes a_1, a_2, a_3, and c. The three axes a_1, a_2, and a_3 are in the basal plane passing through the corners of the hexagon and making between each other an angle of 120^{o}. With the exception of the vicinities of europium and ytterbium the atomic volume decreases by about 5% along the series

TABLE (2.1) The room temperature structural properties and lattice parameter of the rare earth metals. Distances are measured in A°, density in gm cm^{-3}, and atomic volume in cm^3 $mole^{-1}$. Adapted from Taylor and Darby (1972).

ELEMENT	Z	STRUCTURE	a SPACING	c SPACING	c/a RATIO	METALLIC RADIUS	DENSITY	ATOMIC VOLUME	TRANSITION and TRANSITION TEMPERATURE K	MELTING POINT
Lanthanum (La)	57	dhcp	3.769	12.159	1.612	1.877	6.162	22.5	dhcp $\xrightarrow{583}$ fcc $\xrightarrow{1151}$ bcc	1193
Cerium (Ce)	58	dhcp	3.673	11.802	1.607	1.82	6.678	20.70	fcc → dhcp → fcc $\xrightarrow{1003}$ bcc	1068
Praseodymium (Pr)	59	dhcp	3.671	11.831	1.611	1.828	6.769	20.78	dhcp $\xrightarrow{1071}$ bcc	
Neodymium (Nd)	60	dhcp	3.656	11.795	1.613	1.821	7.016	20.60	dhcp $\xrightarrow{1141}$ bcc	1297
Promethium (Pm)	61	dhcp	3.65	11.65	1.60	-	7.26	-	-	1300
Samarium (Sm)	62	rhomb	3.628	26.231	1.607	1.802	7.536	19.0	rhomb $\xrightarrow{1190}$ bcc	1345
Europium (Eu)	63	bcc	4.581	-	-	20.42	5.245	28.91	No transition	1099
Gadolinium (Gd)	64	hcp	3.634	5.781	1.591	1.802	7.886	19.88	hcp $\xrightarrow{1535}$ bcc	1585
Terbium (Tb)	65	hcp	3.606	5.697	1.580	1.782	8.253	19.25	hcp $\xrightarrow{1560}$ bcc	1629
Dysprosium (Dy)	66	hcp	3.593	5.654	1.5735	1.773	8.559	19.03	hcp $\xrightarrow{1657}$ bcc	1680
Holmium (Ho)	67	hcp	3.580	5.627	1.572	1.766	8.799	18.74	hcp $\xrightarrow{1701}$ bcc	1734
Erbium (Er)	68	hcp	3.561	5.593	1.5706	1.757	9.062	18.47	No transition	1823
Thulium (Tm)	69	hcp	3.543	5.571	1.5725	1.746	9.318	18.15	No transition	1818
Ytterbium (Yb)	70	fcc	5.463	-	-	1.940	6.959	24.80	fcc $\xrightarrow{1071}$ bcc	1101
Lutetium (Lu)	71	hcp	3.510	5.567	1.5797	1.734	9.849	17.78	No transition	3600

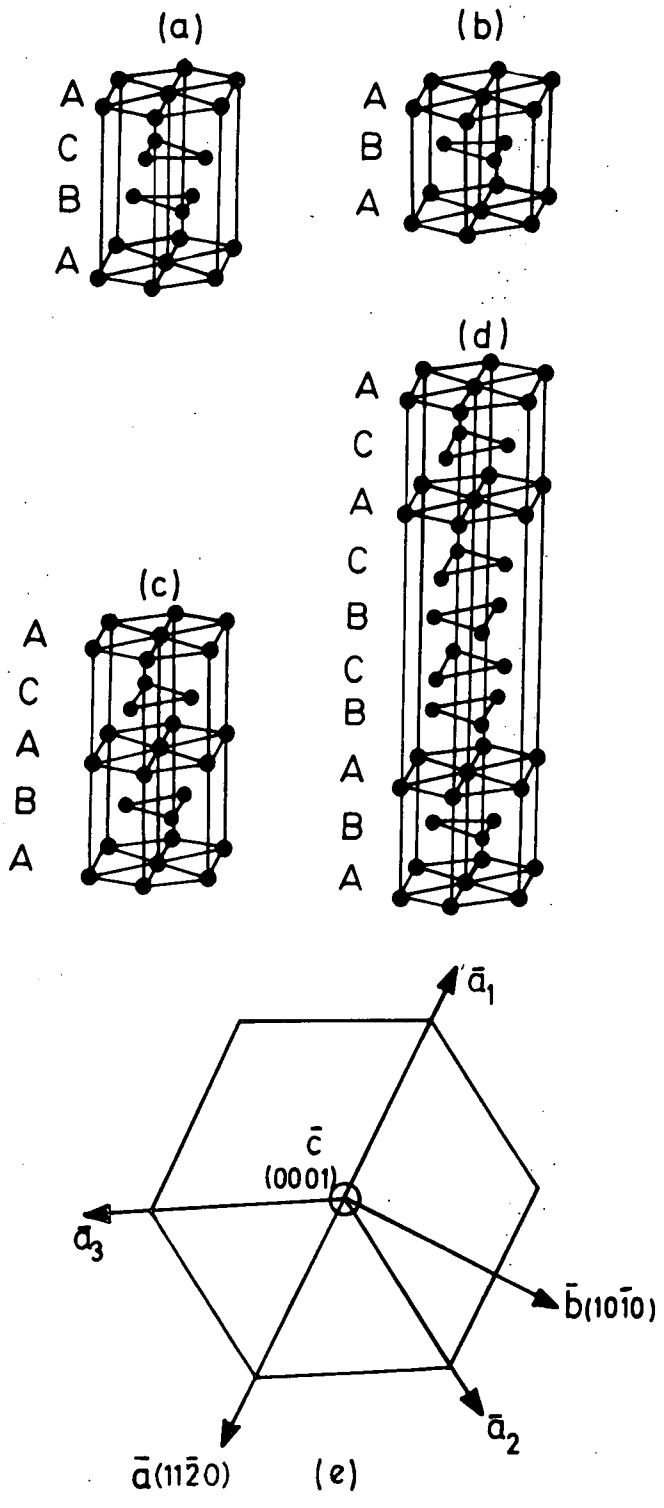

FIG. 2.1 THE FOUR CLOSE PACKED STRUCTURES OBSERVED FOR THE RARE EARTH METALS (a) fcc (b) hcp (c) dhcp (d) Sm-TYPE (e) DEFINITION OF THE AXES IN RECTANGULAR OR HEXAGONAL SYSTEM FOR hcp RARE EARTH METALS.

for the heavy elements. This 'lantnanide contraction' is due to a shrinkage of the 4f electronic shell as the nuclear charge increases. The axial ratios c/a are smaller than the ideal value of $2\sqrt{2/3} = 1.633$ for the heavy metals.

The light rare earths have a more complex double hexagonal structure with a stacking sequence ABACA. . . as shown in Fig. (2.1 c). Samarium has a structure of even greater complexity which is rhombohedral with the stacking sequence ABABCBCAC. . . shown in Fig.(2.1 d). The c/a ratios while still not equal to the ideal value are in excess of 1.6. However, lanthanum is stable in the fcc structure from 310 - 861 K, Elliot (1972). At high temperatures most of the lanthanide group appear to become bcc as we notice from Table (2.1). Europium and ytterbium are divalent in the metallic state while the others are trivalent, so these two elements show large deviations from the rest. Europium has a bcc structure at all temperatures, while Yb crystallizes in the fcc modification as shown in Fig. (2.1 a), and undergoes a change to the bcc structure 30^{o} C below its melting point.

It has been suggested by Taylor and Darby (1972), that the rare earth metals with increasing temperature undergo a structure sequence hcp - (Sm-type) - dhcp-fcc-bcc. This is similar to the behaviour as the atomic number decreases or as an external pressure on the metal is increased. Jayaraman and Sherwood (1964) have suggested that a general trivalent rare earth metal under increasing pressure follows a sequence of the form hcp - (Sm-type) - dhcp-fcc. Johansson (1977) has studied the variation of the Wigner-Seitz radius R_{WS} and the ionic radius R_I as shown in Fig. (2.2), and he found that an increase in the pressure on a specific element will decrease R_{WS} and simulate a lighter element. In alloys it is clear that the same structure sequence appears and the structure of the metal will depend on the

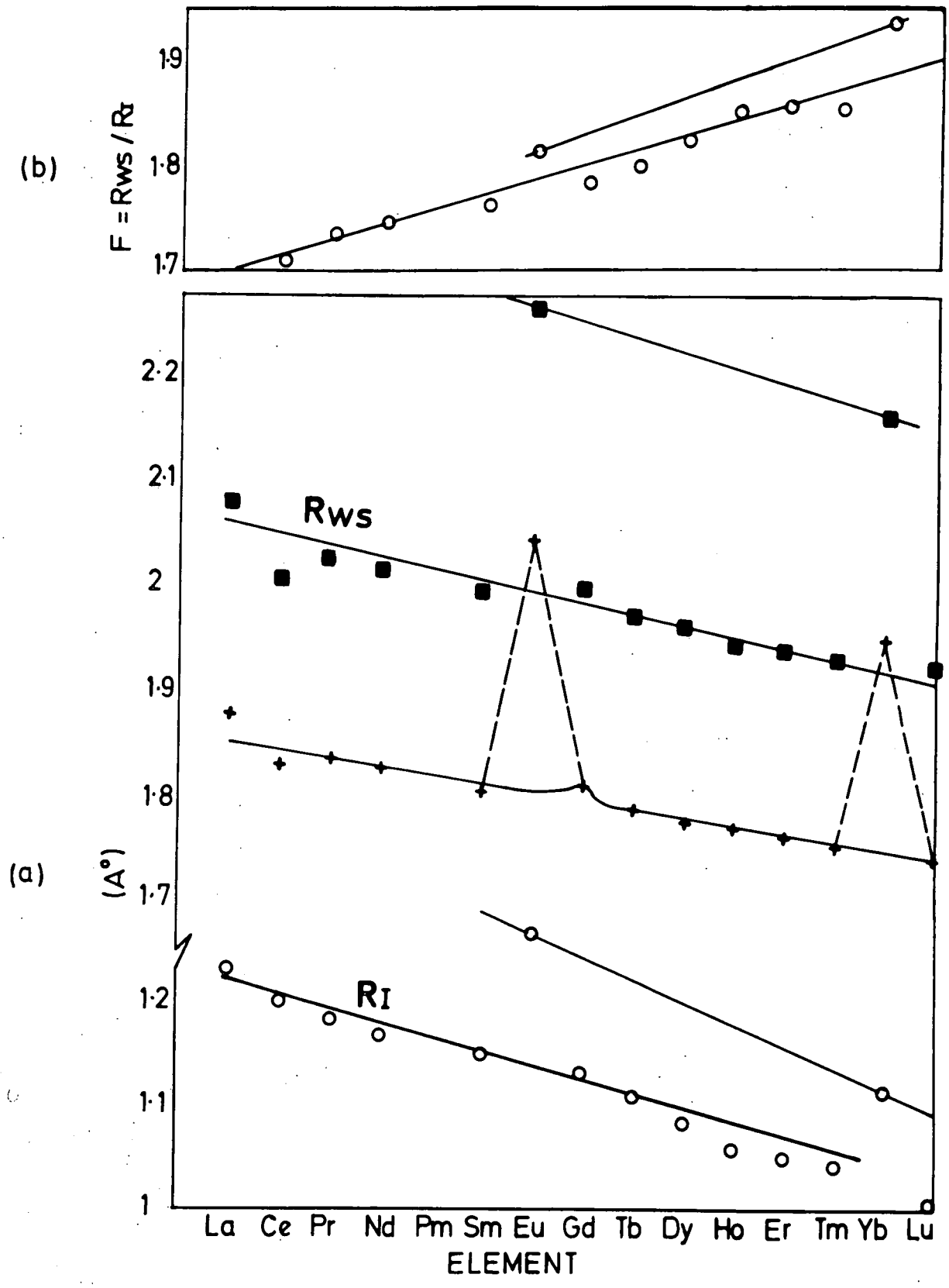

FIG 2·2 a) + METALLIC RADIUS AFTER TAYLOR AND DARBY 1972 o R_I THE IONIC RADIUS, ■ Rws THE WIGNER - SEITZ RADIUS AFTER JOHANSSON 1977.

b) RATIO OF Rws TO R_I

mean atomic number. Alloys over different concentrations between Cerium and Gadolinium, Gd-Pr, Y-Ce, and Y-Pr show the structures hcp - (Sm-type) - dhcp and fcc, Harris et al (1966). If the components of binary alloys lie in the same part of the series, i.e. for alloys of light with light, or heavy with heavy rare earth, no intermediate phases will exist and only the axial ratio and the lattice parameters will vary. Thus the crystal structure of the rare earths is strongly dependent on temperature, pressure, alloying and the atomic number. Finally, it is important to mention the theoretical treatment of the crystal structure of lanthanides by Duthie and Pettifor (1977), where they found that the structure sequence hcp - (Sm-type) - dhcp-fcc could be directly related to the d-band occupancy N_d with the following results:

$N_d < 1.7$ hcp, $1.7 < N_d < 2.3$ Sm-type, $2.3 < N_d < 2.6$ dhcp, and $N_d > 2.6$ fcc.

2.2 Electronic structure of Rare Earth Metals

All the rare earths exhibit similar chemical properties because of the similarity of electronic structure which is given by:

$$1s^2\ 2s^2\ 2p^6\ 3s^2\ 3p^6\ 3d^{10}\ 4s^2\ 4p^6\ 4d^{10}\ 4f^n\ 5s^2\ 5p^6\ 5d^1\ 6s^2$$

where n increases from 0 for Lanthanum (La) to 14 for Lutetium (Lu). In the metallic state the 5d and 6s levels are mixed to give the conduction band. On the other hand the 4f electrons are well localized inside the outer closed shells. The magnetic properties of lanthanides vary from one atom to another, because they depend on the number of f electrons which are responsible for the magnetism in the rare earths. For simplicity it is possible to consider the 4f electrons separately from the other electrons. The magnetic interactions between f electons arise mainly as an indirect effect due to the s-f interaction.

So the localized 4f electrons on a site n of spin $\vec{S}_n$ interact with the conduction electrons of spin $\vec{s}$ $(\vec{r})$ via s-f interaction and give a Hamiltonian of form

$$H = -\sum \Gamma(\vec{r} - \vec{R}_n) \; \vec{s}(\vec{r}) \; . \; \vec{S}_n \qquad \ldots\ldots\ldots(2.1),$$

where $\Gamma(\vec{r} - \vec{R}_n)$ tne interaction constant, Coqblin (1971, 1977) and Elliot (1971). A similar interaction between the conduction electrons and the 4f moment on site m leads to indirect interaction between localized spins on atoms n and m with a Hamiltonian of the form

$$H = -\sum_{n,m} \mathcal{J}(\vec{R}_n - \vec{R}_m) \; \vec{S}_n \; . \; \vec{S}_m \qquad \ldots\ldots\ldots(2.2),$$

where $\mathcal{J}(\vec{R}_n - \vec{R}_m)$ is the exchange integral. This kind of interaction was first discussed by Rudermann, Kittel, Kasuya, and Yosida and is known as RKKY interaction. If the interaction in eq. (2.2) is projected on to the state of total angular momentum, J , it becomes

$$H = -\sum_{n,m} \mathcal{J}(\vec{R}_n - \vec{R}_m) \; \vec{J}_n \; . \; \vec{J}_m \qquad \ldots\ldots\ldots(2.3),$$

where $\mathcal{J} = (g - 1)^2 \mathcal{J}$ and g is the Landé factor.
The total angular momentum J is given as

$$J = L - S \qquad \ldots\ldots\ldots(2.4),$$

for the light rare earths ($n \leq 7$), and

$$J = L + S \qquad \ldots\ldots\ldots(2.5),$$

for the heavy rare earths ($n \geq 7$). The values of the spin angular momentum S, the orbital angular momentum L, and the total angular momentum J as a function of the number of 4f electrons are shown in Fig. (2.3).

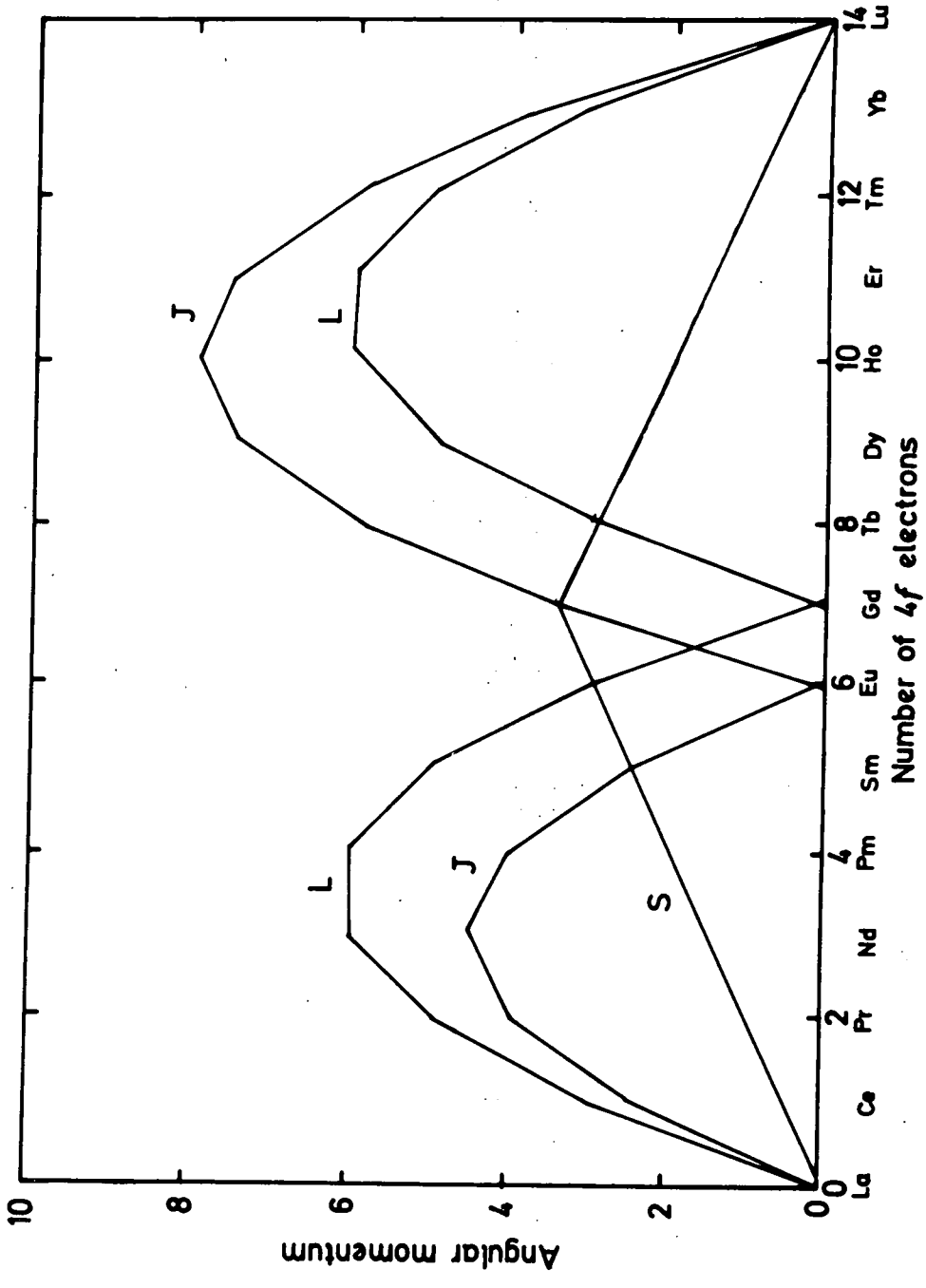

Fig. 2-3 The spin angular momentum S, the orbital angular momentum L, and the total angular momentum J as a function of the number of *4f* electrons, after Chikazumi (1964).

2.3 Magnetic Properties of Rare Earth Metals

The effective magnetic moment of rare earth atoms may be calculated from the expression

$$\mu_{eff} = g\mu_B \sqrt{J\ (J + 1)} \qquad .....(2.6),$$

where g is the Landé g factor given by eq. (1.7) obtained for the light rare earths by eq. (2.4) and for the heavier by eq. (2.5). The effective magnetic moment as a function of number of 4f electrons is shown in Fig. (2.4). Generally each of the heavy rare earth metals has an effective moment in the paramagnetic state which is nearly identical to that of the corresponding trivalent ion, as can be seen for the elements from Gd to Er in Table (2.2), but that of Tm is considerably smaller than the free ion value. The paramagnetic susceptibility is given by the Curie-Weiss law $\kappa = \frac{C}{T - \theta}$. Most of the rare earth elements obey this reasonably well with the exception of La, Pr, Yb, and Lu.

I. The Light Rare Earth Metals

These are more complicated than the heavy rare earths, and they have not been studied in such detail as the heavy ones. However, the first case studied in detail was the pure metal Cerium (Ce) by Coqblin (1971). Lanthanum does not show a magnetic order. It mainly crystallizes in dhcp structure below 583 K, but the fcc phase co-exists below room temperature, and due to this its susceptibility is complicated, Rhyne (1972). Cerium is a magnetic and trivalent metal at normal temperature and pressure in its fcc phase. It is antiferromagnetic at 12.5 K with the dhcp structure, Wilkinson et al (1961), and Koehler (1965). Burr and Ehara (1966) have found that the susceptibility is time dependent at 4.2 K, this is because of the transition from α-fcc to γ-fcc.

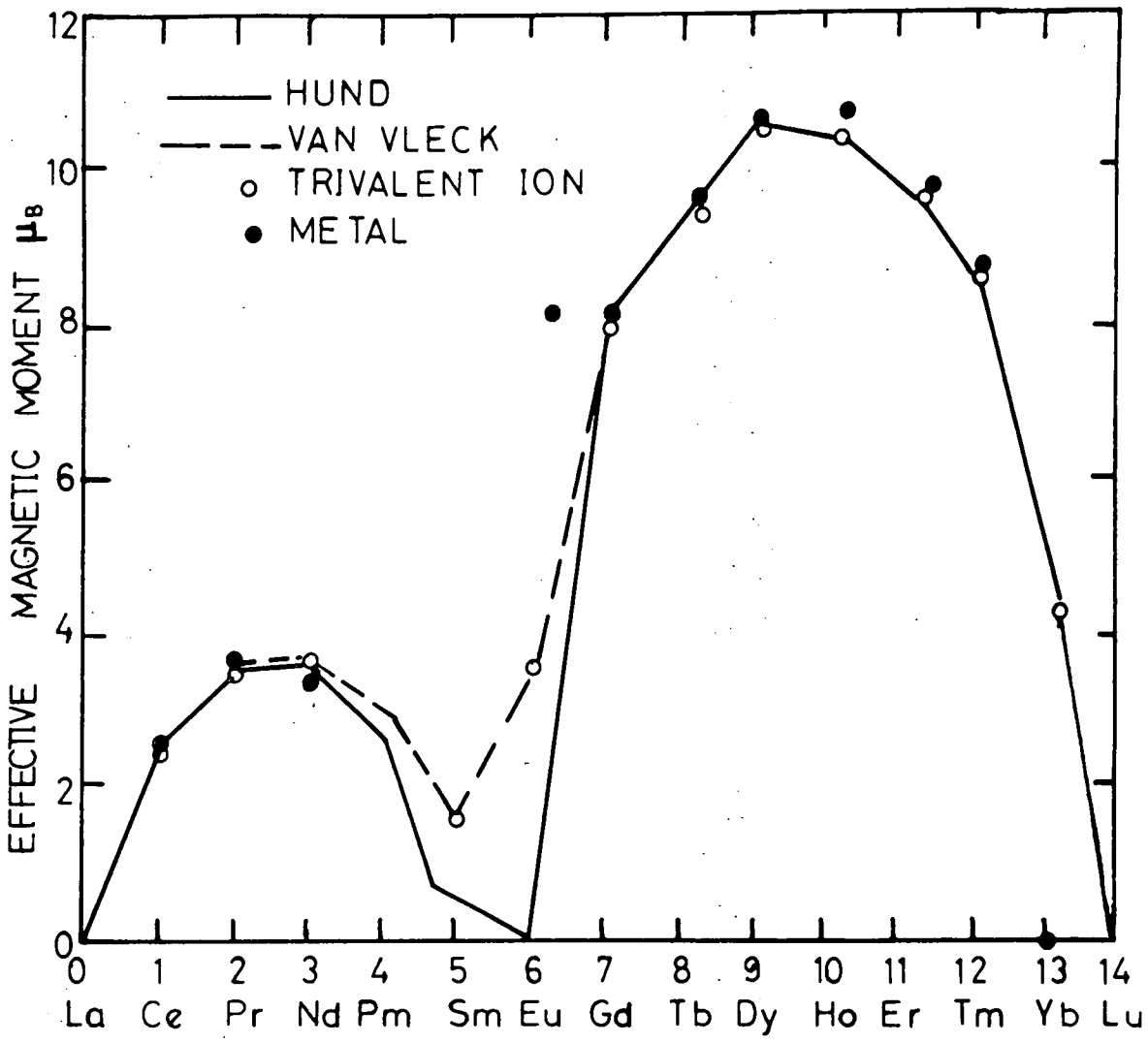

FIG. 2.4 THE EFFECTIVE MAGNETIC MOMENTS FOR RARE EARTHS AS A FUNCTION OF 4f ELECTRONS AFTER TAYLOR AND DARBY 1972

TABLE (2.2): *Summary of the magnetic structures of heavy rare earth metals. The different notations of the table are: (1) Metal. (2) Paramagnetic Curie temperature of polycrystals. (3) Paramagnetic Curie temperature of single crystals with the magnetic field applied along the c-axis. (4) Paramagnetic Curie temperature of single crystals with the magnetic field in the basal plane. (5) Temperatures of the specific heat anomalies. (6) Neel temperature. (7) Structure below the Neel temperature. (8) Intermediate ordering temperature T_H (for Erbium only). (9) Structure below T_H (for Erbium only). (10) Ferromagnetic Curie temperature. (11) Structure below the Curie temperature. (12) Saturation magnetization parallel to the easy magnetization axis (in μ_B). (13) Theoretical values of the magnetic moment for the trivalent rare earths ion (in μ_B),* after Coqblin (1977).

(1) Metal	(2) θ_p(K)	(3) $\theta_{\parallel}$(K)	(4) $\theta_{\perp}$(K)	(5) T_λ(K)	(6) T_N(K)	(7) Structure	(8) T_H(K)	(9) Structure	(10) T_c(K)	(11) Structure T = 4.2 K	(12) μ_{sat} (μ_B)	(13) $g_J J$ (μ_B)
Gd	317	317	317	291.8	$T_N = T_C$ 293.2	Ferromagnetic (g): $(\vec{\mu}, \vec{c})$ angle variable with T					7.55	7.0
Tb	237	195	239	227.7 221	229	Helix (e): $\vec{\mu} \perp \vec{c}$ $\omega_l = 20.5°$ $\omega_{f'} = 18°$			221	Ferro (f): $\vec{\mu} \perp \vec{c}$	9.34	9
Dy	153	121	169	174 83.5	179	Helix (e): $\vec{\mu} \perp \vec{c}$ $\omega_l = 43°$ $\omega_{f'} = 26.5°$			87	Ferro (f): $\vec{\mu} \perp \vec{c}$	10.2	10
Ho	87	73	88	131.6 19.4	133	Helix (e): $\vec{\mu} \perp \vec{c}$ $\omega_l = 51°$ $\omega_{f'} = 33°$			20	Cone (d) $\omega = 30°$ $\omega_f = 30°$	10.34	10
Er	40	61.7	32.5	84 53.5 19.9	80	$\vec{c}$-axis modulated with occurrence of harmonics. $\vec{\mu} \parallel \vec{c}$ (b). $\omega_l = 51.4°$	$T_H = 53$ $\omega = 51.4$	$\vec{c}$-axis modulated with occurrence of harmonics. Helix for $\mu_{\perp}$(c). $\omega_{f'} = 45°$	20	Cone (d) $\omega = 45°$ $\omega_f = 45°$	8	9
Tm	20			55	56	$\vec{c}$-axis modulated: $\vec{\mu} \parallel \vec{c}$(b) $\omega_l = 51.4°$ $\omega_{f'} = 51.4°$			38	Antiphase Ferro. 3–4 (a) $\omega_f = 51.4°$	3.4	.7

Praseodymium was suggested to be antiferromagnetic below 25 K, Cable et al (1964). Neutron diffraction measurements show no magnetic order state for a single crystal, Johansson et al (1970) and Lebech and Rainford (1971). Neodymium shows a quite complex magnetic structure. Moon et al (1964) investigated the magnetic structure of single crystals of Nd by neutron diffraction between 1.6 to 20 K, and they found that Nd shows two magnetic transitions. At $7.5 < T < 19$ K the magnetic structure is one of antiferromagnetic order between neighbouring hexagonal layers B and C while the A layers with cubic nearest-neighbour arrangement remain disordered. At 7.5 K the cubic sites order also.

From measurements of the magnetic susceptibility of samarium by Lock (1957) and Jelinek et al (1965) for a polycrystal of Sm and by Schieber et al (1968) for a single crystal, samarium shows antiferromagnetic behaviour at 14 K. The neutron diffraction measurements show that the spins on hexagonal sites only order antiferromagnetically at 106 K and at 14 K the cubic sites order into ferromagnetic layers, Rhyne (1972).

The last metal of the light rare earths is europium; it becomes antiferromagnetic below 90 K, as has been shown by Bozorth and Van Vleck (1960), from a paramagnetic susceptibility. Also a neutron diffraction study of polycrystalline Eu has shown that the metal becomes antiferromagnetic at 91 K, Koehler (1965).

II. Heavy Rare Earth Metals

The heavy rare earth metals have been studied much more extensively than the light ones for both polycrystalline and single crystal samples, and many reviews have been published for magnetic properties.

Particularly useful reviews are those of Elliott (1972) and more recently of Coqblin (1977). All these elements (with the exception of Yb and Lu) show some form of magnetic ordering at low temperatures. This order is ferromagnetic (Gd, Tb, Dy), helimagnetic (Tb, Dy, Ho), conical (Ho, Er), modulated along c-axis (Er, Tm), or even ferromagnetic antiphase (Tm), Koehler (1965). The magnetization curves show a maximum at the para-antiferromagnetic transition. This occurs at the Néel point (T_N) which is a function of de Gennes factor ξ where $\xi = (g - 1)^2 J(J + 1)$, Weinstein et al (1963), giving an empirical relation for T_N as $T_N \alpha \xi^{2/3}$. This is followed at lower temperatures by a very sharp increase in the magnetization as the ferromagnetic phase occurs, the temperature at which the ferromagnetism is observed in zero applied field is the Curie point (T_C), which is also related to the de Gennes factor. The magnetization measurements of the heavy rare earths show evidence of large magnetocrystalline anistopy which will be discussed in the next chapter. From detailed analyses of the single crystal neutron diffraction results in the appropriate temperature ranges, Koehler (1965) and Koehler (1971), the magnetic configurations of the heavy rare earth metals represented schematically in Fig. (2.5) have been deduced. Some basic physical properties of the heavy rare earth metals are summarized in Table (2.2).

a. Gadolinium

Gadolinium was the fourth ferromagnetic metal to be discovered after Nickel, Cobalt, and Iron. It has no antiferromagnetic phase and the orbital angular momentum is zero as shown in Fig. (2.3). Gadolinium transfers directly to the ferromagnetic state, i.e. the ferromagnetic Curie temperature T_C is the same as the Néel temperature which was first given as 298 K by Trombe (1937) and Elliot et al (1953).

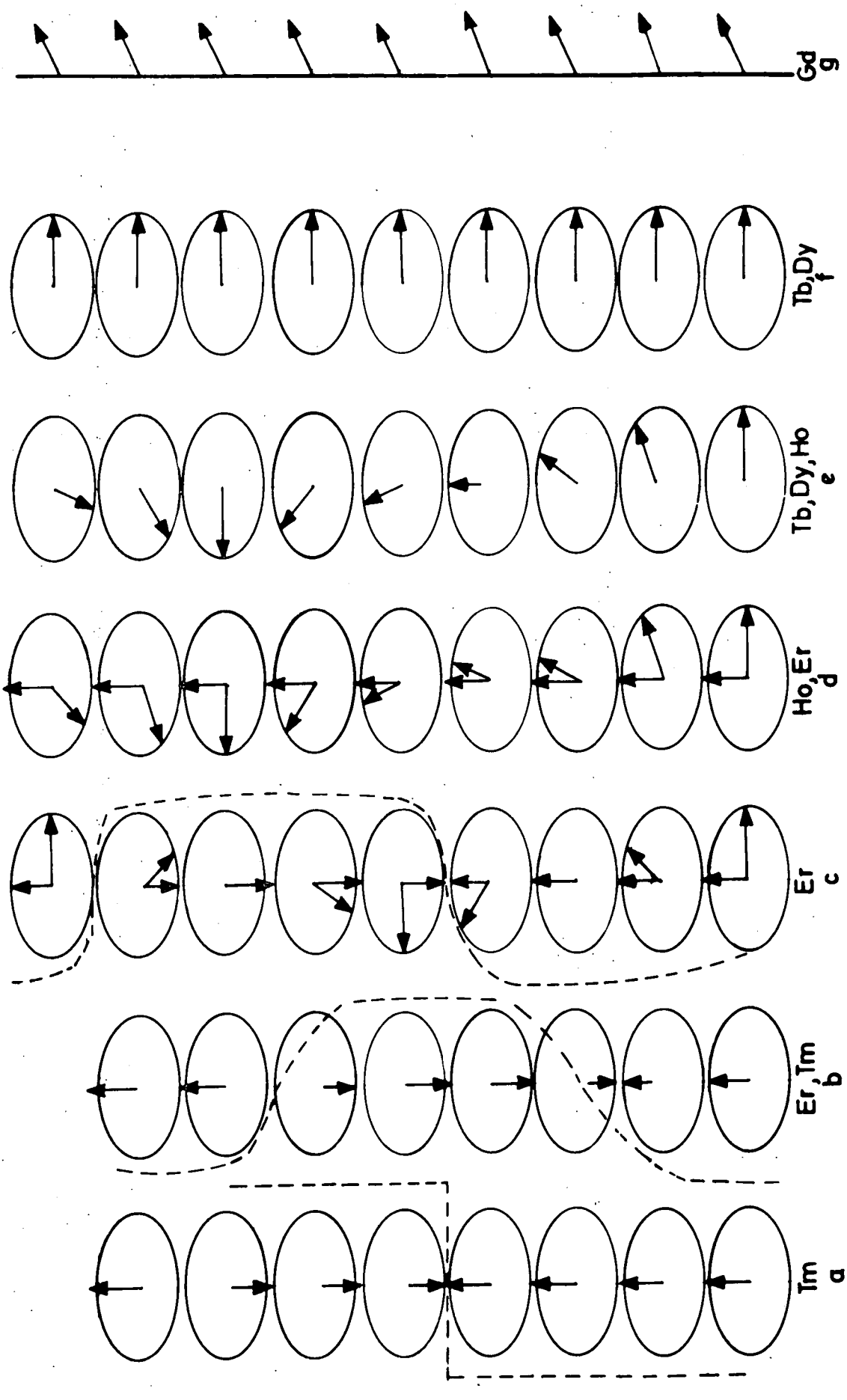

FIG 2·5 SCHEMATIC REPRESENTATION OF THE MAGNETIC STRUCTURES OF HEAVY RARE EARTH METALS; AFTER COQBLIN · 1977

Nigh et al (1963) have measured the resistivity from 4.2 to 380 K and they have found that the b-axis resistivity changes slope at 293.2 K while the c-axis resistivity shows a corresponding change at 292 K as shown in Fig. (2.6). Griffel et al (1957) have given a ferromagnetic Curie temperature of 291.8 K from the thermal dependence of the specific heat as shown in Fig. (2.7). Graham (1964) has found the Curie point to be 293 K from the magnetization study of a single crystal disc of Gd. The magnetic moment as a function of magnetic field applied along the a, b, and c axes of a single crystal below the ferromagnetic Curie temperature has been studied by Nigh et al (1963). This indicated that the c-axis is the easy axis of magnetization just below T_C, as shown in Fig. (2.8). The saturation magnetic moment per gram was found by Rhyne (1972) to be 268.2 emu/g by extrapolation to OK which corresponds to $7.55\,\mu_B$ as shown in Fig. (2.9). Theoretical saturation moment gJ equals $7.00\mu_B$ and thus the excess moment $0.55\,\mu_B$ represents a polarization of the conduction electrons, Rhyne (1972). The paramagnetic Curie temperature is isotropic and equal to $\theta_{\parallel} = \theta_{\perp} = \theta_p = 317$ K. The neutron diffraction data shows that Gd is a normal ferromagnetic below the Curie point. The direction of the moment depends strongly on the temperature as has been found by several workers. Fig. (2.10) shows the temperature dependence of the cone angle which is the angle between the moment direction and the c-axis adapted from Cable and Wollan (1968), using neutron diffraction measurements, and from the torque measurements by Corner et al (1962), Graham (1962), Corner and Tanner (1976), and Smith et al (1978). The easy axis of magnetization is parallel to the c-axis from T_C to 232 K, then it makes an angle with a maximum deviation of 65° near 180 K. As the temperature is further decreased the easy direction moves back towards the c-axis,

FIG. 2·6 THERMAL DEPENDENCE OF THE RESISTIVITY OF Tb AND Gd. IN Gd THE RESIDUAL RESISTIVITY IS SUBTRACTED.

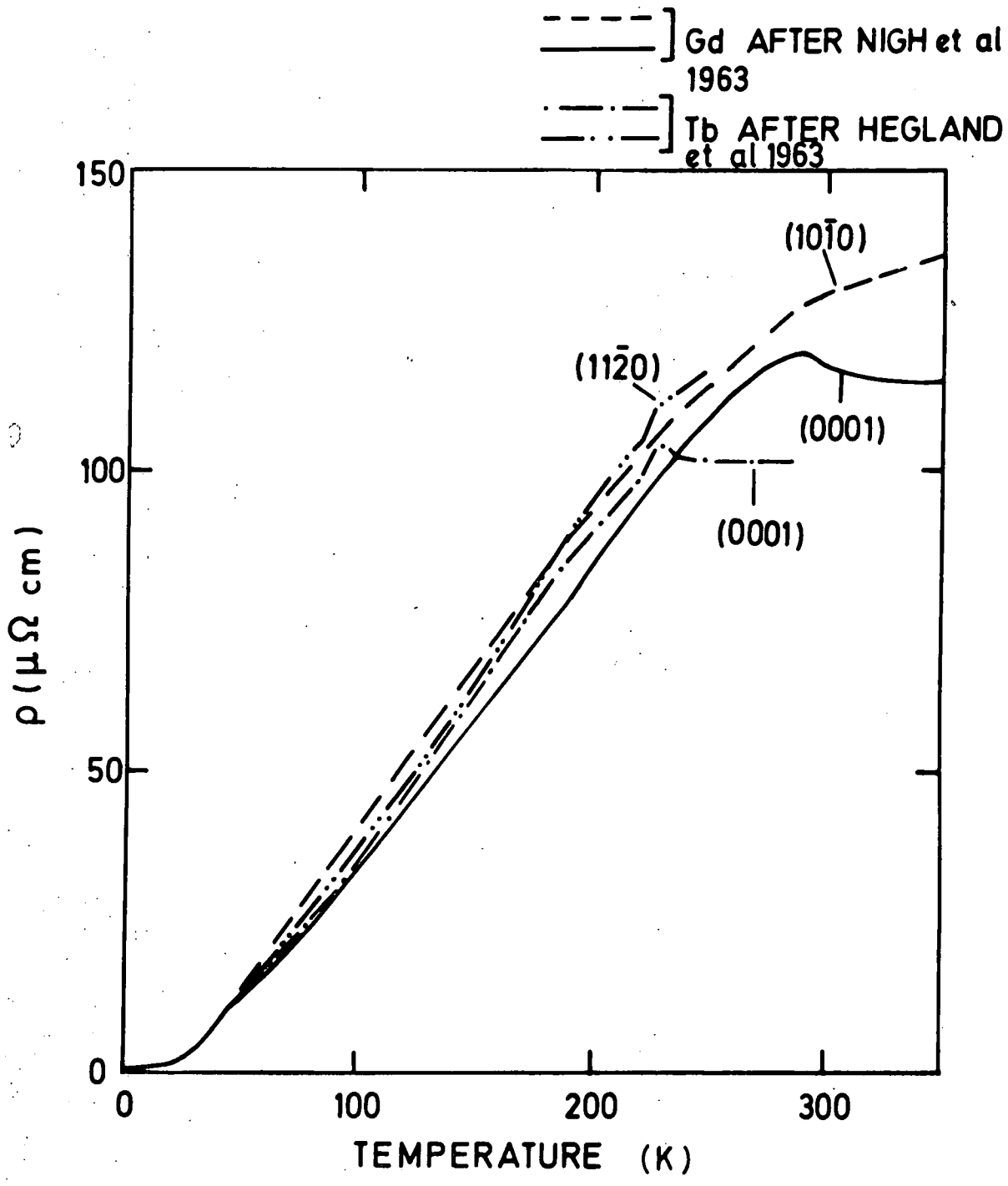

FIG. 2.7 THERMAL DEPENDENCE OF THE SPECIFIC HEAT OF Gd AND Tb

– – – Gd AFTER GRIFFEL et al (1957)

——— Tb AFTER JENNINGS et al (1957)

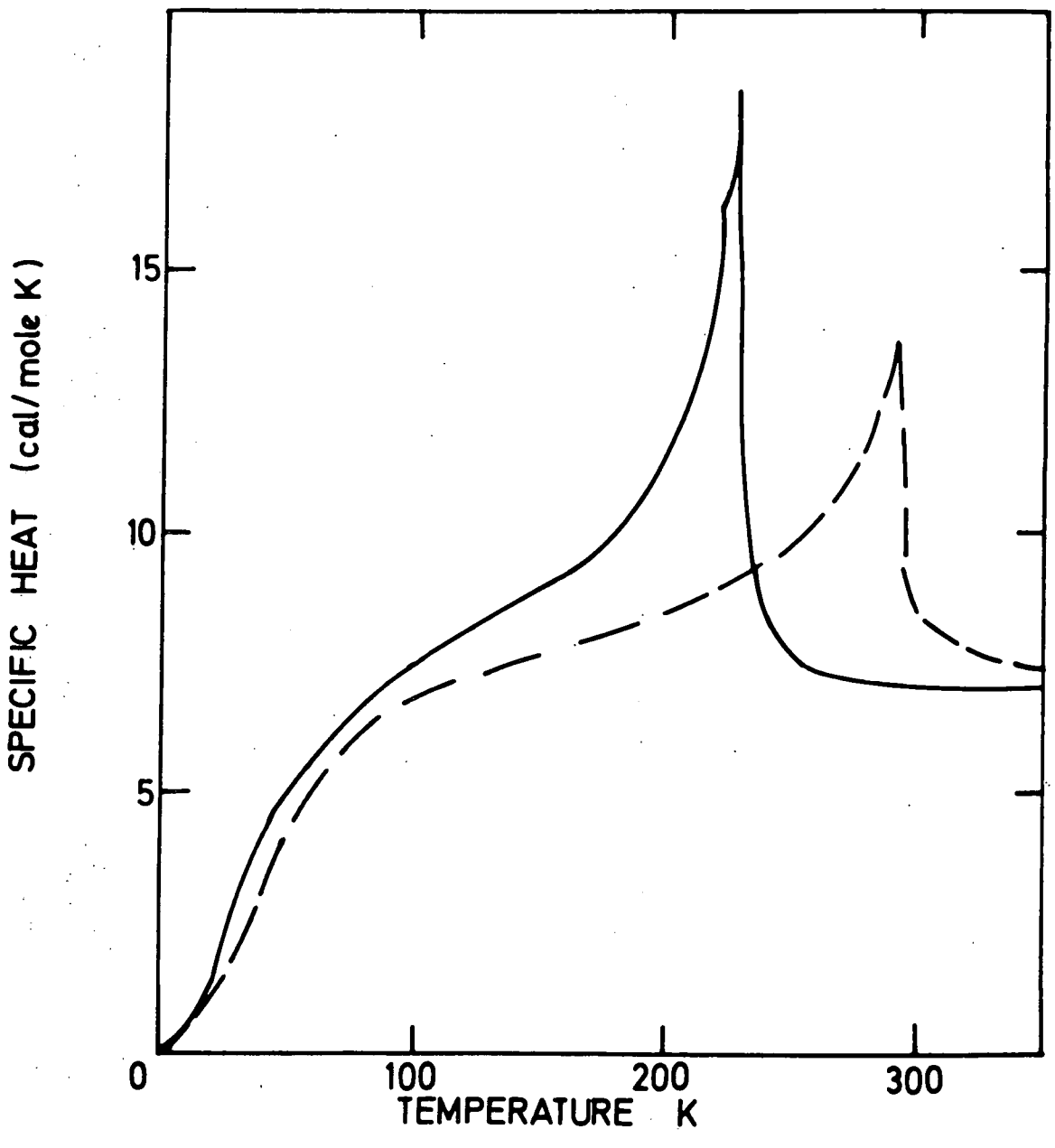

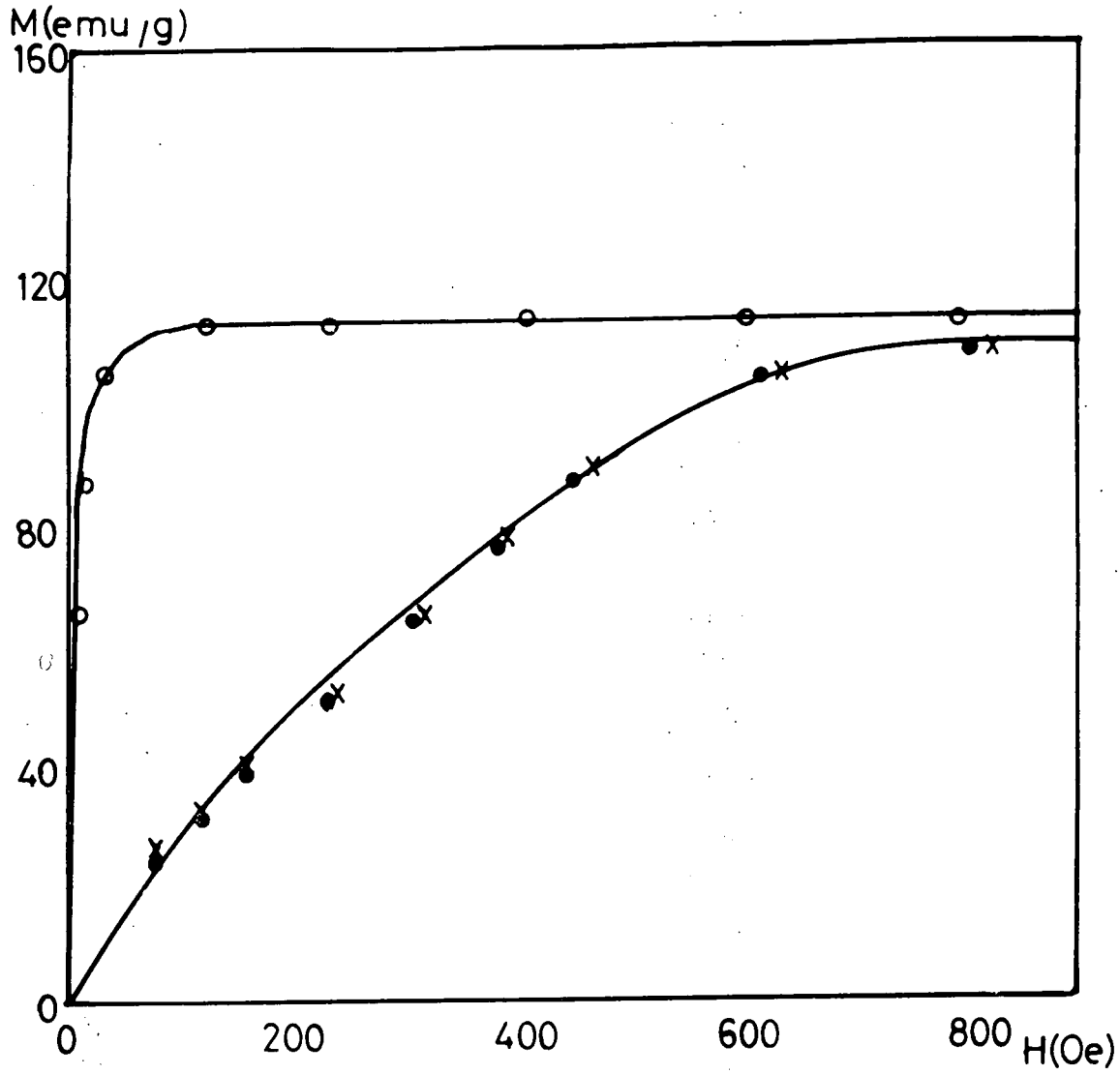

FIG. 2.8 MAGNETIC FIELD DEPENDENCE OF THE MAGNETIC MOMENT OF Gd SINGLE CRYSTALS ALONG THE a-AXIS AT 269.8 K(•), THE b-AXIS AT 270.1 K(x), AND THE c-AXIS AT 270.4 K(o), AFTER NIGH et al 1963

FIG. 2·9 TEMPERATURE DEPENDENCE OF THE MAGNETIC MOMENT IN Gd AND Tb

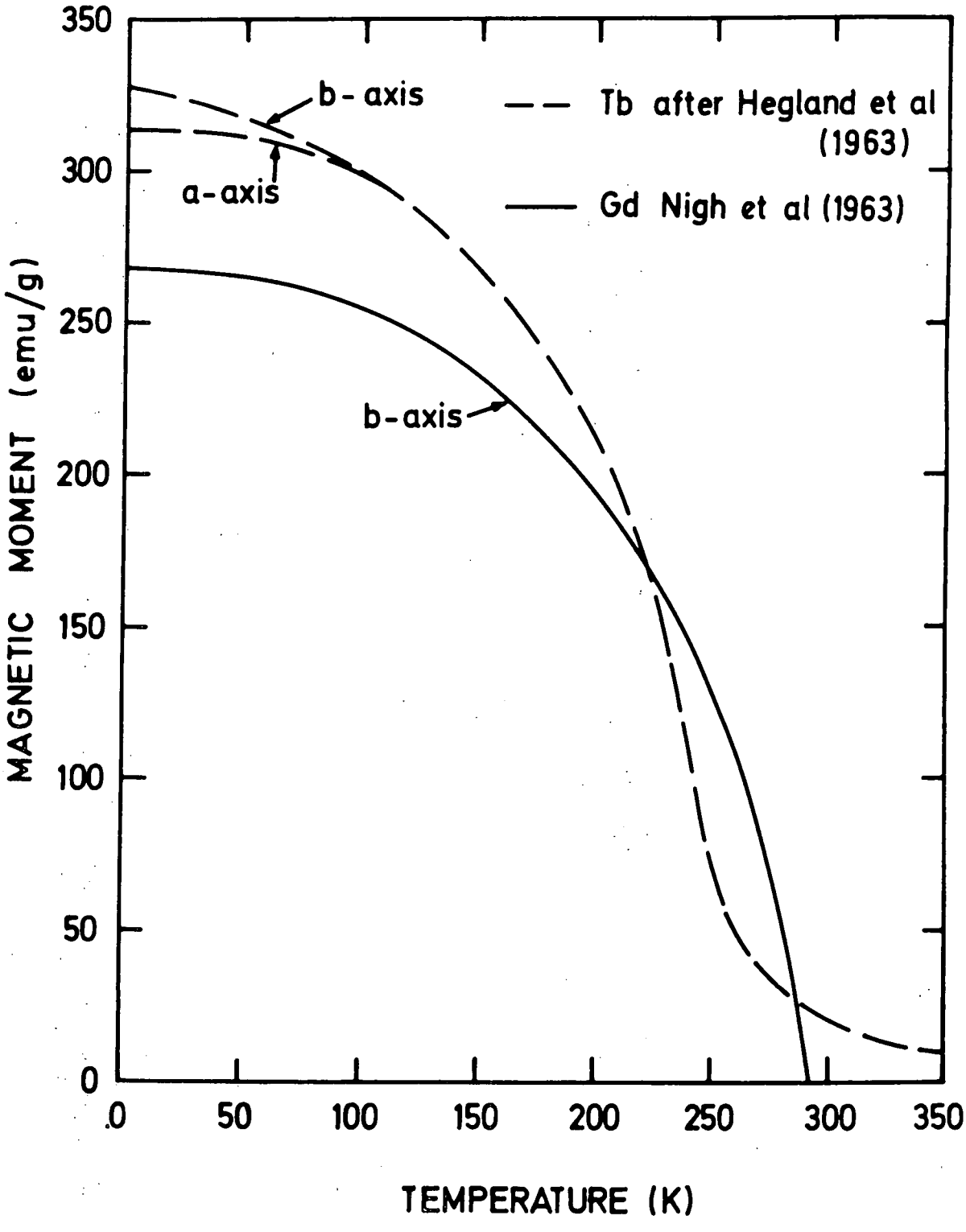

FIG. 2·10 TEMPERATURE DEPENDENCE OF THE ANGLE Φ BETWEEN THE DIRECTION OF THE MAGNETIC MOMENT AND THE C AXIS IN Gd.

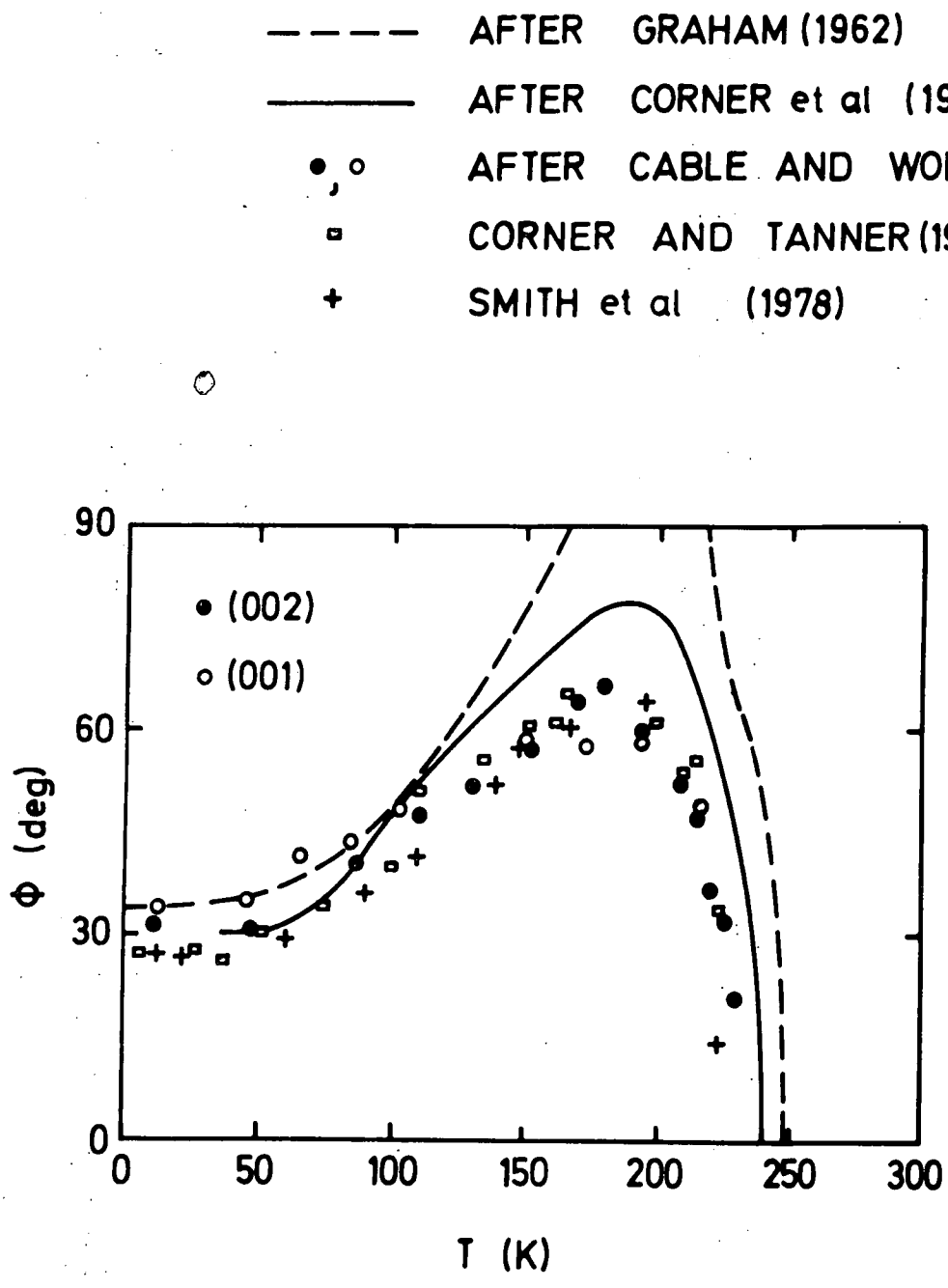

reaching at low temperatures a value of 32^{o}. The discrepancies in the early results have been explained as due to the effect of oxide which varies the easy direction of magnetization as reported by Smith et al (1977). This effect is illustrated in Fig. (2.10).

b. Terbium

The heavy rare earth metals from Terbium to Thulium have at least two magnetic transitions, one corresponding to the Néel point T_N and the other to the Curie point T_C, with $T_N > T_C$. Terbium has the first transition at 229 K from a paramagnetic state to an antiferromagnetically ordered state then another transition at 221 K from this intermediate state to a ferromagnetic state. The paramagnetic Curie temperature is anisotropic and the two measured values parallel and perpendicular to the c-axis are $\theta_{\parallel}$ = 195 K and $\theta_{\perp}$ = 239 K. It is well known now from neutron diffraction measurements, Koehler et al (1963), that Tb has a helical type of ordering in a very small range of temperature from T_N of 229 K to T_C of 221 K. The magnetic structures of Tb are illustrated in Fig. (2.5 e) in the range between T_N and T_C, and by Fig. (2.5 f) for the classical ferromagnetic below T_C. The helical spin configuration in Tb is quite weak energetically. It is destroyed by the application of a magnetic field of less that 200 Oe in the basal plane which induces a fan structure as found by Oothuizen and Alberts (1975) from magnetization measurements on Tb single crystals.

However, as can be seen from the change in resistivity of a Tb single crystal measured by Hegland et al (1963) as a function of temperature with magnetic field applied along the b-axis, Figure (2.11), the broad peak in the resistivity between T_N and T_C disappeared completely only for a field of 11 kOe. Magnetization measurements on a single crystal by Hegland et al confirmed that Terbium is ferromagnetic below 221 and

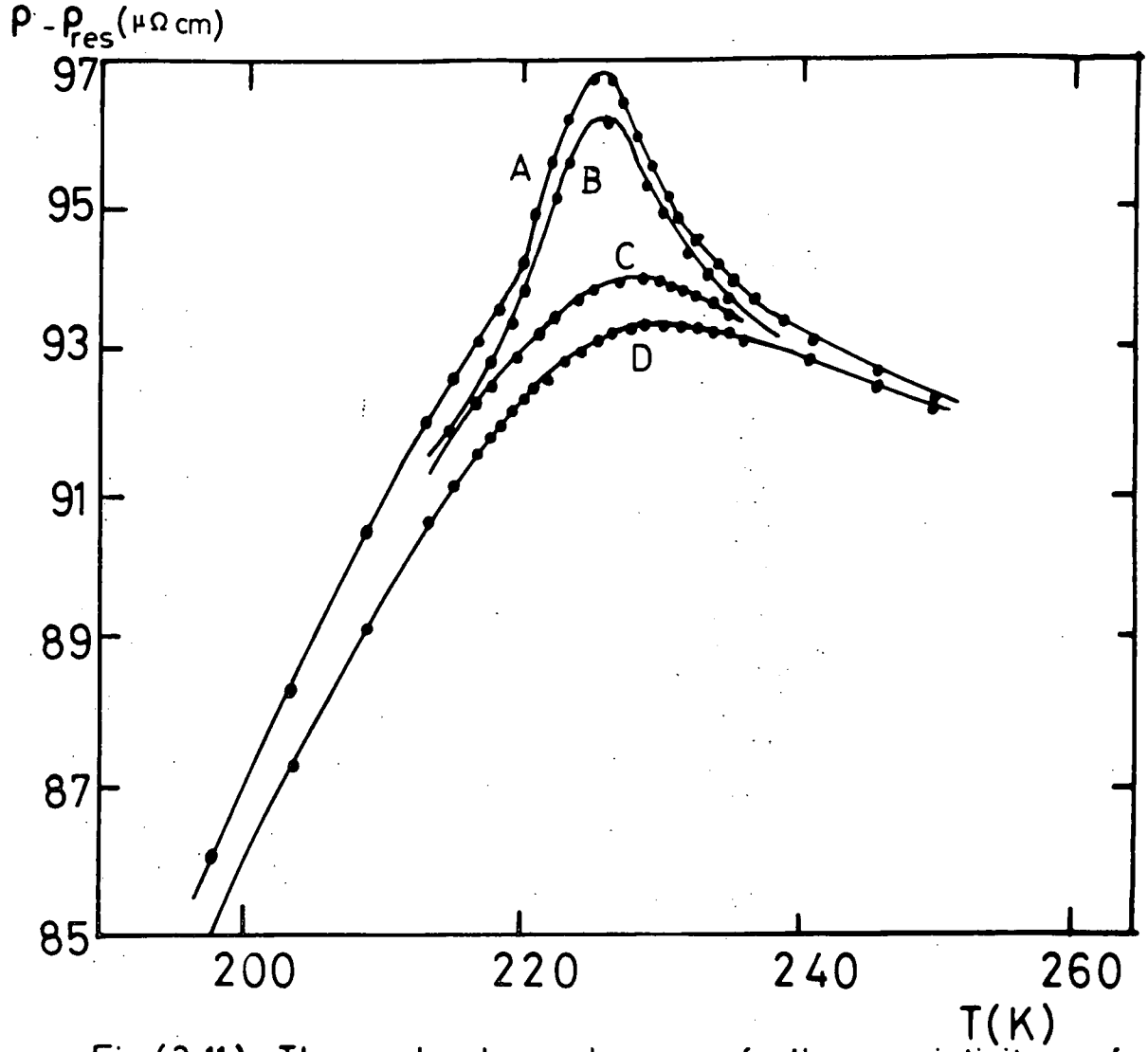

Fig.(2·11) Thermal dependence of the resistivity of a Tb single crystal along the c-axis for different value of the magnetic field applied along the b-axis. The curves A, B, C, and D correspond to a magnetic field of 0, 858, 6700, and 11350 Oe respectively, after Hegland et al (1963).

paramagnetic above 230 K. Because Tb has a very large axial anisotropy we find that the magnetization parallel to the c-axis is much smaller than that in the basal plane as shown in Fig. (2.12). At very low temperature the saturation magnetic moment is 9.34 μ_B as derived from the results shown in Fig. (2.9) in a good agreement with the theoretical value of 9 μ_B the excess moment 0.34 μ_B representing the polarization of the conduction electrons, Roeland et al (1975). The magnetic susceptibility has been measured by Rhyne et al (1968) along the c-axis and reported to be constant with the field at 4 K. The susceptibility near T_N can be represented by

$$\chi = (C/T)\ (A + B_{\pm}\, \varepsilon \ln \varepsilon) \qquad \ldots\ldots\ldots(2.7),$$

where $\varepsilon = |T_N - T| / T_N$. The quantities C, A, and $B_{\pm}$ are constants. The Constants B_+ and B- are associated with $T > T_N$ and $T < T_N$ respectively. If the magnetic susceptibility follows the above equation near both sides of T_N, then a plot of $d(\chi T)/dT$ vs. $\ln \varepsilon$ or $\ln|T_N - T|$ should be a straight line. Arajs et al (1975) have measured the magnetic susceptibility of polycrystalline Terbium below and above T_N. They found that the susceptibility follows Eq. (2.7) below T_N, while it does not above T_N. This means that there is a logarithmic divergence in χ below T_N but not above it.

Often a peak or knee will occur in the specific heat vs. temperature curve; these usually originate in some form of ordering process and may reflect the changes of the magnetic structure. Jennings et al (1957) have measured the total specific heat of Tb between T_N and T_C and they have found that it gives a λ-type anomaly at T_N as shown in Fig. (2.7). The observed total specific heat Cp of the lanthanides is in most cases the sum of four components, the lattice specific heat C_L, the electronic specific heat C_E, the magnetic specific heat C_M which is caused by the interations between the localized 4f electrons

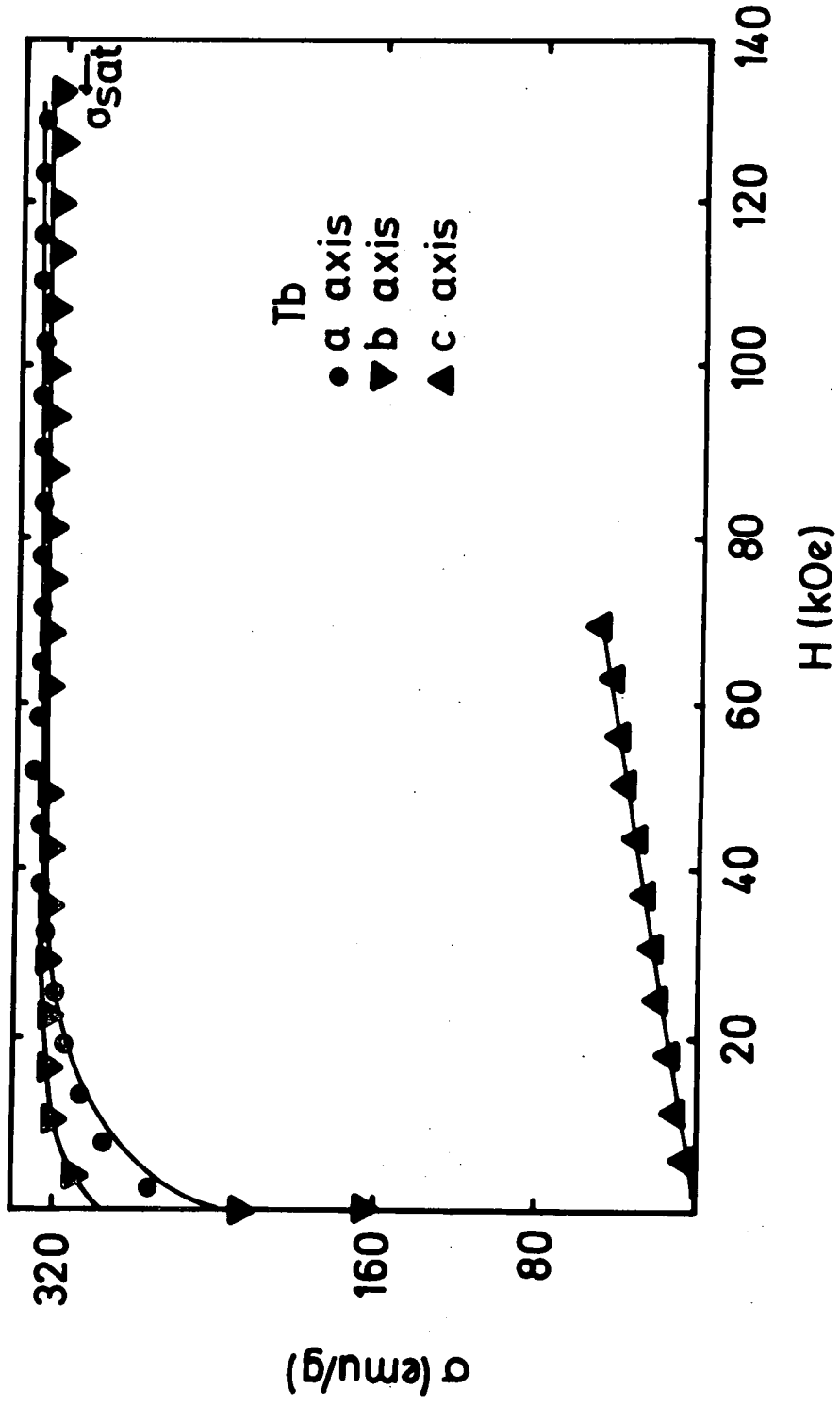

Fig(2.12) Magnetic moment per gram along a, b, and c axis of Tb at 4.2 K after Rhyne et al (1968).

and the nuclear specific heat C_N which results from splitting of the nuclear hyperfine levels with the 4f electrons. Lounasmaa and Sundström (1966) have reported specific heat measurements for Gd, Tb, Dy, and Ho between 3 and 25 K in order to determine the magnetic specific heat. They found an exponential temperature dependence for Tb of the form,

$$C_M = 36\ T^{3/2}\ \exp.\ (-23.5/T)\ \text{mJ/mole K}$$

This agrees with Nira's (1960) theoretical result for an anisotropic ferromagnet, i.e. $C_M = T^{3/2} \exp(-E/kT)$. $E = (K_2K_6)^{1/2}$ the spin wave activation energy, K_2, K_6 being the axial anistropy constants. For Gd

$$C_M = 0.19\ T^{2.7}\ \text{mJ/mole K.}$$

Houmann and Nicklow (1970) have found agreement between the total calculated specific heat and the experimental results at high temperatures for Tb.

c. Dysprosium, Holmium, Erbium, and Thulium

Dysprosium has the same general spin configuration as in Tb except the helical state is stable over a much wider temperature range and the a-axis $(11\bar{2}0)$, is the easy axis of magnetization, Jelinek et al (1965) and Pauthenet (1969). The first transition appears at a Néel temperature of 178.5 K and the second occurs at a Curie point of 85 K, Koehler (1965). The magnetic moment per atom has been found by several workers, Behrendt et al (1958), and Spedding et al (1957) to be $10.2\ \mu_B$ which has to be compared to the theoretical value of $10\ \mu_B$. As in Tb the helical phase between T_N and T_C can be destroyed by the application of a magnetic field, Behrendet et al (1958). Holmium also has two transitions, a Néel point of 130 K and a Curie point of 20 K. The ordered structure is a basal plane helix, but with some distortion between 45 K and the Curie point at which down

to the lowest studied temperature there is a transition to a conical structure with a semi-cone angle about 80^{o} as shown in Fig. (2.5 d) Koehler (1965). The spontaneous moment parallel to the c-axis is $1.7\,\mu_B$ and the basal plane component is $9.7\,\mu_B$. When an external field is applied parallel to the easy b-axis the full moment of $10\,\mu_B$ is developed. The conical state collapses by applying field along the basal plane, Strandburg et al (1962). The magnetization process in Ho is one of the most complex of all rare earths. At low temperatures when a magnetic field is applied the magnetic configuration goes directly to the ferromagnetic structure with the magnetic moment along the b-axis. When the temperature increases the transition occurs by passing through an intermediate fan or incompletely collapsed helical phase, Rhyne (1972) and Coqblin (1977).

Erbium has three magnetic structures; between the Néel temperature of 80 K and an intermediate temperature of 53 K the magnetic moment remains parallel to the c-axis and varies sinusoidally along this axis as shown in Fig. (2.5 b). From 53 K down to the Curie point of 20 K there is a distinct transition in which the perpendicular components of the magnetic moments begin to order and the parallel components tend to form a type of antiphase domain structure in which several layers with moments pointing up along the c-axis are followed by an equal number with moments pointing down, Koehler (1965), and this is illustrated by Fig. (2.5 c). Below T_C the ferromagnetic structure occurs and it is a cone as for Holmium.

Thulium has a magnetic structure similar to that of Erbium, but the magnetic moment remains always parallel to the c-axis. Between the Néel point of 56 K and a temperature of 38 K the antiferromagnetic ordering is the c-axis modulated magnetic structure as shown in Fig. (2.5 b), Koehler (1965). Below 38 K in addition a 3 - 4 antiphase

structure begins to develop as shown in Fig. (2.5 a). At 25 K this squaring up is complete.

d. Ytterbium and Lutetium

Their magnetic properties are unlike those of the other rare earth metals because the 4f shell is full and has fourteen electrons which gives a weakly paramagnetic behaviour, Koehler (1965) and Spedding et al (1957).

CHAPTER 3

THE FREE ENERGY OF A MAGNETIC SYSTEM

3.1 Introduction

Ferromagnetic materials exhibit magnetic properties even in the absence of a magnetic field, due to the fact they become spontaneously magnetized below the Curie temperature. The magnetization is increased when an external magnetic field is applied to the specimen. Moreover the relation between the magnetization M and the applied field H is non-linear and the former rises to a certain saturation value. When the field is removed or decreased gradually the specimen retains some of its magnetization M_R, so a hysteresis effect occurs. However, looking at a specimen as a whole, Weiss suggested that ferromagnetic materials are always magnetically saturated throughout small regions called domains, Carey and Isaac (1966 p.2). Barkhausen (1919), was the first to show the existence of ferromagnetic domains. The actual shapes and arrangements of the magnetic domains in a crystal are determined by a minimisation of five kinds of energy as follows.

3.2 Exchange Energy

As already mentioned the ferromagnetic materials are spontaneously magnetized. This means that the neighbouring moments interact with each other even in the absence of an applied magnetic field. Weiss, (1907) considered the spontaneous alignment of a dipole in a ferromagnet to be caused by the molecular field and this was later explained by Heisenberg (1928) in the terms of exchange energy. If we neglect the anisotropy effects the exchange energy between two moments i and j is given as,

$$W_{ex} = - 2 J S^2 \cos \phi_{ij} \qquad \text{.....(3.1)}$$

where J is the exchange integral which may take either a positive sign which will give rise to ferromagnetism or a negative one which gives rise to other configurations as in (1-2-5) The above equation may be reduced, if the angle between the neighbouring spins is assumed to be small, to,

$$W_{ex} = J S^2 \phi^2 \quad \text{.....(3.2)}$$

3.3 Magnetostatic Energy

Let us consider a ferromagnetic crystal in a uniform magnetization state. If all the spins are parallel to each other, the state has the lowest exchange energy. But free poles on the surface of the crystal produce a magnetic field called demagnetization field B_d opposite to the magnetization M. There is a positive magnetostatic energy due to Coloumb interaction between the magnetic free poles, whose density is given by, Omar, (1975 p. 456)

$$W_m = \tfrac{1}{2} M B_d \quad \text{.....(3.3)}$$

The first theoretical calculation of the magnetostatic energy was obtained by Landau and Lifshitz (1935), Lifshitz (1944), and Néel (1944). The value of B_d has been found by Williams et al, (1949), to depend on the shape of the surface and it is given by,

$$B_d = -\mu_o D M \quad \text{.....(3.4),}$$

where D is the demagnetization factor and equal to unity for a sample in a shape of a thin flat disc normal to the field.

If the crystal is considered as a single domain, this structure has a high magnetostatic energy due to the magnetic poles formed on the end surfaces of the crystal. In order to reduce this energy the crystal divides into domains. This subdivision cannot continue indefinitely because it requires some energy to create the wall or boundary separating two domains magnetized in different directions.

Landau and Lifshitz, (1935) showed that the subdivision continues until the energy required to form further domain wall is greater than the consequent reduction in the magnetostatic energy.

3.4 Domain Wall Energy

The change in direction of the magnetization between one domain and the next occurs through a transition layer which is called the domain wall, first investigated by Bloch, (1932). A rotation of atomic moment through 180^{o} between adjacent atomic sites would involve an extremely high value of exchange energy, tnus the domains wall must have a finite width. If within the wall the rotation takes place gradually over n sites, the exchange energy may be shown to be reduced by a factor of order n. Domain walls can be classified according to the angle of rotation of the magnetization. In a 180^{o} wall spin rotates by π from one domain to the other. Similarly 90^{o} walls and walls such as 71^{o}, and 109^{o} walls may exist. The wall characteristics are not only determined by the exchange energy, but also by the magnetic anisotropy energy wich will be discussed in the next section. The effect of this is to reduce the wall thickness. Thus although the exchange energy favours the formation of a thick wall, the anistropy energy limits this thickness. The wall thickness and energy can be estimated by minimizing the sum of these two energies. For a 180^{o} wall Kittel and Galt, (1956), have given,

$$\gamma = W_{ex} + W_{k}$$

$$\gamma = \frac{J S^2 \pi^2}{N a^2} + K N a$$

.....(3.5),

where W_{ex} is the exchange energy, W_{k} the anistropy energy, J the exchange integral, S the total spin, N the number of layers in which

the spins rotate by 180°, a the lattice constant, and K the anistropy constant. By minimizing γ with respect to N it is readily shown that the width of the wall is given by

$$\delta = N\,a = \sqrt{\frac{J\,S^2\pi^2}{K\,a}} \qquad \text{.....(3.6)}$$

3.5 Magnetocrystalline Anisotropy Energy

3.5.1 Introduction

Weiss, (1907), suggested that in a demagnetized single crystal, the domain magnetization could lie in any direction. But experiments on ferromagnetic materials show that magnetization can proceed more readily in certain directions, there being "easy" and "hard" directions. Iron crystals, for example, are more easily magnetized in the [100] directions than in [111] directions. So the magnetic properties of crystals are anisotopic and the magnetic energy of the system will depend on the direction of the magnetization vector. The difference in the energy between the easy and hard directions may be called the magnetic anisotropy energy. Magnetic anistropy can also be produced by applying mechanical stress to the materials (magnetostrictive anistropy), or may be due to the shape of the specimen. These effects should not be confused with the intrinsic effect related to the crystal structure and called magnetocrystalline anistropy.

3.5.2 Origins of Magnetocrystalline Anisotropy

The magnetic anisotropy energy E_k for a hexagonal symmetry can be written in Hamiltonian form as follows, Rhyne, (1972 p. 155) and Coqblin, (1977 p. 195)

$$H = E_a = K_2^o\, Y_2^o(\theta) + K_4^o\, Y_4^o(\theta) + K_6^o\, Y_6^o(\theta) + K_6^6 \sin^6\theta \cos 6\phi \qquad \text{.....(3.7)}$$

where θ is the polar angle from the c-axis [0001] to the magnetization vector and ϕ is the azimuthal angle in the basal plane measured from the a-axis $[11\bar{2}0]$ to the magnetization vector.

$Y_l^o(\theta)$ represents the spherical harmonic $Y_l^o(\theta, \phi)$ of l and $m = o$ values.

The first three anisotropy coefficients K and accompanying harmonics describe the dominant uniaxial anisotropy, while the K_6^6 refers to the six fold basal plane component.

An alternative set of anisotropy constants may be defined by Mason's equation, Mason (1954), for hexagonal structures in polar co-ordinates as,

$$E_a = K_1 \sin^2\theta + K_2 \sin^4\theta + K_3 \sin^6\theta + K_4 \sin^6\theta \cos 6\phi \quad \ldots\ldots\ldots(3.8),$$

where θ and ϕ are as in Eq. (3.7).

Two models have been proposed to account for the anisotropy energy. Firstly in addition to mutual coupling between electron orbital and spin moments there is also an interaction between the spins and the crystal lattice via the spin-orbit coupling. Through this interaction the localized spins of a single ion situated in a crystalline electrostatic field arising from neighbouring ions will have preferred directions with respect to the symmetry axes of that field and hence with respect to the crystallographic axes. This is called the single-ion model, Darby and Isaac (1974).

If the anisotropy arises from the coupling between pairs of spins such as pseudo-dipolar interaction this is known as a two-ion model.

a. Single-ion Anisotropy

In iron-group ferro or antiferromagnetics containing ions such as Fe^{3+} and Mn^{2+} the magnetic moment which is due to the spin moments of the 3d electrons is not coupled directly with the crystal lattice.

Thus the magnetic anisotropy energy arises from the indirect coupling between the spin and the crystal lattice via the spin-orbit coupling and the orbit-lattice coupling. Such a single-ion model can also be expected to apply to the rare earth metals where the unpaired electrons of the 4f shell are responsible for the magnetic moment, but because of a strong L-S coupling magnetic anisotropy is caused by a direct coupling between the orbit and the lattice, Yosida (1968). The Hamiltonian of a single-ion can be represented by, Darby and Isaac (1974),

$$H = g\mu_B \underline{H}_m \cdot \underline{S} + V_c(r) + H_{SL} + \mu_B \underline{H}_o \cdot (\underline{L} + 2\underline{S}) \quad \ldots\ldots\ldots(3.9),$$

where H_m is the molecular field used to represent the exchange interaction of a single-ion with its neighbours.

H_{SL} is the spin-orbit coupling, V_c is the potential of the crystalline field and H_o is an external field.

For the iron transition group Wolf (1957) has calculated the anisotropy energy in terms of parameters entering the spin Hamiltonian for a single-ion, the form of the Hamiltonian depending on the symmetry of the surroundings and the magnitude of the spin. For a spin in a lattice of cubic symmetry the operator which represents the one-ion anisotropy can be written with reference to the principal axes ξ, η, and ζ of the crystalline field.

$$H = \mu_B \underline{H}_m \underline{S} + \frac{1}{6} a (S_\xi^4 + S_\eta^4 + S_\zeta^4) + D S_a^2 + f S_a^4 \quad \ldots\ldots\ldots(3.10),$$

where S_ξ, S_η, and S_ζ are the components of the total spin of the ion S parallel to the ξ, η and ζ axes.

a is the direction of the axial distortion.

a, D, and f represent the amount of axial distortion.

In rare earth metals and compounds the carriers of magnetic moments

are 4f electrons and they are closely bound within the outer shells. As a result of the large L-S coupling, the total angular momentum $J = L \pm S$ is a good quantum number. Therefore, the single-ion anistropy Hamiltonian is given by the crystalline field potential itself. For a hexagonal structure it can be expressed in terms of J_x, J_y, and J_z with reference to the hexagonal axes as, Stevens (1952)

$$\begin{aligned} H_A = {} & \alpha A_2^0 \langle r^2 \rangle [2J_z^2 - J(J+1)] + \beta A_4^0 \langle r^4 \rangle [35 J_z^4 - 30 J_z^2 J(J+1) \\ & + 3 J^2 (J+1)^2 + 25 J_z^2 - 6 J(J+1)] + \gamma A_6^0 \langle r^6 \rangle [231 J_z^6 \\ & - 315 J(J+1) J_z^4 + 105 J^2 (J+1)^2 J_z^2 - 5 J^3 (J+1)^3 \\ & + 735 J_z^4 - 525 J(J+1) J_z^2 + 40 J^2 (J+1)^2 + 294 J_z^2 - 60 J(J+1)] \\ & + \gamma A_6^6 \langle r^6 \rangle 1/2 [(J_x + iJ_x)^6 + (J_x - iJ_y)^6] \end{aligned}$$

.....(3.11)

The above equation can be represented in an alternative form given by Elliot and Stevens (1953).

$$\begin{aligned} H_A = {} & \alpha A_2^0 \langle r^2 \rangle Y_2^0(J) + \beta A_4^0 \langle r^4 \rangle Y_4^0(J) \\ & + \gamma A_6^0 \langle r^6 \rangle Y_6^0(J) + \gamma A_6^6 \langle r^6 \rangle [Y_6^6(J) + \bar{Y}_6^6(J)] \end{aligned}$$

.....(3.12),

where A^m's are the crystal field potential calculated for the tripositive ions and α, β, γ are constants determined by J, L, and S for f electrons. $\langle r^n \rangle$ represents the average of r^n. Stevens (1952) has obtained the anisotropy energy from Eq. (3.11) at the absolute zero of temperature as,

$$E_A = D P_2 (\cos\theta) + E P_4 (\cos\theta) + F P_6 (\cos\theta) + G \sin^6\theta \cos 6\phi$$

.....(3.13),

which is another form of Eq. (3.7)

$$D = 2\alpha A_2^0 \langle r^2 \rangle J^2 \qquad E = 8\beta A_4^0 \langle r^4 \rangle J^4$$

$$F = 16\gamma A_6^0 \langle r^6 \rangle J^6 \qquad G = \gamma A_6^6 \langle r^6 \rangle J^6$$

b. Two-ion Model

The single-ion anisotropy energy is very small for an S-state ion such as Gd^{3+} because it has no orbital moments in the free-ion state or it vanishes identically in some cases such as for an effective spin S = 1/2, Yosida (1968) and Darby and Isaac (1974). In such cases the anisotropic interaction between pairs of ions must be important in the magnetic anisotropy. The origin of the two-ion anisotropy as follows. Since the interaction energy between the electronic charge clouds depends upon their shape and the shape of a cloud depends upon the direction of its spin through the spin orbit coupling, so the energy depends upon the direction of the spins.

The simplest mechanism is the magnetic dipole-dipole interaction in which two spins $\underline{S}_i$ and $\underline{S}_j$ on ions separated by vector $\underline{R}_{ij}$ are coupled to give a Hamiltonian of form,

$$H_D = \sum_{i<j} E_{ij} \left[\underline{S}_i \cdot \underline{S}_j - 3 \left(\underline{S}_i \cdot \underline{R}_{ij} \right) \left(\underline{S}_j \cdot \underline{R}_{ij} \right) \underline{R}_{ij}^{-2} \right] \qquad \ldots\ldots\ldots(3.14)$$

where $E_{ij} = g^2 \mu_B^2 / R_{ij}^3$. Generally this is too small to account for the observed anisotropy.

Van Vleck (1937) proposed an interaction between spins $\underline{S}_i$ and $\underline{S}_j$ to treat the source of ferromagnetism of metallic Ni, now referred to as a pseudo-dipolar interaction. This used a similar expression to Eq. (3.14) but with the constant E_{ij} replaced by an empirical constant D_{ij} which was evaluated from experimental results. He also needed to include quadrupole-quadrupole terms in his treatment.

The general form of interaction energy between two spins $\underline{S}_1$ and $\underline{S}_2$ is given by Darby and Isaac as,

$$H_{12} = \underline{S}_1 . \underline{J} . \underline{S}_2 + d(\underline{S}_1 \times \underline{S}_2) + \underline{S}_1 \underline{S}_2 : j : \underline{S}_1 \underline{S}_2 + \text{higher terms} \qquad \ldots\ldots\ldots(3.15)$$

where J and j are tensors of second and fourth rank respectively. The dipole interaction and the isotropic exchange interaction have the form of the first term. The second term has been predicted by

Dzyaloshinski (1958), which arises from certain second order perturbation terms involving the L-S coupling and the exchange interaction. The interaction gives an origin of the weak (or Parasitic) ferromagnetism, Yosida (1968). The pseudo-dipolar interaction between two spins appears in the third term.

3.5.3 Variation of Anistropy Coefficients with Temperature

It is necessary to know the thermal dependence of the anistropy coefficients before we can study the magnetoelastic effects. The main principle of calculating the temperature variation of the magnetic anistropy energy consists of averaging the anisotropy energy of the spins at various temperatures.

This has been discussed by Callen and Callen (1966) and a full explanation of the theoretical treatment is given by Coqblin (1977 p. 360). Following the calculation of Callen and Callen (1966) for a single-ion model, the theoretical dependences of the anisotropy coefficients of order $l = 2, 4, 6$ are given as follows,

$$K_l(T) = K_l(0) \frac{I_{l+\frac{1}{2}}[\mathcal{L}^{-1}(m)]}{I_{\frac{1}{2}}[\mathcal{L}^{-1}(m)]} = K_l(0)\, \hat{I}_{l+\frac{1}{2}}[\mathcal{L}^{-1}(m)] \quad \text{.....(3.16),}$$

where $\hat{I}$ is the reduced hyberbolic Bessel function, $\mathcal{L}^{-1}$ is the inverse of the Langevin function, and $m = \frac{M(T)}{M(0)}$ is the reduced magnetization. The above equation should be correct for all temperature ranges.

In the low temperature region where $\frac{M(T)}{M(0)} \sim 1$ Callen and Callen have found that the anisotropy constants follow the $[l(l+1)/2]$-power law as

$$\frac{K_l(T)}{K_l(0)} = 1 - \frac{l(l+1)}{2}[1 - m] \simeq [m]^{l(l+1)/2} \quad \text{.....(3.17)}$$

Another limit concerns the case where $\frac{M(T)}{M(0)}$ is very small, i.e. when T is very close to T_C, the anisotropy constants can then be represented as, Coqblin (1977),

$$\frac{K_l(T)}{K_l(0)} \simeq \frac{3^l}{(2l+1)!!}\left[\frac{M(T,H)}{M(0,0)}\right] \qquad \ldots\ldots\ldots(3.18),$$

where $(2l+1)!!$ denotes $1 \times 3 \times 5 \times \ldots\ldots\ldots (2l+1)$

At temperatures above T_C the anisotropy constants would be expected, according to Rhyne (1972) to vary as,

$$K(T) \alpha m^l \qquad \ldots\ldots\ldots(3.19)$$

The above results have been established for the single-ion mechanism as it is an important contributor to magnetic anisotropy effects in the rare earth elements. For the two-ion model the situation is more complicated and the $l(l+1)$ power law will fail, all that can be said with rigor is that the low and high temperature limits are $m^{l(l+1)/2}$ and m^l Callen and Callen (1966).

3.6 Magnetostriction and Magnetoelastic Energy

3.6.1 Introduction

Magnetostriction is the change in the shape of a crystal during the process of magnetization. The strain $\frac{\delta l}{l}$ due to magnetostriction is very small typically between 10^{-3} and 10^{-6} and it varies with the field as shown in Fig. (3.1), and finally reaches the saturation value λ. This study deals with both its origin and its temperature and field dependence. Tsuya et al, (1964) have reported a theory for heavy rare earth metals. Clark et al, (1965), have discussed the theory of magnetostriction of hexagonal-close-packed crystals, but most of the details of the theoretical calculations have been described

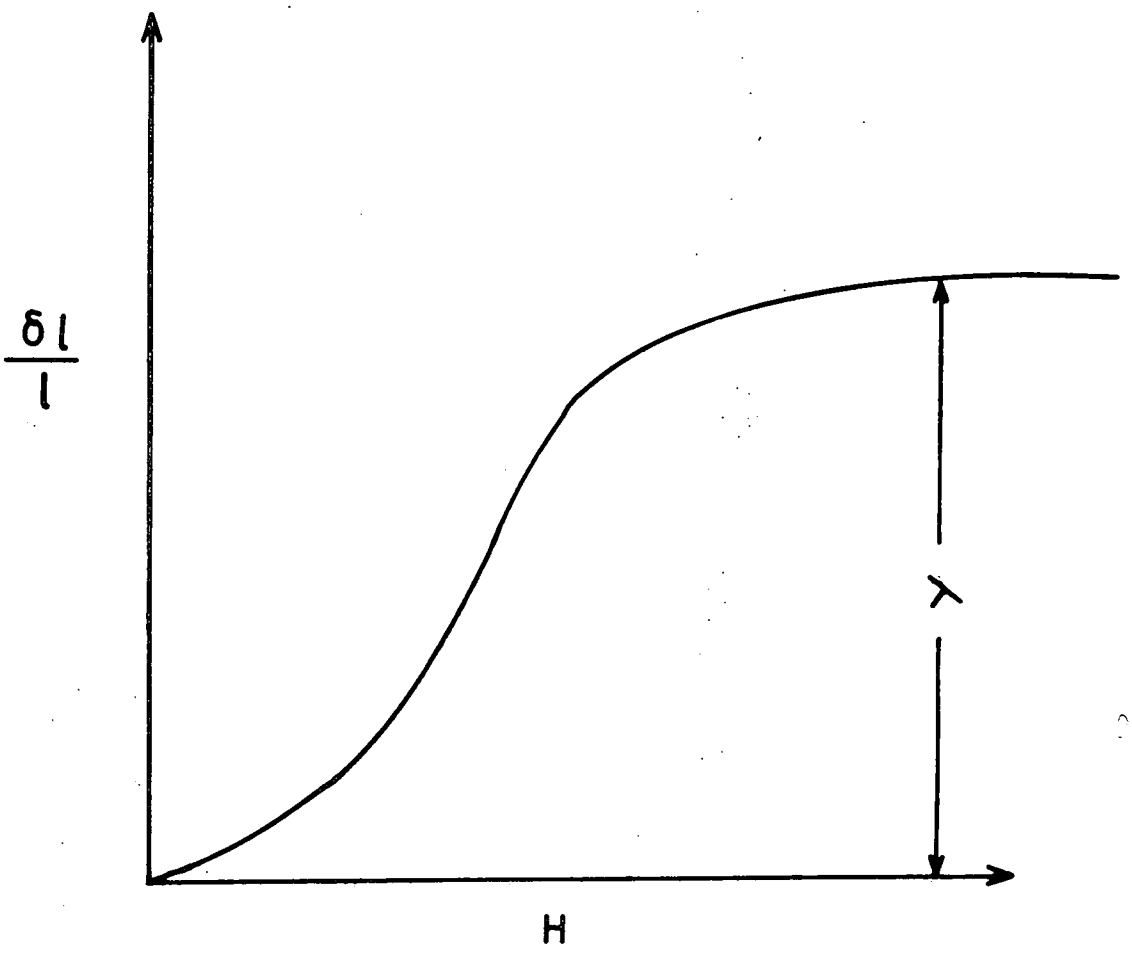

FIG. 3.1 MAGNETOSTRICTION AS A FUNCTION OF THE FIELD INTENSITY.

by Callen and Callen in a series of papers, (1963, 1965, 1966), and a later review by Callen, (1968) reviewed the work on magnetostriction since 1961. A brief review of theory has been given by Rhyne, (1972) and a fairly complete account of the theoretical basis is given by Coqblin (1977 p. 381).

3.6.2 Theory of Magnetostriction

The magnetostriction arises from the modulation by the strain of single-ion energies such as the anisotropy energy and crystal-field splittings; it should also include the two-ion magnetoelastic terms, which are required to describe the strain dependence of the exchange energy (isotropic and anisotropic) and the dipole-dipole energy. Phenomenologically the Hamiltonian of the system can be written, Callen and Callen, (1965) as,

$$H = H_m + H_e + H_{me} + H_a \qquad \text{.....(3.21),}$$

where H_m is the Hamiltonian of the spin system, H_e is the elastic energy ($\frac{1}{2}C\varepsilon^2$), where ε is the strain.

H_{me} is the magnetoelastic interaction, coupling the spin system to the strain, and H_a is the magnetocrystalline anisotropy energy.

The magnetoelastic energy H_{me} has been given by Clark et al, (1965) as

$$H_{me} = -\sum_{\mu,j}\sum_{\iota} B_j^{\mu,\iota} \sum_i \varepsilon_i^{\mu,j} \sum_f K_i^{\mu,\iota}(S_f) - \sum_{\mu,j}\sum_{\iota,i}\varepsilon_i^{\mu,j}\sum_{f,g} D_j^{\mu,\iota}(f,g)\, K_i^{\mu,\iota}(S_f,S_g)$$

$$\text{.....(3.22),}$$

$B_j^{\mu,\iota}$ and $D_j^{\mu,\iota}$ are one ion and two ion temperature independent magnetoelastic coupling coefficients. $\varepsilon_i^{\mu,j}$ are the irreducible strains. $K_i^{\mu,\iota}(S_f)$ and $K_i^{\mu,\iota}(S_f,S_g)$ are respectively the symmetry polynomial in the spin components of spin f and spins f and g.

In this expression l is the degree of the symmetry polynomial. For a hexagonal crystal, keeping only terms in $l = 2$, H_{me} reduced by Tsuya et al, (1964) to give,

$$H_{me} = [\{ B_1^{\alpha,2}(\varepsilon_{xx} + \varepsilon_{yy}) + B_2^{\alpha,2}\varepsilon_{zz} \}(J_z^2 - 1/3) + B^{\gamma,2}\{ 1/4(J_x^2 - J_y^2)(\varepsilon_{xx} - \varepsilon_{yy}) + J_x J_y \varepsilon_{xy} \} + B^{\varepsilon,2}\{ J_y J_z \varepsilon_{yz} + J_z J_x \varepsilon_{zx} \}] / (2J^2 - J)$$

.....(3.23)

The superscripts α , γ , and ε identify the three possible magnetostriction modes, α the fully symmetric strain mode in which the hexagonal symmetry is unchanged, γ is the shearing mode which distorts the basal plane, ε is a shearing mode containing the unique axes.

Minimizing the free energy with respect to the strain, and transforming these hexagonal strains to Cartesian strains, the magnetostriction expression for crystals of hexagonal close packed symmetry given by Clark et al (1965), and as corrected by Callen, (1968) is as follows,

$$\frac{\delta l}{l} = \lambda = \sum_{i,j} \varepsilon_{i,j} \beta_i \beta_j$$

.....(3.24)

$$\frac{\delta l}{l} = \lambda = \lambda_1^{\alpha,0}(1 - \beta_z^2) + \lambda_2^{\alpha,0}\beta_z^2 + \lambda_1^{\alpha,2}(1 - \beta_z^2)(\alpha_z^2 - \tfrac{1}{3}) + \lambda_2^{\alpha,2}\beta_z^2(\alpha_z^2 - \tfrac{1}{3}) + \lambda^{\gamma,2}[\tfrac{1}{2}(\beta_x^2 - \beta_y^2)(\alpha_x^2 - \alpha_y^2) + 2\beta_x \beta_y \alpha_x \alpha_y] + 2\lambda^{\varepsilon,2}(\beta_x \alpha_x + \beta_y \alpha_y)\beta_z \alpha_z$$

.....(3.25)

Here α_x, α_y, and α_z are the direction cosines of the magnetization and, β_x, β_y, and β_z are those of the strain (measuring) directions. The two fully symmetric terms $\lambda_1^{a,0}$, $\lambda_2^{a,0}$ are independent of the magnetization direction. They arise from the two-ion interaction term in the Hamiltonian and depend only upon the magnitude of M. The coefficient $\lambda_1^{a,0}$, refers to the strain measured in a basal plane direction, and $\lambda_2^{a,0}$ refers to the strain along c-axis. They are related to the anomalous thermal expansion. The symbols α, ε and γ describe the strain modes of magnetostriction as already stated and as shown in Fig. (3.2). The coefficients of Eq. (3.25) can be related to the general Eq. (3.22), Clark et al (1965), as,

$$\lambda_1^{a,0} = \sum_{f,g} [\, 1/3\, \tilde{D}_1^{a,0}(f,g) - 1/2\, \tilde{D}_2^{a,0}(f,g)] < S_f . S_g > ,$$

$$\lambda_2^{a,0} = \sum_{f,g} [\, \tilde{D}_1^{a,0}(f,g) + \tilde{D}_2^{a,0}(f,g)] < S_f . S_g > ,$$

$$\lambda_1^{a,2} = [\, 1/3\, \tilde{B}_1^{a,2} - 1/2\, \tilde{B}_2^{a,2}\,] < (S_f^{\zeta})^2 - 1/3\, S(S+1) >$$

$$+ \sum_{f,g} [\, 1/3\, \tilde{D}_1^{a,2}(f,g) - 1/2\, \tilde{D}_2^{a,2}(f,g)\,]$$

$$x < S_f^{\zeta} S_g^{\zeta} - 1/3\, S_f . S_g > ,$$

$$\lambda_2^{a,2} = [\, 1/3\, \tilde{B}_1^{a,2} + \tilde{B}_2^{a,2}\,] < (S_f^{\zeta})^2 - 1/3\, S(S+1) >$$

$$+ \sum_{f,g} [1/3\, \tilde{D}_1^{a,2}(f,g) + \tilde{D}_2^{a,2}(f,g)] \, x < S_f^{\zeta} S_g^{\zeta} - 1/3\, S_f . S_g > ,$$

$$\lambda^{\gamma,2} = \tilde{B}^{\gamma,2} < (S_f^{\zeta})^2 - 1/3\, S(S+1) >$$

$$+ \sum_{f,g} \tilde{D}^{\gamma,2}(f,g) < S_f^{\zeta} S_g^{\zeta} - 1/3\, S_f . S_g > ,$$

$$\lambda^{\varepsilon,2} = \tilde{B}^{\varepsilon,2} < (S_f^{\zeta})^2 - 1/3\, S(S+1) >$$

$$+ \sum_{f,g} \tilde{D}^{\varepsilon,2}(f,g) < S_f^{\zeta} S_g^{\zeta} - 1/3\, S_f . S_g >$$

.....(3.26)

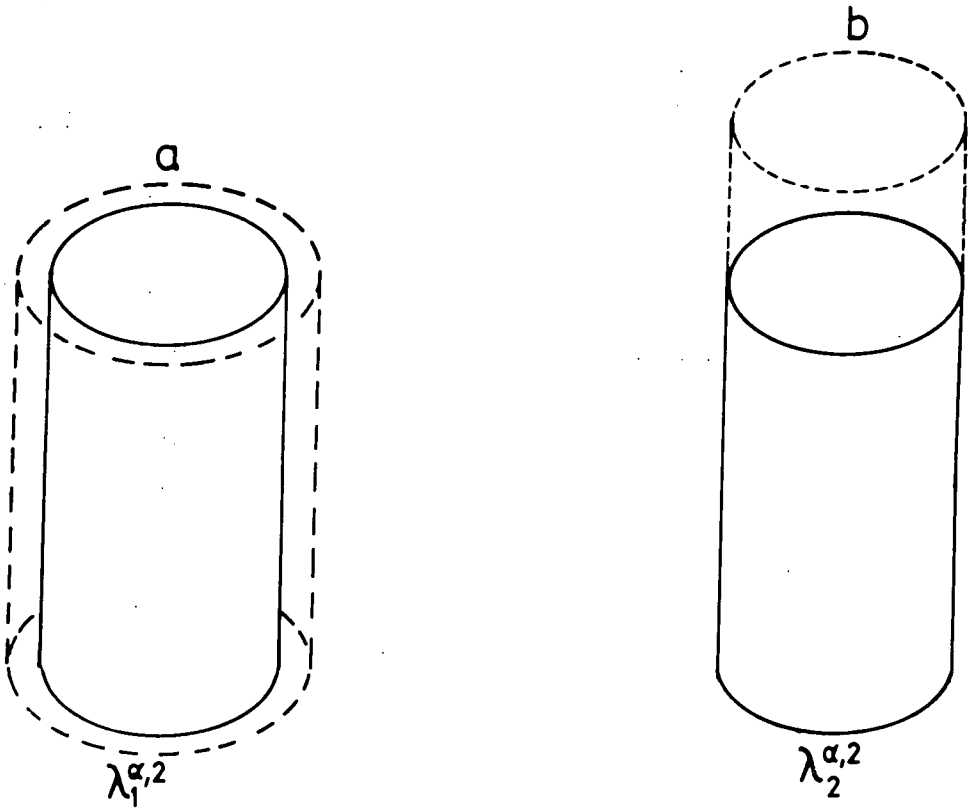

FIG 3·2 THE FOUR POSSIBLE MAGNETOSTRICTION MODES

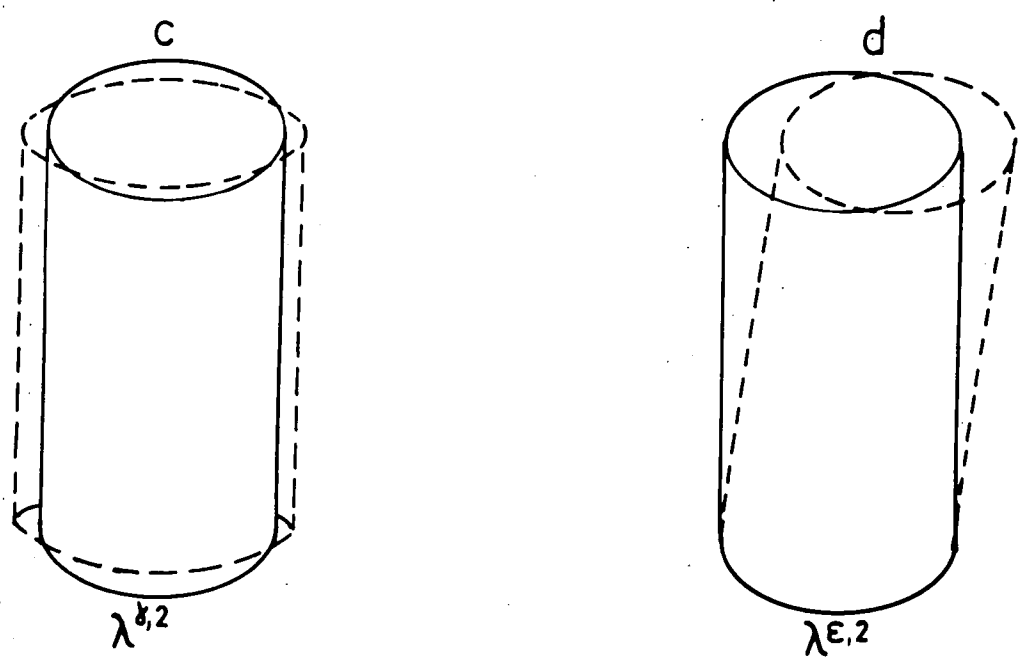

Callen and Callen, (1965) have introduced another six magnetostriction coefficients $\lambda^{a}_{11}, \lambda^{a}_{12}, \lambda^{a}_{21}, \lambda^{a}_{22}, \lambda^{\gamma}, \lambda^{\epsilon}$.

and they have given the equivalent formula as,

$$\frac{\delta l}{l} = 1/3\,\lambda^{a}_{11}(T,H) + \frac{1}{2\sqrt{3}}\,\lambda^{a}_{12}(T,H)(\alpha_z^2 - 1/3)$$
$$+ \sqrt{3}\,\lambda^{a}_{21}(T,H)\,(\beta_z^2 - 1/3) + 3/2\;\lambda^{a}_{22}(T,H)\,(\alpha_z^2 - 1/3)\,(\beta_z^2 - 1/3)$$
$$+ 2\lambda^{\gamma}(T,H)\,[\,1/4(\alpha_x^2 - \alpha_y^2)(\beta_x^2 - \beta_y^2) + \alpha_x\,\alpha_y\,\beta_x\,\beta_y\,]$$
$$+ 2\lambda^{\epsilon}(T,H)\,[\,\alpha_x\,\alpha_z\,\beta_x\,\beta_z + \alpha_y\,\alpha_z\,\beta_y\,\beta_z\,] \qquad \ldots\ldots\ldots(3.27)$$

The relations between the coefficients of Clark et al (1965) and those of Callen and Callen (1965) as calculated by Coqblin (1977) including corrections are

$$\lambda^{a,0}_{1} = 1/3\,(\,\lambda^{a}_{11} - \sqrt{3}\,\lambda^{a}_{21})$$
$$\lambda^{a,0}_{2} = 1/3\,(\,\lambda^{a}_{11} + 2\sqrt{3}\,\lambda^{a}_{21})$$
$$\lambda^{a,2}_{1} = \frac{1}{2\sqrt{3}}\,(\,\lambda^{a}_{12} - \sqrt{3}\,\lambda^{a}_{22})$$
$$\lambda^{a,2}_{2} = \frac{1}{2\sqrt{3}}\,(\,\lambda^{a}_{12} + 2\sqrt{3}\,\lambda^{a}_{22})$$
$$\lambda^{\gamma,2} = \lambda^{\gamma} \quad \text{and} \quad \lambda^{\epsilon,2} = \lambda^{\epsilon} \qquad \ldots\ldots\ldots(3.28)$$

A higher order formula up to $l = 4$ has been given by Mishima et al, (1976) as,

$$\lambda = \lambda^{a,0}_{1}\,(1 - \beta_z^2) + \lambda^{a,0}_{2}\,\beta_z^2 + \lambda^{a,2}_{1}\,(1 - \beta_z^2)(\alpha_z^2 - 1/3)$$
$$+ \lambda^{a,2}_{2}\,\beta_z^2\,(\alpha_z^2 - 1/3) + \lambda^{\gamma,2}\,[\,1/2\,(\beta_x^2 - \beta_y^2)(\alpha_x^2 - \alpha_y^2) + 2\,\beta_x\,\beta_y\,\alpha_x\,\alpha_y\,]$$
$$+ 2\,\lambda^{\epsilon,2}\,(\beta_x\,\alpha_x + \beta_y\,\alpha_y)\,\beta_z\,\alpha_z + \lambda^{a,4}_{1}\,(1 - \beta_z^2)(7\,\alpha_z^4 - 6\,\alpha_z^2 + 3/5)$$
$$+ \lambda^{a,4}_{2}\,\beta_z^2\,(7\,\alpha_z^4 - 6\,\alpha_z^2 + 3/5) + \lambda^{\gamma,4}\,[\,1/2\,(\beta_x^2 - \beta_y^2)(\alpha_x^2 - \alpha_y^2)$$
$$+ 2\,\beta_x\,\beta_y\,\alpha_x\,\alpha_y\,]\,(7\,\alpha_z^2 - 1) + 2\,\lambda^{\epsilon,4}\,(\beta_x\,\alpha_x + \beta_y\,\alpha_y)\,\beta_z\,\alpha_z\,(7\,\alpha_z^2 - 3)$$
$$+ \lambda^{\delta,4}\,[\,8\,\beta_x\,\beta_y\,\alpha_x\,\alpha_y\,(\alpha_x^2 - \alpha_y^2) - (\beta_x^2 - \beta_y^2)\,(\alpha_x^4 + \alpha_y^4 - 6\,\alpha_x^2\,\alpha_y^2)\,] \qquad \ldots\ldots\ldots(3.29)$$

For higher order terms of $\lambda^{a,8}_{i}$, they have derived the magnetostriction to be as;

$$\lambda = \lambda_1^{a,6} (1 - \beta_z^2) \left[\frac{176}{5} \alpha_z^6 - 48 \alpha_z^4 + 16 \alpha_z^2 - \frac{16}{21} \right]$$
$$+ \lambda_2^{a,6} \beta_z^2 \left[\frac{176}{5} \alpha_z^6 - 48 \alpha_z^4 + 16 \alpha_z^2 - \frac{16}{21} \right]$$
$$+ \lambda_1^{a,8} (1 - \beta_z^2) \left[\frac{1144}{7} \alpha_z^8 - \frac{4576}{15} \alpha_z^6 + 176 \alpha_z^4 - 32 \alpha_z^2 + \frac{8}{9} \right]$$
$$+ \lambda_2^{a,8} \beta_z^2 \left[\frac{1144}{7} \alpha_z^8 - \frac{4576}{15} \alpha_z^6 + 176 \alpha_z^4 - 32 \alpha_z^2 + \frac{8}{9} \right]$$

.....(3.30)

A third magnetostriction expression, which has been frequently used in the analysis of experimental work, has been given by Mason (1951, 1954) up to fourth order for hcp structures as,

$$\frac{\delta l}{l} = A \left[2 \alpha_x \alpha_y \beta_x + (\alpha_x^2 - \alpha_y^2) \beta_y \right]^2 + B \alpha_z^2 \left[(\alpha_x^2 - \alpha_y^2) (\beta_x^2 - \beta_x^2) \right.$$
$$\left. + 4 \alpha_x \alpha_y \beta_x \beta_y \right] + C \left[(\alpha_x^2 - \alpha_y^2) (\beta_x^2 - \beta_y^2) + 4 \alpha_x \alpha_y \beta_x \beta_y \right]$$
$$+ D (1 - \alpha_z^2) (1 - \beta_z^2) + E \alpha_z^2 \beta_z^2 (1 - \alpha_z^2) + F \alpha_z^2 (1 - \alpha_z^2)$$
$$+ G \beta_z^2 (1 - \alpha_z^2) + H \alpha_z \beta_z (\alpha_x \beta_x + \alpha_y \beta_y) + I \alpha_z^2 \beta_z (\alpha_x \beta_x + \alpha_y \beta_y)$$
$$+ J \alpha_z^2 (1 - \beta_z^2) + K \alpha_z^2 \beta_z^2 .$$

.....(3.31)

The six constants C, D, G, H, J, and K are linear combinations of the magnetostriction constants of Callen and Callen in Eq. (3.27), or of those of Clark et al in Eq. (3.25), and can be related to each other as follows,

$$C = 1/2 \ \lambda^{\gamma,2} \qquad D = \lambda_1^{a,0} - 1/3 \ \lambda_1^{a,2}$$

$$G = \lambda_2^{a,0} - 1/3 \ \lambda_2^{a,2} \qquad H = 2 \ \lambda^{\varepsilon,2}$$

$$J = \lambda_1^{a,0} + 2/3 \ \lambda_1^{a,2}$$

$$K = \lambda_2^{a,0} + 2/3 \ \lambda_2^{a,2}$$

.....(3.32)

The five constants A, B, E, F, and, I are the fourth order magnetostriction constants.

If the equation of Clark et al up to $l = 4$ which has been derived by Mishima et al, (1976) Eq. (3.29), is compared with that of Mason's formula Eq. (3.31), A to K can be calculated and given as follows,

$$A = \frac{4}{3}\lambda^{\delta,4} \qquad B = -\lambda_1^{a,0} - \frac{2}{3}\lambda_1^{a,2} - \frac{43}{5}\lambda_1^{a,4} + \frac{7}{2}\lambda^{\gamma,4} + \frac{2}{3}\lambda^{\delta,4}$$

$$C = 1/2\,(\lambda^{\gamma,2} - \lambda^{\gamma,4})$$

$$D = \lambda_1^{a,0} - 1/3\,\lambda_1^{a,2} + 3/5\,\lambda_1^{a,4} - 2/3\,\lambda^{\delta,4}$$

$$E = -\lambda_1^{a,0} - 2/3\,\lambda_1^{a,2} - 8/5\,\lambda_1^{a,4} + 7\,\lambda_2^{a,4} - 1/3\,\lambda^{\delta,4}$$

$$F = \lambda_1^{a,0} + 2/3\,\lambda_1^{a,2} + 8/5\,\lambda_1^{a,4} - 1/3\,\lambda^{\delta,4}$$

$$G = \lambda_2^{a,0} - 1/3\,\lambda_2^{a,2} - 7/80\,\lambda_2^{a,4}$$

$$H = 2\,\lambda^{\varepsilon,2} + 11/4\,\lambda^{\varepsilon,4} \qquad I = 11/3\,\lambda^{\varepsilon,4}$$

$$J = \lambda_1^{a,0} + 2/3\,\lambda_1^{a,2} + 29/16\,\lambda_1^{a,4} + 1/3\,\lambda^{\delta,4}$$

$$K = \lambda_2^{a,0} + 2/3\,\lambda_2^{a,2} + 73/80\,\lambda_2^{a,4}$$

.....(3.33)

3.6.3 Determination of Magnetostriction Constants

The formula of Clark et al Eq. (3.25) will be used in this discussion. This equation can be reduced by choosing a certain plane and direction of measurements.

(i) If the direction of measurements is the b-axis in the ab plane, we can substitute α's and β's as follows,

$$\alpha_x = \sin\theta \qquad \beta_x = 0$$

$$\alpha_y = \cos\theta \qquad \beta_y = 1$$

$$\alpha_z = 0 \qquad \beta_z = 0$$

.....(3.34)

The strain is, $\left[\frac{\delta l}{l}\right]_b = \lambda_1^{a,0} - 1/3\ \lambda_1^{a,2} + 1/2\ \lambda^{\gamma,2} \cos 2\theta$

.....(3.35)

The reference state when $\theta = 0$ is,

$$\left[\frac{\delta l}{l}\right]_b^{\theta=0} = \lambda_1^{a,0} - 1/3\ \lambda_1^{a,2} + 1/2\ \lambda^{\gamma,2}$$

.....(3.36)

And the b-axis strain between this reference state and any other state where the magnetic moment makes an angle ψ with the b-axis may be written as,

$$\left[\frac{\delta l}{l}\right]_b^{\theta=\psi} - \left[\frac{\delta l}{l}\right]_b^{\theta=0} = 1/2\ \lambda^{\gamma,2} (\cos 2\psi - 1)$$

.....(3.37)

or

$$\left[\frac{\delta l}{l}\right]_b^{\theta=90} - \left[\frac{\delta l}{l}\right]_b^{\theta=0} = -\ \lambda^{\gamma,2}$$

.....(3.38)

(ii) The strain along the b-axis for the bc plane can be calculated if we substitute as follows,

$$\alpha_x = 0 \qquad \beta_x = 0$$

$$\alpha_y = \cos\theta \qquad \beta_y = 1$$

$$\alpha_z = \sin\theta \qquad \beta_z = 0$$

.....(3.39)

And the strain is,

$$\left[\frac{\delta l}{l}\right]_b = \lambda_1^{a,0} + 1/6\ \lambda_1^{a,2} + 1/4\ \lambda^{\gamma,2} + (1/4\ \lambda^{\gamma,2} - 1/2\ \lambda_1^{a,2}) \cos 2\theta$$

.....(3.40)

Thus

$$\left[\frac{\delta l}{l}\right]_b^{\theta=\psi} - \left[\frac{\delta l}{l}\right]_b^{\theta=0} = (1/4\ \lambda^{\gamma,2} - 1/2\ \lambda_1^{a,2}) (\cos 2\psi - 1)$$

.....(3.41)

and

$$\left[\frac{\delta l}{l}\right]_b^{\theta=90} - \left[\frac{\delta l}{l}\right]_b^{\theta=0} = -\ (1/2\ \lambda^{\gamma,2} - \lambda_1^{a,2})$$

.....(3.42)

(iii) And if the strain measurements are along the c-axis in the bc plane we find that,

$$\alpha_x = 0 \qquad \beta_x = 0$$
$$\alpha_y = \sin\theta \qquad \beta_y = 0$$
$$\alpha_z = \cos\theta \qquad \beta_z = 1$$

.....(3.43)

and the strain is,

$$\left[\frac{\delta l}{l}\right]_c = \lambda_2^{a,0} + 1/6\ \lambda_2^{a,2} + 1/2\ \lambda_2^{a,2} \cos 2\theta$$

.....(3.44)

Thus

$$\left[\frac{\delta l}{l}\right]_c^{\theta=\psi} - \left[\frac{\delta l}{l}\right]_c^{\theta=0} = 1/2\ \lambda_2^{a,2} (\cos 2\psi - 1)$$

.....(3.45)

and if $\psi = 90^\circ$ we find:

$$\left[\frac{\delta l}{l}\right]_c^{\theta=90} - \left[\frac{\delta l}{l}\right]_c^{\theta=0} = -\ \lambda_2^{a,2}$$

.....(3.46)

(iv) Finally to calculate $\lambda^{\varepsilon,2}$ we have to measure the strain along a direction of 45° from the c-axis, this means that,

$$\alpha_x = 0 \qquad \beta_x = 0$$
$$\alpha_y = \sin\theta \qquad \beta_y = 1/\sqrt{2}$$
$$\alpha_z = \cos\theta \qquad \beta_z = 1/\sqrt{2}$$

.....(3.47)

And the strain along this direction is given by,

$$\left[\frac{\delta l}{l}\right]_{45^\circ}^{\theta} = 1/2\ (\lambda_1^{a,0} + \lambda_2^{a,0}) + 1/12\ (\lambda_1^{a,2} + \lambda_2^{a,2}) + 1/8\ \lambda^{\gamma,2}$$
$$+ [\ 1/4\ (\lambda_1^{a,2} + \lambda_2^{a,2}) - 1/8\ \lambda^{\gamma,2}\ ] \cos 2\theta + 1/2\ \lambda^{\varepsilon,2} \sin 2\theta$$

.....(3.48)

And,

$$\left[\frac{\delta l}{l}\right]_{45^o}^{\theta=\psi} - \left[\frac{\delta l}{l}\right]_{45^o}^{\theta=0} = \left[\, 1/4\, (\, \lambda_1^{\alpha,2} + \lambda_2^{\alpha,2}\,) - 1/8\, \lambda^{\gamma,2}\,\right] (\cos 2\psi - 1) + 1/2\, \lambda^{\varepsilon,2} \sin 2\psi$$

.....(3.49)

Thus, if we take ψ to be 45^o we find:

$$\left[\frac{\delta l}{l}\right]_{45^o}^{\theta=45^o} - \left[\frac{\delta l}{l}\right]_{45^o}^{\theta=0} = 1/8\, \lambda^{\gamma,2} - 1/4\, \lambda_1^{\alpha,2} - 1/4\, \lambda_2^{\alpha,2} + 1/2\, \lambda^{\varepsilon,2}$$

.....(3.50)

3.6.4 Magnetoelastic Coefficients of Gadolinium

The experimental procedure for determination of the magnetostriction constants will be discussed in Chapter 5. In this section we will give an account of previous measurements on single crystals. The thermal and field dependence of magnetostriction have been studied on heavy rare earths in particular Gadolinium by many people. Gadolinium has a small magnetostriction compared to the other heavy rare earths. The first data for magnetostriction on single crystals of gadolinium were obtained by Bozorth and Wakiyama, (1963), who used strain gauge techniques to measure the magnetostriction λ and the thermal expansion α from 4.2 K to the Curie point. They used a simplified expression for the magnetostriction $\frac{\delta l}{l}$ with only four independent constants λ_A, λ_B, λ_C and λ_D. This formula has been given by Bozorth, (1954), as,

$$\frac{\Delta l}{l} = \lambda_A \left[\, (\alpha_x \beta_x + \alpha_y \beta_y)^2 - \alpha_z \beta_z\, (\alpha_x \beta_x + \alpha_y \beta_y)\right] + \lambda_B \left[\, (1 - \alpha_z^2)(1 - \beta_z^2) - (\alpha_x \beta_x + \alpha_y \beta_y)^2\,\right] + \lambda_C \left[\, (1 - \alpha_z^2)\, \beta_z^2 - \alpha_z \beta_z\, (\alpha_x \beta_x + \alpha_y \beta_y)\,\right] + 4\, \lambda_D\, \alpha_z \beta_z\, (\alpha_x \beta_x + \alpha_y \beta_y)$$

.....(3.51)

The relation between these four magnetostriction constants λ_A, λ_B, λ_C and λ_D and the six constants in formula of Clark et al Eq. (3.25), has

been given by Rhyne, (1972), as,

$$\lambda^{\gamma,2} = \lambda_A - \lambda_B$$

$$\lambda_1^{a,2} = -1/2\ (\ \lambda_A + \lambda_B\ ) \qquad \lambda_2^{a,2} = -\lambda_C$$

$$\lambda^{\varepsilon,2} = 2\ \lambda_D - 1/2\ (\ \lambda_A + \lambda_C\ )$$

.....(3.52)

Alstad and Legvold, (1964) have obtained similar values of magnetostriction coefficients for Gadolinium using also strain gauge techniques. Fig. (3.3) shows the four $l = 2$ magnetostriction constants of Gadolinium as a function of temperature between 4.2 and 340 K' after Alstad and Legvold, (1964). Coleman and Pavlovic, (1965) have measured the temperature dependence of the magnetostriction constants at various fields above 77 K and also have measured precisely the forced magnetostriction near the Curie temperature. To represent the magnetostriction Coleman and Pavlovic have used a formula which has been given by Birss, (1959) as,

$$\lambda = R_o + R_1 \beta_z^2 + (R_2 + R_3 \beta_z^2)\ (1 - \alpha_z^2) + [\ R_4 \alpha_z \beta_z + R_5\ (\alpha_x \beta_x + \alpha_y \beta_y)\ ]\ (\alpha_x \beta_x + \alpha_y \beta_y)$$

.....(3.53)

The terms R_o and R_1 are the exchange magnetostriction constants which are independent of the direction of magnetization and depend only on the magnitude of the magnetization. R_2 to R_5 are the anistropic magnetostriction constants which depend on the direction as well as the magnitude of the magnetization; these four constants can be related to Eq. (3.51), Coleman and Pavlovic, (1965), as follows,

$$R_5 = \lambda_A - \lambda_B \qquad R_3 = \lambda_C - \lambda_B$$

$$R_4 = 4\ \lambda_D - \lambda_C - \lambda_A \qquad R_2 = \lambda_B$$

.....(3.54)

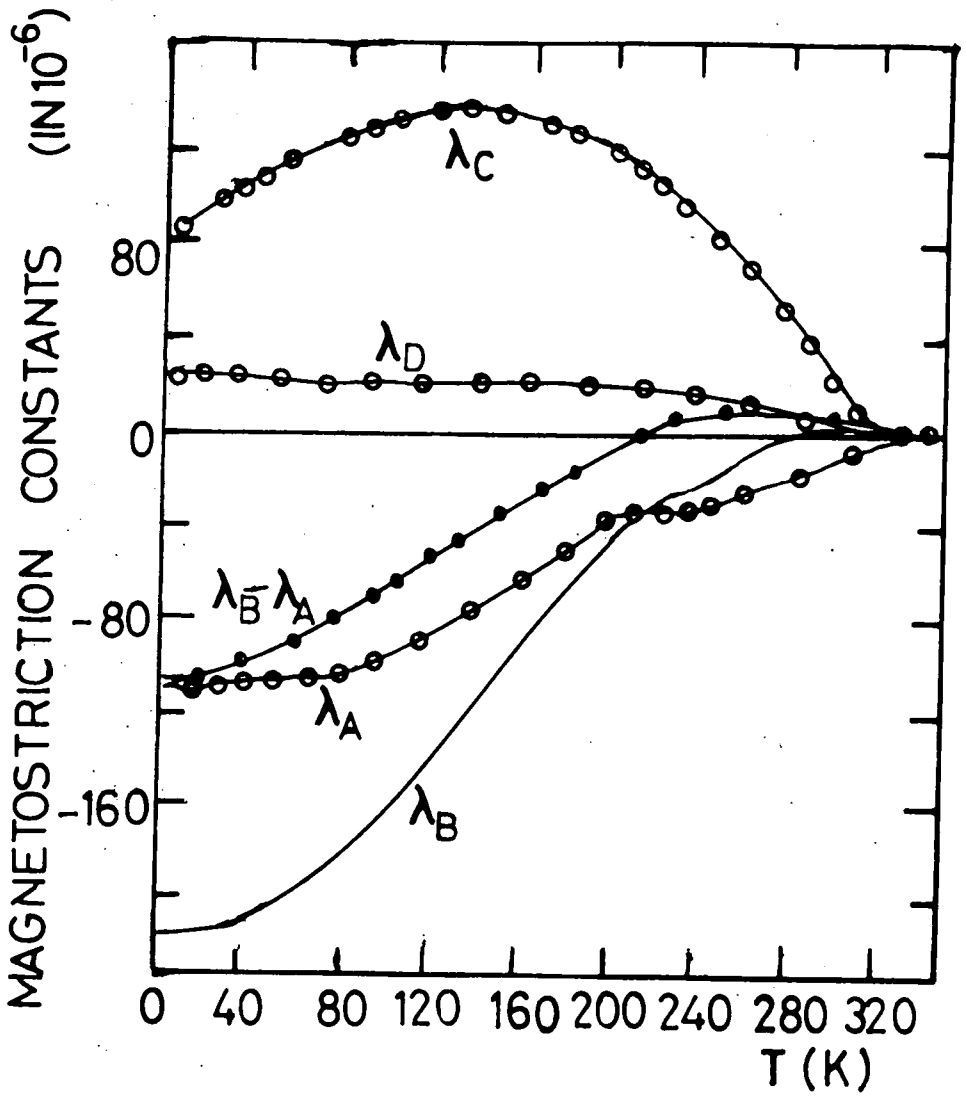

FIG. 3.3 THE MAGNETOSTRICTION CONSTANTS OF Gd DEFINED BY Eq.(3.51) AS A FUNCTION OF TEMPERATURE, AFTER ALSTAD AND LEGVOLD 1964

Coleman and Pavlovic have shown that the forced exchange magnetostriction is field dependent having a peak between 220 K and 320 K. The constants in Eq. (3.53), are an admixture of those of order $l = 2$ and $l = 4$. Consequently the coefficient R_5 can be associated with the Callen and Callen coefficient λ^{γ} or that designated by Clark et al $\lambda^{\gamma,2}$ i.e. $R_5 = \lambda^{\gamma}$

Callen and Callen, (1965), have accounted for the full temperature dependence of λ^{γ} or R_5 using the data of Coleman, (1964). This is shown in Fig. (3.4) and it is clear from the figure that the coefficient changes sign before vanishing at the Curie temperature. The change in sign was theoretically explained by Callen and Callen (1965) as the results of the contribution of both the one-ion magnetoelastic coupling and the two-ion one.

$$\lambda^{\gamma} = 351 \times 10^{-5} \hat{I}_{5/2}(x) - 243 \times 10^{-6} m^2(T,H), \qquad \ldots\ldots\ldots(3.55)$$

Where $\hat{I}_{5/2}(x)$ is a higher order reduced byperbolic Bessel function. The temperature dependence of the lattice parameters for Gadolinium has been studied by Darnell, (1963). The c-axis was found to increase with decreasing temperature below the Curie point.

Mishima et al, (1976) have measured the saturation magnetostriction of Gadolinium between 4.2 K and 330 K. To fit the experimental results they have to go up to 8-th order terms in the formula of Clark et al. They have obtained a value of $\lambda^{\gamma,2}$ equal to 108×10^{-6} at 4.2 K. The magnetostriction constants from $\lambda_1^{a,2}$ to $\lambda_2^{a,8}$ at 4.2 K are as follows,

$$\lambda_1^{a,2} = 145 \times 10^{-6} \qquad \lambda_1^{a,4} = -13 \times 10^{-6}$$
$$\lambda_1^{a,6} = 6.6 \times 10^{-6} \qquad \lambda_1^{a,8} = -2.4 \times 10^{-6}$$

In the ac plane an anomalous saturation was observed along the c and a axes. Below 77 K they observed minima around $\theta = 75^{\circ}$ and 105° in

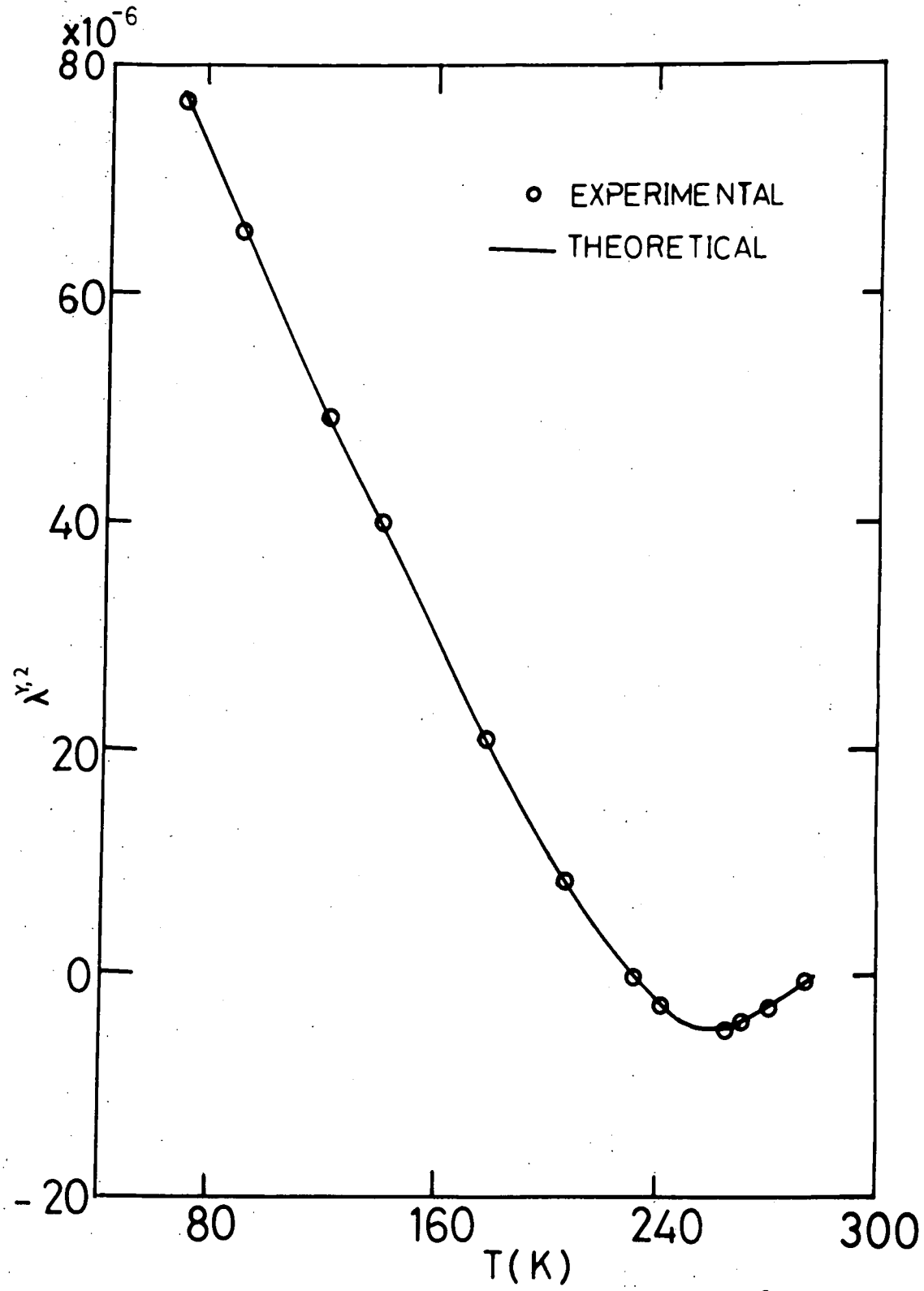

FIG. 3.4 TEMPERATURE DEPENDENCE OF $\lambda'^{,2}$ OF Gd. EXPERIMENTAL DATA FROM COLEMAN 1964 THEORETICAL CURVE CALCULATED BY Eq.(3.55), AFTER CALLEN AND CALLEN 1965.

the saturation magnetostriction versus field direction curve. These inflection points decrease with increasing temperature and disappear completely at 77 K .

The magnetostriction constants $\lambda_2^{a,2}$ to $\lambda_2^{a,8}$ at 4.2 K are given as,

$$\lambda_2^{a,2} = -125 \times 10^{-6} \qquad \lambda_2^{a,4} = -14.3 \times 10^{-6}$$

$$\lambda_2^{a,6} = 7.8 \times 10^{-6} \qquad \lambda_2^{a,8} = -3.9 \times 10^{-6}$$

They have also measured the magnetostriction constants $\lambda^{\varepsilon,2}$ and $\lambda^{\varepsilon,4}$ as 22.1×10^{-6} and 3.6×10^{-6} respectively. Fig. (3.5) shows the temperature dependence of the second order magnetostriction constants $\lambda_1^{a,2}$, $\lambda_2^{a,2}$ $\lambda^{\gamma,2}$ and $\lambda^{\varepsilon,2}$. $\lambda^{\gamma,2}$ shows a good agreement with the measurements of Bozorth and Wakiyama, (1963) and Alstad and Legvold, (1965), the values of the higher order magnetostriction constants are about 10 times smaller than the second order constants.

The forced magnetostriction of Gadolinium is independent of the field direction, but depends on the field strength. Bozorth and Wakiyama, (1963) and Coleman and Pavlovic, (1965) have measured the forced magnetostriction of Gadolinium single crystals. It was found that the forced magnetostriction coefficient $\lambda_{\parallel}$, measured parallel to the hexagonal axis is in absolute magnitude about 20 times larger than $\lambda_{\perp}$, which is measured perpendicular to the hexagonal axis. Both $\lambda_{\parallel}$ and $\lambda_{\perp}$ depend strongly on temperature, and present extremum near the Curie point while tending to zero at low and high temperatures. Tonegawa, (1964) has calculated a theoretical forced magnetostriction for Gadolinium single crystals. His calculations were based on Yosida and Watabe's theory (1962), in which they have shown that the exchange interaction between 4f spins in rare earth metals is mainly due to indirect exchange interation via the conduction electrons. The forced magnetostriction of Gadolinium has been obtained by calculating the strain dependence of this indirect exchange interaction. The theoretical

Fig (3.5)

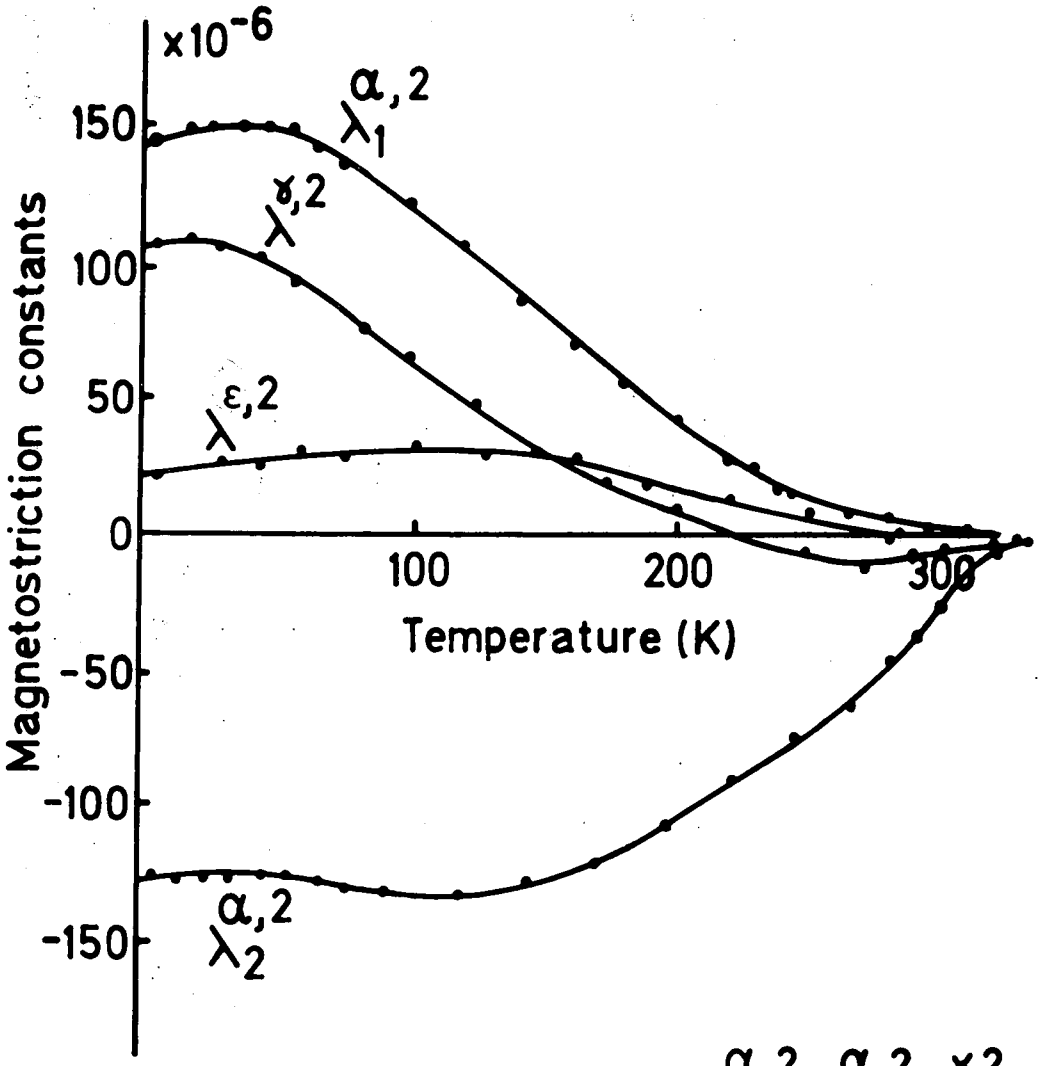

Magnetostriction constants, $\lambda_1^{\alpha,2}$, $\lambda_2^{\alpha,2}$, $\lambda^{\gamma,2}$ and $\lambda^{\varepsilon,2}$ of Gd as functions of temperature after Mishima et al (1976)

curves are shown in Fig. (3.6) for two applied magnetic fields 11.6 kOe and 17.4 kOe, the curve also shows the data of the forced magnetostriction coefficients $\lambda_{\parallel}$ and $\lambda_{\perp}$ obtained by Bozorth and Wakiyama, (1963), Coleman and Pavlovic, (1965) have given the following empirical expression for the forced magnetostriction,

$$\lambda = A H^{n} + B \qquad \ldots\ldots\ldots(3.56),$$

where A,B, and n are functions of temperature.

Related to the forced magnetostriction is the anomalous thermal expansion which arises from the dominant contribution of the forced magnetostriction to the measured lattice parameter. Bozorth and Wakiyama, (1963) have determined the shape of the α vs. T curve for the a and c axes, which is shown in Fig. (3.7), It is clear from this figure that the thermal expansion coefficient measured along the c-axis shows a sharp dip, while that measured along the a-axis exhibits a sharp peak.

3.6.5. Magnetoelastic Coefficents of Terbium

Terbium has a large magnetostriction compared with Gadolinium. Many data are available for the magnetostriction of Terbium, but the most complete are those of Rhyne and Legvold, (1965) and those of du Plessis, (1968). The a, b and c axis lattice parameters as a function of temperature for Terbium have been obtained using x-ray methods by Darnell, (1963). Rhyne and Legvold, (1965) have measured the magnetostriction of Terbium single crystals from 4 to 350 K in applied fields up to 30 kOe by strain gauge methods. Because of the high magnetocrystalline anisotropy of Terbium magnetic fields considerably in excess of those normally available in the laboratory are necessary to produce significant rotation of the magnetic moment out of the basal plane, Rhyne and Legvold, (1965) have assumed $\alpha_z = 0$ in Eq. (3.31), i.e.

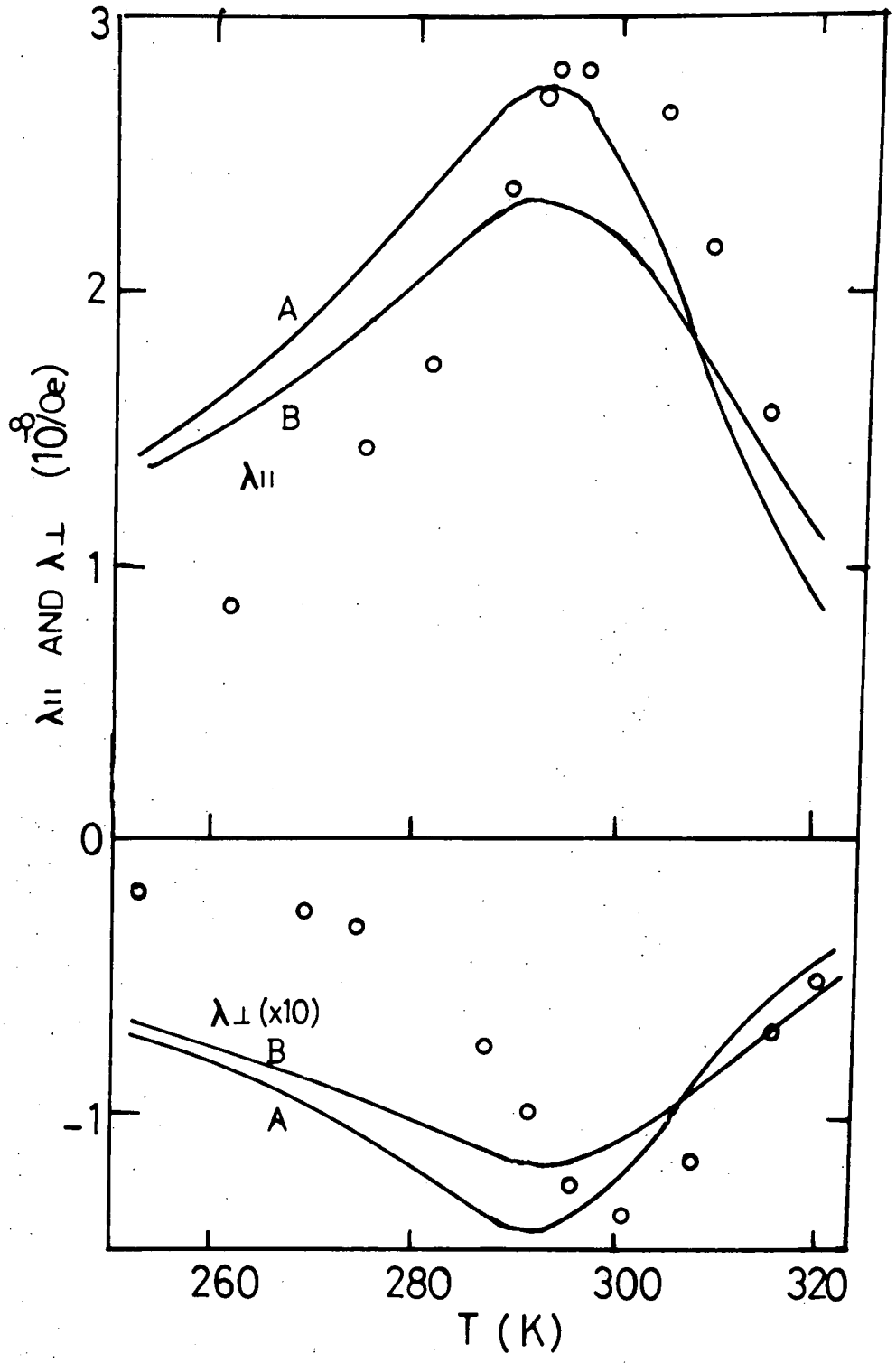

FIG. 3.6 FORCED MAGNETOSTRICTION COEFFICIENT OF Gd, $\lambda_{\parallel}$ AND $\lambda_{\perp}$ PARALLEL AND PERPENDICULAR TO THE HEXAGONAL AXIS RESPECTIVELY. CURVE A AND CURVE B CORRESPOND TO EXTERNAL MAGNETIC FIELD OF 11.6 kOe AND 17.4 kOe, AFTER TONEGAWA 1964

—— THEORETICAL

o EXPERIMENTAL BY BOZORTH AND WAKIYAMA 1963

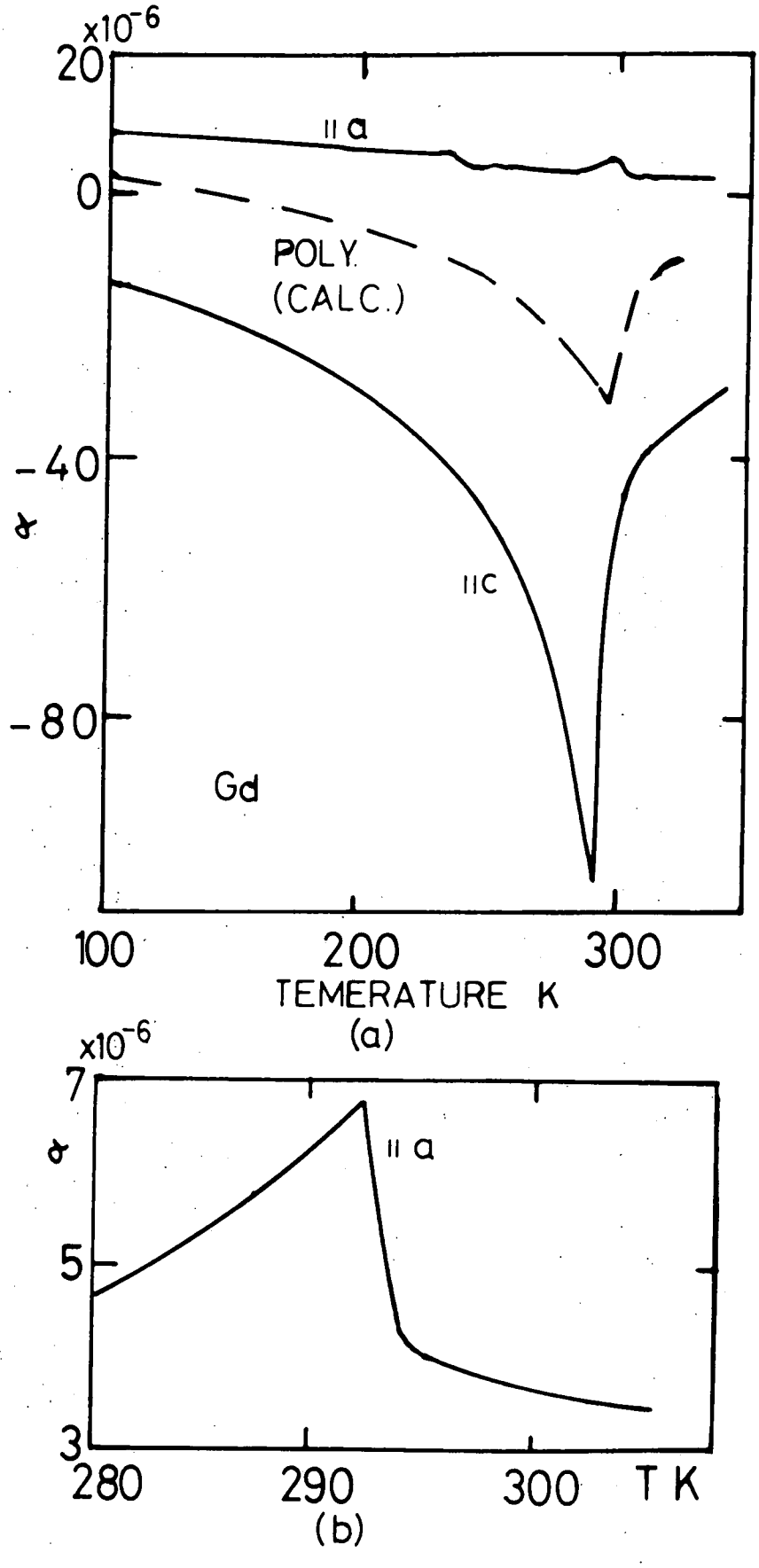

FIG. 3.7 THERMAL EXPANSION COEFFICIENTS $\alpha = (1/l)(dl/dT)$, AFTER BOZORTH AND WAKIYAMA 1963.

$$\left[\frac{\delta l}{l}\right]_{\chi_Z=0} = A\left[2\alpha_x\alpha_y\beta_x + (\alpha_x^2 - \alpha_y^2)\beta_y\right]^2$$
$$+ C\left[(\alpha_x\beta_x + \alpha_y\beta_y)^2 + (\alpha_x\beta_y + \alpha_y\beta_x)^2\right]$$
$$+ D(1-\beta_z^2) + G\beta_z^2$$

.....(3.57)

Using this equation they have measured the constants A, C, D, and G while du Plessis has used the formula of Clark et al Eq. (3.25). The constants A, C, D, and G may be determined by different measurements of the strain $\frac{\delta l}{l}$ along different directions β . The values of $\lambda^{\gamma} = 2C$ are in agreement for both Rhyne and Legvold, (1965) and du Plessis, (1968), except below 125 K . Fig. (3.8) shows the values of the two constants A, and C as measured by Rhyne and Legvold, (1965) at 30 kOe. The theoretical calculations of the temperature dependence of the constants A, and C by Callen and Callen, (1963), give

$$\frac{\delta l}{l}(T) = \frac{\delta l}{l}(0)\,\frac{I_{l+\frac{1}{2}}[\mathcal{L}^{-1}(m)]}{I_{\frac{1}{2}}[\mathcal{L}^{-1}(m)]}$$

.....(3.58),

where I is a modified Bessel function $\mathcal{L}^{-1}$ is the inverse of the Langevin function and $m_n = M(T) / M(0)$ is the reduced magnetization. The theoretical curves for C and A have been plotted also by Rhyne and Legvold using the above equation and the magnetic moment data of Hegland et al, (1963). The value of C (T = 0) used was 4.3×10^{-3} and the value of A (T = 0) was 2.14×10^{-3}. The two constants λ^{γ} and A were measured by du Plessis, (1968) between 77 K and 350 K . Fig. (3.9) shows the temperature variation of λ^{γ} , measured at an external field 16.4 kOe, also, it was shown by du Plessis that the data are very well fitted by the $\hat{I}_{5/2}[\mathcal{L}^{-1}(m)]$ over the whole temperature range while the m_n^3 law is satisfactory up to about 200 K as shown in Fig. (3.9). By extrapolation to the value at 0 K , this gives a value of $\lambda^{\gamma} = 8.5 \times 10^{-3}$.

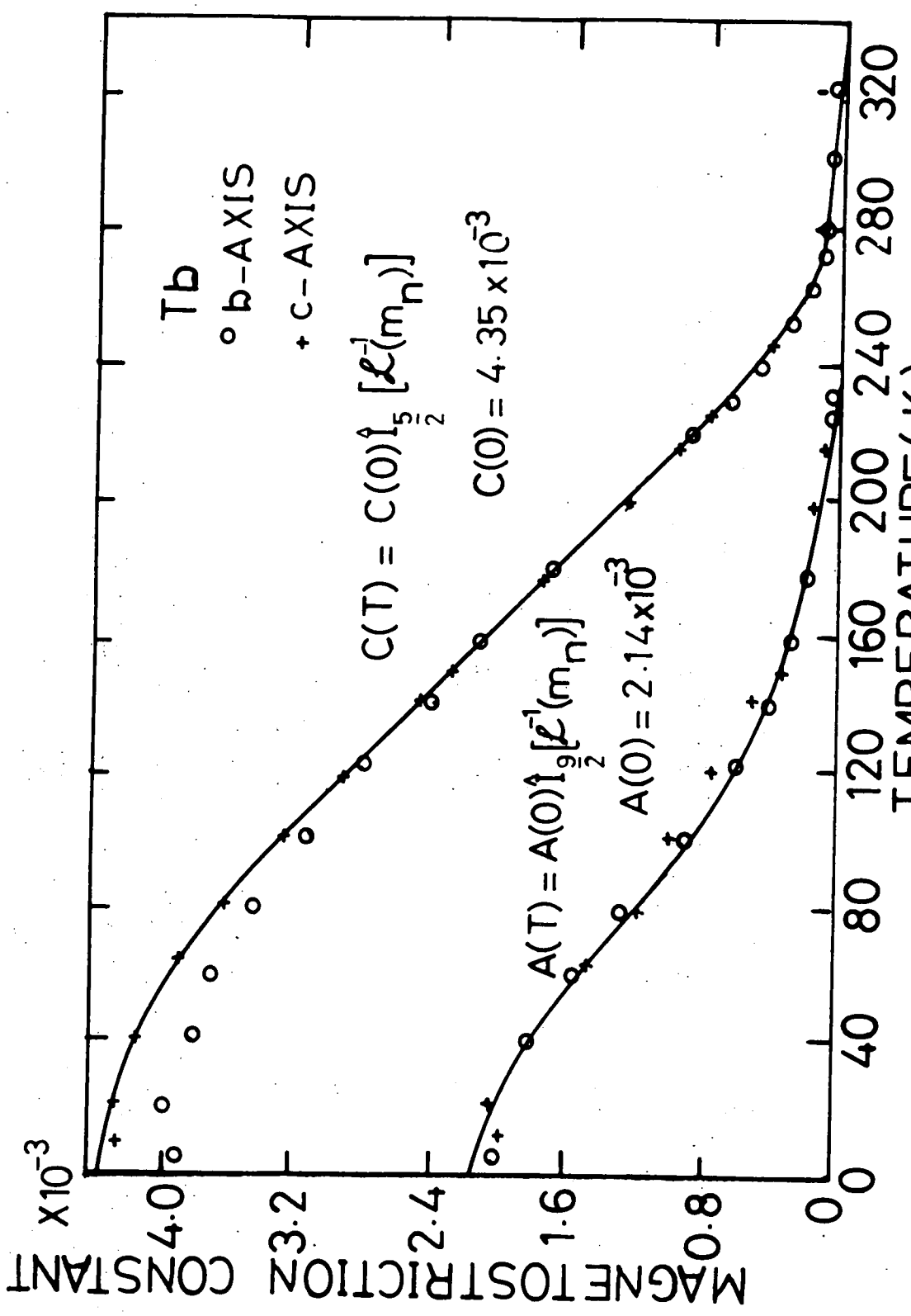

FIG. 3.8 MAGNETOSTRICTION CONSTANTS A AND C AT 30 kOe, AFTER RHYNE AND LEGVOLD 1965.

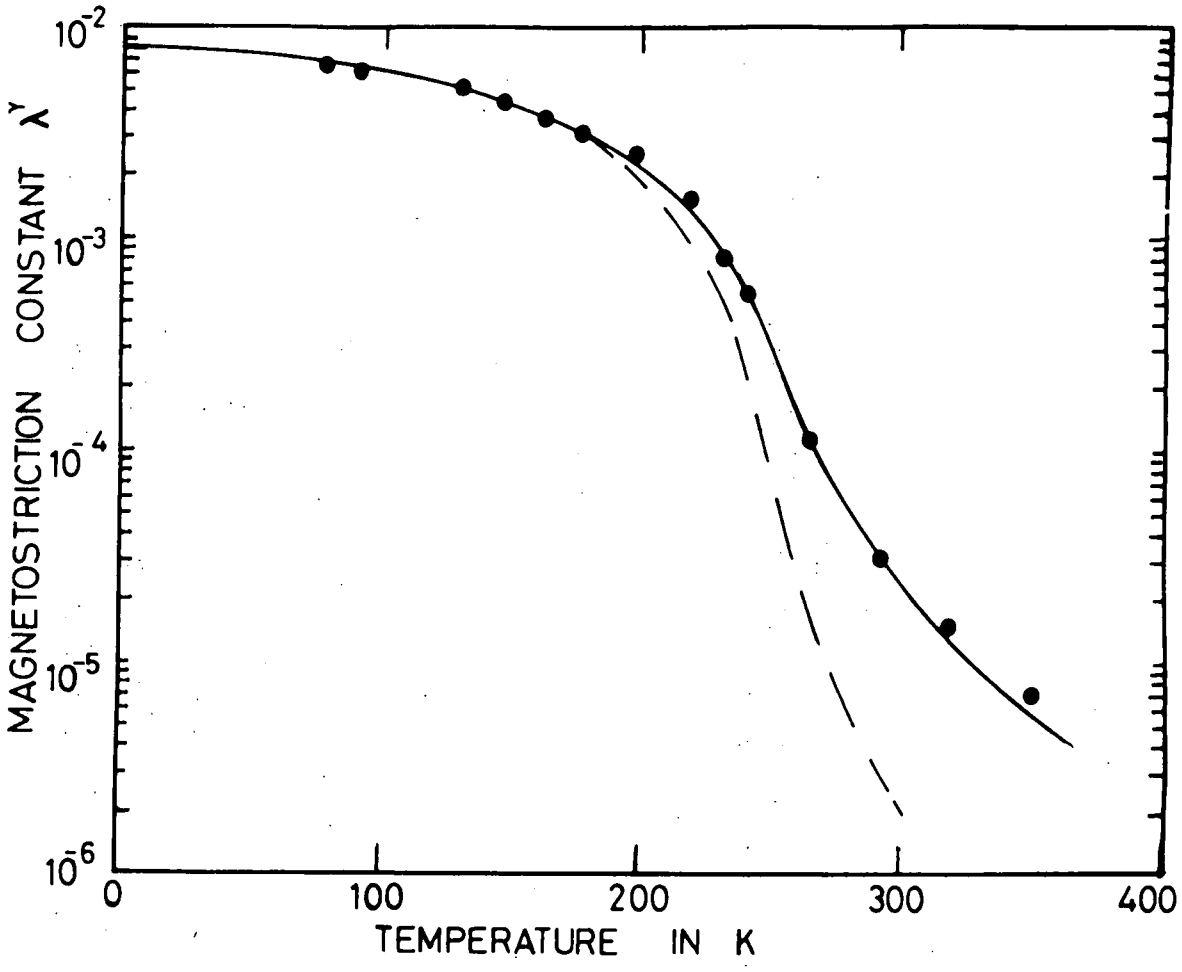

Fig. (3.9) The temperature variation of λ^γ measured at an external field of 16.4 kOe for Tb.
The solid line is given by $\lambda^\gamma(0)\hat{I}_{5/2}\left[\mathcal{L}^{-1}(m_n)\right]$,
where $\lambda^\gamma(0) = 8500 \times 10^{-6}$ The broken line is given by the lower temperature limit $\lambda^\gamma(0)m_n^3$, after du Plessis (1968)

The second order coefficient has been determined by du Plessis, (1968), and he has found that this coefficient follows a $\hat{I}_{9/2}$ law with a normalization value of A (0) = 2.5×10^{-3}. The coefficients A, C, D, and G have been extrapolated to zero applied field by Rhyne and Legvold, (1965) and yield values for D, and G of $D_o = -1.6 \times 10^{-3}$ and, $G_o = 4 \times 10^{-3}$, the extrapolated values are shown in Fig. (3.10). Du Plessis has determined the thermal dependence of $\lambda^{\varepsilon,2}$ and $\lambda_2^{a,2}$. Their variation with temperature is quite well fitted by the $\hat{I}_{5/2}[\mathcal{L}^{-1}(m)]$ function as shown in Fig. (3.11), where fairly linear curves were obtained, except for $\lambda^{\varepsilon,2}$ when the temperature is very close to the Curie temperature. The ratio $\lambda^{\varepsilon,2}/\lambda^{\gamma,2}$ is expected to be the same for the heavy rare earths, it is equal to about 0.6, but for Terbium it gives an anomalous value of 2.35, du Plessis, (1968).

Rhyne and Legvold, (1965) and du Plessis, (1968) in more detail have measured the forced magnetostriction, also measured by Alberts and du Plessis, (1968). The forced magnetostriction is the slope of the linear magnetostriction at high applied fields. Fig. (3.12) shows the forced magnetostriction in the a, b, and c directions as obtained by Rhyne and Legvold, (1965), from the slope above saturation of the strain vs. field curves in a field up to 30 kOe. As seen in this figure the forced magnetostriction presents a maximum around the Néel temperature. Du Plessis has found similar results for a and c-axis measurements for a field up to 20 kOe. The temperature dependence of the c-axis thermal expansion has been given by du Plessis, (1968). An anomaly has been observed at 225 K with a peak value -104×10^{-6} and $-65 \times 10^{-6}/K^{-1}$ at zero and 14 kOe applied field respectively, as shown in Fig. (3.13). Since the helical structure collapses at low field, the fact that the curves for both zero field and 14 kOe peak at the same temperature is evidence that this occurs at the Néel point, du Plessis, (1968).

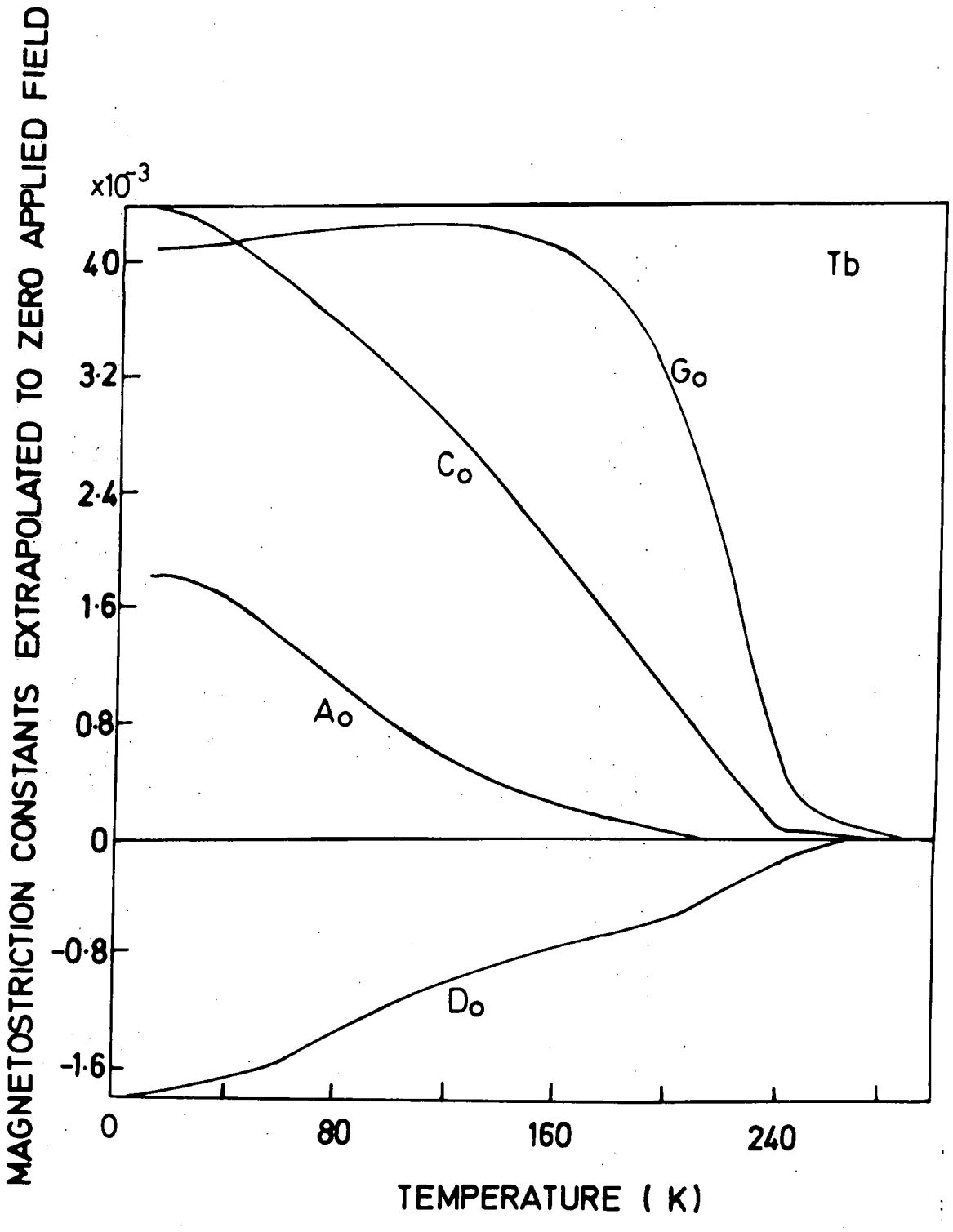

FIG.3·10 MAGNETOSTRICTION CONSTANTS A_o, C_o, D_o AND G_o. THE SUBSCRIPT o INDICATES THE VALUES HAVE BEEN EXTRAPOLATED TO ZERO APPLIED FIELD, AFTER RHYNE AND LEGVOLD 1965

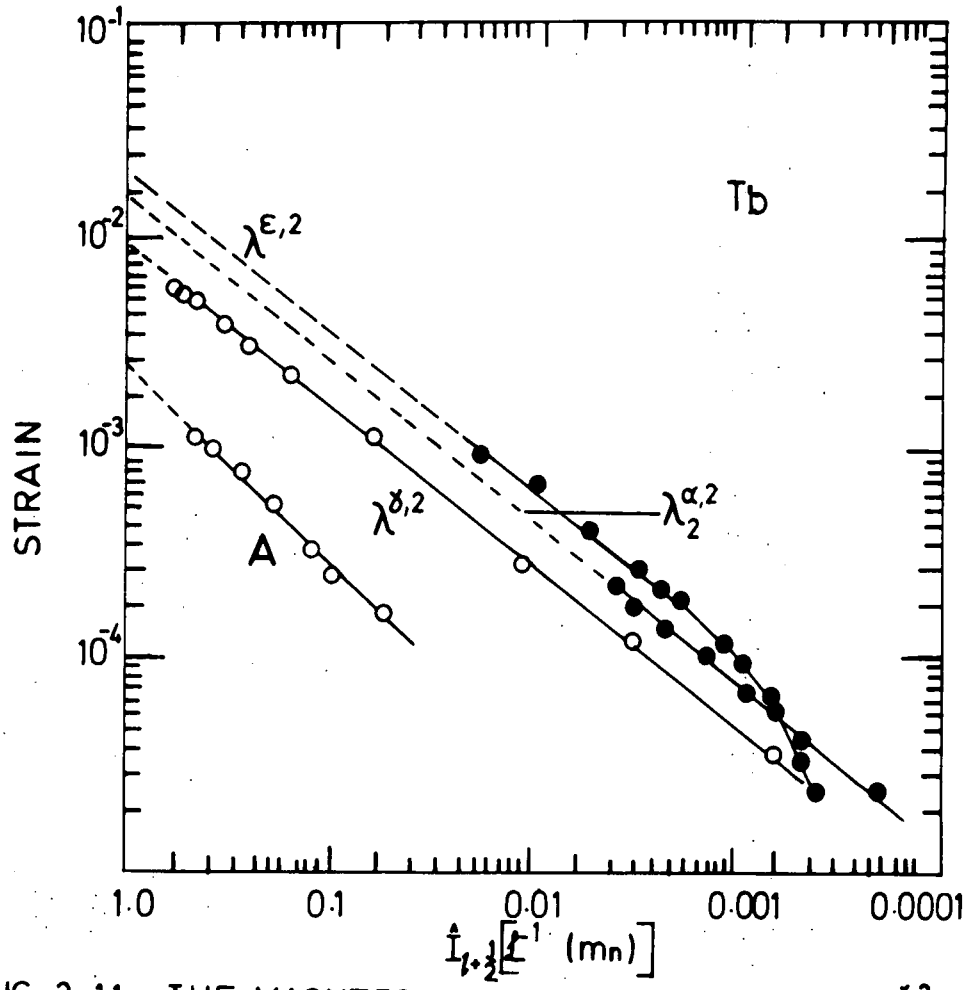

FIG. 3·11 THE MAGNETOSTRICTION COEFFICIENTS $\lambda^{\gamma,2}$, $\lambda^{\varepsilon,2}$ AND $\lambda_2^{\alpha,2}$ VERSUS $\hat{I}_{5/2}[\ell^{-1}(mn)]$ AND A VERSUS $\hat{I}_{9/2}[\ell^{-1}(mn)]$ THE MAGNETIZATION HAS BEEN VARIED BY VARYING THE TEMPERATURE IN THE FERROMAGNETIC REGION AND BY VARYING TEMPERATURE AND FIELD STRENGTH IN THE PARAMAGNETIC REGION, AFTER DU PLESSIS 1968

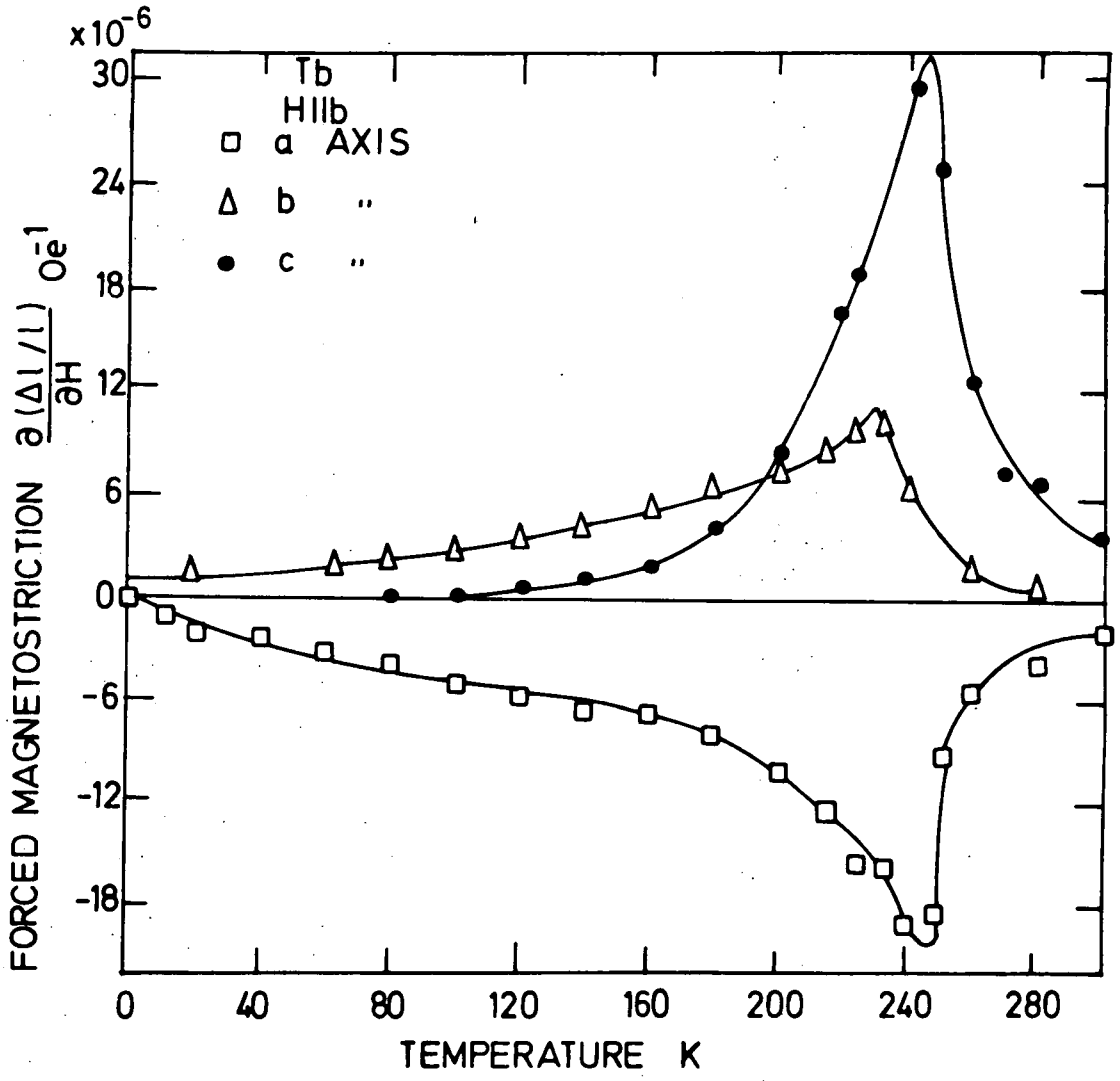

FIG 3·12 FORCED MAGNETOSTRICTION IN THE a-,b-, AND c-AXIS DIRECTIONS AFTER RHYNE AND LEGVOLD 1965.

FIG 3·13 THE TEMPERATURE DEPENDENCE OF THE ZERO FIELD C AXIS THERMAL EXPANSION COEFFICIENT IS DEPICTED WITH A SOLID LINE. THE DOTTED LINE REPRESENTS THE COEFFICIENT MEASURED AT 14 Koe AFTER DU PLESSIS 1968

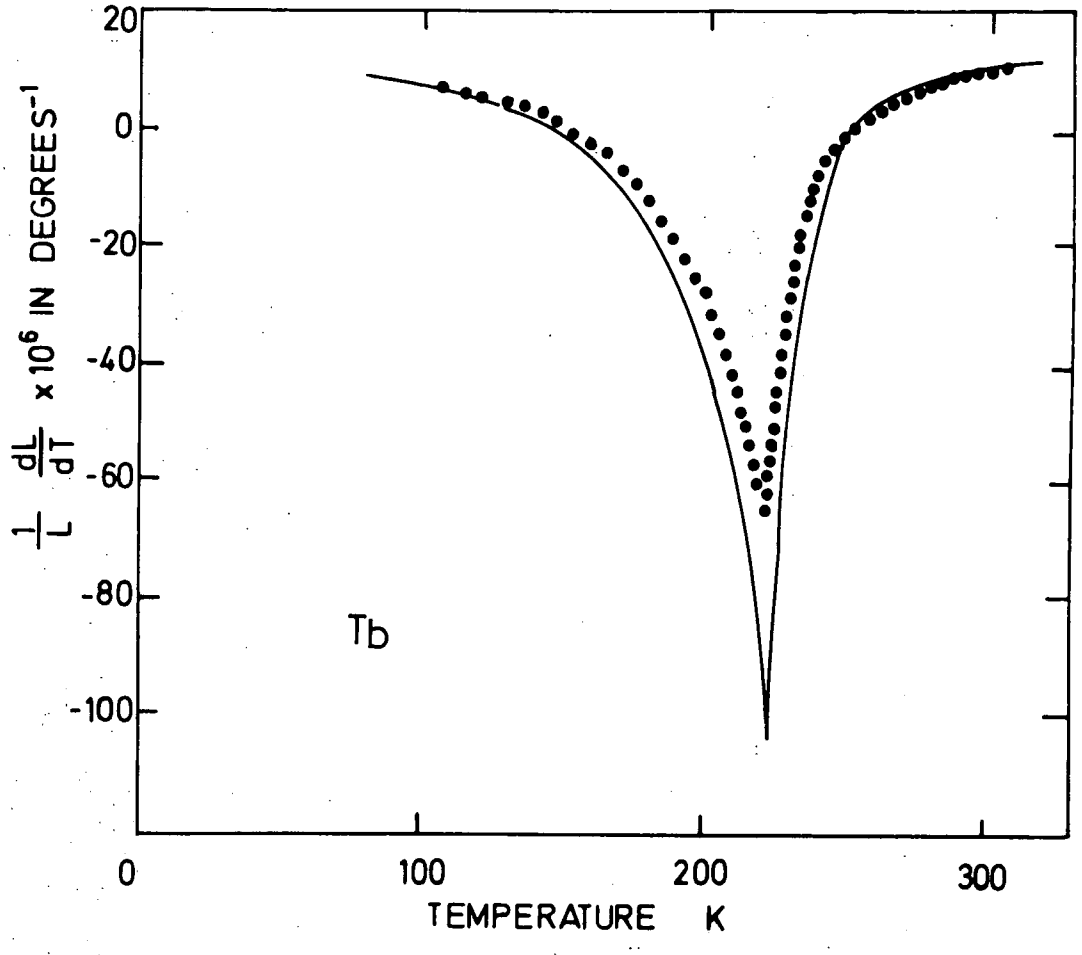

3.6.6. Elastic Constants

Due to the relatively low order symmetry of rare earths there are five independent elastic constants. For the hcp structure the classical elastic energy can be represented as follows, Coqblin, (1977),

$$E_e = 1/2\, C^a_{11}\, (\varepsilon^{a,1})^2 + C^a_{12}\, \varepsilon^{a,1}\, \varepsilon^{a,2} + 1/2\, C^a_{22}\, (\varepsilon^{a,2})^2$$

$$+ 1/2\, C^\gamma [\, (\varepsilon^\gamma_1)^2 + (\varepsilon^\gamma_2)^2\,] + 1/2\, C^\varepsilon [\, (\varepsilon^\varepsilon_1)^2 + (\varepsilon^\varepsilon_2)^2\,]$$

.....(3.59)

The strain $\varepsilon^{\mu,j}_i$ are related to the usual strain defined with respect to Cartesian axes, x, y, z, as follows,

$$\varepsilon^{a,1} = \varepsilon_{xx} + \varepsilon_{yy} + \varepsilon_{zz}$$

$$\varepsilon^{a,2} = 1/2\sqrt{3}\, [\, 2\, \varepsilon_{zz} - \varepsilon_{xx} - \varepsilon_{yy}\,]$$

$$\varepsilon^\gamma_1 = 1/2\, (\, \varepsilon_{xx} - \varepsilon_{yy})$$

$$\varepsilon^\gamma_2 = \varepsilon_{xy}$$

$$\varepsilon^\varepsilon_1 = \varepsilon_{yz}$$

$$\varepsilon^\varepsilon_2 = \varepsilon_{xz}$$

.....(3.60)

The elastic stiffness constants C^μ_{ik} are related to the five independent Cartesian stiffness constants by the following relations.

$$C^a_{11} = 1/9\, (2\, C_{11} + 2\, C_{12} + 4\, C_{13} + C_{33})$$

$$C^a_{22} = 2/3\, (\, C_{11} + C_{12} - 4\, C_{13} + 2\, C_{33})$$

$$C^a_{12} = 2/3\sqrt{3}\, (-\, C_{11} - C_{12} + C_{13} + C_{33})$$

$$C^\gamma = 2\, (C_{11} - C_{12}) = 4\, C_{66}$$

$$C^\varepsilon = 4\, C_{44}$$

.....(3.61)

The five independent elastic constants C_{11}, C_{12}, C_{13}, C_{33}, and C_{44}, can be measured by propagating longitudinal and shear waves in directions parallel, perpendicular and at angle 45° to the c-axis, Palmer and Lee, (1972). The five single crystal elastic constants of Gadolinium

and Terbium have measured by Palmer et al, (1974), within the temperature range 4.2 to 300 K. In Gadolinium there is a very pronounced change in the c-axis compressional mode constant C_{33} at the magnetic ordering temperature. In Gadolinium also the elastic constants are hardly affected by a magnetic field, with the exception of C_{33} where a large ΔC effect is observed at about 220 K at which the magnetization just begins to deviate from the c-axis. This is in reasonable aggreement with the magnetocrystalline anisotropy results from which the temperature was found to be at 240 K, Corner, et al (1962), Smith et al (1978). In Terbium also it was found by Palmer et al (1974) that there is an anomaly in C_{33} at T_C. Pollina and Luthi, (1968, 1969) have measured the attenuation of sound in Gadolinium and Terbium, a sharp peak in longitudinal attenuation being observed at T_C. In Terbium two transition points have been at T_N and T_C. To explain their results Pollina and Luthi, have adopted a two spin-phonon coupling mechanisms.

(1) a magnetostrictive coupling (spin orbit type magnetostriction), and

(2) a volume magnetostrictive coupling (two-ion or forced magnetostriction).

Finally, it is found that the thermal dependence of the elastic constants of Gadolinium and Terbium, is relatively weak and becomes significant only in the vicinity of the transition temperatures.

CHAPTER 4

Magnetic Properties of Alloys of Gd and Tb

4.1 Introduction

We can prepare magnetic substances which have various kinds of magnetic properties by alloying rare earth metals with each other or with other metals. The methods of greatest use in the study of the magnetic properties of rare earth alloys fall into two groups, direct magnetization measurements and neutron diffraction methods. Both have been used to study the magnetic structure of the alloys.

From the magnetic point of view it has been found by Weinstein et al (1963) that in the Dy-Y alloys the Néel temperature T_N was proportional to the 2/3 power of the Y concentration. Then Child et al (1965) found that in the R-Y alloys where R is rare earth metal generally a 2/3 power law was obeyed. They found that T_N follows a universal law versus ξ of the form,

$$T_N = 46.7\, \xi^{2/3} \qquad \ldots\ldots\ldots(4.1),$$

where ξ is the mean value of the de Gennes factor. This is defined as

$$\xi = c\,(g-1)^2\, J(J+1) \qquad \ldots\ldots\ldots(4.2),$$

where c is the atomic concentration of the rare earth. The Néel temperatures for alloys R-R, where both constituents are heavy rare earth metals, follow the same universal law. For R-R alloys ξ is given as, Bozorth (1967),

$$\xi = c_1\, \xi_1 + c_2\, \xi_2 \qquad \ldots\ldots\ldots(4.3),$$

where c_1 and c_2 are the atomic concentrations of the two components. The Curie point behaviour variation with temperature does not appear to follow a universal law but is different for each system of R-R alloys.

Gadolinium binary alloys

Gadolinium has the highest ordering temperature T_C = 293 K of all the rare earth metals, and it is ferromagnetic at all temperatures below its Curie Point. One of the alloy series which has been extensively studied is that with Y which has the same crystal structure as Gd, nearly the same atomic volume and exhibits simple paramagnetism over all the temperature range. The first magnetization measurements were made by Thorburn et al (1958). For alloys of high Gd content paramagnetic to ferromagnetic transitions are observed with decreasing temperature. As Gd content is decreased the transition to ferromagnetic ordering is replaced by one to anti-ferromagnetic ordering, ferromagnetic ordering appearing at a lower temperature. Child and Cable (1969) have made measurements of the neutron diffraction from Gd-Y alloys and found that Gd-Y alloys are ferromagnetic above 70 at % Gd and also they found that the angle Φ between the magnetic moment and the c-axis for the ferromagnetic alloys remains constant and equal to 70^{o} at all temperatures. Ito (1973) has measured the magnetization, magnetocrystalline anisotropy, electrical resistivity, thermal expansion and magnetostriction of Gd-Y alloys. He found that the alloys show ferromagnetism at high content of Gd and antiferromagnetism at low content. The ordering temperature decreases nearly linearly with Gd content. Because the behaviour of Gd cannot be accounted by the one-ion model of Callen and Callen (1965), alone, Ito has found that the temperature dependence of the magnetocrystalline anisotropy can be greatly simplified by the addition of non-magnetic Y. The thermal expansion, the magnetostriction, and the electrical resistivity were all found to be anisotropic in both magnetic regions.

Gadolinium-heavy rare earth metal alloys have been studied by several workers. Bozorth and Suits (1964) have studied the magnetization of Gd-Dy alloys. The Gd rich alloys are ferromagnetic in the whole

temperature range in which ordering occurs, while the Dy rich alloys have a ferromagnetic structure at low temperature and a helical structure between T_N and T_C. The magnetocrystalline anisotropy of Gd-Dy alloy has measured by Tajima and Chikazumi (1967) for 1.3 wt% Dy-Gd alloys and they found that the anisotropy constants are all in agreement with those estimated from single ion model.

Magnetostriction and thermal expansion of single crystals of Gd-Dy alloys have been investigated by Nikitin et al (1976) and they have found that along the c-axis the magnetostriction is mainly due to a two-ion mechanism, while along the a-axis both two-ion interactions and the one-ion interactions must be taken into account. Bozorth and Gambino (1966) have studied the magnetization of Gd-Er, Gd-Ho, Gd-Lu and determined the values of T_N and T_C. The magnetic behaviour of the first three alloys is close enough to that of Gd-Dy alloys, while Gd-Lu alloys are also ferromagnetic for high content of Gd, but the transition from the antiferromagnetic phase to a ferromagnetic phase takes place through at least one intermediate 'fan' structure. Gd-Sc alloys are also ferromagnetic for about 70% Gd and the Curie temperature T_C and the paramagnetic Curie temperature θ_p decreases more rapidly in Gd-Sc alloys than in Gd-Y alloys, Nigh et al (1964). The Gadolinium-rich alloys are ferromagnetic at all temperatures in the range of ordering, while Gd-poor alloys have at least one region of antiferromagnetic-type ordering. The Néel temperatures follow Eq.(4.1), and the Curie temperatures decrease with decreasing Gd content.

Tb-binary alloys

One system which has been well studied is the Tb-Y alloy system. Neutron diffraction measurements have been made by Koehler et al (1963) on a series of Tb-Y alloys in order to study the influence of magnetic dilution on the magnetic properties of the rare earth metals. They found that introduction of Y into Tb reduces the Néel temperature and

produces a helical phase. At 30 at% Yttrium and above the spontaneous transformation to the ferromagnetic structure was not observed for zero applied field even for temperatures down to 4.2 K. Koehler (1965) has found that for Tb-Y and Tb-Lu alloys the Néel temperatures follow Eq. (4.1) from neutron diffraction measurements. Nikitin et al (1977a) have found from magnetization measurements that alloys with more than 35 at% Yttrium show no transformation to the ferromagnetic state for zero applied field all the way to 4.2 K.

Magnetostriction measurements have also been made by Nikitin et al (1977a) and they found that the measurements on the basal plane samples yield results which follow the single-ion theory, while the magnetostriction measured along the c-axis cannot be adequately described by the single-ion theory. Vorobev et al (1977)have found from x-ray diffraction measurements on Tb-Y alloys that dilution with Y leads to a decrease in magnetostriction.

Tb-Ho alloys have been studied by both magnetization and neutron diffraction techniques. Spedding et al (1969) have investigated the magnetic properties of this system and they found that the Néel temperature and the polycrystalline paramagnetic Curie temperature decreases almost linearly with Ho content to the pure Ho values; also they have observed that the alloying does not significantly affect the anistropy, the b direction being preferred as in the parent metals and the c direction being the hard direction in all cases. The same samples of Tb-Ho have been studied by Spedding et al (1970) using the neutron diffraction technique, and they have found that the helical structure is present between T_N and T_C in the whole concentration range.

Tb alloys with other heavy rare earth metals such as Tb-Dy, Tb-Er, Tb-Tm, and Tb-Lu have been studied by Bozorth and Gambino (1966) using the neutron diffraction technique. In all these alloys the variation of

Néel temperature is well represented by Eq. (4.1). The Tb-Sc alloys are similar to Tb-Y and Tb-Lu alloys as has been found by Child and Koehler (1966). Chatterjee (1972) has studied the magnetic properties of a series of alloys between Tb and Sc for both single and polycrystals. He found that the Néel temperatures follow a $T_N \alpha \xi^{4/3}$ dependence unlike the other systems. Also he found that the thermal dependence of the magnetostriction constants $\lambda^{\gamma,2}$ for $Tb_{0.89}Sc_{0.11}$ and $Tb_{0.825}Sc_{0.175}$ are reasonably well fitted with the single-ion theory. The anisotropy of Tb-Sc alloys follows the single ion theory as has been found by Welford (1975).

Recently Nikitin et al (1977b)have studied the concentration dependences of magnetic, magnetoelastic and electric properties of single crystals of Tb-Gd alloys, and they have found that the magnetic anisotropy and magnetostriction are due mainly to single-ion interactions. Their results for magnetostriction and thermal expansion are shown in Fig (4.1) The values of the thermal expansion coefficients at 320 K change very little in a wide range of concentration. The spontaneous magnetostriction λ_{oc} along the c-axis and λ_{ob} along b-axis were obtained by subtracting the phonon part of the thermal expansion $(\frac{\Delta l}{l})_{ph}$ (which has been obtained from the thermal expansion curves of Lu) from the experimental $(\frac{\Delta l}{l})^{\parallel}$ and $(\frac{\Delta l}{l})^{\perp}$ curves measured in a magnetic field applied along the easy magnetization axis. They found that $\lambda^{\gamma,2}$ decreases linearly with increase in concentration of Gd. The effective magnetic moment per atom μ_{eff} decreases linearly with increasing Gd content in the alloys with $\mu_{eff} = 7.9\ \mu_B$ for Gd and $\mu_{eff} = 9.6\ \mu_B$ for Tb as shown in Fig. (4.3). The paramagnetic Curie point $\theta_p^{\perp}$ (magnetization in the basal plane) and $\theta_p^{\parallel}$ (magnetization along the hexagonal axis) were found to increase monotonically with increasing Gd content, while the difference $\Delta\theta_p = \theta_p^{\perp} - \theta_p^{\parallel}$ decreases as shown in Fig. (4.2) and (4.3). The paramagnetic Curie

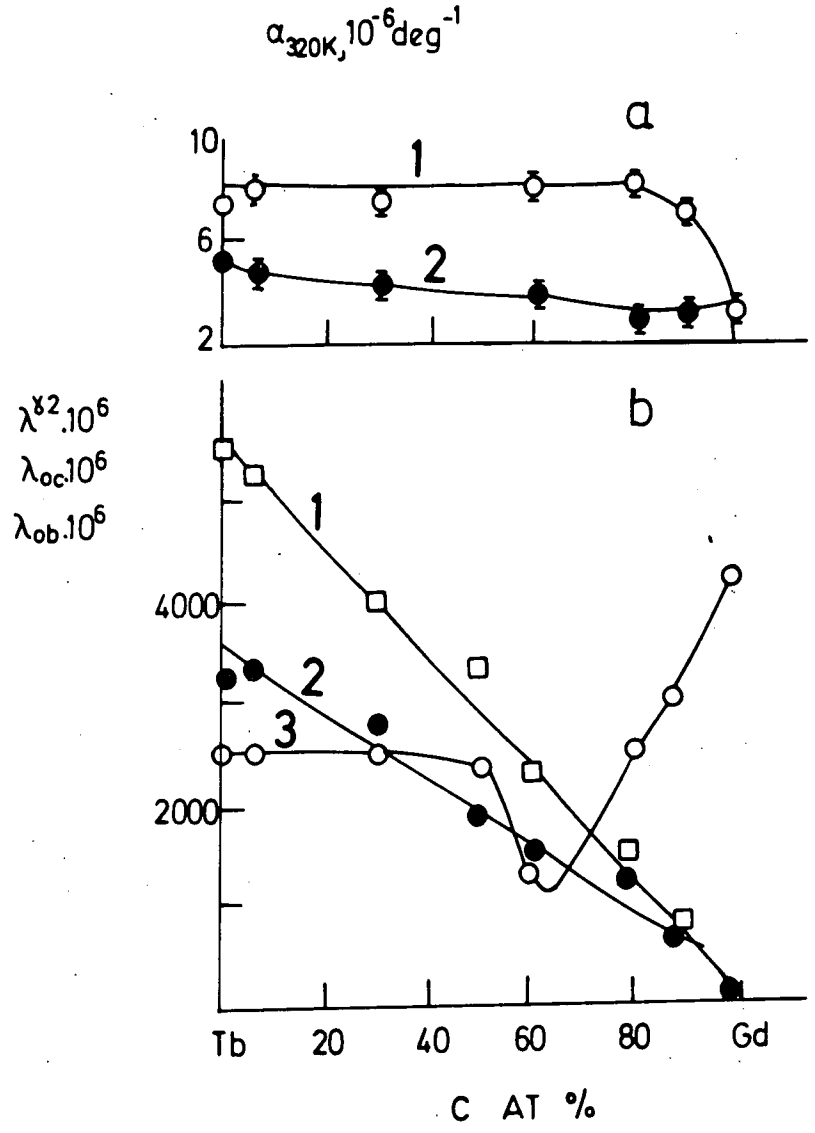

FIG 4·1 MAGNETOELASTIC PROPERTIES OF Tb–Gd ALLOY;
a) COEFFICIENT OF THERMAL EXPANSION AT 320 K ALONG THE HEXAGONAL AXIS (CURVE 1) AND IN THE BASAL PLANE (CURVE 2) b) MAGNETOSTRICTION CONSTANT $\lambda^{\gamma 2}$ (LINE 1) SPONTANEOUS STRICTION ALONG THE b – AXIS λ_{ob} (LINE 2) SPONTANEOUS STRICTION λ_{oc} ALONG C – AXIS (CURVE 3) TEMPERATURE 4·2 K AFTER NIKITIN et al 1977 b

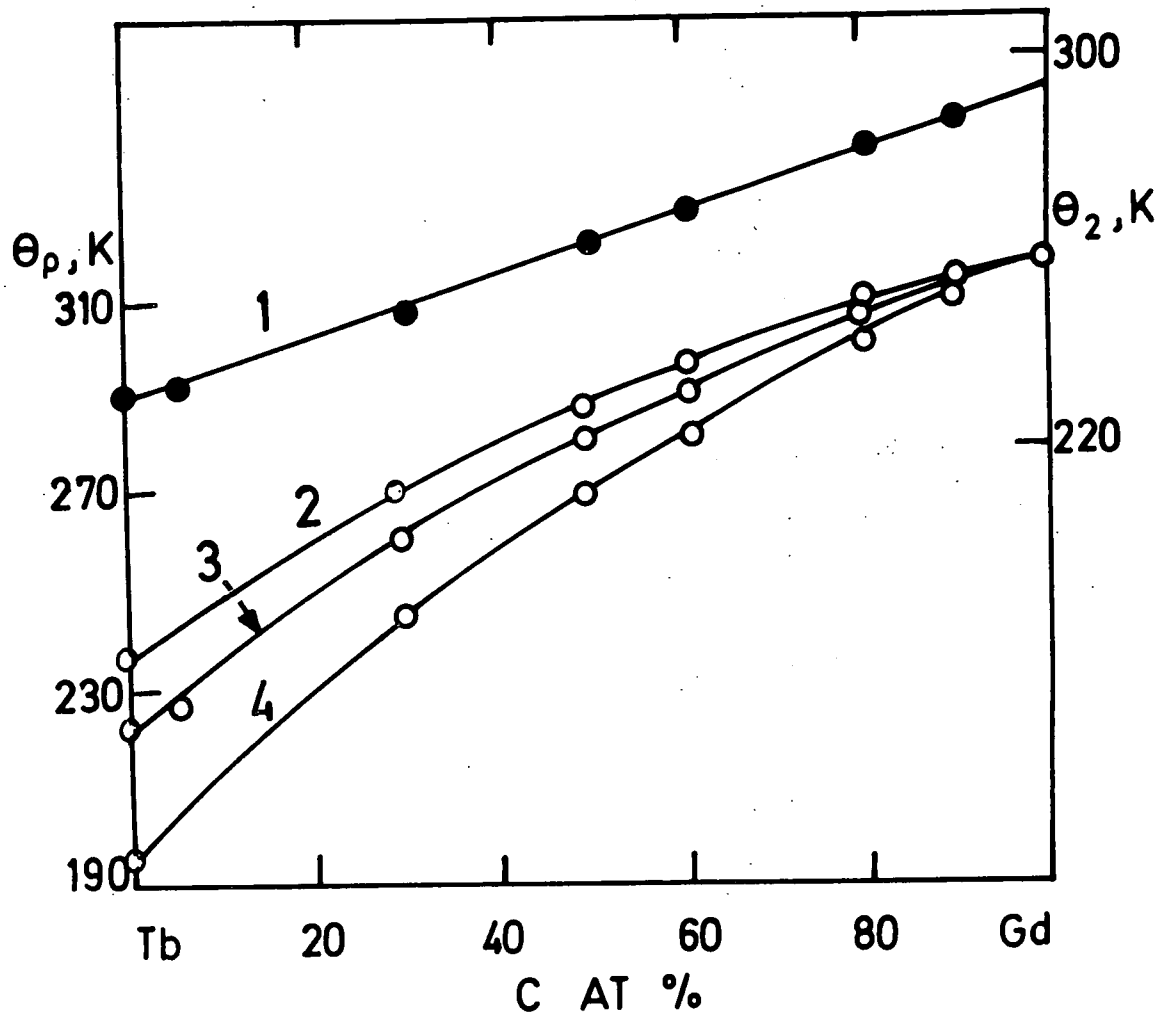

FIG. 4.2 CRITICAL TEMPERATURE OF MAGNETIC ORDERING θ_2 (1) AND PARAMAGNETIC CURIE POINTS $\theta_p^{\perp}$ (2), θ_p^{POLY} (3), $\theta_p^{\parallel}$ (4) FOR ALLOYS OF THE Tb-Gd SYSTEM, AFTER NIKITIN et al 1977b

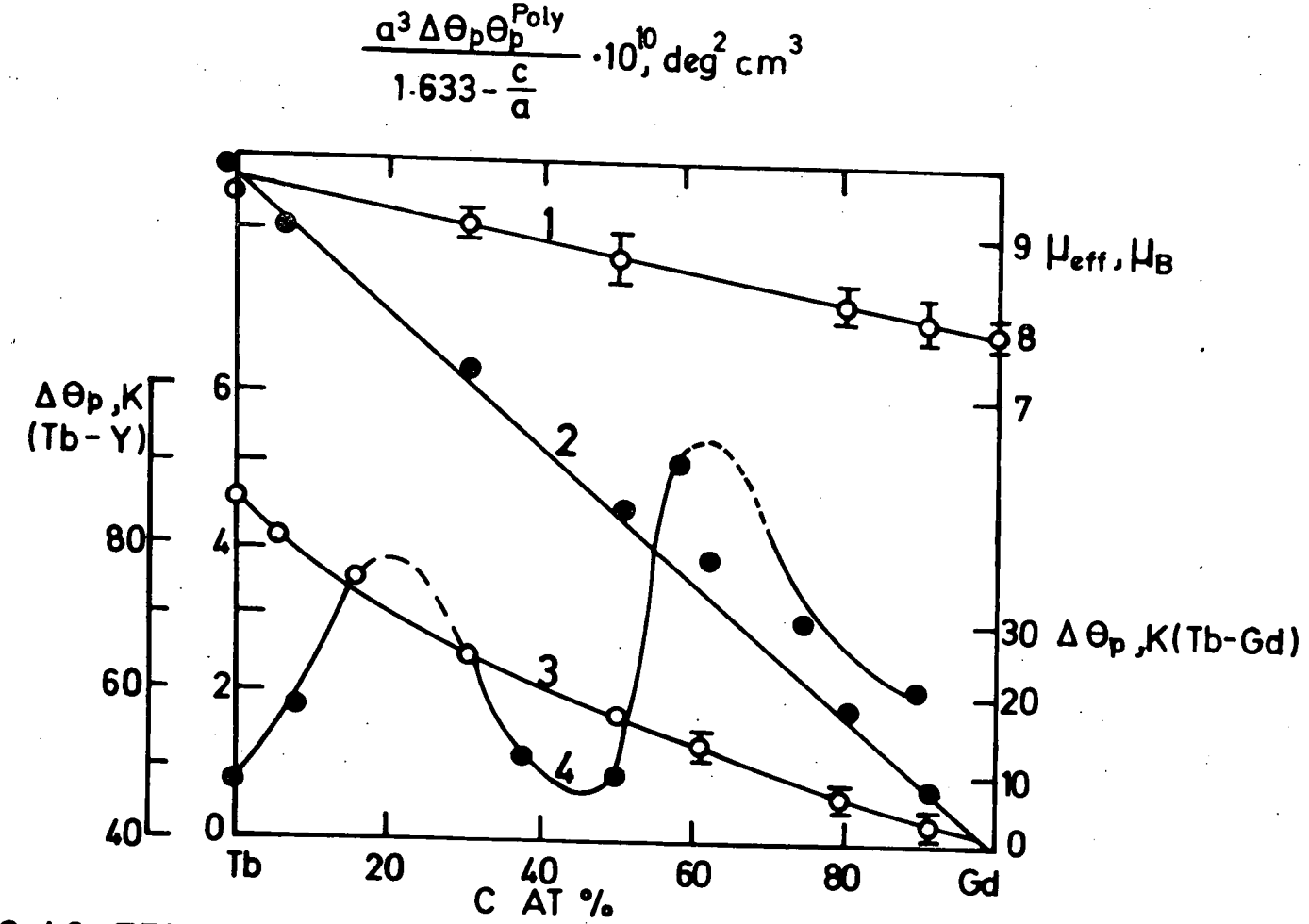

FIG. 4.3 EFFECTIVE MAGNETIC MOMENT μ_{eff} (1) AND MAGNETIC ANISOTROPY OF ALLOYS OF THE SYSTEM Tb-Gd CURVE-2 PLOT OF $a^3\Delta\Theta_p\Theta_p^{POLY}/(1.633-c/a)$; 3 ANISOTROPY OF THE MAGNETIC CURIE POINTS 4 ANISOTROPY OF THE PARAMAGNETIC CURIE POINTS IN ALLOYS OF THE Tb-Y SYSTEM AFTER NIKITIN et al 1977 b

temperature θ_p^{pol} for a polycrystal calculated from the formula $\theta_p^{pol} = \frac{1}{3}(2\theta_p^{\perp} + \theta_p^{\parallel})$ has a nonlinear dependence on the alloy composition as shown in Fig. (4.2). The uniaxial magnetic anisotropy constant K_2^o has been estimated by Nikitin et al (1977b) from the expression $K_2^o \sim a^3 \Delta\theta_p \theta_p^{\parallel}/(1.633 - c/a)$ obtained by Kasuya (1966) and they have found that K_2^o decreases linearly with increasing Gd concentration in Tb-Gd alloys.

CHAPTER 5

SPECIMENS, EXPERIMENTAL APPARATUS AND TECHNIQUES

5.1 Specimens

The specimens containing 50 and 75 per cent of Tb, were grown from the melt at the Centre for Materials Science, University of Birmingham, by melting the desired weights of Gd and Tb together. The parent metals Gd and Tb were purified using the solid state electrotransport technique. The application of this technique to the purification of rare earth metals has been discussed by Jordan (1974). The specimens containing 5 and 20 per cent of Tb were grown by Dr. D.A.Hukin at Clarendon Laboratory, Oxford, using levitated melt in Water Cooled Ag Crucible. Single crystals of Gd-Tb alloys of compositions $Gd_{0.95}\ Tb_{0.05}$, $Gd_{0.80}\ Tb_{0.20}$, $Gd_{0.50}\ Tb_{0.50}$, and $Gd_{0.25}\ Tb_{0.75}$ were cut by electrospark erosion at the Centre for Materials Science, except for the $Gd_{0.80}\ Tb_{0.20}$ samples containing b and c axes which were cut at Sunderland Polytechnic. All the ingots for single crystal cutting were oriented initially at Durham using the back reflection x-ray Laue method. Before cutting the samples from the $Gd_{0.80}\ Tb_{0.20}$ ingot, it was necessary first to make the grain boundaries visible; this was achieved by etching in very dilute nitric acid then washing in acetone. A suitable grain was chosen and then the ingot was fixed on an adjustable goniometer using equal amounts of Durofix and granulated carbon. The grain was oriented by the back reflection Laue method until two main axes were centred on the picture. The ingot was rotated by 180° and another picture was taken of the reflection from the back surfaces to check if the grain passed to the other surface of the ingot. A slice of thickness about 1.5 mm was cut from the oriented grain using electrospark erosion, the cutting being done under paraffin and a wire slice being employed. The slice was polished mechanically using 6M2 diamond lapping compound followed by 1M4 diamond lapping compound

and then polished chemically in 50% nitric acid - 50% acetic acid followed by a thorough wash in acetone. The slice was again examined by the Laue technique to check that the orientation had been retained accurately during the cutting cycle. Finally a disc was cut from the slice using the electrospark erosion, with a cylindrical tool.
All the specimens were in the shape of discs of diameter about 5 mm and of thickness about 1 mm. The samples can be split into two groups according to their orientation. The first group containing a and b axes lying in the plane of the disc and with the c-axis perpendicular to the plane. The second group contained specimens which were cut to contain b and c axes lying in the plane with the a-axis perpendicular to the plane. All the specimens were polished mechanically and chemically as described before.

5.2 Determination of Specimen Orientation by the Back Reflection Laue Method

The Laue method is one of the simplest of all techniques for obtaining diffraction photographs. The specimen was fixed on a brass block and then mounted on two circle adjustable goniometer. Its angles were set to zero using a travelling microscope so that one edge of the block was vertical. A collimated x-ray beam of wide wave length range fell upon the crystal surface. A 57 high speed Polaroid film was placed between the radiation source and the specimen so that the diffracted radiation could be recorded as a series of spots. The camera used was a very simple Polaroid cassette, consisting of a film holder and fluorescent screen. The crystal was mounted at 3 cm from the film plane. An exposure time of about 10 minutes was adequate using a Mo anode tube and a current of 30 mA at 30 kV. Since the beam had been incident almost normally on the surface of the disc the diffraction pattern was close

to that expected for the appropriate crystal plane. After the first picture the intersection of zones nearest to the middle of the picture was chosen and the sample orientation adjusted to move this to the centre of the film. The angles through which the specimen must be rotated were measured on the film using a Wulff net, and then the goniometer arcs were appropriately adjusted and a further exposure made. A 90^{o} rotation was made some times, so that the beam was parallel to the crystal plane, to check that the reflection obtained was characteristic of the appropriate axis. Finally a rotation of the crystal was made on the goniometer about the x-ray beam axis so that one principal axis lay vertically while the other was horizontal. The axes were finally identified by comparing the pictures with computed basal plane and b and c axis diffraction patterns for hcp crystals.

5.3 Magnetostriction Measurement

Since magnetostriction is a small change in specimen length due to a magnetic field applied, it requires an accurate method of determination. Several methods can be used such as the x-ray diffraction method, the effect of the change of length on the air gap of a capacitor, or the resistive strain gauge technique.

Because the x-ray diffraction method involves bulky equipment, this means it is an inconvenient method to be used in this experiment, since the bore of the magnet is only 4.75 cm. The capacitor method suffers from the difficulty of operation at low temperature. Also due to the simplicity of the strain gauge method, this led to the choice of the resistive strain gauge technique. Unfortunately using this method there are inherent sources of error,

(i) the magnetoresistance effect, but this is negligibly small for Karma gauges which have been used in this experiment as discussed by Greenough and Underhill (1976),

(ii) slight misalignments of the gauge with respect to the desired crystallographic direction, however the gauge can be carefully aligned, and if there was any doubt the crystal was reoriented again after fixing the gauge using the surface on which no gauge was fixed,

(iii) the uncertainty in the gauge factor and its variation with temperature, but the gauge factor quoted by the manufacturer was found to be reasonably accurate for the calculation of strain as will be discussed in Section 5.3.

Mechanical strain in materials is frequently measured by the resistive strain gauge technique and this technique has been the most widely used to measure magnetostriction since it was introduced by Goldman (1947). The gauge is cemented directly to the surface of the sample under test so that changes in length are detected by changes in the resistance of the gauge. The magnitude of the change in resistance can be determined since,

$$R = \rho \frac{l}{A} \qquad .....(5.1),$$

where l is the total length, A is the cross-section area and ρ is the resistivity of the wire.

A measure of the gauge sensivitity is the relative change in resistance per relative change in length, or the gauge factor K,

$$K = (\Delta R/R)/(\Delta l/l) \qquad .....(5.2)$$

The gauge factor is given by, Brophy (1977),

$$K = 1 + 2\sigma + l \frac{d\rho}{dl} \qquad .....(5.3),$$

where σ is Poisson's ratio for the wire material.

As clear from the above equation the change in the resistance arises from changes in the wire dimensions because of mechanical strain. There is also the possibility of changes in resistivity, with strain. In metal-wire or metal-foil gauges the third term in Eq. (5.3) is

negligible particularly for Karma gauges as said before. Assuming the volume does not change Poisson's ratio is 0.5 and hence K =2. A Wheatstone bridge is usually used to measure the change in the resistance of strain gauges. In this method two gauges can be used, one bound to the specimen while thermal and magnetoresistive compensation can be achieved by connecting a dummy gauge in another arm of the bridge. In this experiment a dummy gauge was cemented to the surface of a copper disc and this was placed in the same thermal and magnetic environment. The active and the dummy gauges were electrically connected in adjacent arms of a Wheatsone bridge as shown in Fig. (5.1b). For the special case of a Wheatstone bridge with three equal arms as shown in Fig. (5.1a), if the detector system has an input impedance much larger than R the signal voltage due to a very small resistance change ΔR may be obtained following Smith (1971). Thus

$$V_1 = \frac{R}{2R} \quad V = \frac{V}{2}$$

and

$$V_2 = V(R + \Delta R)/(R + R + \Delta R) = \frac{V}{2}\left[(1 + \Delta R/R)/(1 + \Delta R/2R)\right]$$

$$= \frac{V}{2}\left[(1 + \delta)/(1 + \frac{\delta}{2})\right],$$

where $\delta = \Delta R/R$ the fractional unbalance.

Using the approximation

$$1/(1 + z) \approx 1 - z \qquad \text{for z small,}$$

we find

$$V_2 \approx \frac{V}{2}\left[(1 + \delta)\ (1 - \frac{\delta}{2})\right] \approx \frac{V}{2}\ (1 + \delta/2)$$

thus

$$e = V_2 - V_1 = \frac{V}{2}\ (1 + \frac{\delta}{2}) - \frac{V}{2} = V\ \delta\ /4 = \frac{V}{4}.\ \frac{\Delta R}{R}$$

.....(5.4)

By substituting from Eq. (5.2) we find

$$e = \frac{VK}{4}\ (\frac{\Delta l}{l})$$

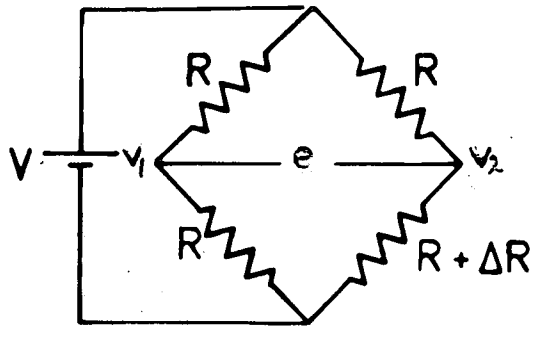

FIG 5.1a

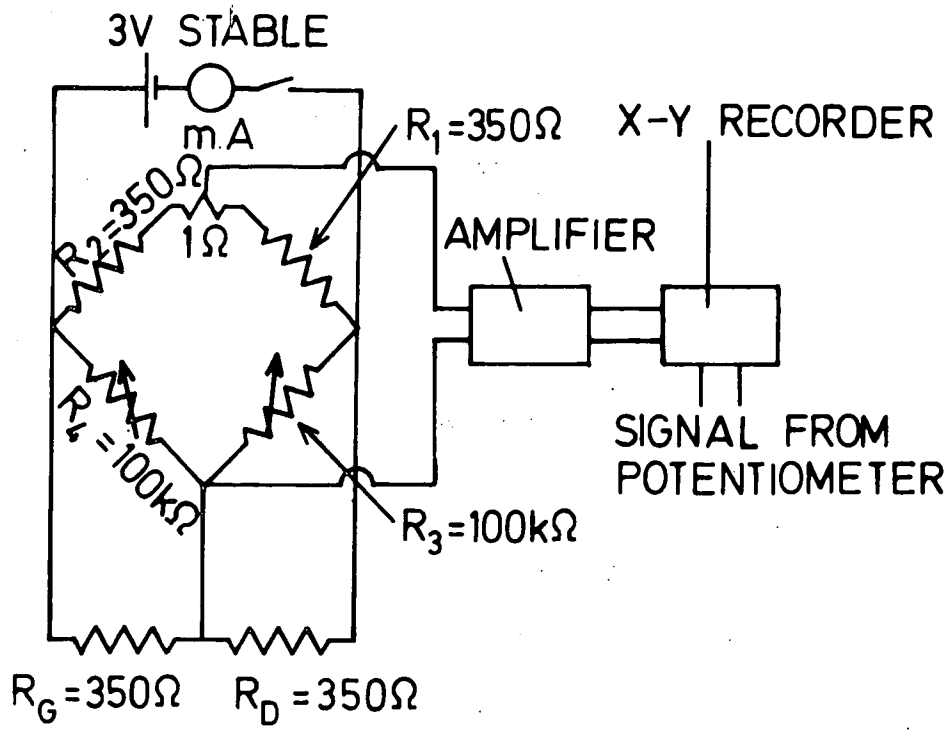

R_G IS THE ACTIVE GAUGE RESISTANCE
R_D IS THE DUMMY GAUGE RESISTANCE

FIG 5.1b

THE WHEATSTONE BRIDGE CIRCUIT.

Or,

$$\frac{\Delta l}{l} = \frac{4e}{VK} \qquad \text{.....(5.5)}$$

Hence variation in the supply voltage V leads to error in the strain, so an accurate voltage-stabilizer should be used. The voltage-stabilized power supply which was used has been developed and fully discussed by Unvala and Green (1974). The circuit is shown in Fig. (5.2). The input voltage 27 V was initially supplied from three PP6 batteries to ensure stability but this was finally changed to a 27 volts stabilized D.C. power unit supplied from the mains. No problems of spurious pick-up associated with the 50 Hz mains supply were found.

The output voltage of the first integrated circuit μA741 is stabilized at about 12 V. This is used as a power supply to the second integrated circuit μA741. The output of the second integrated circuit is stabilized by the two transistors BFY 52 and BC 479 to 3 volts.

Since the strain is very small, the output voltage e is small also, for example with a strain of 10^{-5} and using a 3 volts bridge supply and strain gauges with gauge factor of 2 an output of about 10 μV, is obtained so that an amplifier was necessary. The amplifier must be of a low drift type, so as not to degrade the accuracy of the system. An amplifier circuit was built to use with the strain gauge bridge; this has been fully described by Unvala et al (1976). The circuit is shown in Fig. (5. 3). The transistor MAT-01H was changed by another transistor type, NPN-2C444 BFY 82 which has the same characteristic as the first one. This transistor was followed by an integrated circuit operational amplifier type 308. The gain of the combination is determined by the feed back through VR_2 and VR_3; in this circuit switchable gains of x10 and x100 were used.

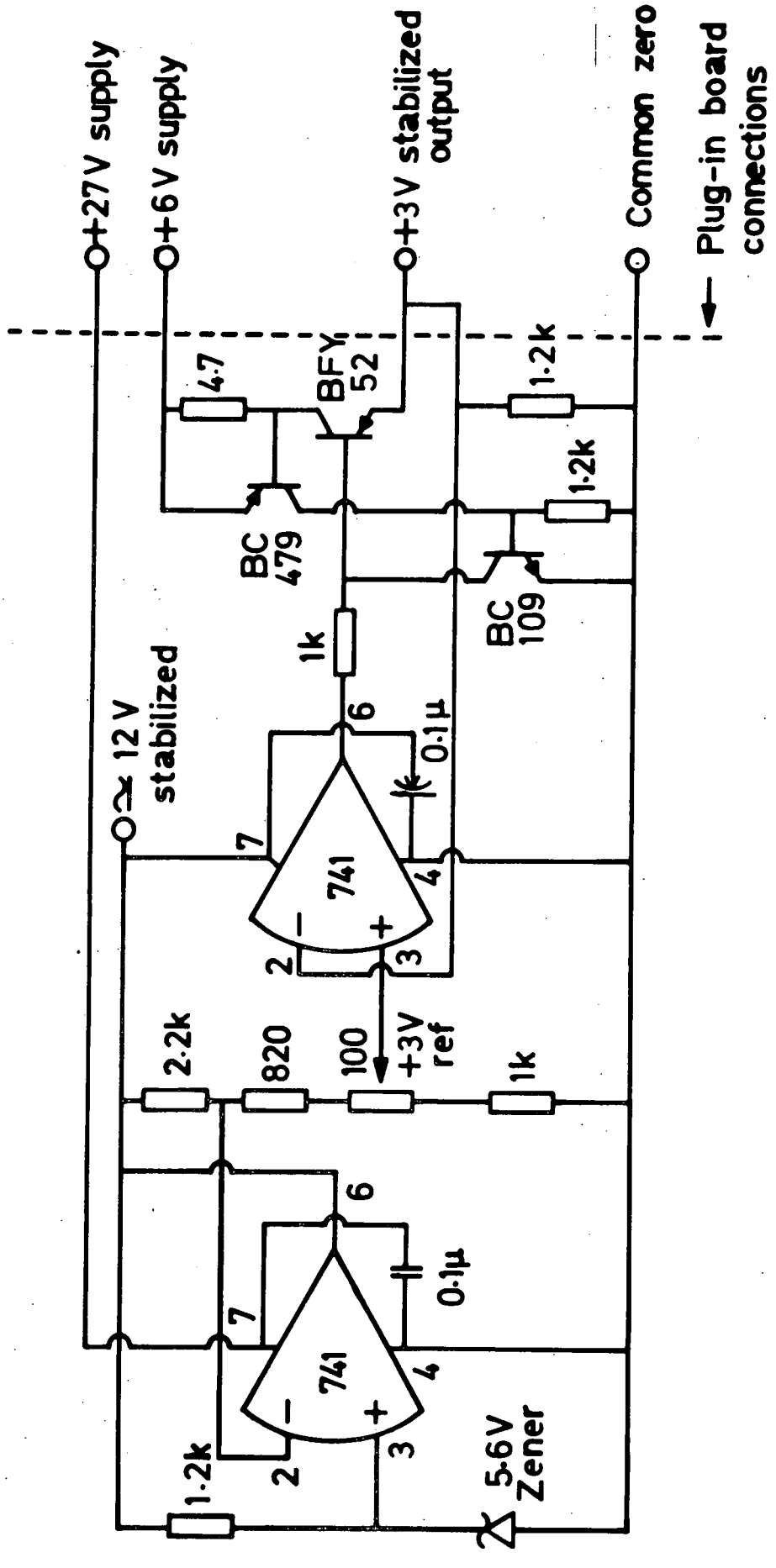

Fig(5-2) Circuit for stabilizer for 3V power supply, after Unvala and Green(1974).

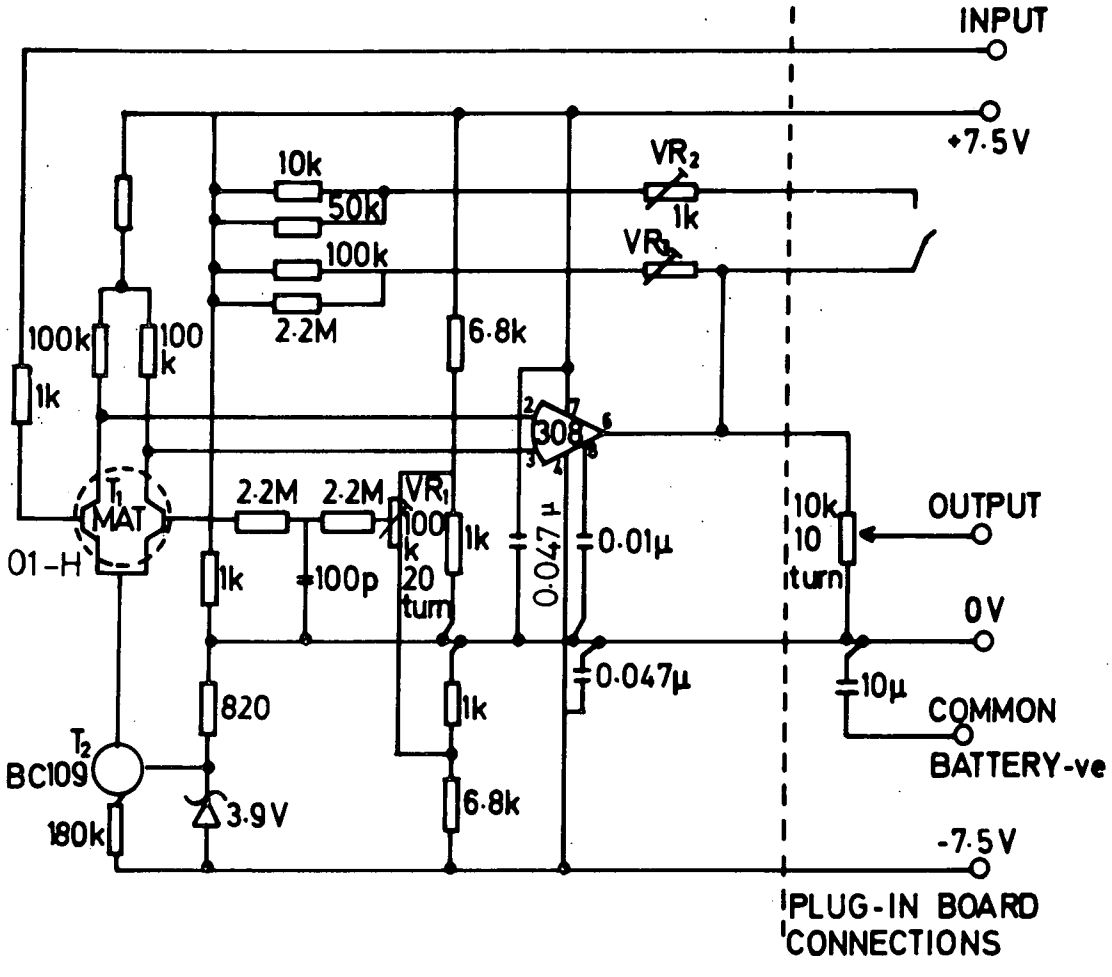

Fig(5.3) Circuit of amplifier using MAT-01H/308 combination, after Unvala et al (1976)

To provide the +7.5 V|0V|-7.5 V supply for the amplifier PP6 batteries were initially used, but later this was changed to a stabilized DC power unit supplied from the mains.

5.4 Fixing the Gauge(s) on the Crystal

Karma gauges were used, type WK-06-050AR-350, where:

W indicates that the gauge is fully incorporated in glass-fibre reinforced epoxyphenolic resin with high-endurance lead wires,

K shows the foil alloy, a nickel-chromium alloy being used for high performance self temperature compensated gauges,

06 is the self-temperature-compensation (S-T-C) number which is the approximate thermal expansion coefficient in PPM/F° of the structural material on which the gauge is to be used,

050 is the active gauge length in mils,

AR describes the grid and tab geometry, and

350 is the gauge resistance in ohms.

The gauge factor is 2.04 ± 1% at 297 K and it varies with temperature as shown in Fig. (5.4). The WK-series have one of the widest operational temperature ranges, between 4 K and 563 K.

M-Bond 610 adhesive was used for bonding the strain gauges. It is useful for temperatures ranging from 4 K to 500 K.

The axes of the crystal having been identified, the brass block on which the crystal was mounted was transfered to a microscope with a rotatable disc provided with a circular scale divided into 360°. The block was fixed on the rotatable disc using Durofix, then the disc was rotated until one of the cross-lines of the eyepiece was parallel to one edge of the block. Then the disc was rotated clock or anti-clockwise by an angle equal to the angle through which the goniometer was rotated during the orientation to set one of the crystal axes

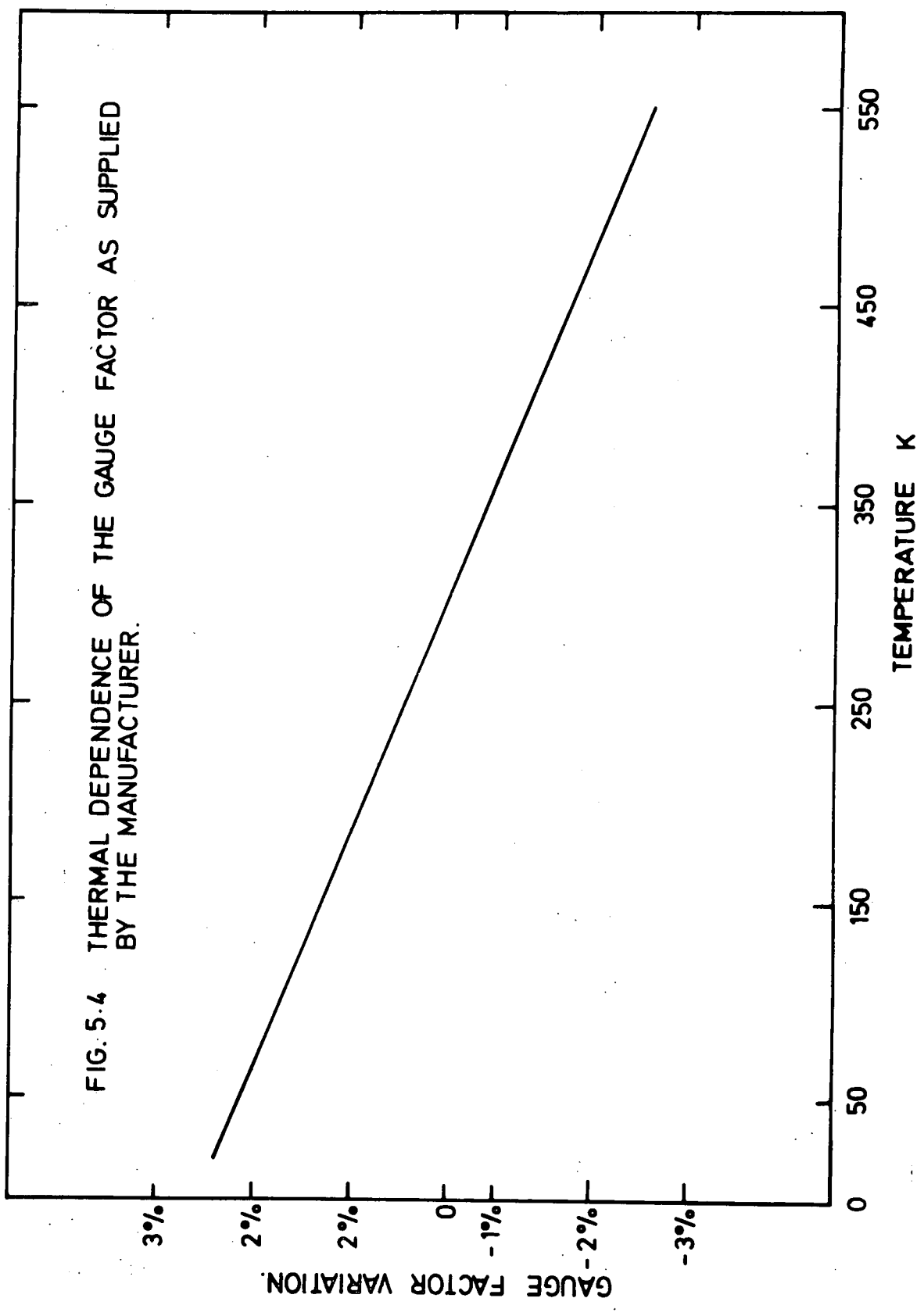

FIG. 5.4 THERMAL DEPENDENCE OF THE GAUGE FACTOR AS SUPPLIED BY THE MANUFACTURER.

vertical. By doing this two axes of the crystal, a and b for basal plane samples and b and c for b-c axes samples, were directed along the cross-lines of the eyepiece. The crystal was carefully cleaned with acetone, then the crystal and the gauge were coated with a thin layer of M-Bond 610 adhesive. The adhesive was permitted to dry for about 30 minutes. Then the gauge was placed along a chosen axis. The gauge was overlaid with a piece of thin teflon sheet and this was covered with a metal plate. The crystal was removed from the microscope and clamped using spring clamps to apply pressure during the curing cycle. The clamped specimen was placed into a cool oven and the temperature raised gradually to the desired level. Time verses temperature recommendations for curing M-Bond 610 adhesive are given in Fig. (5.5); all the specimens were cured for 2 hours at 150°C. Upon completion of the curing cycle the oven temperature was allowed to drop to room temperature before removing the clamping pieces. Finally the specimen was washed in acetone.

For the basal plane samples one gauge was fixed along a b-axis, and for b and c axis samples two gauges were fixed. Firstly one gauge was fixed along a b-axis and the sample was cured, then the sample was fixed on a microscope glass slide and another gauge was fixed along the c-axis on the other side of the disc (perpendicular to the b-axis gauge) under the microscope. Later a third gauge was fixed on the b-c axis samples along a direction at 45° to the c-axis after polishing off the c-axis gauge. These gauges were required to permit the determination of the various magnetostriction constants as described in section 3.6.3.

5.5 The Magnet

To saturate the specimens a high magnetic field was required especially for those of high Tb content. The 13 Tesla superconducting magnet at

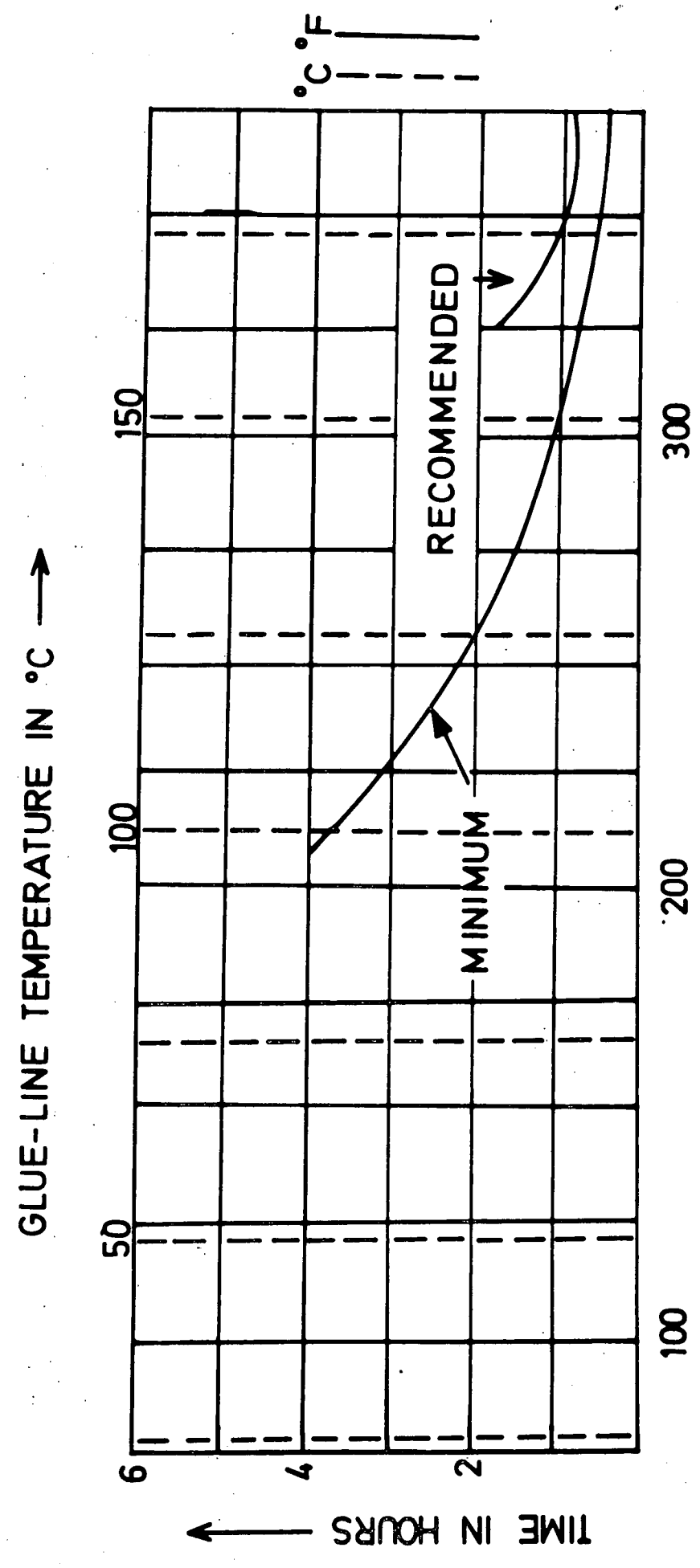

FIG. 5.5 TIME VERSUS TEMPERATURE RECOMMENDATION FOR CURING M-BOND 610 ADHESIVE AS SUPPLIED BY THE MANUFACTURE.

the Physics Department of the University of Nottingnam was used. The magnet consists of a pair of coils with cold bore of 45.7 mm and a split of 15 mm. Fig. (5.6) shows a section of the magnet in horizontal position. The magnet may be used with its axis vertical or with one of the split holes vertical. The former arrangement was used for the present measurements. Access to tne magnet is via the top plate of the containing dewar. A variable temperature insert was designed to go with tne cold bore of 45.7 mm and this can be suspended from the top plate of tne containing dewar.

To operate the magnet first it should be cooled to 4.2 K. This is achieved by filling tne inner space with liquid nitrogen, taking about 70 litres, and keeping it at that temperature for about 15 hours. Then the remnant of the nitrogen is transferred to the outer space by applying pressure with nelium gas. On completing this process the magnet will be at about 77 K. The inner space is now evacuated. This is followed by transfering liquid helium into the inner space using the desired amount required for tne experiment; usually 60 litres would give about 8 hours running for the first transfer.

Another magnet was used to run the experiments between 77 K and room temperature at Durham. This magnet consists of a solenoid giving a field of 1 Tesla. The magnet is an oil cooled solenoid. The oil was pumped through the solenoid within a closed recirculating system. The closed circulating system was jacketed by three additional heat exchangers, these were cooled directly with water from the mains supply. The solenoid was wound with copper strip and enclosed in a brass cylinder which had Tufnol end pieces; the terminals of the solenoid were brought out through these end plates. The power for the solenoid was derived from a Brentford stabilized D.C. supply. The voltage across the solenoid could be swept up to 120 volts for a current of

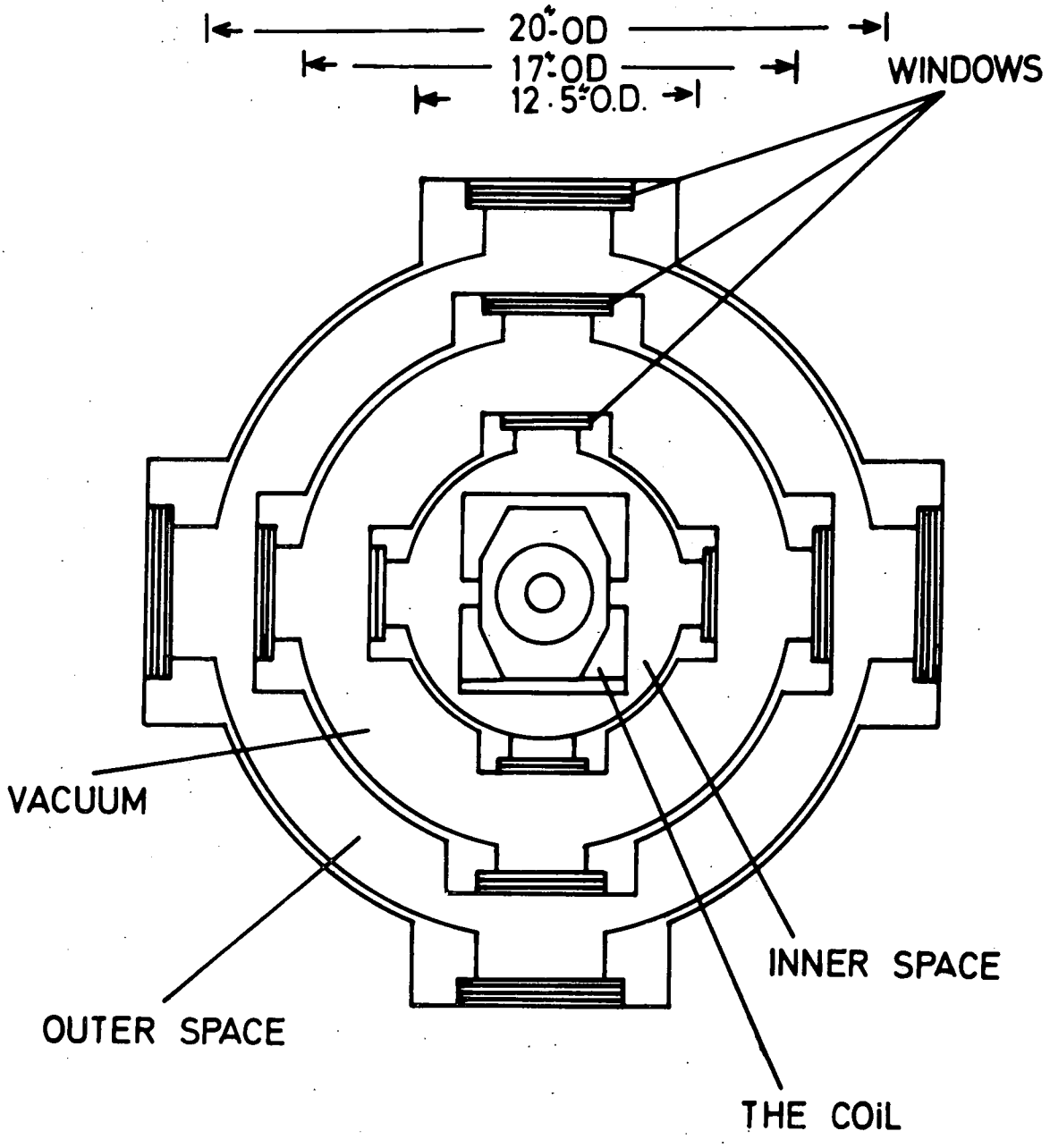

FIG. 5·6 SECTION SHOWING THE MAGNET IN HORIZONTAL POSITION.

120 amps. The supply had two modes of operation, the current stabilized and the voltage stabilized modes. It was used in the former. The magnetic field due to the solenoid was calibrated by Mundell (1976) using a flux meter and Hall probe, Fig. (5.7) shows the calibration curve for this solenoid. This magnet could be used to saturate the samples with low Tb content, 5% and 20%, and was used for the low field measurements for the specimens of other compositions. The temperature was varied between 77 K and room temperature by evacuating the sample space which was surrounded by a stainless steel tube as shown in Fig. (5.10b). This tube was immersed in liquid nitrogen, and a cartridge heater immediately below the specimen holder used to raise the sample temperature in conjunction with a temperature controller (see Section 5.7).

5.6 The Measuring Assembly

Since the magnetic field in both solenoids is vertical, this required a gear mechanism to rotate the sample in a vertical plane. Figs (5.8a) and (5.8b) show the arrangement which has been used to rotate the sample, where a helical pinion and rack were used to give 180° of rotation. All was constructed from brass. Fig. (5.8b) shows a vertical view of this arrangement. Initially, to hold the crystal a small piece of vero-board was fixed using Araldite on a brass plate which was soldered to the pinion. The crystal was fixed with Durofix on the vero-board, but this was unsatisfacotry because the bond between the crystal and the vero-board was found to be too weak to retain the crystal when acted on by the forces produced by the magnetic field. Another arrangement was finally used consisting of a small box as shown in Fig. (5.8a) where now the crystal was bonded with Durofix in the box and held firmly inside the box by pressing it with a small pad of cotton wool and closing the box with a lid. The strain gauge leads come out of the box from three holes by the edge of the box and are connected to insulated copper pins

FIG. 5·7 SOLENOID CALIBRATION, MAGNET CURRENT VS MAXIMUM FIELD (FLUXMETER) AFTER MUNDELL (1976)

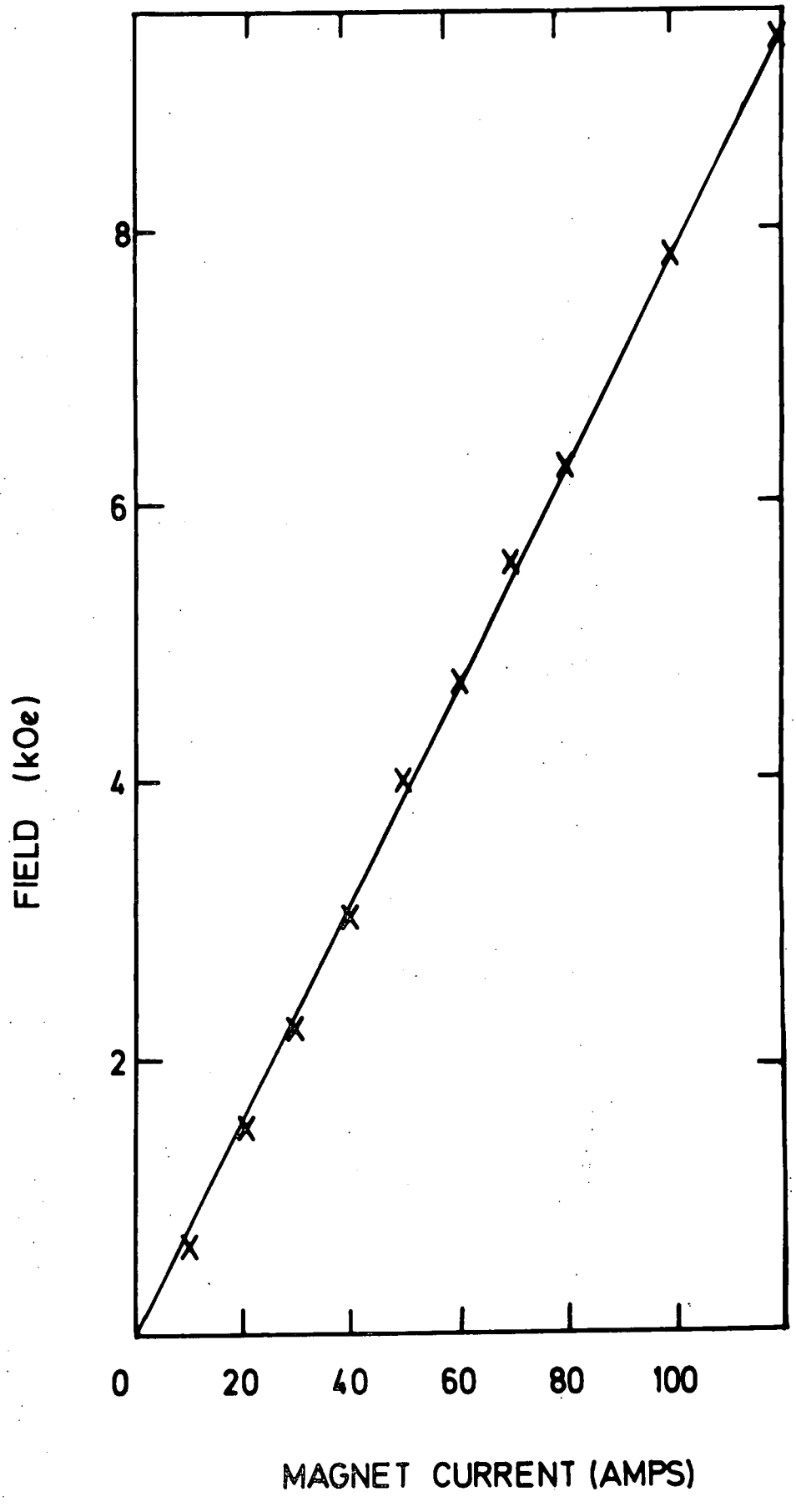

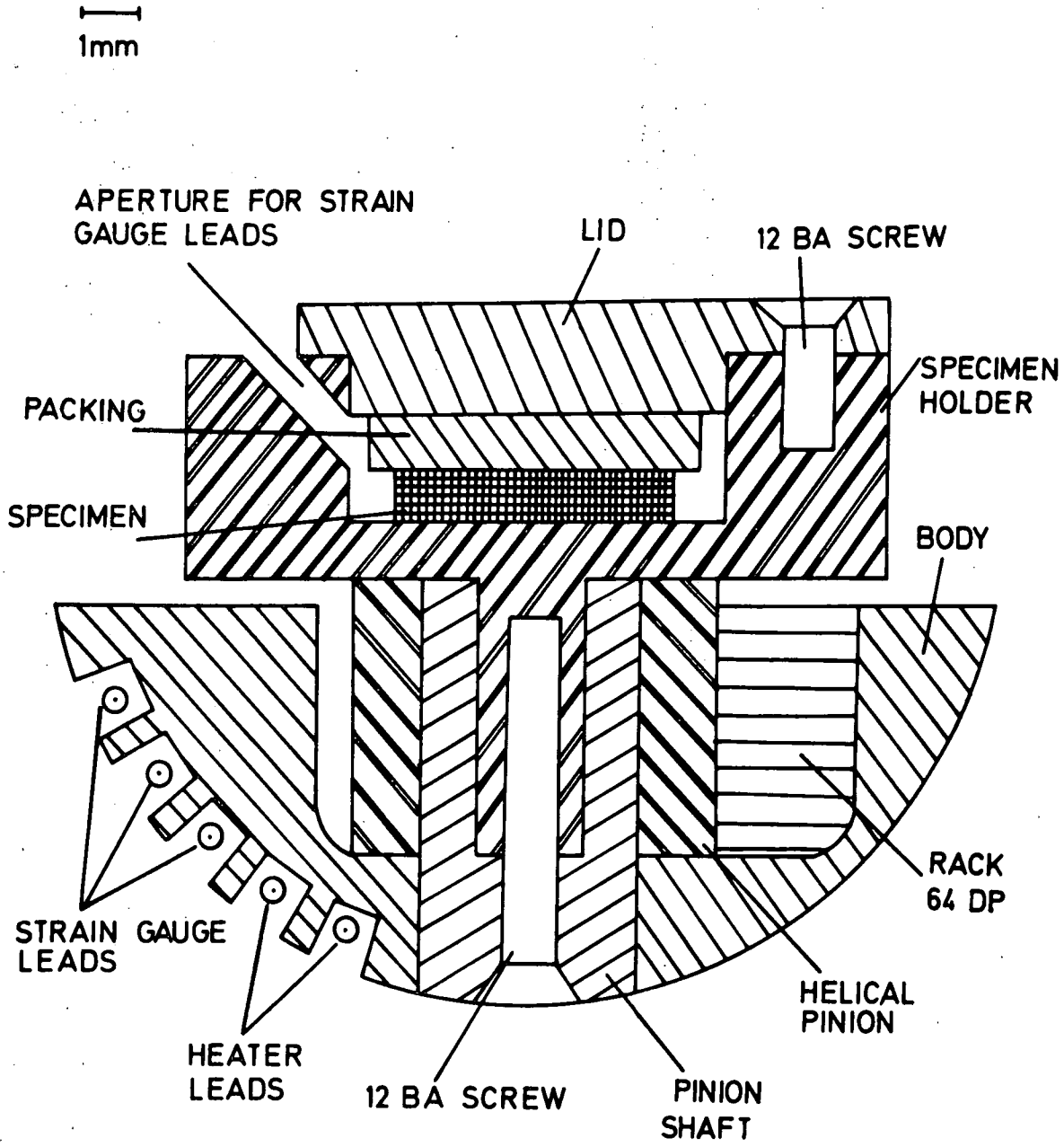

FIG. 5·8a VERTICAL SECTION SHOWING THE HELICAL PINION ARRANGEMENT AND THE CRYSTAL HOLDER, ALL MADE FROM BRASS.

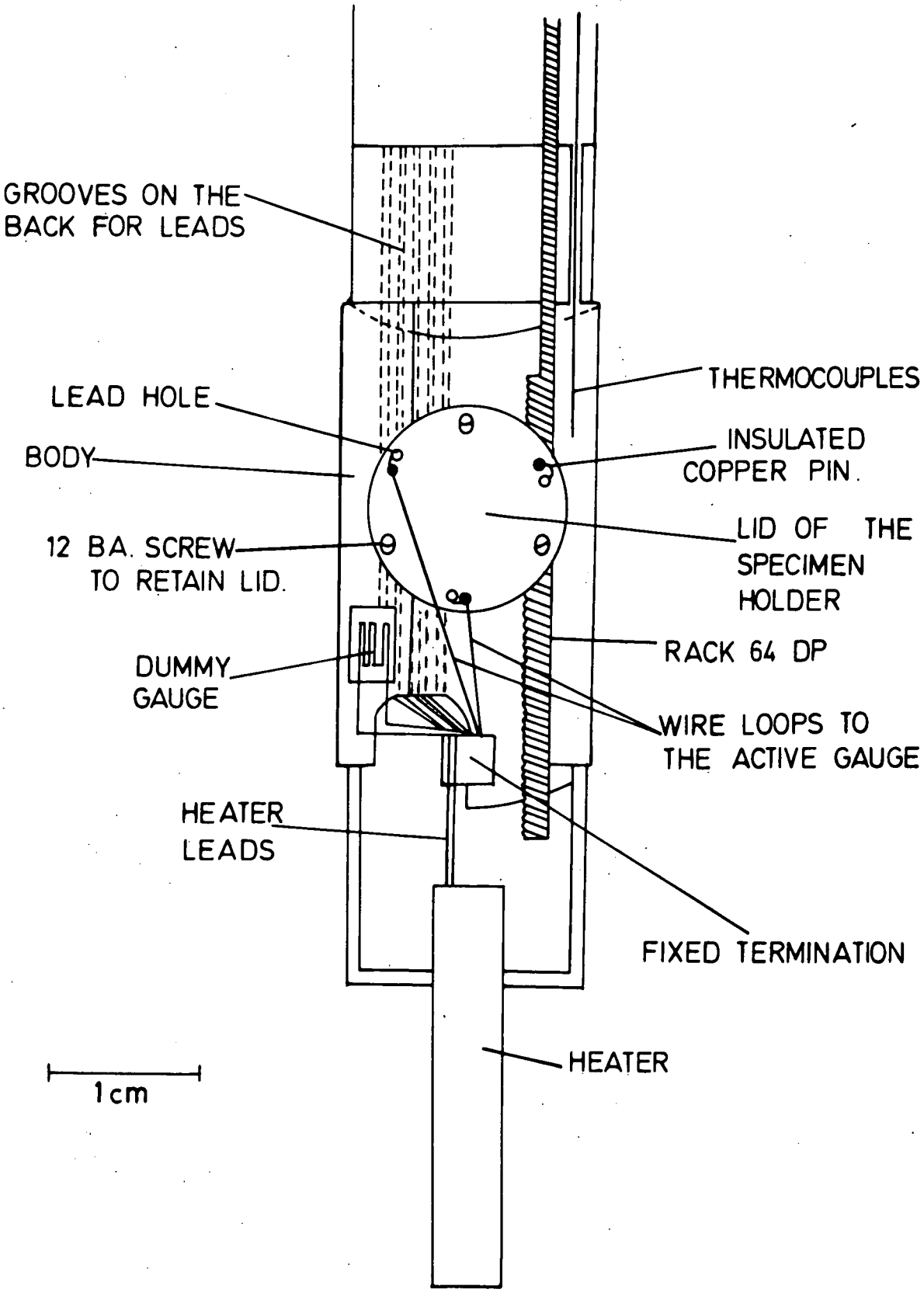

FIG. 5·8b VERTICAL VIEW OF THE MEASURING ASSEMBLY.

on the surface of the box. From these connections are made to fixed terminations using loops of enamel insulated copper wire of SWG 32. A coaxial cable was used between the fixed terminations and the strain gauge bridge, the cable coming out of the insert through a vacuum feed-through connection.

Fig. (5.9) shows the top mechanism of the rotation where a push-pull rotor drive motion was used to drive the rack. A voltage proportional to the angle through which the crystal had been rotated with respect to the magnetic field direction was obtained by mounting a potentiometer on the drive shaft. The set-up of the apparatus is shown in Fig. (5.10a). Experiments were carried out in the temperature range 4.2 K to 250 K. The temperatures were measured by using Au + 0.03 at % Fe vs Chromel thermocouples.

5.7 The Variable Temperature Insert

A variable temperature insert designed by the Nottingham group was modified to go with the experiment as shown in Fig. (5.10a). Temperatures above 4.2 K were obtained by passing a current through either a heater resistance cartridge of 40 ohms capable of carrying a current of about 0.85 amperes and fixed below the sample, or using a heating coil of resistance 80 ohms capable of carrying 0.5 amperes wound around the inner tube in the variable temperature insert. The temperature was controlled by using a Thor temperature controller Model 3010 II to provide the heater current. The error voltage can be measured up to 1 mV, which can give a temperature stability of 0.01 K. The desired temperatures were measured by taking the output voltage from the controller and converting this to temperature using a table and graph provided by the manufacturers of the thermocouple wire. In addition direct readings were obtained from an Oxford temperature controller Model DTC2 connected on parallel with the Thor Model. The temperatures were stabilized to $\pm$ 0.1 K.

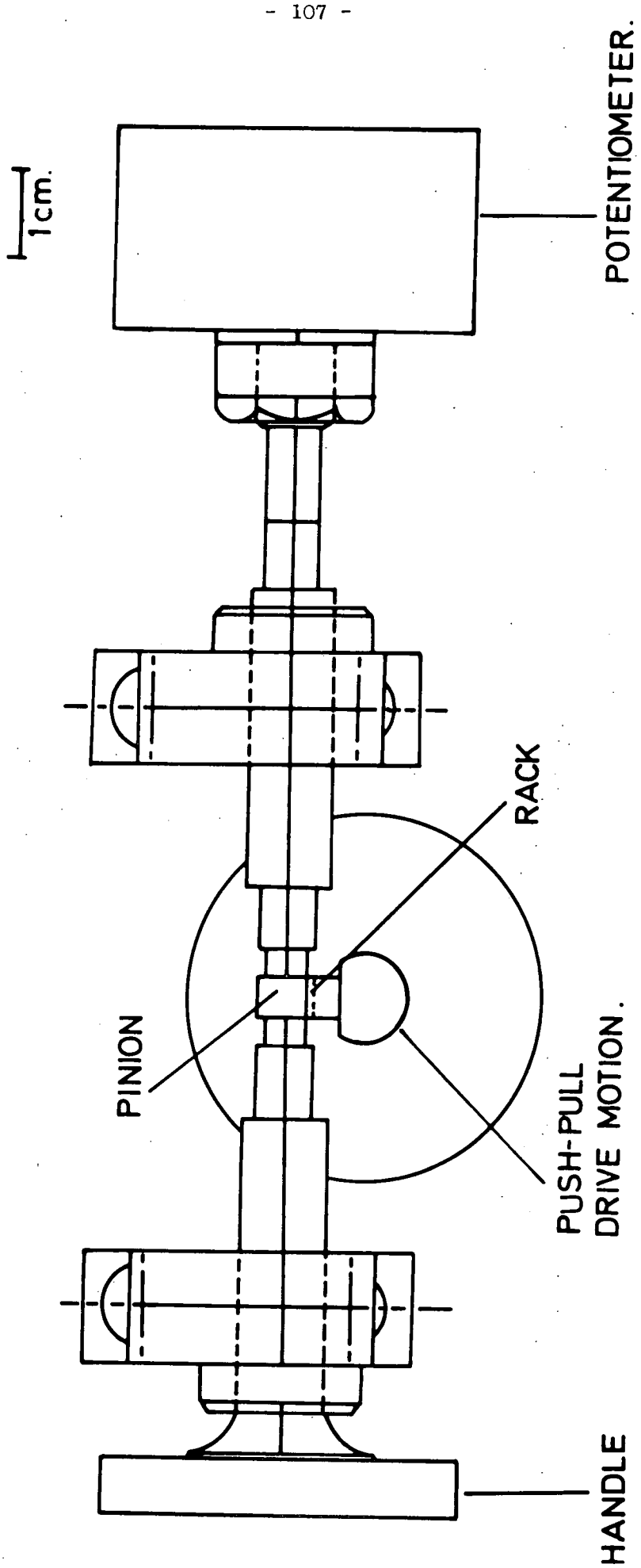

FIG. 5·9 HORIZONTAL SECTION SHOWING THE TOP ARRANGEMENT TO DRIVE THE PINION.

FIG. 5·10a CROSS SECTION OF THE EXPERIMENTAL ARRANGEMENT.

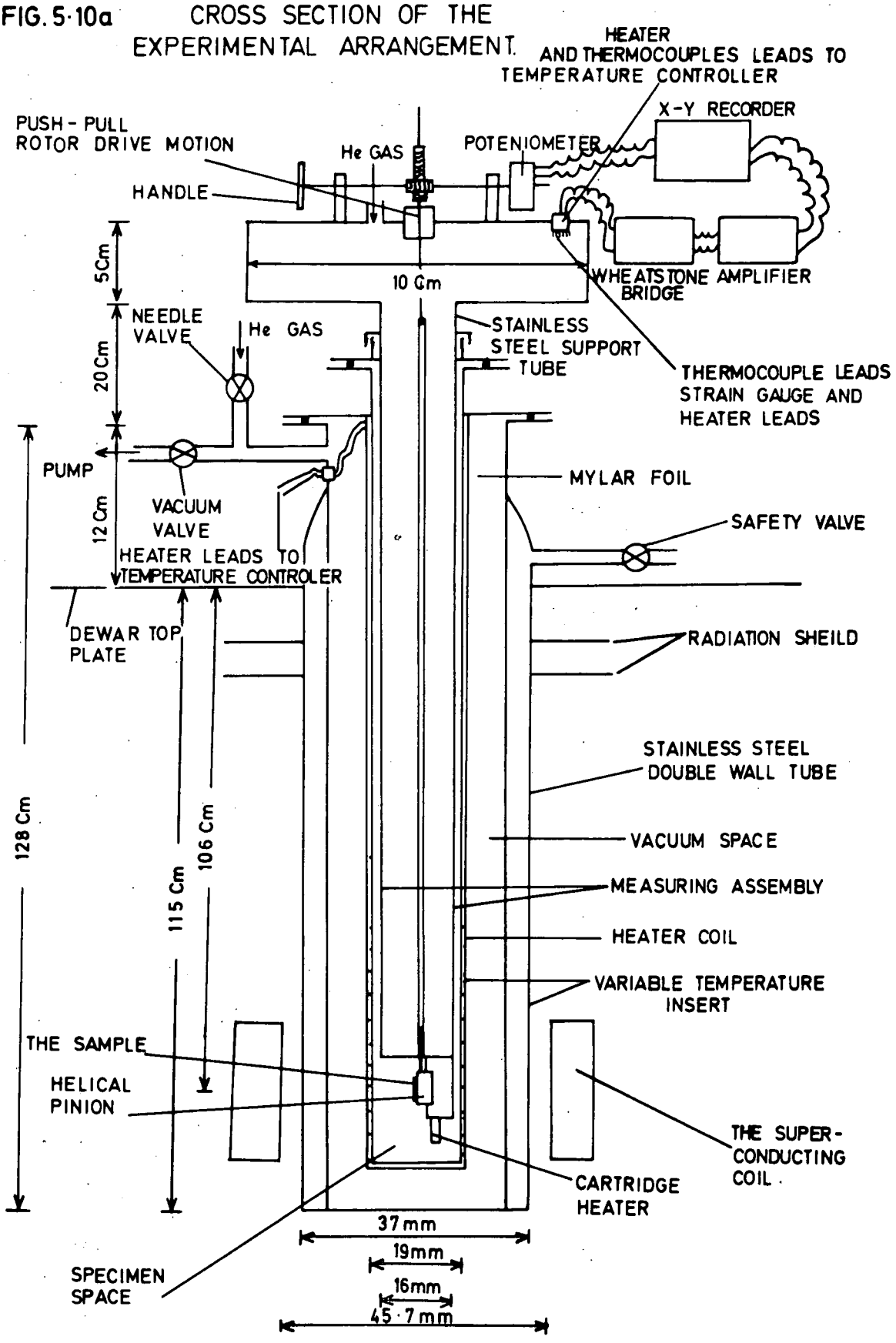

FIG. 5.10 b THE VARIABLE TEMPERATURE INSERT FOR MEASUREMENTS BETWEEN 77K AND ROOM TEMPERATURE USING THE OIL COOLED SOLENOID.

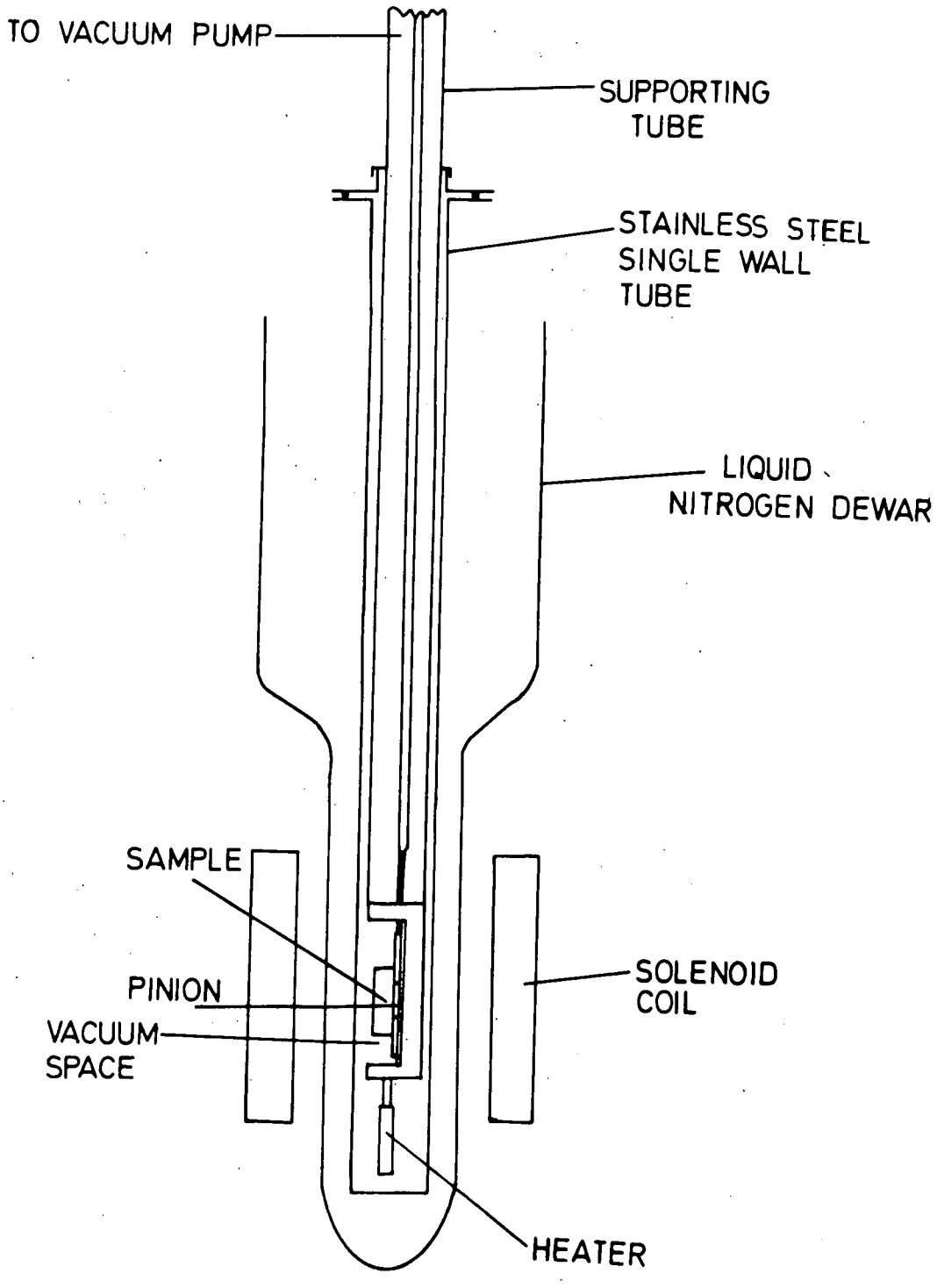

To run the experiments the variable temperature insert was evacuated down to about 10^{-2} torr before it was inserted inside the magnet. Then to cool the specimen space which was filled with helium gas under atmospheric pressure, a small amount of helium gas was introduced using a needle valve to the vacuum space, providing good heat conduction between the liquid helium and the specimen. This small amount of helium gas was sufficient to cool the sample down to about 30 K, then a larger amount of helium was introduced to the vacuum space to cool the sample to 4.2 K. To heat the sample the helium gas was evacuated first from the vacuum space and then the heater could be used while the specimen was kept in helium gas at atmospheric pressure in the specimen space.

5.8 Calibration of the Measuring Assembly

Since there is no way to calibrate the strain gauge after it has been fixed a separate measurement was made on a nickel crystal disc whose surface was a (110) plane in order to calibrate the measuring system. Two gauges were fixed, one along [001] and another along [1$\bar{1}$0]. The expression for magnetostriction in cubic crystals is given by Chikazumi (1964 p. 170) as

$$\frac{\Delta l}{l} = 3/2 \quad \lambda_{100} \left(\alpha_x^2 \beta_x^2 + \alpha_y^2 \beta_y^2 + \alpha_z^2 \beta_z^2 - \tfrac{1}{3}\right)$$

$$+ 3 \ \lambda_{111} \left(\alpha_x \alpha_y \beta_x \beta_y + \alpha_y \alpha_z \beta_y \beta_z + \alpha_z \alpha_x \beta_z \beta_x\right)$$

.....(5.6),

where α's and β's are the direction cosines of the magnetization and the strain respectively. As in Chapter 3 for hexagonal crystals the above equation can be simplified by choosing a particular measuring direction.

(i) The strain along [00$\bar{1}$] can be found if we substitute α's and β's as follows

$$\beta_x = \beta_y = 0 \qquad \beta_z = 1$$

$$\alpha_x = \alpha_y = 1/\sqrt{2} \sin\theta \qquad \alpha_z = \cos\theta$$

i.e.

$$\frac{\delta l}{l} = 3/4 \ \lambda_{100} \cos 2\theta + 1/4 \ \lambda_{100}$$

or

$$\left[\frac{\delta l}{l}\right]^{\theta=90} - \left[\frac{\delta l}{l}\right]^{\theta=0} = -3/2 \ \lambda_{100} \qquad \text{.....(5.7)}$$

(ii) The strain along [1$\bar{1}$0] can be found if we substitute α's and β's as follows

$$\beta_x = \beta_y = 1/\sqrt{2} \qquad \beta_z = 0$$

$$\alpha_x = \alpha_y = 1/\sqrt{2} \sin\theta \qquad \alpha_z = \cos\theta$$

and the strain will be

$$\frac{\delta l}{l} = -3/8 \ (\lambda_{100} + \lambda_{111}) \cos 2\theta - 1/8 \ (\lambda_{100} + 3\lambda_{111})$$

or

$$\left[\frac{\delta l}{l}\right]^{\theta=90} - \left[\frac{\delta l}{l}\right]^{\theta=0} = 3/4 \ (\lambda_{100} + \lambda_{111}) \qquad \text{.....(5.8)}$$

Fig (5.11) shows the variation of length in the [00$\bar{1}$] direction of the nickel at 250 K as it was rotated in the magnetic field. Fig. (5.12) shows the magnetostriction at 250 K along [1$\bar{1}$0]. Curves of similar amplitude were obtained at 77 K. Figs. (5.13) and (5.14) show the field dependence of magnetostriction along [00$\bar{1}$] and [1$\bar{1}$0] respectively. For all of these results the gauge factor supplied by the makers was used to calculate the strain. From these curves the magnetostriction constants λ_{100} and λ_{111} may be then calculated yielding

$$\lambda_{100} = -(44 \pm 3.2) \times 10^{-6}$$

$$\lambda_{111} = -(23 \pm 4) \times 10^{-6} \qquad \text{at 250 K}$$

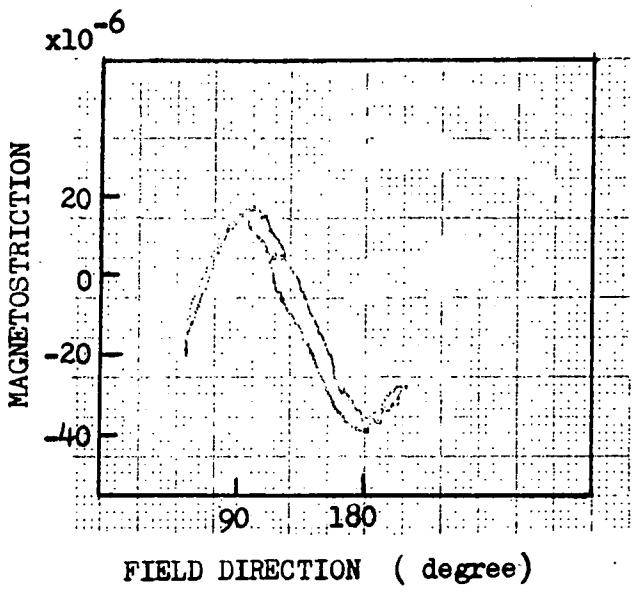

Fig. (5.11) Magnetostriction in Ni along [001] at 250 K and 1 Tesla, as a function of field direction.

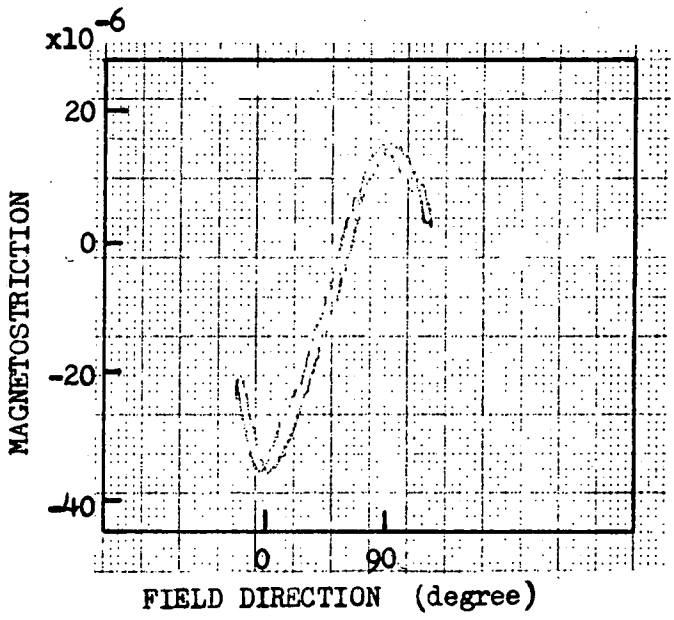

Fig. (5.12) Magnetostriction in Ni along [110] at 250 K and 1 Tesla, as a function of field direction.

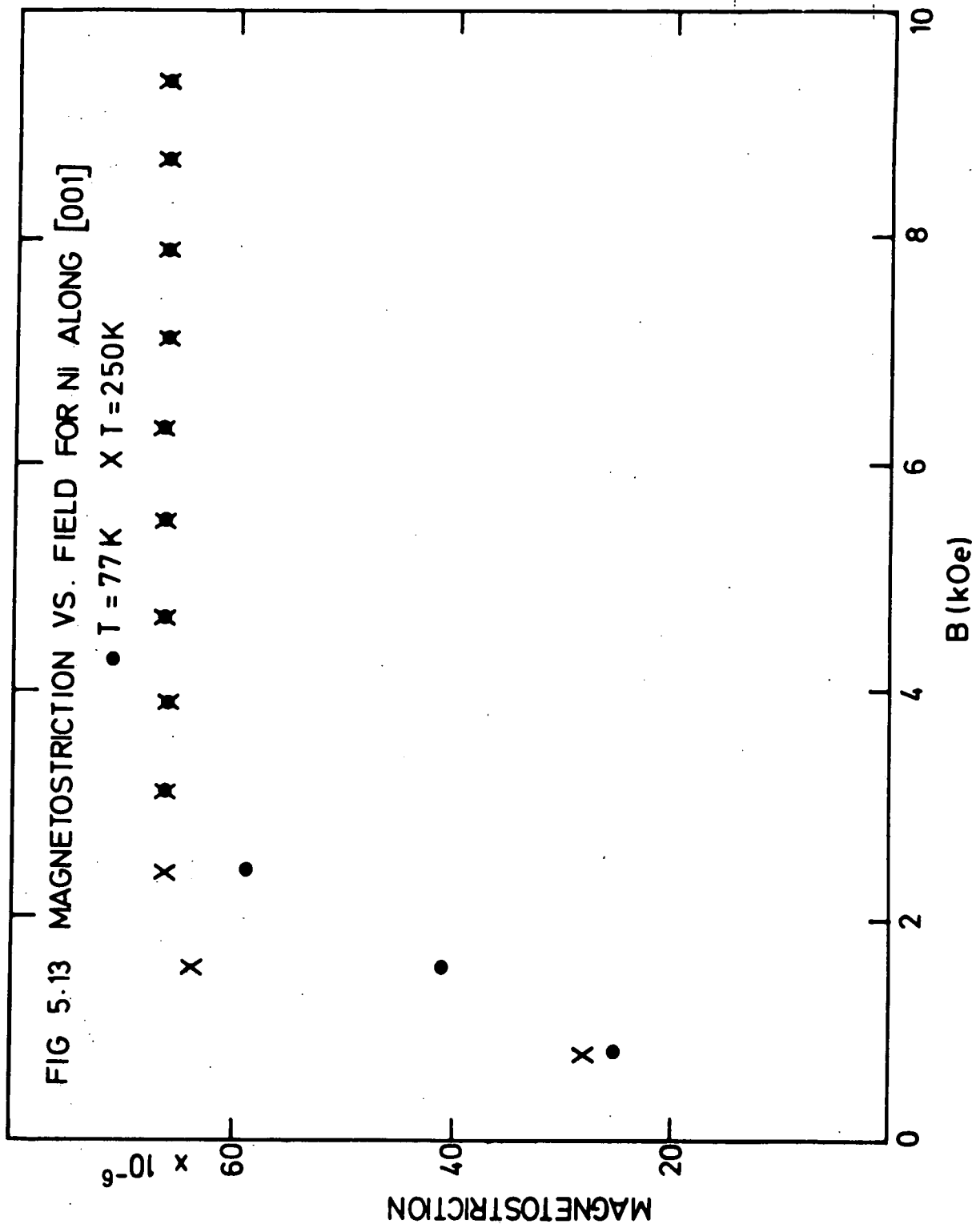
FIG 5.13 MAGNETOSTRICTION VS. FIELD FOR Ni ALONG [001]
● T = 77 K X T = 250 K
MAGNETOSTRICTION
x 10⁻⁶
60
40
20
0
2
4
6
8
10
B (kOe)

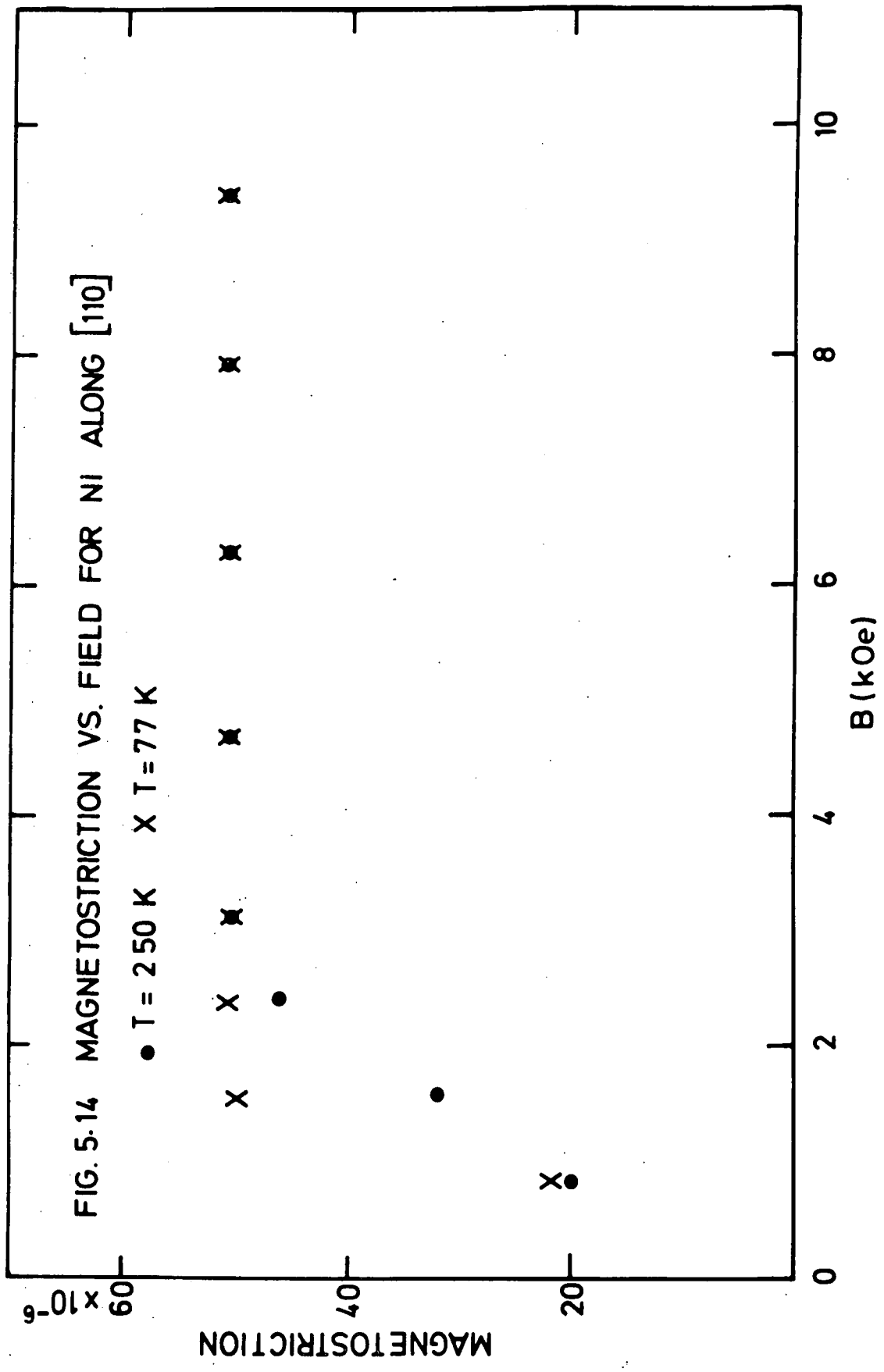
FIG. 5.14 MAGNETOSTRICTION VS. FIELD FOR NI ALONG [110]
● T = 250 K X T = 77 K
MAGNETOSTRICTION
× 10⁻⁶
60
40
20
0
2
4
6
8
10
B (kOe)

which in a good agreement wi tn values quoted by Chikazumi (1964 p. 173) as,

$$\lambda_{100} = -45.9 \times 10^{-6} \qquad \text{at room temperature}$$
$$\lambda_{111} = -24.3 \times 10^{-6}$$

These results weretaken as a reasonable justification for using tne gauge factors quoted by the makers of the gauges to calculate strain. An added check was obtained as described in Chapter 6.

CHAPTER 6

RESULTS AND DISCUSSION

6.1 Introduction

Measurements of magnetostriction for Gd-Tb alloys were carried out in the temperature range from 4.5 K to 250 K. Magnetic fields of up to 13 Tesla were available, but most of the samples were found to saturate before reaching the highest value of the field. To analyze the results the expression of Clark et al, Eq. (3.25), was used. The four magnetostriction coefficients $\lambda^{\gamma,2}$, $\lambda_2^{\alpha,2}$, $\lambda_1^{\alpha,2}$, and $\lambda^{\varepsilon,2}$ were obtained in accordance with the plane of measurement as given in Table (6.1).

TABLE (6.1) Magnetostriction coefficient of order 2.

Plane	Gauge Direction	Direction of saturation		Coefficient Obtained
		Initial	Final	
Basal plane	b	a	b	$-\lambda^{\gamma,2}$
b and c	c	b	c	$-\lambda_2^{\alpha,2}$
b and c	b	c	b	$-(\frac{\lambda^{\gamma,2}}{2} - \lambda_1^{\alpha,2})$
b and c	45° to c	c	45° to c	$(\frac{\lambda^{\gamma,2}}{8} - \frac{\lambda_2^{\alpha,2}}{4} - \frac{\lambda_1^{\alpha,2}}{4} - \frac{\lambda^{\varepsilon,2}}{2})$

The present study considers the magnetostriction coefficients up to only order 2. The curves obtained included high order coefficients and cannot be fully represented using only the cos 2θ term in Eq. (3.25). However, higher terms are very small as will be discussed later and only the amplitude of the curves were taken to analyze the results. The results of the measurements of the magnetostriction coefficients $\lambda^{\gamma,2}$, $\lambda_2^{\alpha,2}$, $\lambda_1^{\alpha,2}$, and $\lambda^{\varepsilon,2}$ will be discussed in that order.

6.2 The Magnetostriction Coefficient $\lambda^{\gamma,2}$

6.2.1 The Field Dependence of $\lambda^{\gamma,2}$

Measurements of $\lambda^{\gamma,2}$ were obtained for alloys of the four compositions

$Gd_{0.95}Tb_{0.05}$, $Gd_{0.80}Tb_{0.20}$, $Gd_{0.50}Tb_{0.50}$, and $Gd_{0.25}Tb_{0.75}$. Fig. (6.1) shows the saturation magnetostriction in the basal plane for $Gd_{0.80}Tb_{0.20}$ as a function of magnetic field direction at 6 K as the crystal was rotated in the magnetic field. The curve in Fig. (6.1) is not due to a cos 2θ dependence only, but the curves were simplified by raising the temperature above 80 K and curves similar to Fig. (6.2) were obtained. Also by increasing Tb content in the alloys the discrepancy from cos 2θ was less observed even at low temperatures as shown in Fig. (6.3). A similar shape of curve to Fig. (6.1) and Fig. (6.2) was obtained for the composition containing 5% Tb and to Fig. (6.3) for composition containing 50% Tb.

The field dependencies of $\lambda^{\gamma,2}$ for the four compositions are shown in Figs. (6.4), (6.6), (6.8), and (6.10) for various temperatures. The coefficients were positive over all temperature and field ranges. The crystals of low Tb content (Tb = 5% and Tb = 20%) tend to saturate at about 0.5 Tesla. As we increase the concentration of Tb the samples need a higher magnetic field. For a concentration of 50% of Tb about 1.5 Tesla was sufficient for saturation while the sample containing 75% was found to saturate at about 2 Tesla. However, in the later case a small positive slope is still detectable at 10 Tesla.

6.2.2 Temperature Dependence of $\lambda^{\gamma,2}$ Using Single-ion Theory.

The temperature dependence of the magnetostriction coefficients $\lambda^{\gamma,2}$ for the four compositions are shown in Figs. (6.5), (6.7), (6.9) and (6.11) respectively. The temperature dependence of the coefficient $\lambda^{\gamma,2}$ can be correlated with one of the Callen and Callen equations (1965). Using a classical field Hamiltonian they have found for one-ion interaction that the temperature dependence of the related magnetostriction coefficient is given by

$$\frac{\Delta l}{l}(T) = \frac{\Delta l}{l}(0) \frac{I_{l+\frac{1}{2}}[\mathcal{L}^{-1}(m)]}{I_{\frac{1}{2}}[\mathcal{L}^{-1}(m)]} \quad \text{.....(6.1),}$$

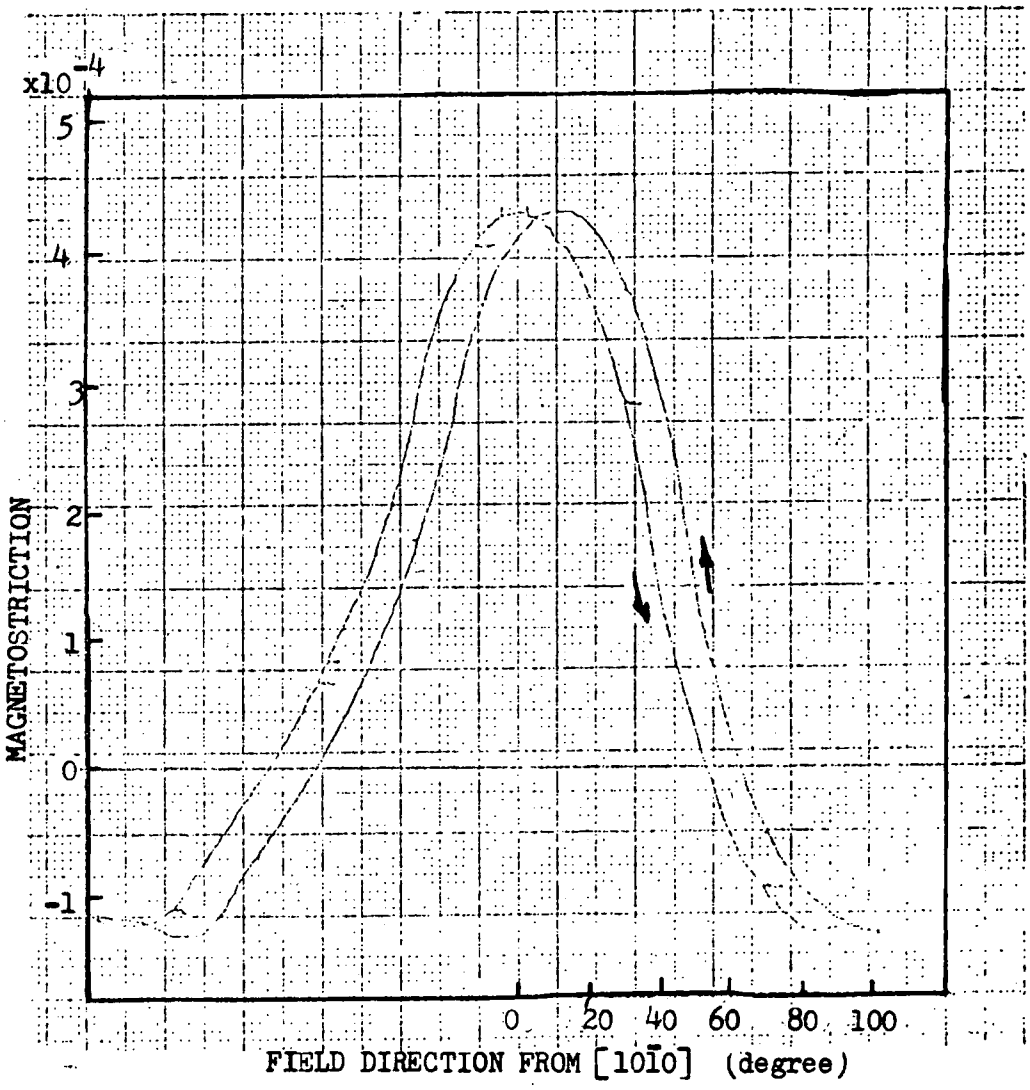

Fig.(6.1) Magnetostriction measured along the b-axis in the basal plane as a function of field direction at 6 K and 2 Tesla, for $Gd_{0.80}Tb_{0.20}$.

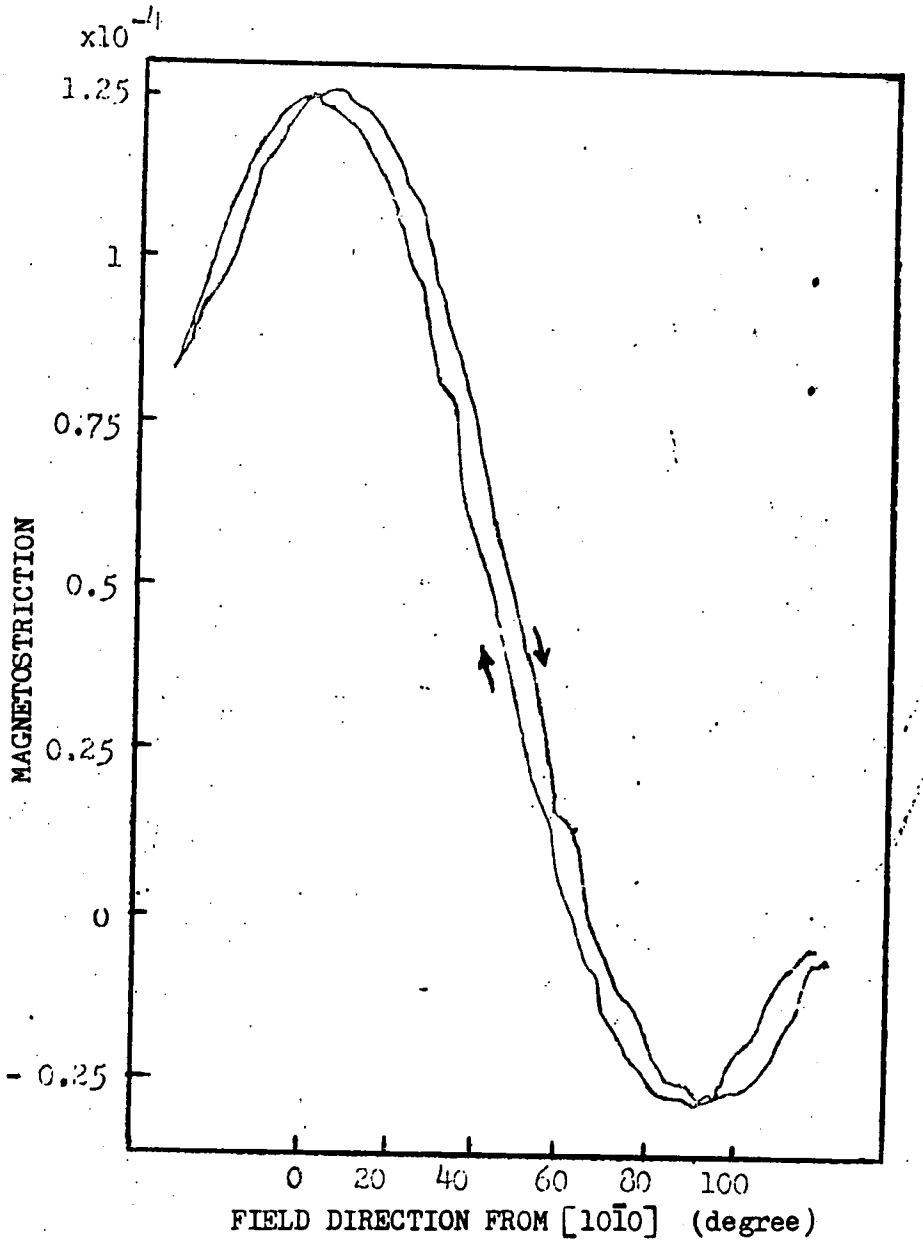

Fig.(6.2) Magnetostriction measured along the b-axis in the basal plane as a function of field direction at 200 K and 1 Tesla, for $Gd_{0.80}Tb_{0.20}$.

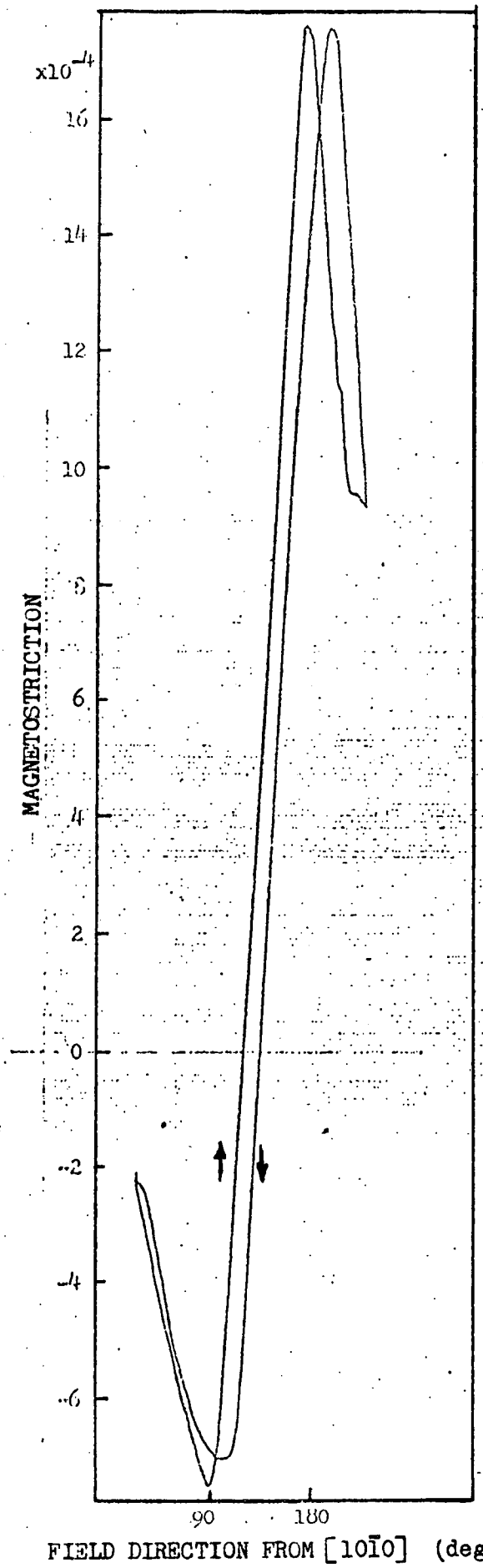

Fig.(6.3) Magnetostriction measured along the b-axis in the basal plane as a function of field direction at 8.9 K and 10 Tesla, for $Gd_{0.25}Tb_{0.75}$.

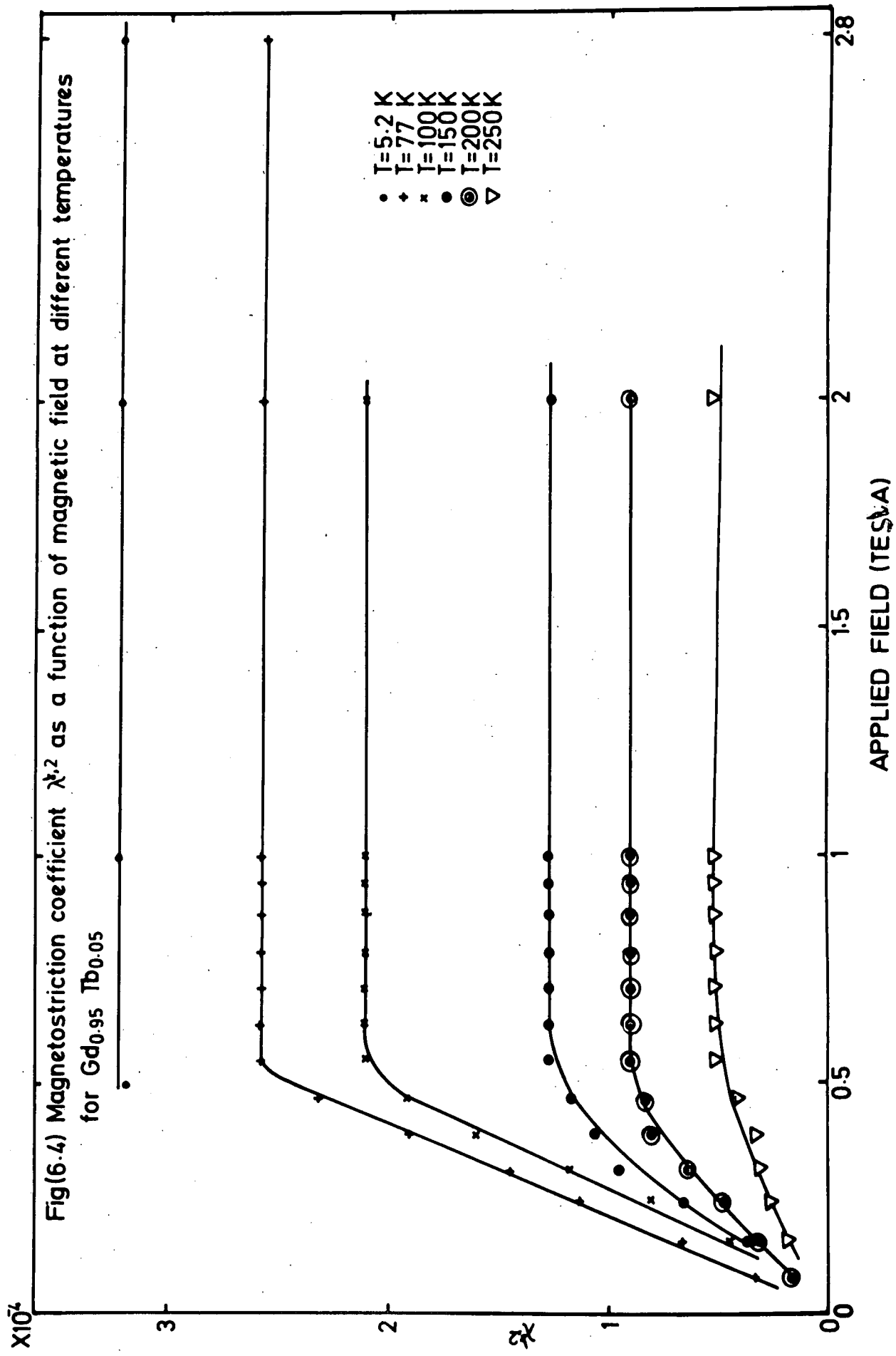

Fig(6.4) Magnetostriction coefficient λ^2 as a function of magnetic field at different temperatures for $Gd_{0.95}$ $Tb_{0.05}$

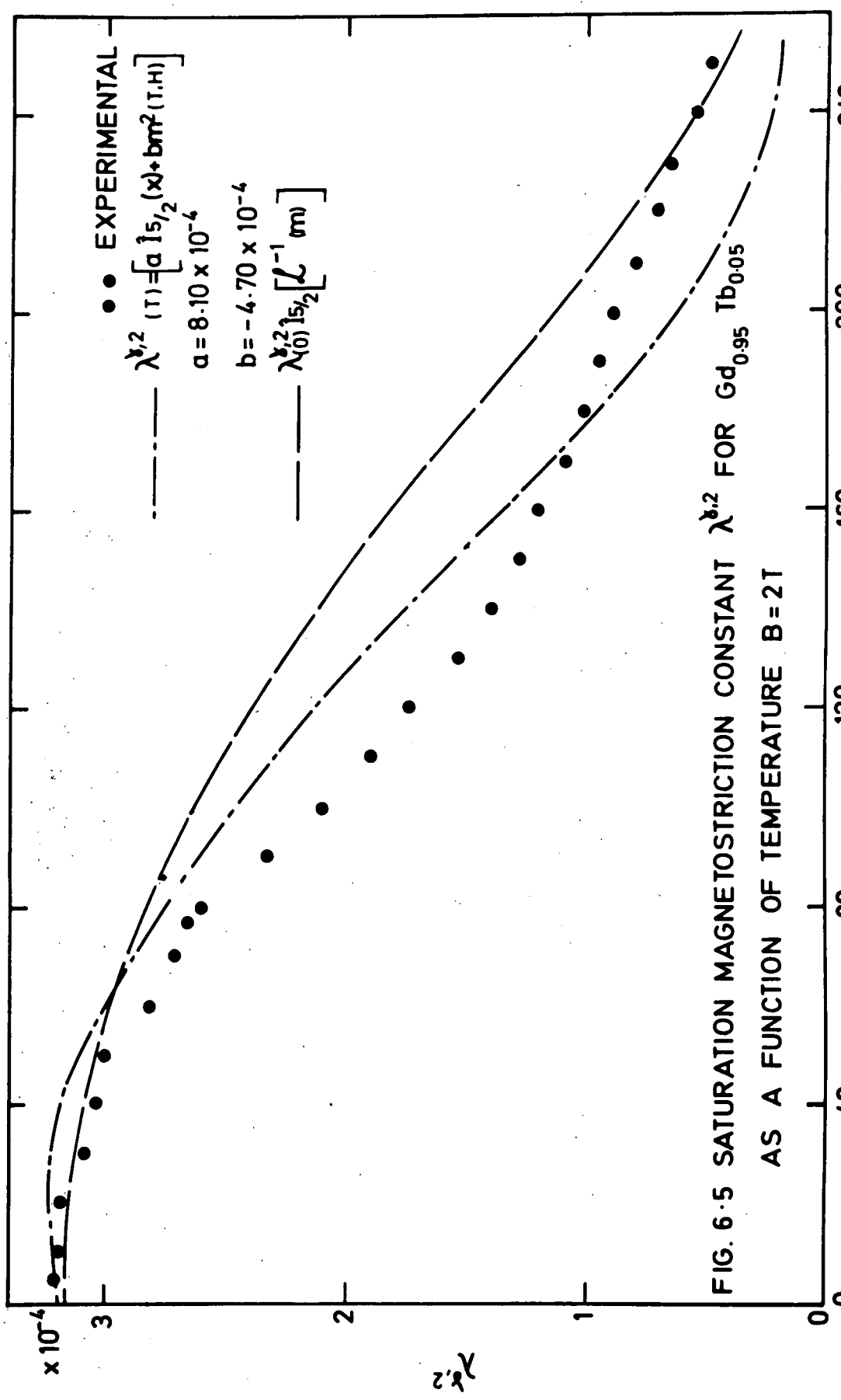

FIG. 6·5 SATURATION MAGNETOSTRICTION CONSTANT $\lambda^{\gamma,2}$ FOR $Gd_{0.95}\ Tb_{0.05}$ AS A FUNCTION OF TEMPERATURE B = 2 T

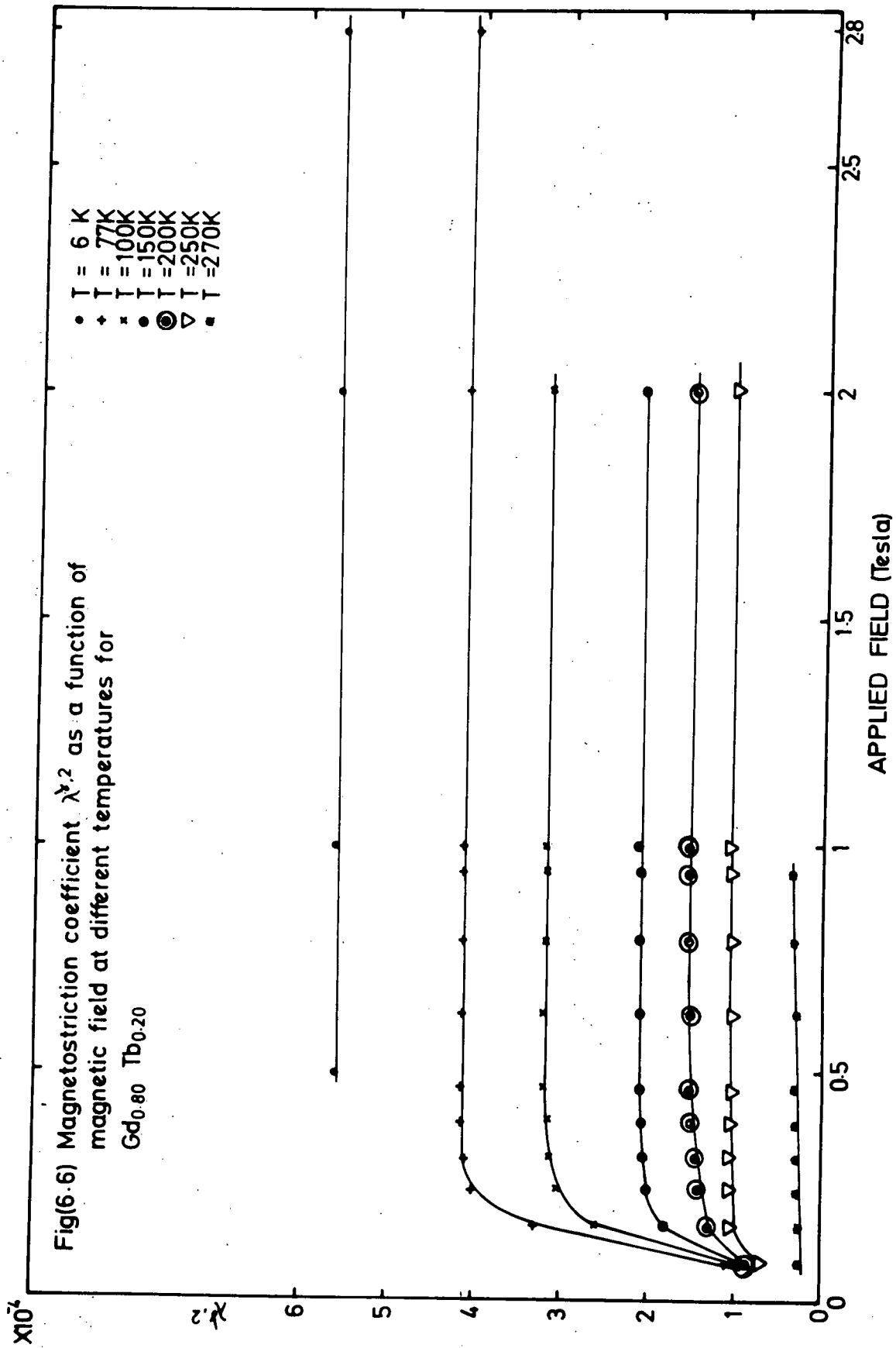

Fig(6.6) Magnetostriction coefficient $\lambda^{\gamma,2}$ as a function of magnetic field at different temperatures for $Gd_{0.80}$ $Tb_{0.20}$

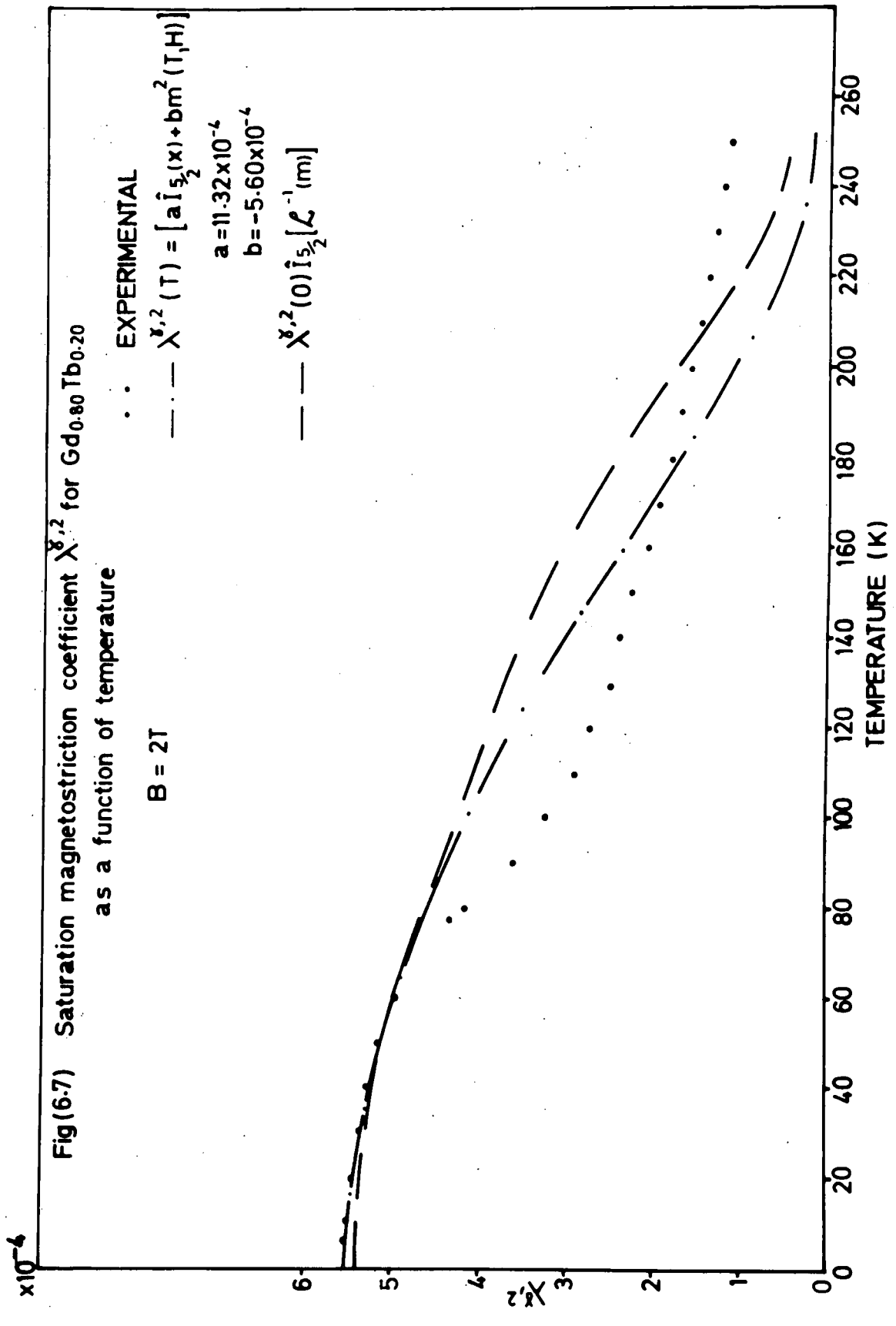
Fig(6·7) Saturation magnetostriction coefficient $\lambda^{\gamma,2}$ for $Gd_{0.80}Tb_{0.20}$
as a function of temperature
B = 2T
· · EXPERIMENTAL
— · — $\lambda^{\gamma,2}(T) = [a\hat{I}_{5/2}(x) + bm^2(T,H)]$
a = 11·32×10⁻⁴
b = −5·60×10⁻⁴
— — $\lambda^{\gamma,2}(0)\hat{I}_{5/2}[\mathcal{L}^{-1}(m)]$
×10⁻⁴
$\lambda^{\gamma,2}$
0
1
2
3
4
5
6
0
20
40
60
80
100
120
140
160
180
200
220
240
260
TEMPERATURE (K)

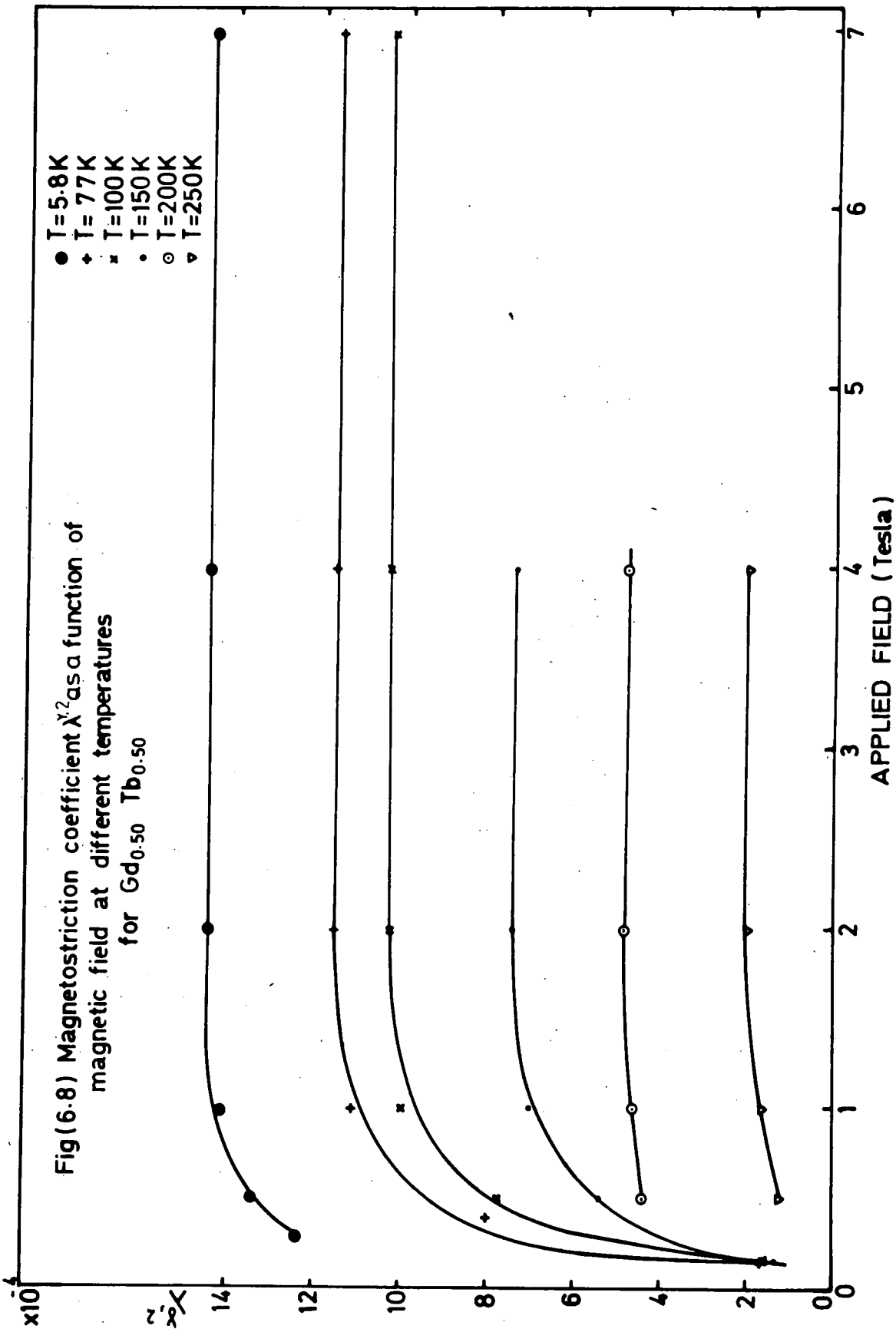

Fig(6.8) Magnetostriction coefficient λ^2 as a function of magnetic field at different temperatures for $Gd_{0.50}$ $Tb_{0.50}$

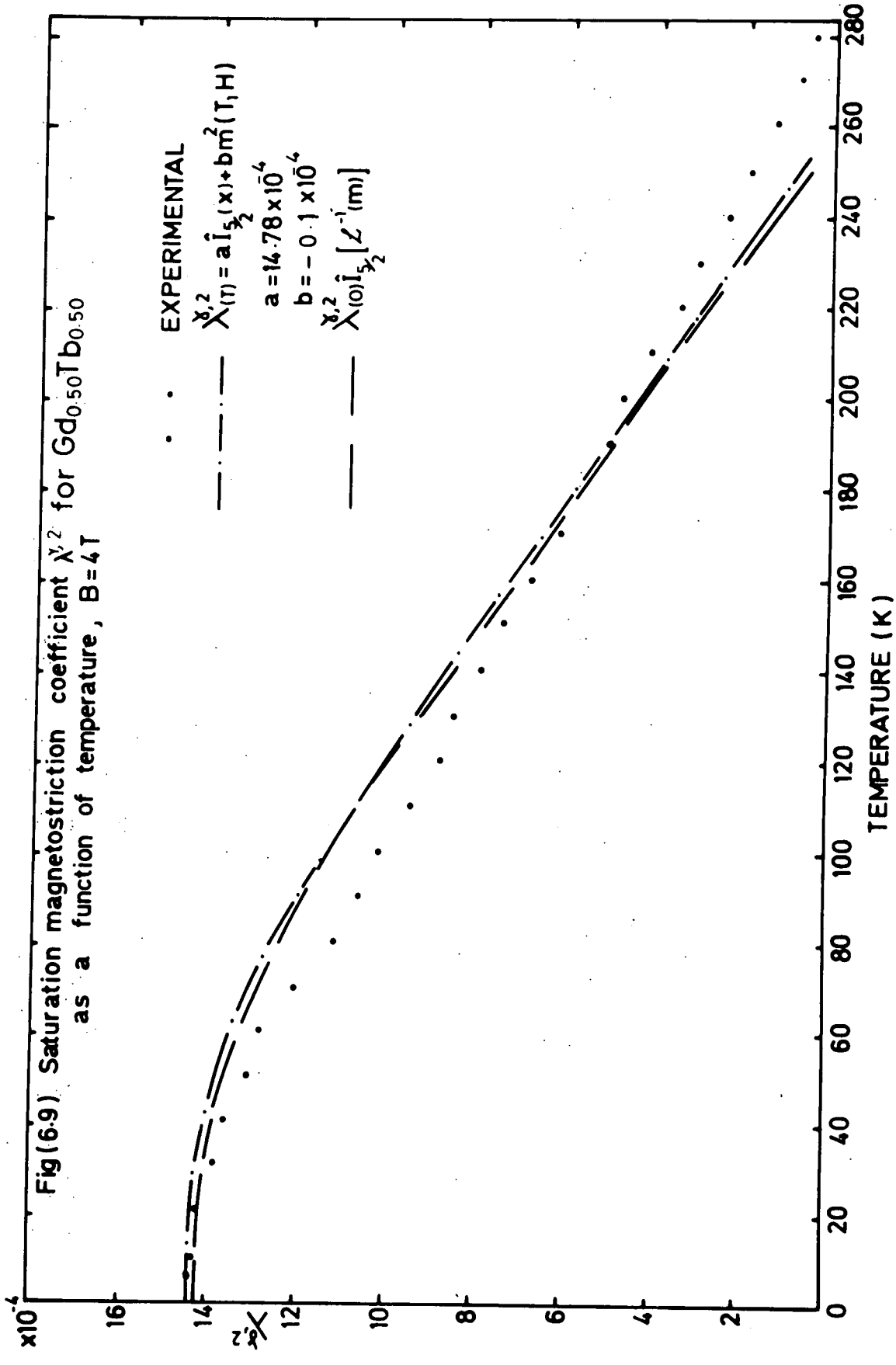
Fig(6.9) Saturation magnetostriction coefficient $\lambda^{\gamma,2}$ for $Gd_{0.50}Tb_{0.50}$ as a function of temperature, B=4 T
EXPERIMENTAL
$\lambda^{\gamma,2}_{(11)} = a\hat{I}_{5/2}(x) + bm^2(T,H)$
a = 14.78 x 10⁻⁴
b = - 0.1 x 10⁻⁴
$\lambda^{\gamma,2}_{(10)}\hat{I}_{5/2}[\mathcal{L}^{-1}(m)]$
x10⁻⁴
$\lambda^{\gamma,2}$
TEMPERATURE (K)

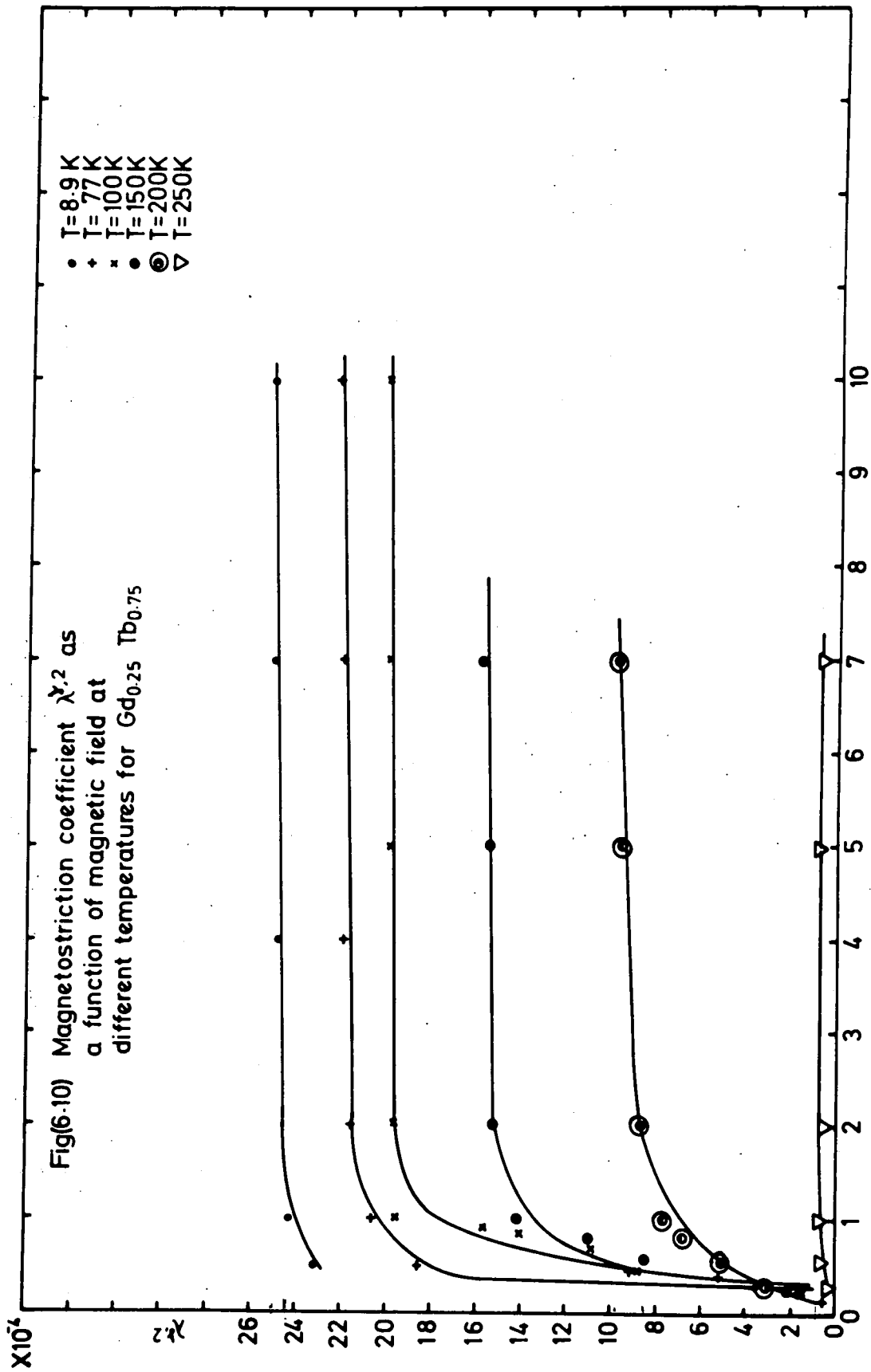

Fig(6.10) Magnetostriction coefficient λ'^2 as a function of magnetic field at different temperatures for $Gd_{0.25}$ $Tb_{0.75}$

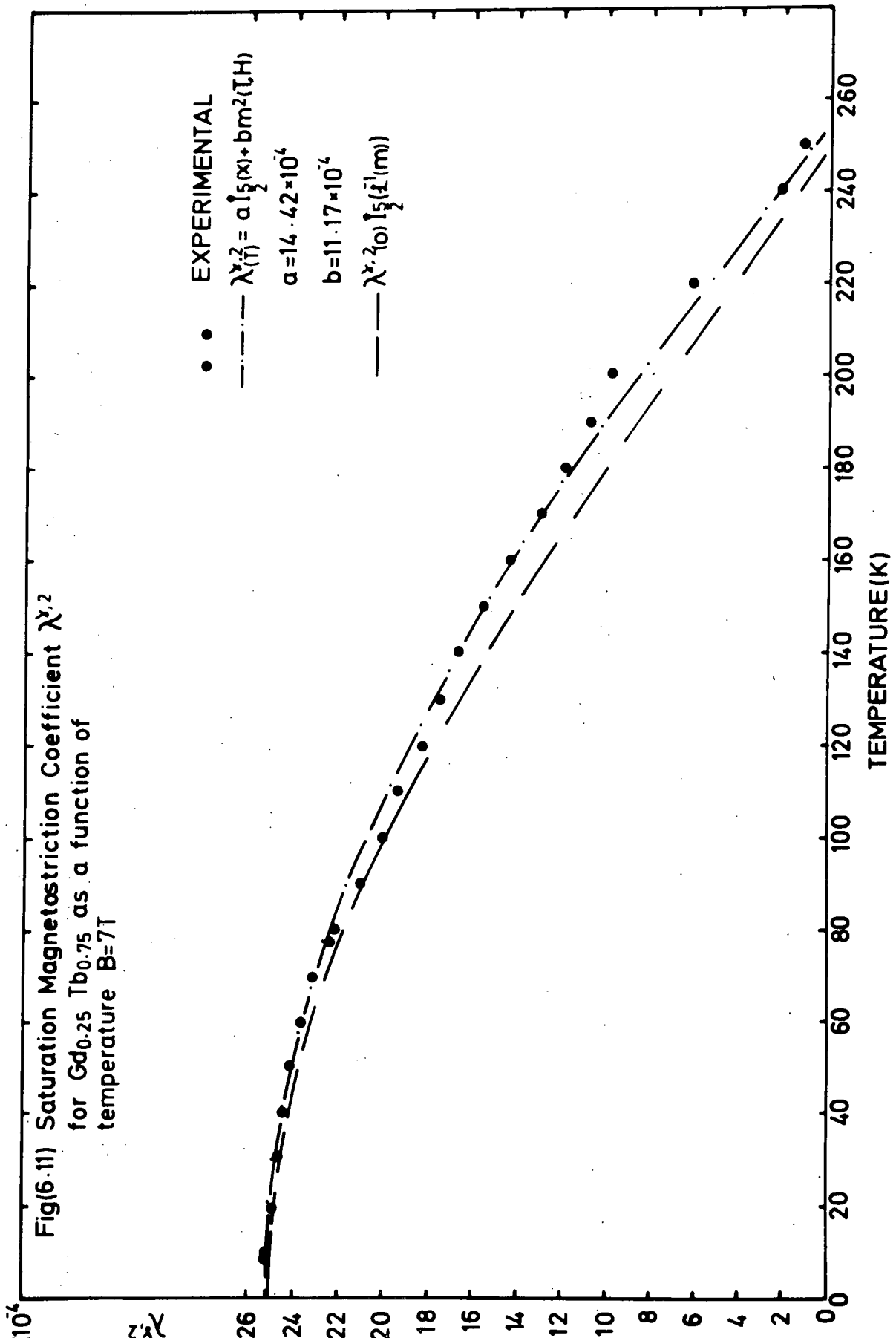

Fig(6.11) Saturation Magnetostriction Coefficient $\lambda^{\gamma,2}$ for $Gd_{0.25}\ Tb_{0.75}$ as a function of temperature B=7T

where I, $\mathcal{L}^{-1}$, and m take the meanings quoted in Chapter 3.

This may be written,

$$\frac{\Delta l}{l}(T) = \frac{\Delta l}{l}(0)\,\hat{I}_{l+\frac{1}{2}}[\mathcal{L}^{-1}(m)] = \frac{\Delta l}{l}(0)\,\hat{I}_{l+\frac{1}{2}}(x) \qquad \ldots\ldots\ldots(6.2),$$

where $x = [\mathcal{L}^{-1}(m)]$ and $\hat{I}_{l+\frac{1}{2}}$ is the reduced hyperbolic Bessel function which is the ratio of the hyperbolic Bessel function of order $(l + \frac{1}{2})$ to the hyperbolic Bessel function of order $\frac{1}{2}$. The argument x is to be considered as a parameter to be expressed in terms of the magnetization by inversion of the relationship given by Callen and Callen (1965) as

$$m = \hat{I}_{3/2}(x) = \coth x - \frac{1}{x} \qquad \ldots\ldots\ldots(6.3),$$

where $\hat{I}_{3/2}(x)$ is the familiar Langevin function.

In practice experimental values of m are usually available and corresponding values of x required. To facilitate this a graph, Fig. (6.12) was plotted so that direct reading of x could be made.

No magnetization values were available for Gd-Tb alloys and time did not allow the assembly of equipment to measure these so approximate values were estimated as follows.

The magnetization values of Tb obtained by Hegland et al (1963) and the magnetization values of Gd obtained by Nigh et al (1963) were plotted on one graph. The antiferromagnetic ordering in Tb is very easily overpowered to produce ferromagnetic alignment above the ordering temperature and since the values of Hegland et al were measured at 18 kOe, it was necessary to force the value of M_s to zero at the ordering temperature of 221 K. The values of the magnetic ordering temperatures and the low field magnetic moments for Gd-Tb alloys have been obtained by Nikitin et al (1977b), as shown in Fig. (4.2) and Fig. (4.3). These values were plotted on the same graph and lay between the values for the pure metals. Curves were then interpolated between the curves for the pure metals, starting and finishing at the critical temperature of the

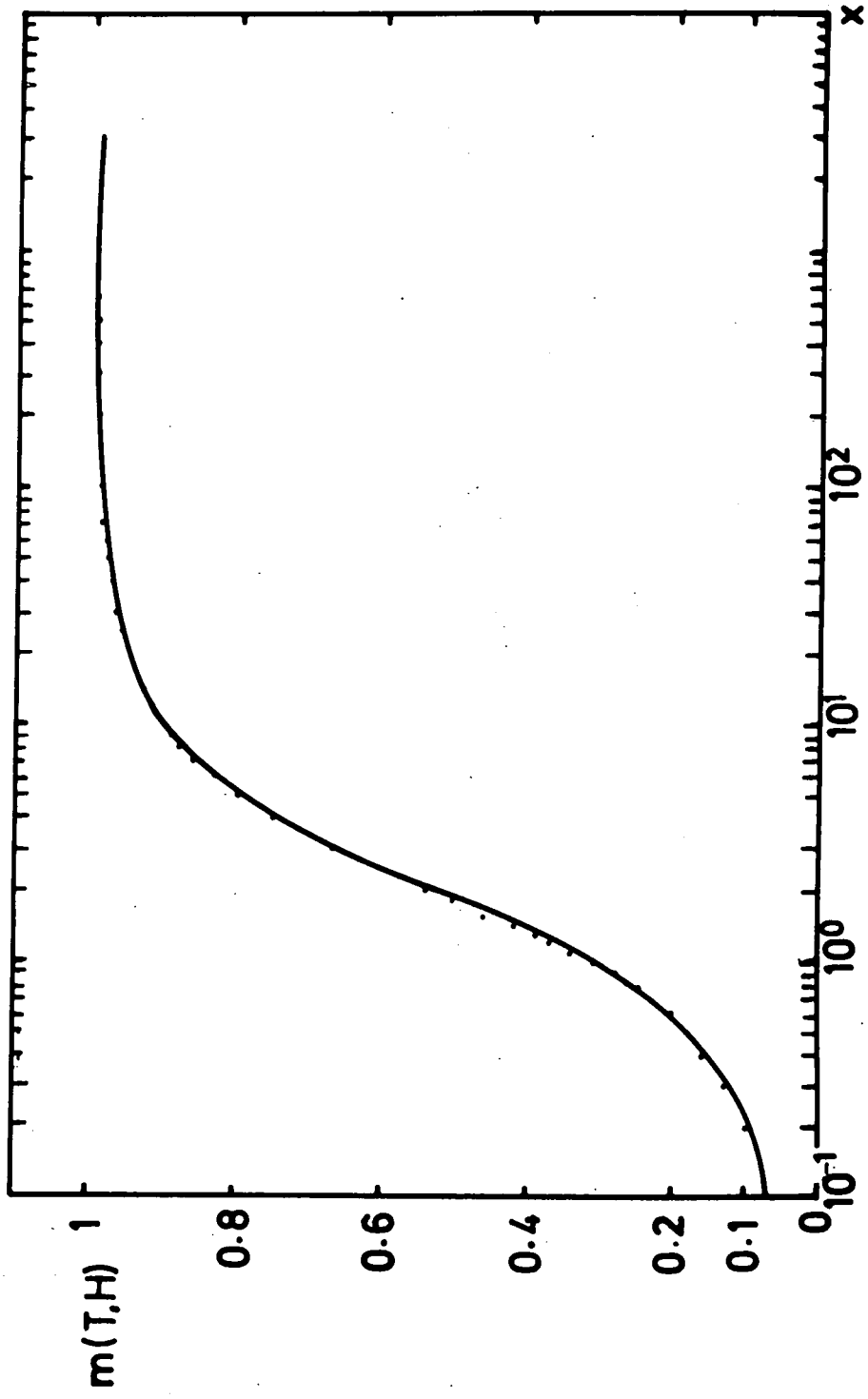

Fig(6.12) Graph showing form of relation given by the equation $m(T,H) = \text{Coth}\, x - \frac{1}{x}$

magnetic ordering and the low temperature magnetization for each composition of the Gd-Tb alloys. These curves give the magnetization of the alloys as shown in Fig. (6.13).

For $l = 2$ Eq. (6.2) wil be

$$\frac{\Delta l}{l}(T) = \frac{\Delta l}{l}(0)\ \hat{I}_{5/2}(x) \qquad \text{.....(6.4)}$$

This equation gives the temperature dependence of the strain calculated from the single-ion theory. The values of $\hat{I}_{5/2}(x)$ were obtained from data given by Welford (1975), shown in Appendix II and the theoretical magnetostriction coefficients $\lambda^{\gamma,2}$ were calculated from Eq. (6.4) by replacing the strain $\frac{\Delta l}{l}$ by the term $\lambda^{\gamma,2}$.

Normalization values of $\lambda^{\gamma,2}_{(0)}$ for the alloys were taken as,

$\lambda^{\gamma,2}_{(0)} = (3.22 \pm 0.4) \times 10^{-4}$ for $Gd_{0.95}Tb_{0.05}$

$\lambda^{\gamma,2}_{(0)} = (5.5 \pm 0.2) \times 10^{-4}$ for $Gd_{0.80}Tb_{0.20}$

$\lambda^{\gamma,2}_{(0)} = (14.4 \pm 1) \times 10^{-4}$ for $Gd_{0.50}Tb_{0.50}$

$\lambda^{\gamma,2}_{(0)} = (25.3 \pm 0.3) \times 10^{-4}$ for $Gd_{0.25}Tb_{0.75}$

Fig. (6.14) shows the temperature dependence of $\lambda^{\gamma,2}$ for the four alloys used, more details are given in Figs. (6.5), (6.7), (6.9), and (6.11). In each of these figures the experimental points are compared with curves based on Eq. (6.4). It is clear from the last four figures that $\lambda^{\gamma,2}$ does not follow the simple single-ion relation for the low Tb content. This theory gives consistently higher value of $\lambda^{\gamma,2}$ for Tb concentrations of 5% and 20%. The results for the $Gd_{0.95}Tb_{0.05}$ alloy follow the single-ion curve up to about 50 K, then higher values were obtained by the theory. The same drift was obtained beyond 70 K for the $Gd_{0.80}Tb_{0.20}$ alloy. The system $Gd_{0.50}Tb_{0.50}$ was better fitted by the single-ion curve, but this still gave a considerably higher value. The alloy with Tb content of 75% was well fitted by the single-ion mechanism, but at temperatures above 240 K the single-ion curve tends to fall well below the experimental values.

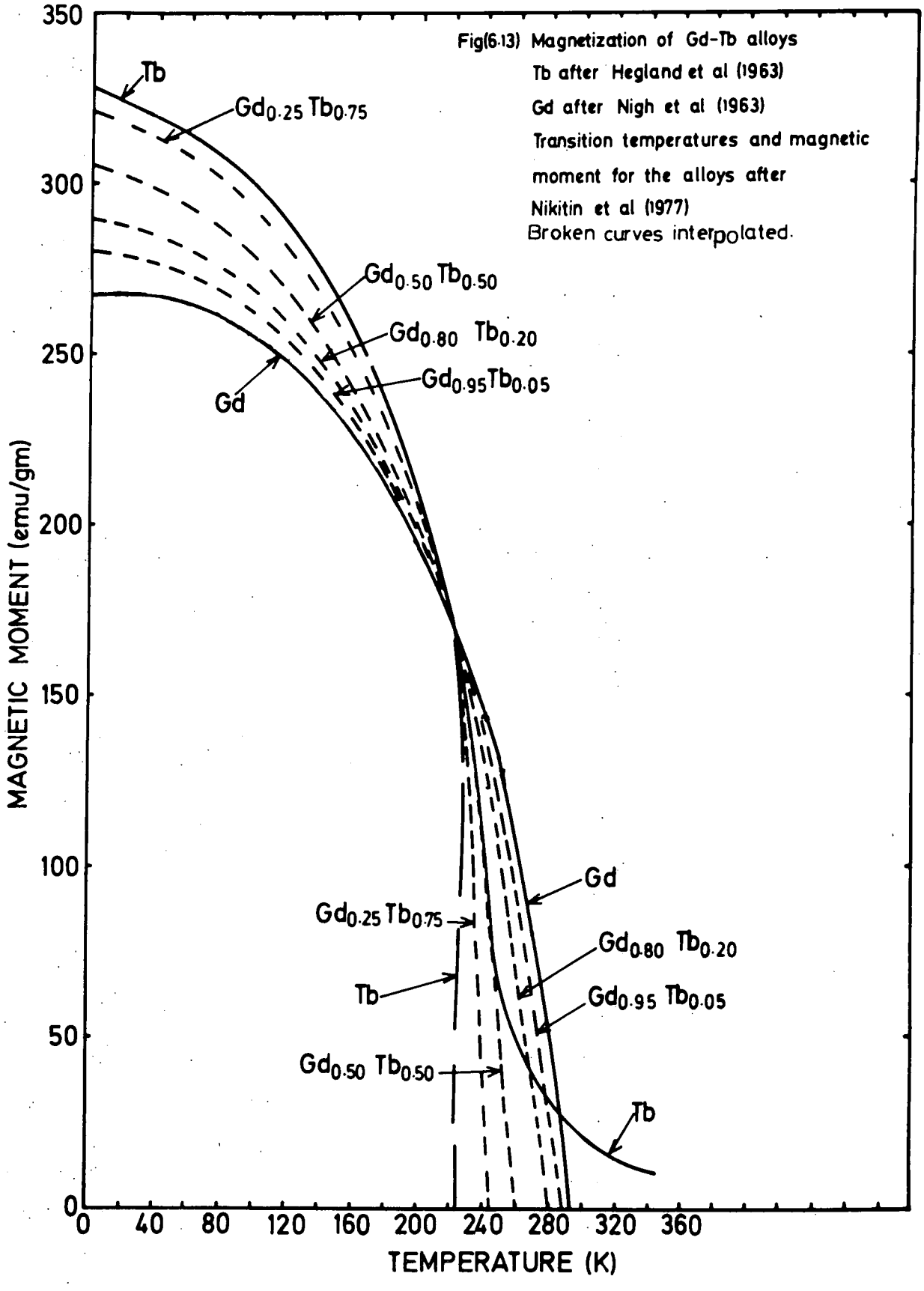

Fig(6.13) Magnetization of Gd-Tb alloys
Tb after Hegland et al (1963)
Gd after Nigh et al (1963)
Transition temperatures and magnetic moment for the alloys after Nikitin et al (1977)
Broken curves interpolated.

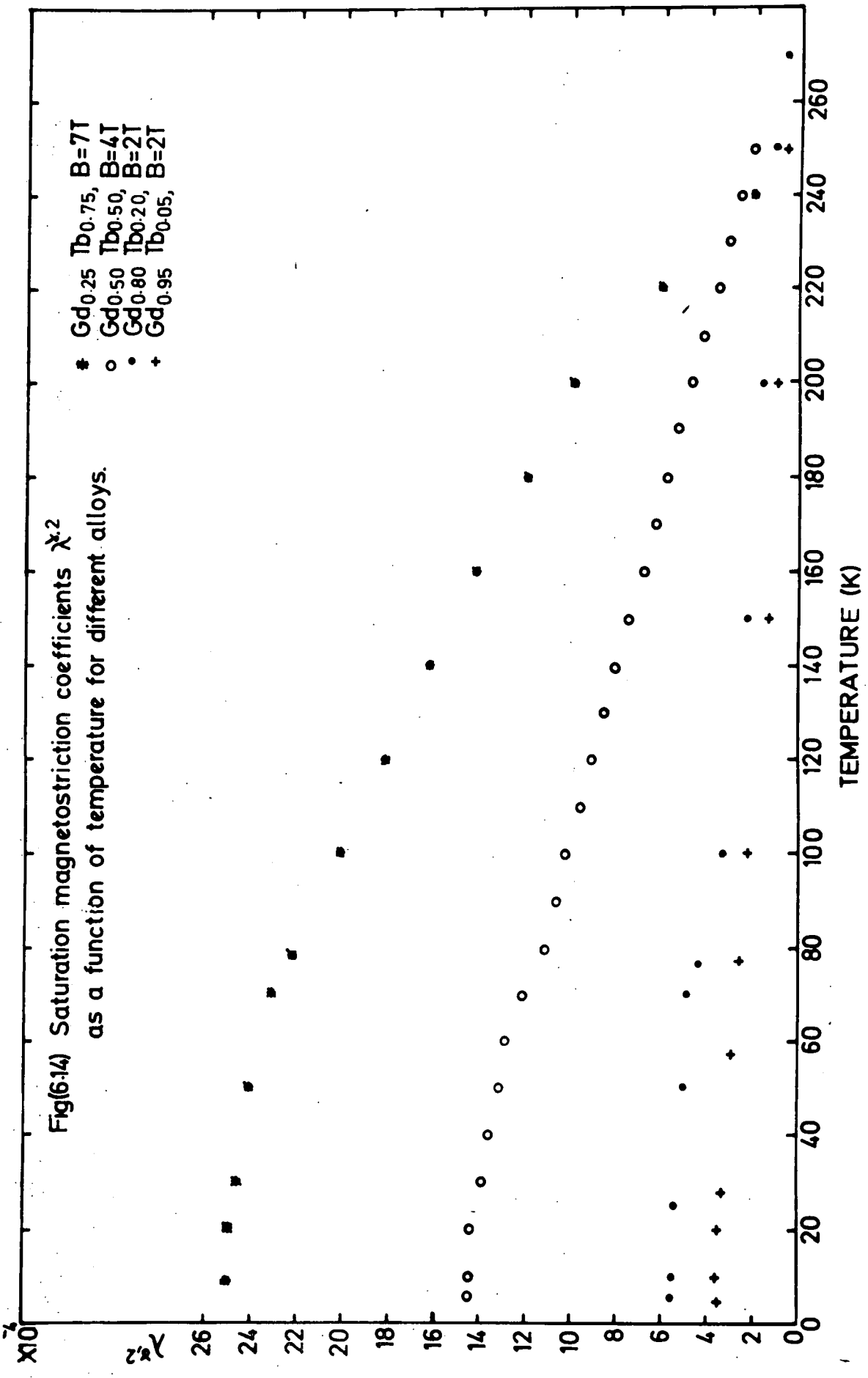

Fig(6.14) Saturation magnetostriction coefficients λ^{2}_{2} as a function of temperature for different alloys.

If the logarithm of the measured values is plotted against $\hat{I}_{5/2}(x)$ a straight line of slope equal to unity should be obtained if the system follows the single-ion theory as suggested by Tasuya et al (1964). Fig. (6.15) shows a log/log plot of the coefficient $\lambda^{\gamma,2}$ against $\hat{I}_{5/2}\,[\mathcal{L}^{-1}(m)]$. It is clear from this figure that the system $Gd_{0.25}Tb_{0.75}$ follows the single-ion theory with a slope very close to unity except at the high temperature of 240 K which is near to the Néel point. The results for other compositions do not fit well to the straight line suggested by Tasuya et al. It is not unreasonable to suppose that the single-ion theory will be inadequate for alloys containing a high proportion of Gd.

6.2.3. Temperature Dependence of $\lambda^{\gamma,2}$ Using an Expression Containing a Term Representing a Two-ion Mechanism.

In the case of Gadolinium Callen and Callen (1965) have found that the magnetostriction coefficient $\lambda^{\gamma,2}$ data obtained from Coleman (1964) were fitted well by the expression,

$$\lambda^{\gamma,2}(T) = a\,\hat{I}_{5/2}(x) + b\,m^2\,(T,H) \qquad .....(6.5)$$

The first term indicates the single-ion mechanism and a takes a form,

$$a = \left[\frac{(2S+3)!}{5!\,(2S-2)!}\right]^{\frac{1}{2}} \quad \frac{1}{C^{\gamma}} \sum_{f} \tilde{B}^{\gamma}(f) \qquad .....(6.6)$$

The second term indicates the two-ion interaction and b has been given as

$$b = \frac{\sqrt{6}\;S}{(S+1)(2S+1)} \quad \frac{1}{C^{\gamma}} \sum_{(f,g)} \tilde{D}^{\gamma}(f,g) \qquad .....(6.7)$$

$\tilde{B}^{\gamma}(f)$ and $\tilde{D}^{\gamma}(f,g)$ are the single-ion and two-ion magnetoelastic coupling constants as mentioned in Section (3.6), C is the elastic constant, and S is the spin operator.

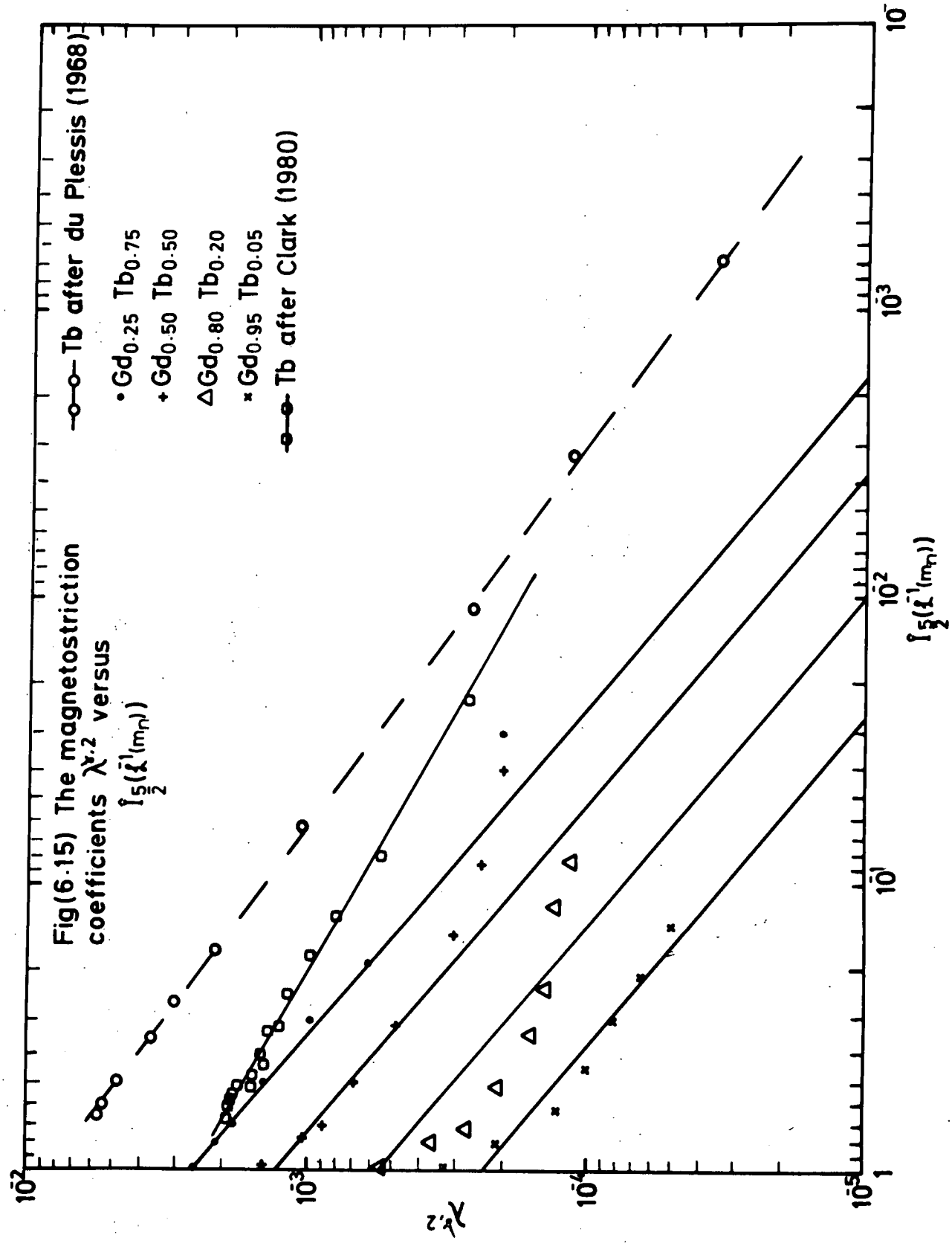

Fig(6.15) The magnetostriction coefficients $\lambda^{\gamma,2}$ versus $f_{\frac{5}{2}}(\xi^{-1}(m_\eta))$

The term x in Eq. (6.5) is to be expressed in terms of the reduced magnetization m by Eq. (6.3).

A computer program, shown in detail in Appendix I, was used to calculate the values of $\lambda^{\gamma,2}(T)$ from Eq. (6.5) using a least squares technique to obtain the values of a and b which best fit the experimental results. The values of the magnetization as a function of temperature were obtained as described before. From these results values of $\hat{I}_{5/2}(x)$ were obtained using the data given in Appendix II. Figs. (6.5), (6.7), (6.9), and (6.11) show the temperature dependence of $\lambda^{\gamma,2}$ for the four alloy compositions used and the values of a and b giving the best fit. Table (6.2) shows the variation of the two terms a and b with the composition of the alloy.

TABLE (6.2): The variation of a and b with the alloy composition for $\lambda^{\gamma,2}$.

Composition	a x 10^4	b x 10^4
Gd, after Callen & Callen (1965)	3.51	-2.43
$Gd_{0.95}Tb_{0.05}$	8.10	-4.70
$Gd_{0.80}Tb_{0.20}$	11.3	-5.60
$Gd_{0.50}Tb_{0.50}$	14.78	-0.10
$Gd_{0.25}Tb_{0.75}$	14.4	11.17
Tb, after Clark (1980)	-37.10	58

The values of the coefficient $\lambda^{\gamma,2}$ obtained for the sample $Gd_{0.95}Tb_{0.05}$ by the experiment still do not follow the curve representing Eq. (6.5) even at very low temperatures, though the curve lies generally closer than that based on Eq. (6.2). For a content of 20% of Tb the experimental results follow Eq. (6.5) well up to about 70 K, then higher values were obtained using the theory up to 170 K above which lower values were obtained. For the $Gd_{0.50}Tb_{0.50}$ sample there was little difference between the values calculated using the single-ion theory or those using Eq. (6.5). The specimen with 75% Tb gives a somewhat better fit using Eq. (6.5) than with the single-ion mechanism. Fig. (6.16a) shows the saturation values of magnetostriction coefficient $\lambda^{\gamma,2}$ for the four compositions used and the pure metals, Gd after Mishima et al (1976) and Tb after du Plessis (1968). Note that the $\lambda^{\gamma,2}$ scale is logarithmic. A very large change of $\lambda^{\gamma,2}$ was observed by adding a small amount of Tb to the alloy. The curves obtained for the specimens containing 5%, 20%, and 50% of Tb do not fall so rapidly as those for the elements in the higher temperature region, but at 75% Tb the curve is similar to that for Tb. Clark (1980) has measured the magnetostriction coefficent $\lambda^{\gamma,2}$ of a Tb single crystal using the x-ray diffraction technique between 135 K and the Curie point of 217 K at zero applied field. His values are about 2.5 times smaller than those of du Plessis (1968) and Rhyne and Legvold (1965). The single-ion theory was used to compare Clark's experimental results with values calculated from Eq. (6.4) as shown in Fig. (6.16b). The normalized $\lambda^{\gamma,2}_{(0)}$ was obtained by extrapolating the value at 135 K to 0 K. This was achieved by fitting the $\hat{I}_{5/2}(x)$ curve to the experimental point at 135 K and then using it as an extrapolation function. The magnetization values were obtained from the neutron diffraction measurements by Dietrich and Als-Nielsen (1967). They measured the spontaneous magnetization from the intensity of magnetic reflections in neutron diffraction peaks as a

Fig(6.16a) Saturation magnetostriction coefficient $\lambda^{\gamma,2}$ as a function of temperature, for different alloys and the pure metals.
Tb after du Plessis (1968)
Gd after Mishima et al (1976)

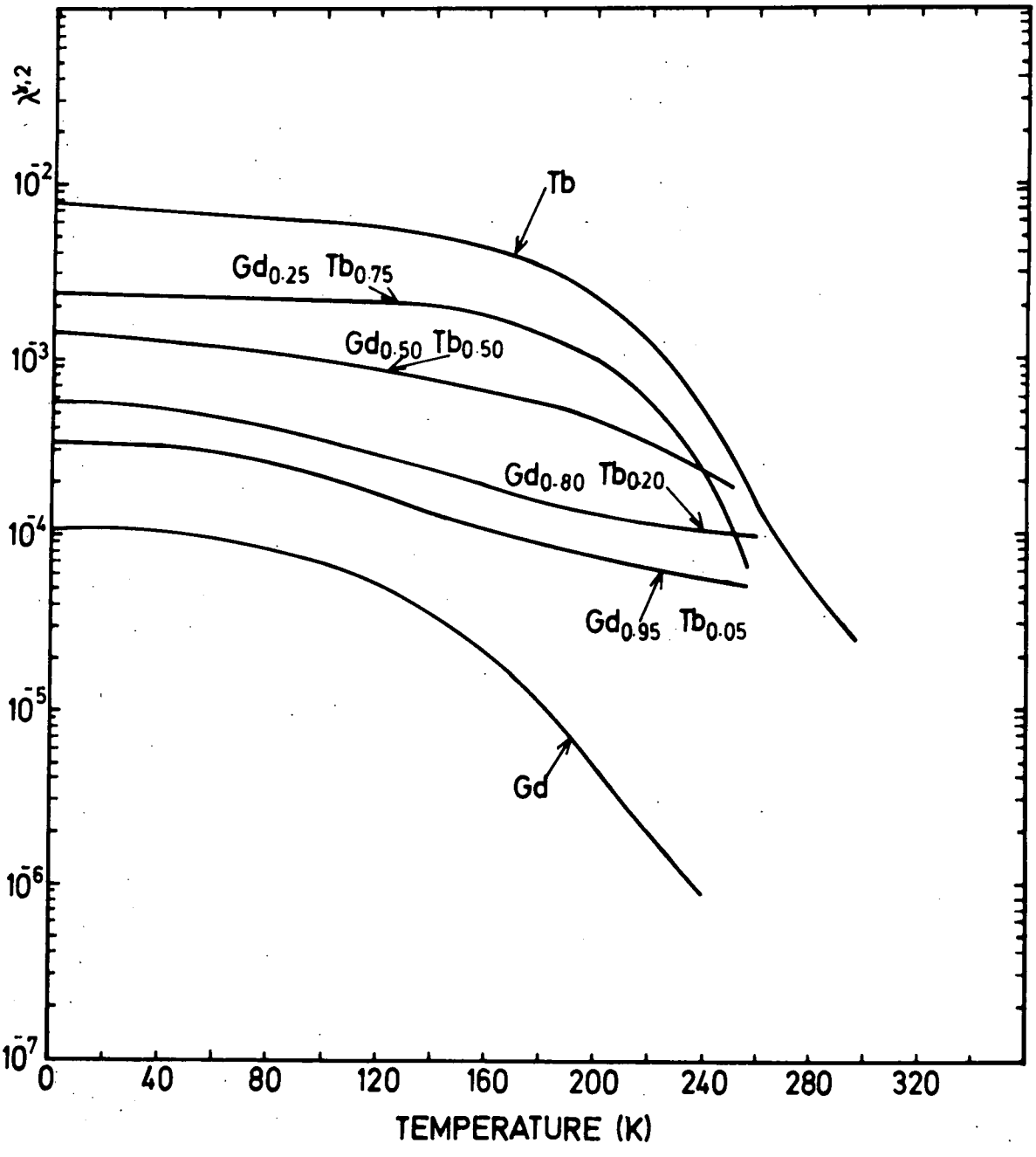

function of temperature between 100 K and the Curie point of 216 K. The curve was extrapolated to 0 K. The values of $\hat{I}_{5/2}(x)$ were obtained from the tables in Appendix II.

It is clear from Fig.(6.16b) that the single-ion theory does not give a reasonable representation of magnetostriction values measured at zero field. While it is possible to draw a straight line along the experimental points on a log/log plot of $\lambda^{\gamma,2}$ versus $\hat{I}_{5/2}(x)$ as shown in Fig. (6.15), this line does not lie with a similar slope to those for the alloys or the pure metal Tb. It is clear from Fig. (6.16b) that by introducing a term representing a two-ion interaction as in Eq. (6.5) the values calculated from this gave a reasonable representation of the temperature variation of the experimental results. Appropriate values of a and b are given in Table (6.2)

6.2.4 Variation of $\lambda^{\gamma,2}$ with alloy composition.

Fig. (6.17) shows the normalized saturation magnetostriction coefficients (at 0 K) as a function of alloy composition. The results obtained do not agree with those reported by Nikitin et al (1977b), who found that $\lambda^{\gamma,2}$ increases linearly with increasing Tb concentration. The present results are capable of being represented by an exponential relation.

$$\lambda^{\gamma,2}_{(0)} = A\, e^{BC} \qquad \text{.....(6.8),}$$

where A and B are constants having the values,

$$A = 81.10 \times 10^{-4}$$

$$B = -0.04$$

and C is the concentration of Gd in the alloy.

Fig. (6.17) shows the values to lie on a smooth curve which extrapolates to the values given by Mishima for pure Gd and by du Plessis for Tb. This gives another reasonable justification for using the gauge factors quoted by the makers of the strain gauges to calculate the strain.

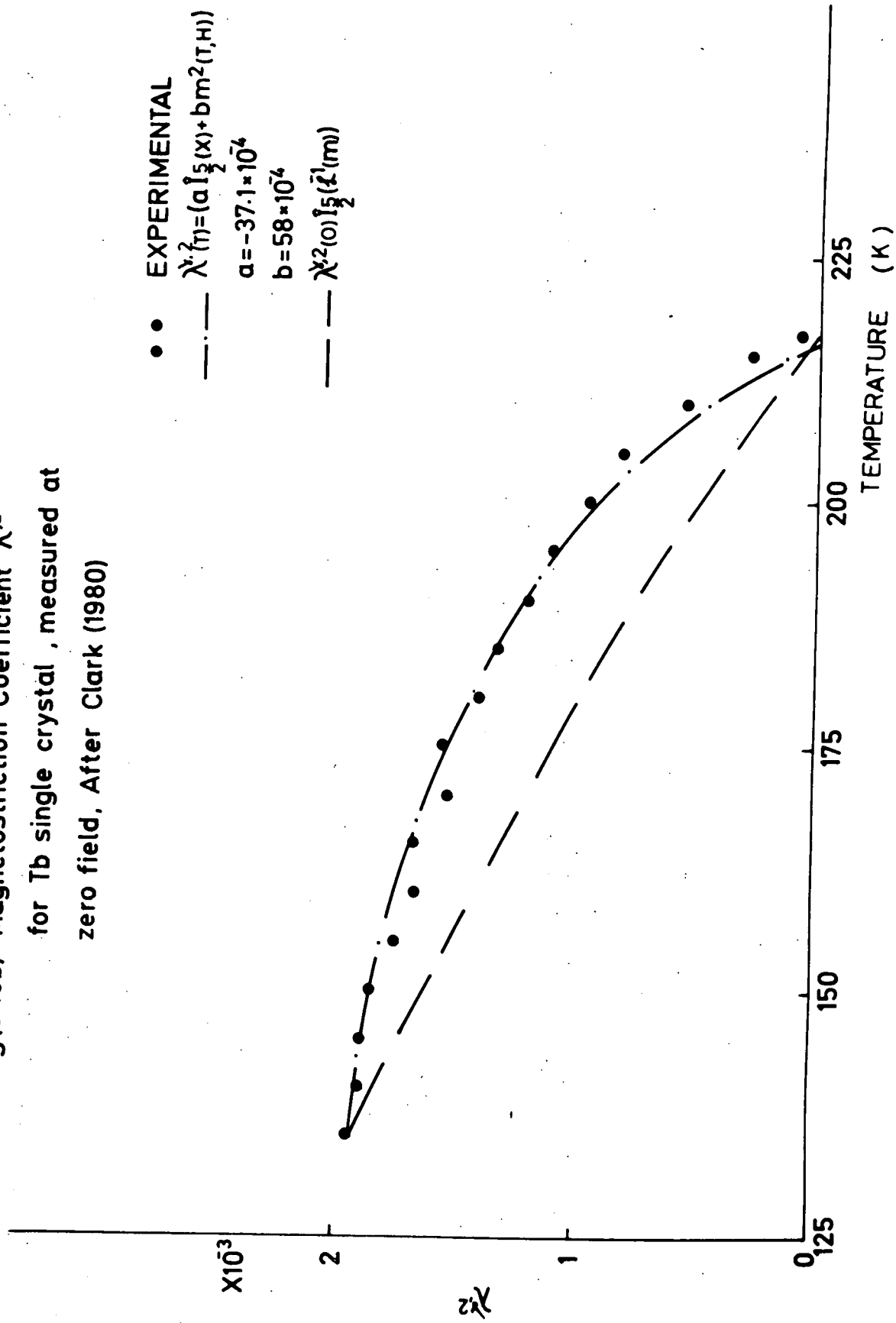

Fig (6.16b) Magnetostriction Coefficient $\lambda^{\gamma,2}$ for Tb single crystal, measured at zero field, After Clark (1980)

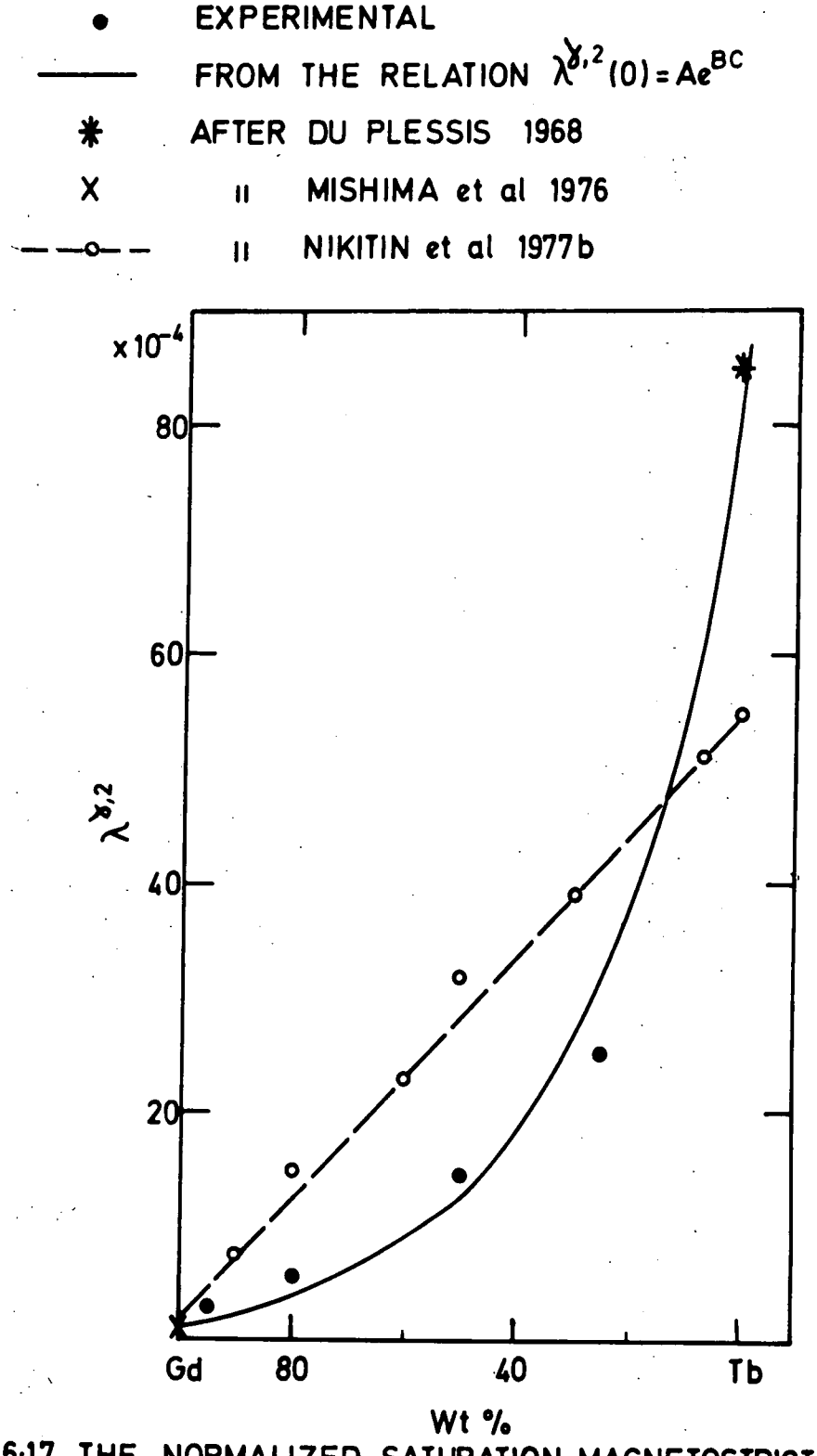

FIG. 6·17 THE NORMALIZED SATURATION MAGNETOSTRICTION COEFFICIENT $\lambda^{\gamma,2}$ AS A FUNCTION OF ALLOYS COMPOSITION.

6.3 The Magnetostriction Coefficient $\lambda_2^{\alpha,2}$

6.3.1 The Field Dependence of $\lambda_2^{\alpha,2}$

The coefficient $\lambda_2^{\alpha,2}$ can be determined by a 90° rotation measuring the strain along the c-axis in a b-c axis sample. Figs. (6.18), (6.19), and (6.20) show the variation of magnetostrictive strain along the c-axis for $Gd_{0.95}Tb_{0.05}$ as the crystal was rotated in the magnetic fields of 0.5, 1 and 4 Tesla respectively. Figs. (6.21), (6.22), (6.23), and (6.24) show similar results at a field of 1 Tesla as the temperature was raised from 8.8 K to 77 K for the specimen $Gd_{0.80}Tb_{0.20}$. These curves show anomalous behaviour in the region of the minimum which splits into a double minimum with a crateriform profile. The minima are at approximately 90° to the b-axis and the splitting is about 10°. These anomalies disappear on raising the field when the minima tend to become very sharp as shown in Fig. (6.19) and Fig. (6.20). Also they decrease with increasing temperature and disappear completely at about 70 K as shown in Figs. (6.21) to (6.24).

The curves cannot be represented by Eq. (3.25) of $l = 2$ or Eq. (3.29) of $l = 4$ with the term in cos 2θ alone. Similar anomalies were observed in the magnetostriction measurements on Gd by Mishima et al (1976) at $\theta = 75°$ and to represent these inflection points adequately they had to use a higher order magnetostriction expression as quoted in Eq. (3.30) with $l = 6, 8$. Rodbell and Moore (1964) observed in ferromagnetic resonance measurements on Gd that there is an inflection point at $\theta = 78°$ at 4.2 K and 20 K and they had to use higher order anisotropy constants with $l = 4, 6, 8$, i.e. out to $K_8 \sin^{16}\theta$. No similar anomalies were observed for the two samples $Gd_{0.50}Tb_{0.50}$ and $Gd_{0.25}Tb_{0.75}$. The curves show another anomalous behaviour in the region of the maximum where the magnetostriction value reaches a higher value before it decreases to the minimum. These anomalies were observed for the two samples containing 20% and 50% of Tb, and did not disappear with raising the temperature up

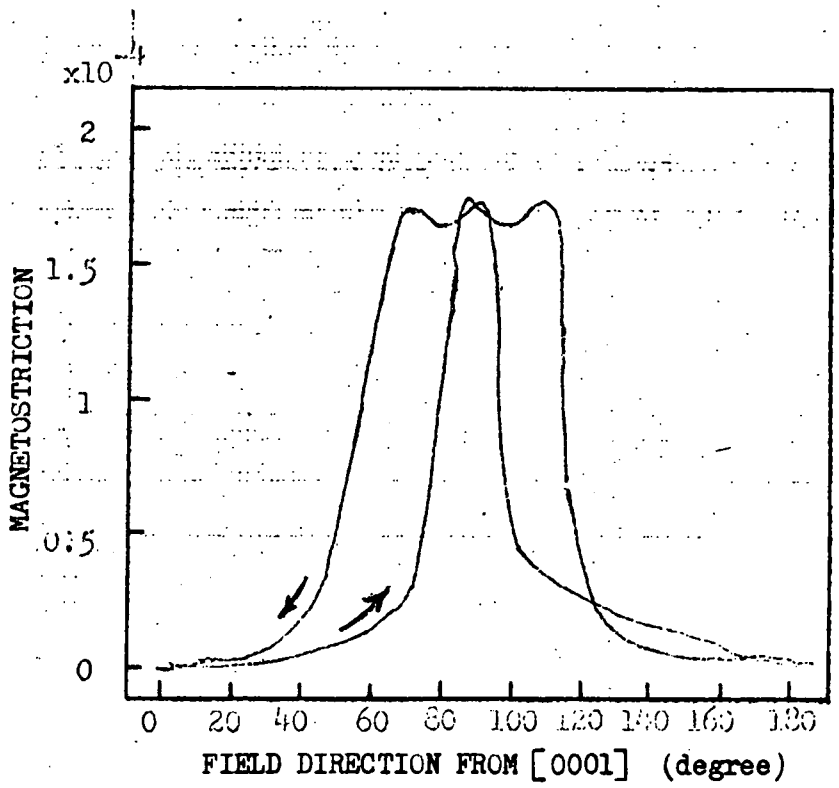

Fig.(6.18) Magnetostriction measured along c-axis in plane containing b and c axes as a function of field direction at 5.8 K and 0.5 Tesla, for $Gd_{0.95}Tb_{0.05}$.

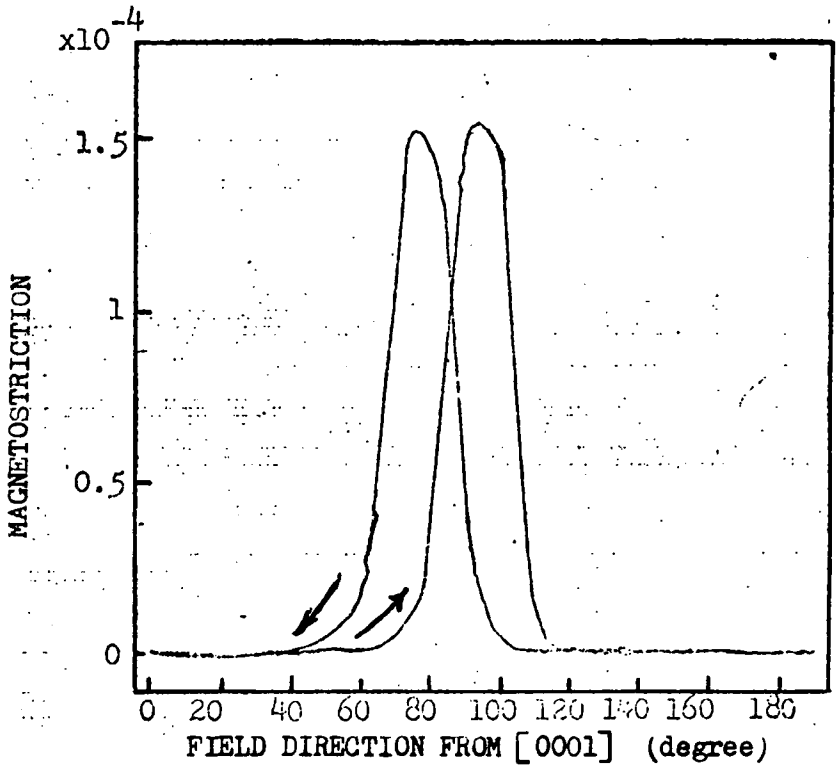

Fig.(6.19) Magnetostriction measured along c-axis in plane containing b and c axes as a function of field direction at 5.8 K and 1 Tesla, for $Gd_{0.95}Tb_{0.05}$.

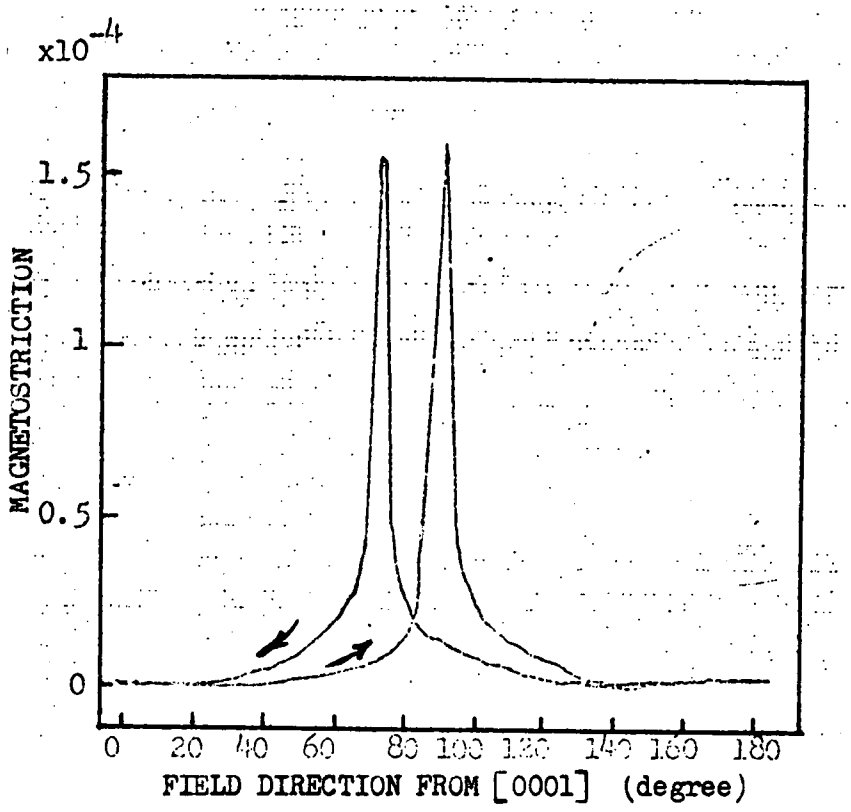

Fig.(6.20) Magnetostriction measured along c-axis in plane containing b and c axes as a function of field direction at 5.8 K and 4 Tesla, for $Gd_{0.95}Tb_{0.05}$.

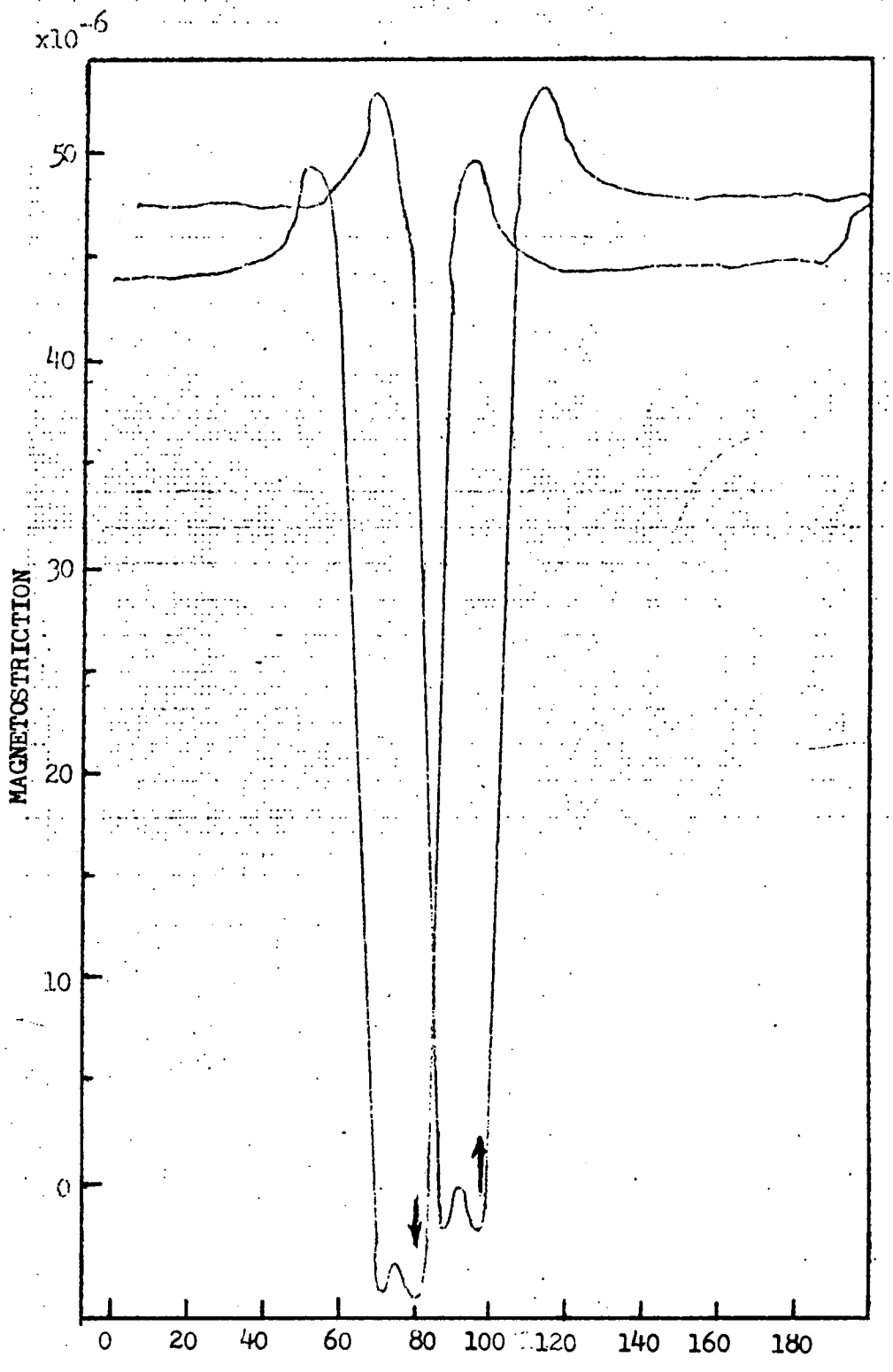

Fig.(6.21) Magnetostriction measured along c-axis in plane containing b and c axes as a function of field direction at 8.8 K and 1 Tesla, for $Gd_{0.80}Tb_{0.20}$.

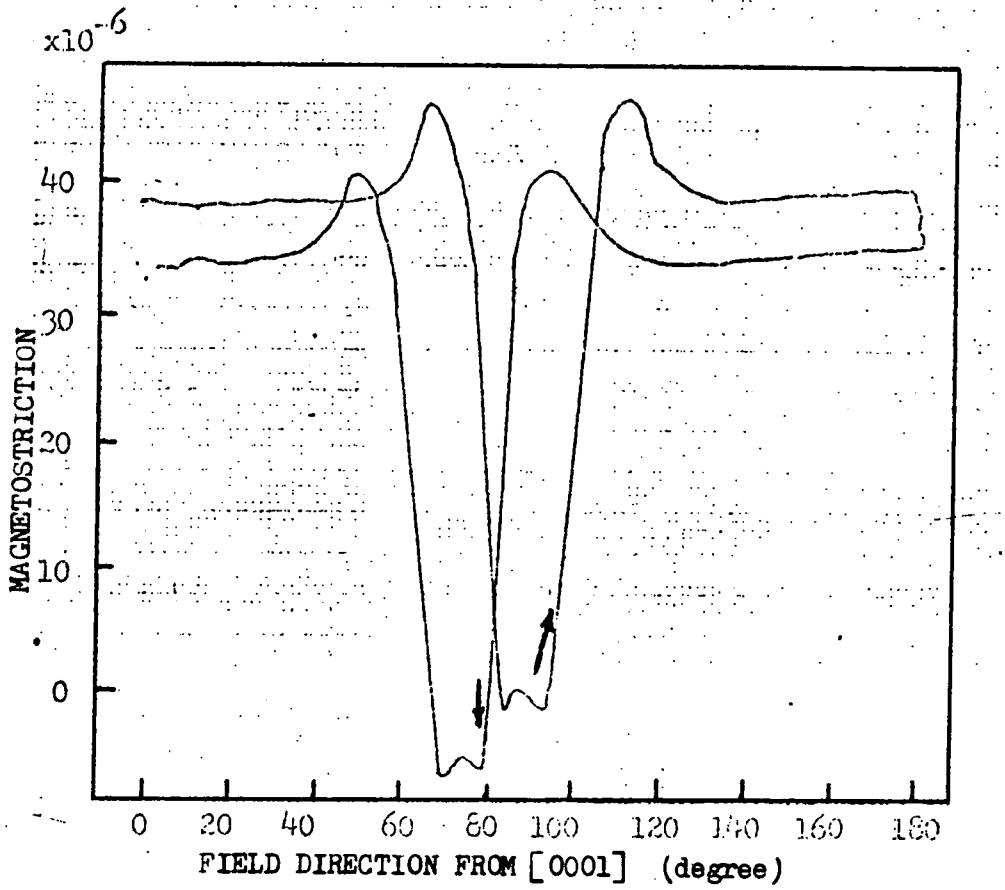

Fig.(6.22) Magnetostriction measured along c-axis in plane containing b and c axes as a function of field direction at 50 K and 1 Tesla, for $Gd_{0.80}Tb_{0.20}$.

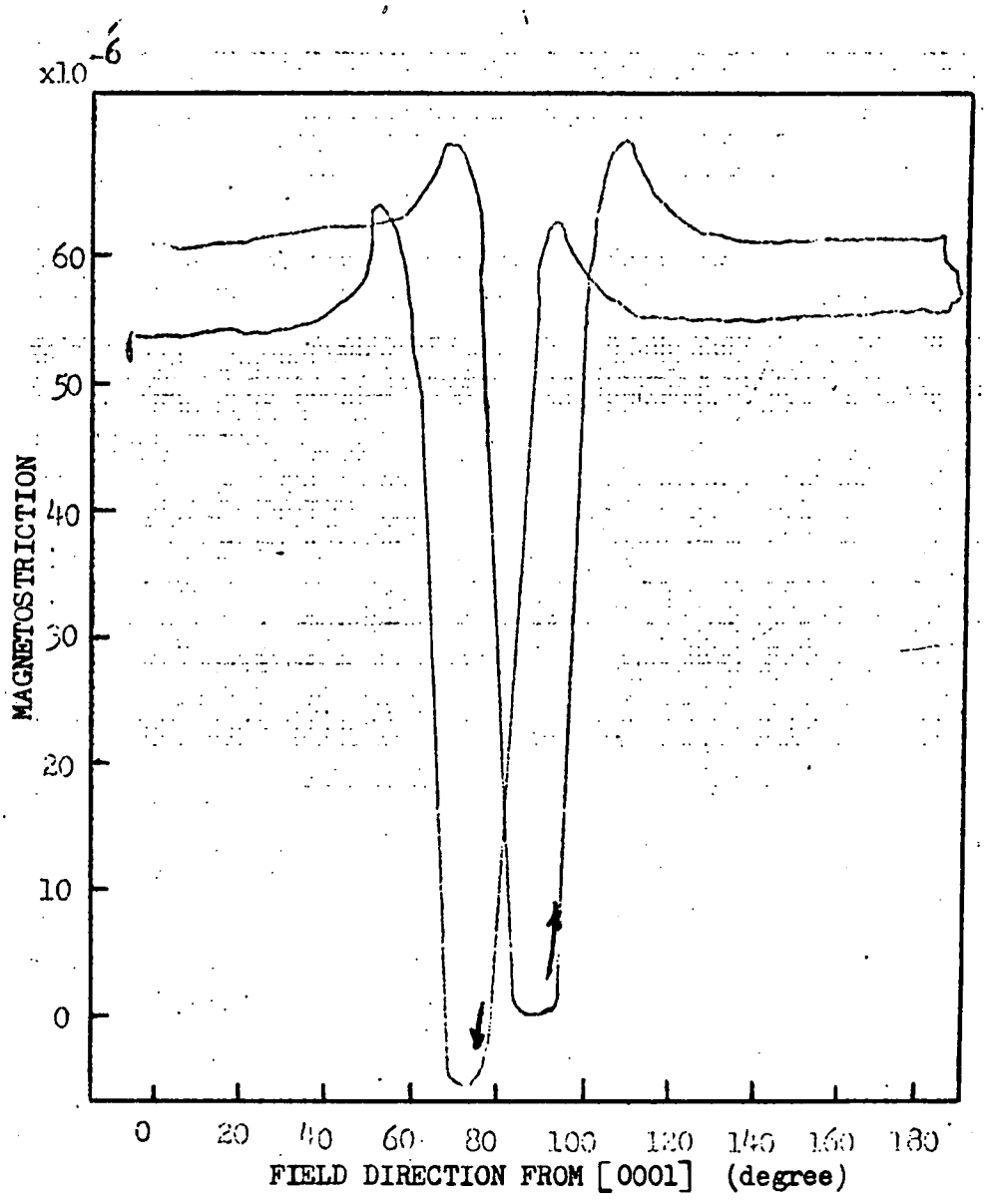

Fig.(6.23) Magnetostriction measured along c-axis in plane containing b and c axes as a function of field direction at 60 K and 1 Tesla, for $Gd_{0.80}Tb_{0.20}$.

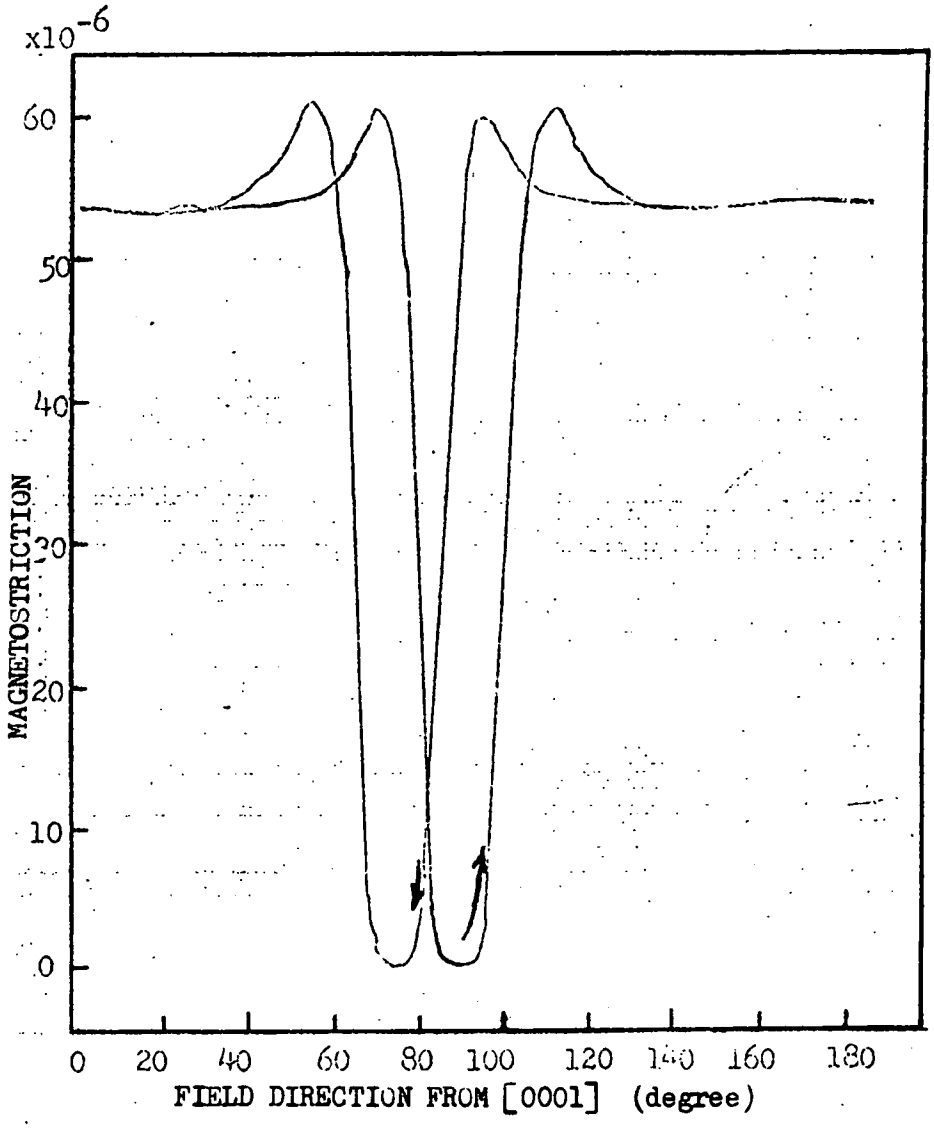

Fig.(6.24) Magnetostriction measured along c-axis in plane containing b and c axes as a function of field direction at 77 K and 1 Tesla, for $Gd_{0.80}Tb_{0.20}$.

to the highest temperature studied. No similar anomalies were observed either in the region of minimum or maximum for the sample $Gd_{0.25}Tb_{0.75}$. The magnetostriction coefficients $\lambda_2^{\alpha,2}$ as a function of magnetic field at different temperatures were obtained by taking the amplitude of the change in length recorded. Results for the sample containing 5%, 20%, 50% and 75% of Tb are shown in Figs. (6.25), (6.27), (6.29), and (6.31) respectively. The sample $Gd_{0.95}Tb_{0.05}$ gave negative values of $\lambda_2^{\alpha,2}$ while for the other samples positive values were obtained. The specimen with concentration of 5% was found to saturate along the c-axis at about 0.5 Tesla. The sample with 20% Tb was found to saturate at about 0.8 Tesla and the specimen with 50% Tb was saturated at about 2 Tesla. However, for the sample containing 75% Tb even 13 Tesla was not enough to produce saturation.

6.3.2 Temperature Dependence of $\lambda_2^{\alpha,2}$ Using Single-ion Theory.

No corrections for higher order magnetostriction coefficients of $l = 4$, 6, 8 were applied; however these terms are very small as reported by Mishima et al (1976) and according to the classical single-ion theory they have a temperature dependence given by $\hat{I}_{9/2}(x)$ and $\hat{I}_{13/2}(x)$ which causes them to decrease rapidly with increasing temperature, Clark et al (1965). Temperature dependencies of $\lambda_2^{\alpha,2}$ for the four compositions are shown in Figs. (6.26), (6.28), (6.30), and (6.32) respectively. Normalized saturation values for the samples were taken as,

$$\lambda_2^{\alpha,2}(0) = -(1.55 \pm 0.3) \times 10^{-4} \qquad \text{for } Gd_{0.95}Tb_{0.05}$$

$$\lambda_2^{\alpha,2}(0) = (0.65 \pm 0.2) \times 10^{-4} \qquad \text{for } Gd_{0.80}Tb_{0.20}$$

$$\lambda_2^{\alpha,2}(0) = (1.15 \pm 0.2) \times 10^{-4} \qquad \text{for } Gd_{0.50}Tb_{0.50}$$

$$\lambda_2^{\alpha,2}(0) = (27.6 \pm 0.5) \times 10^{-4} \qquad \text{for } Gd_{0.25}Tb_{0.75}$$

The values of $\lambda_2^{\alpha,2}$ were then calculated from the single-ion expression Eq. (6.4) and curves are shown alongside the experimental results. It may be observed that there is rather poor agreement with the experimental values for the first three alloys containing 5%, 20% and 50% of Terbium.

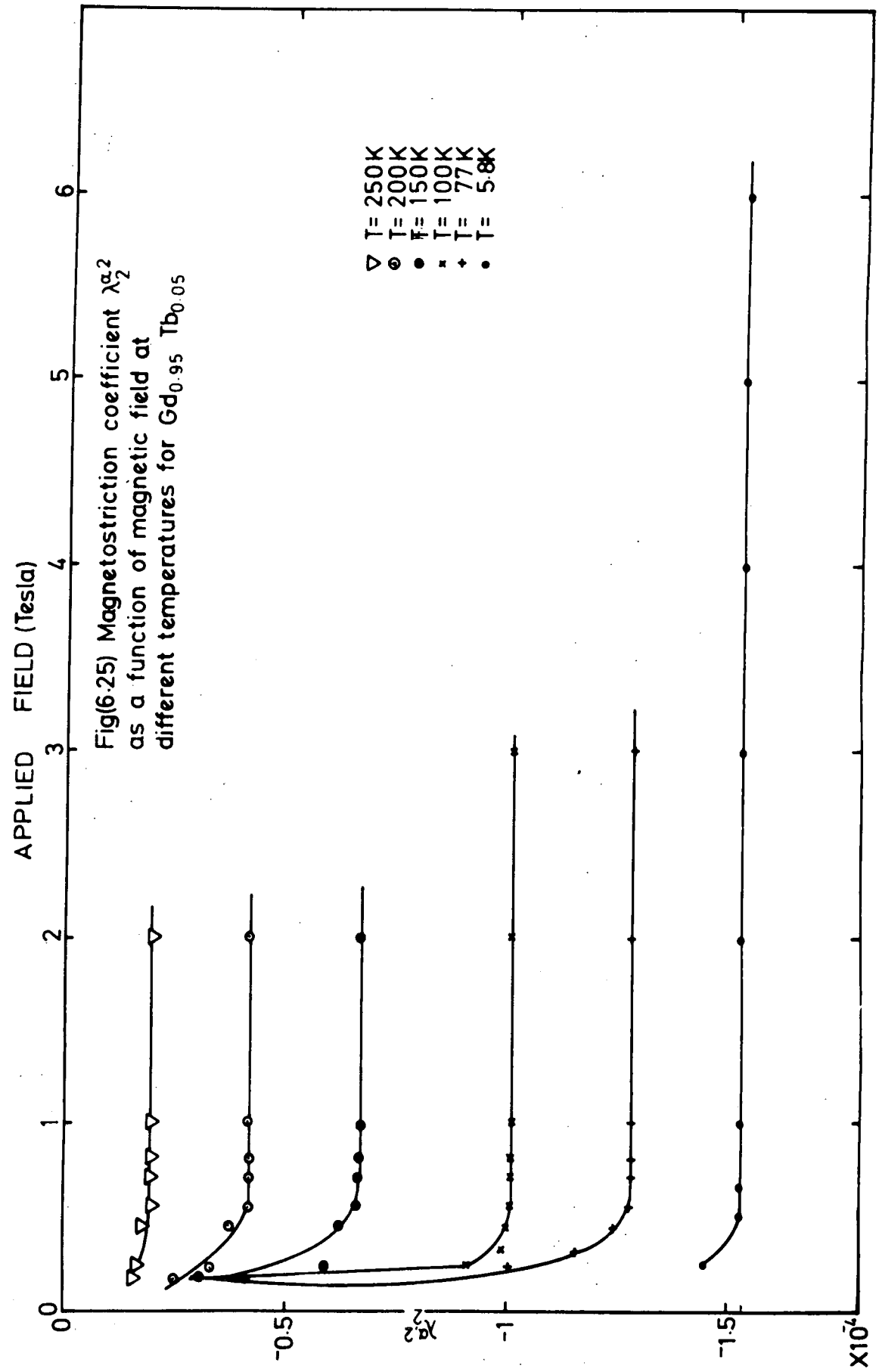

Fig(6.25) Magnetostriction coefficient $\lambda_2^{\alpha 2}$ as a function of magnetic field at different temperatures for $Gd_{0.95}$ $Tb_{0.05}$

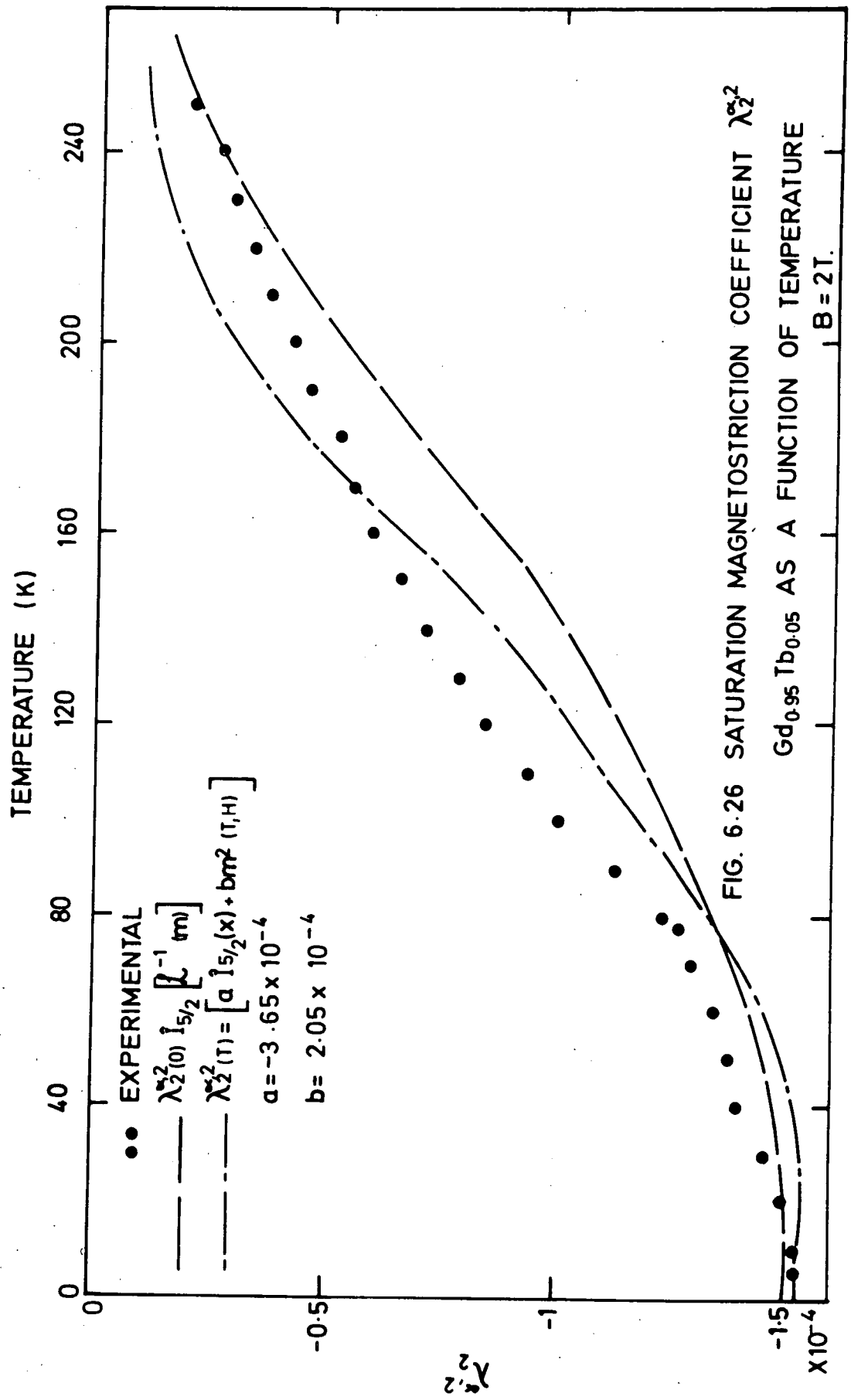

FIG. 6.26 SATURATION MAGNETOSTRICTION COEFFICIENT λ_2^{*2}

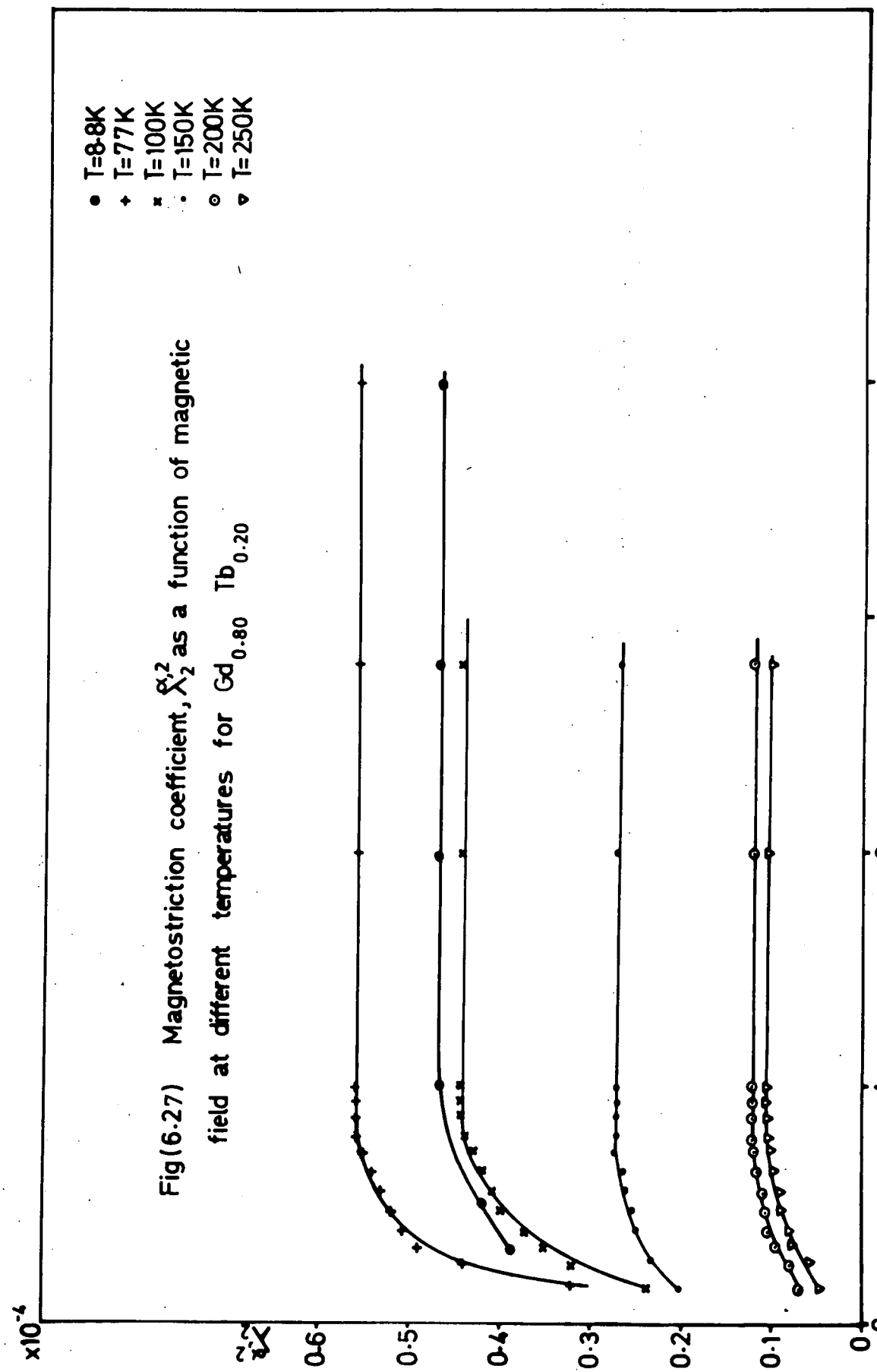

Fig(6·27) Magnetostriction coefficient, $\chi_2^{\alpha,2}$ as a function of magnetic field at different temperatures for $Gd_{0.80}$ $Tb_{0.20}$

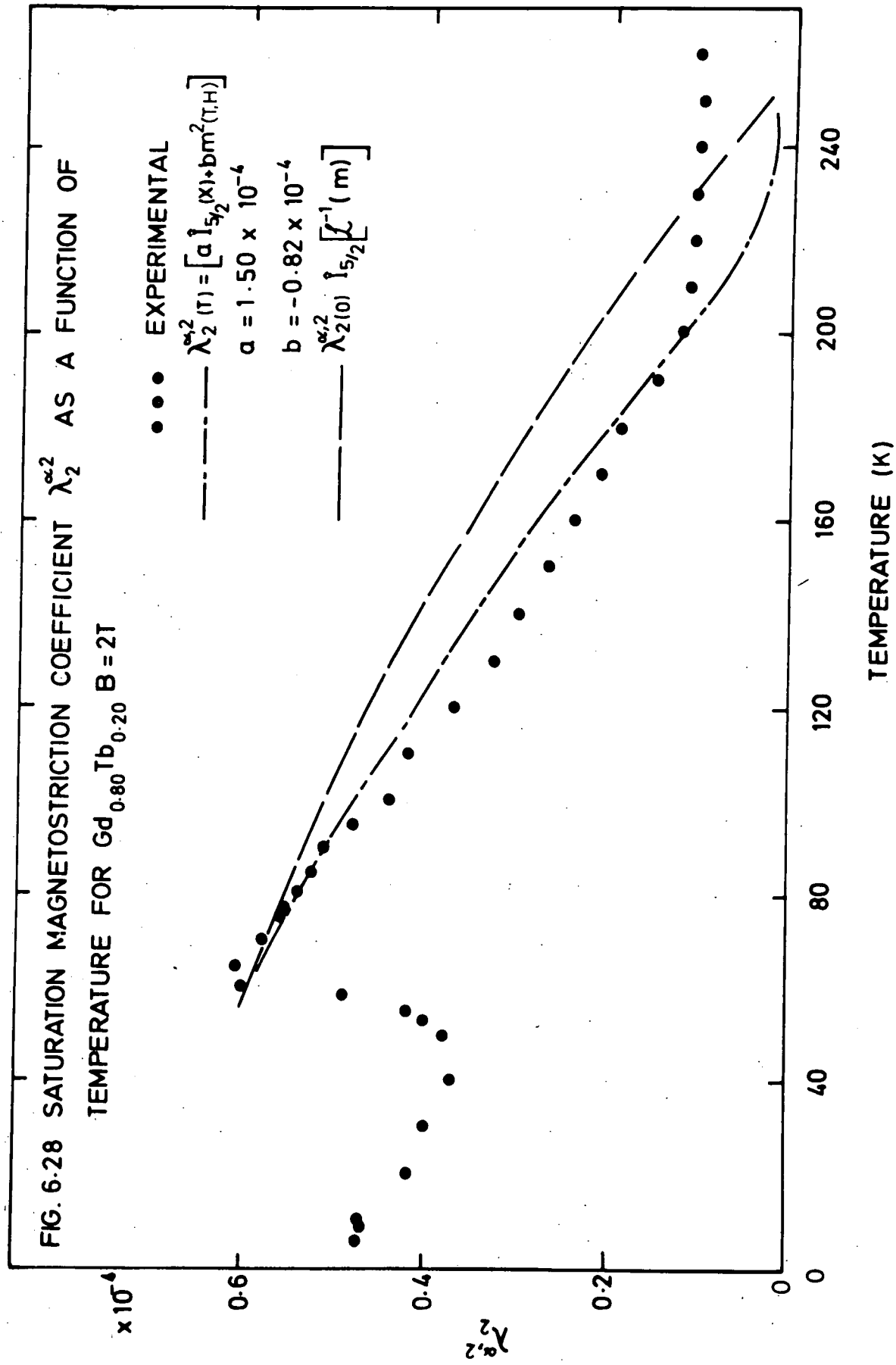

FIG. 6·28 SATURATION MAGNETOSTRICTION COEFFICIENT $\lambda_2^{\alpha 2}$ AS A FUNCTION OF TEMPERATURE FOR $Gd_{0.80}Tb_{0.20}$ B = 2T

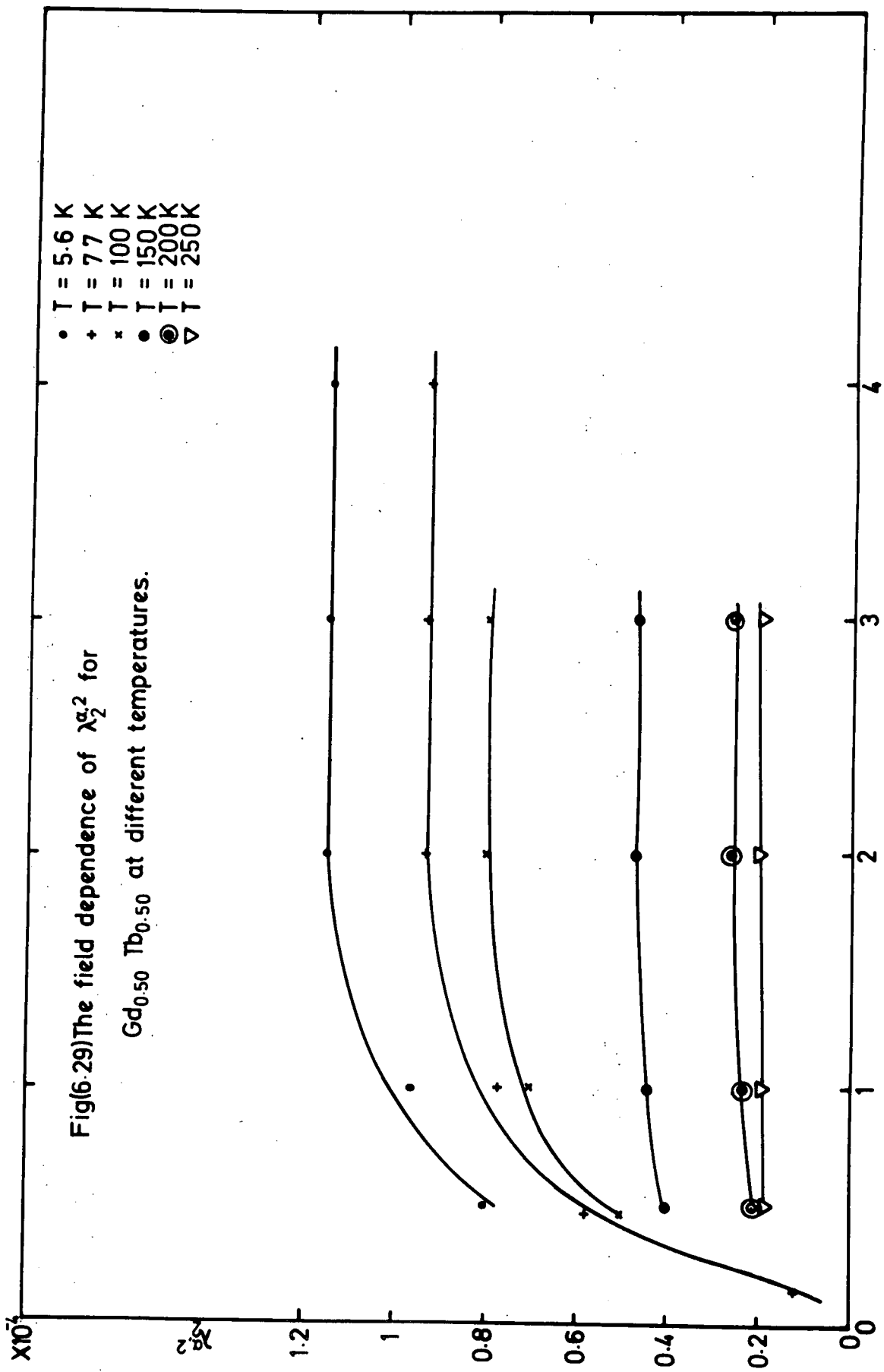

Fig(6.29)The field dependence of $\lambda_2^{\alpha 2}$ for $Gd_{0.50}$ $Tb_{0.50}$ at different temperatures.

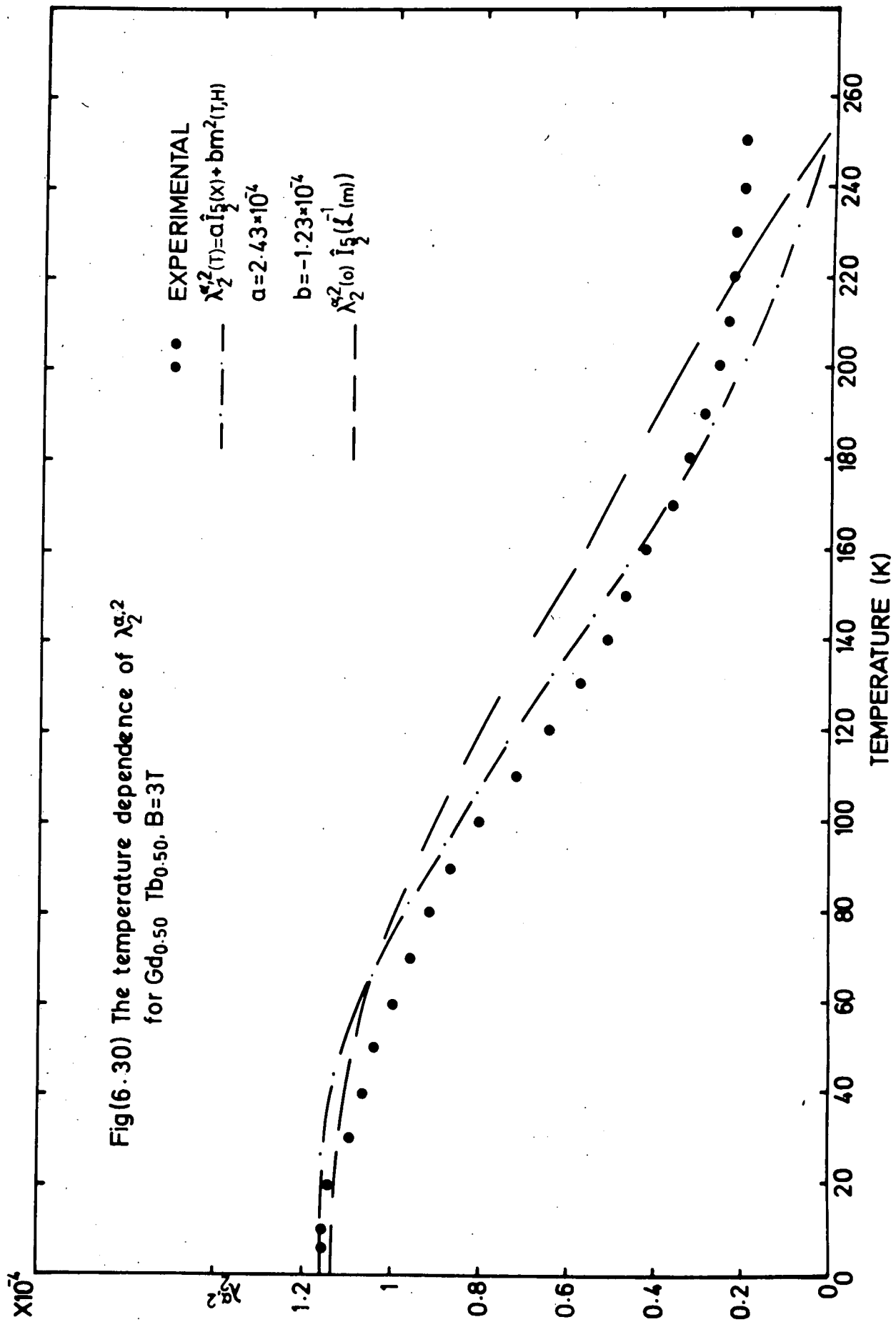

Fig(6.30) The temperature dependence of $\lambda_2^{\alpha,2}$ for $Gd_{0.50}$ $Tb_{0.50}$, B=3T

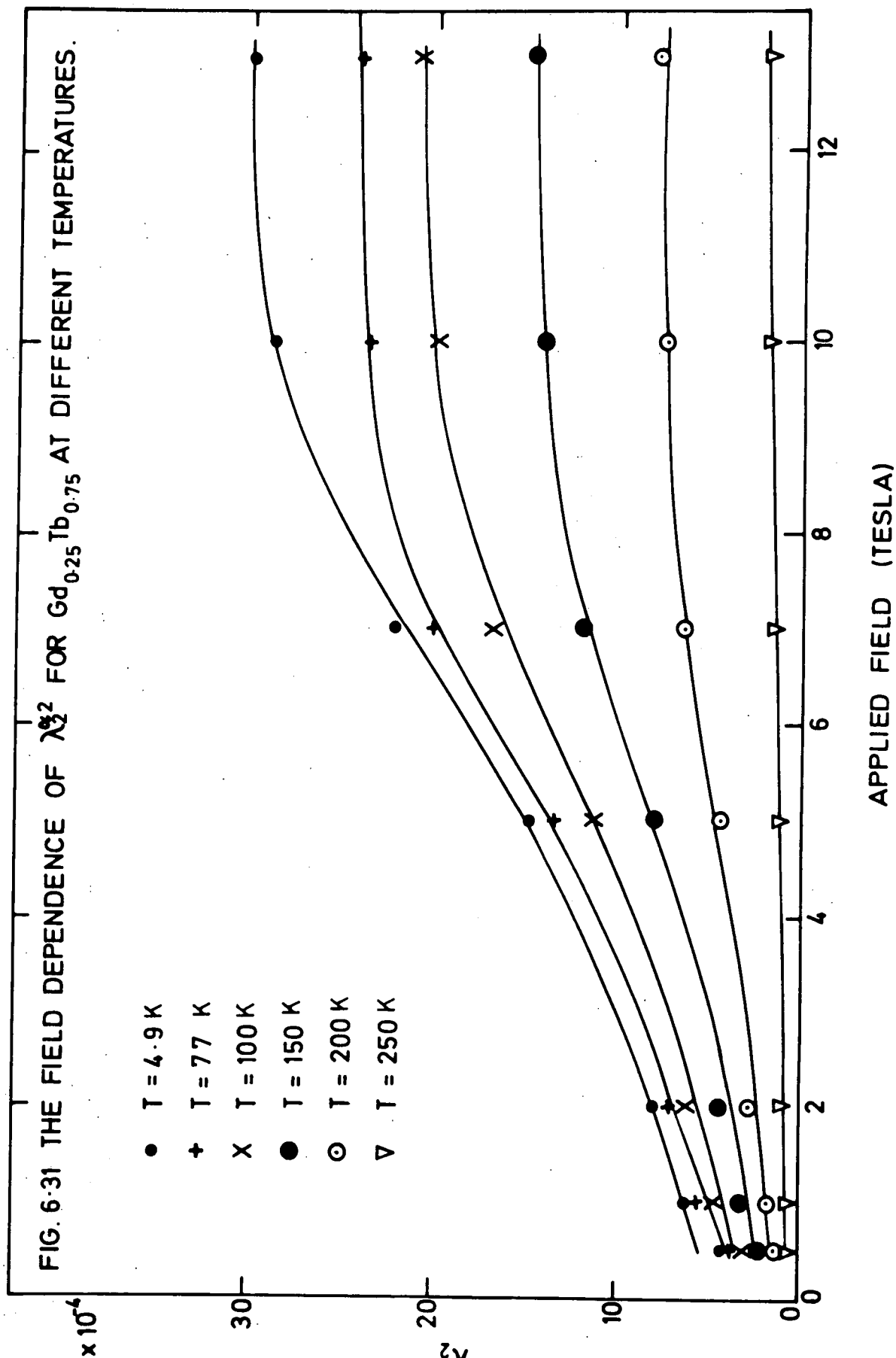
FIG. 6·31 THE FIELD DEPENDENCE OF λ*2 FOR Gd0·25Tb0·75 AT DIFFERENT TEMPERATURES.
T = 4·9 K
T = 77 K
T = 100 K
T = 150 K
T = 200 K
T = 250 K
λ*2
x 10⁻⁴
0
10
20
30
0
2
4
6
8
10
12
APPLIED FIELD (TESLA)

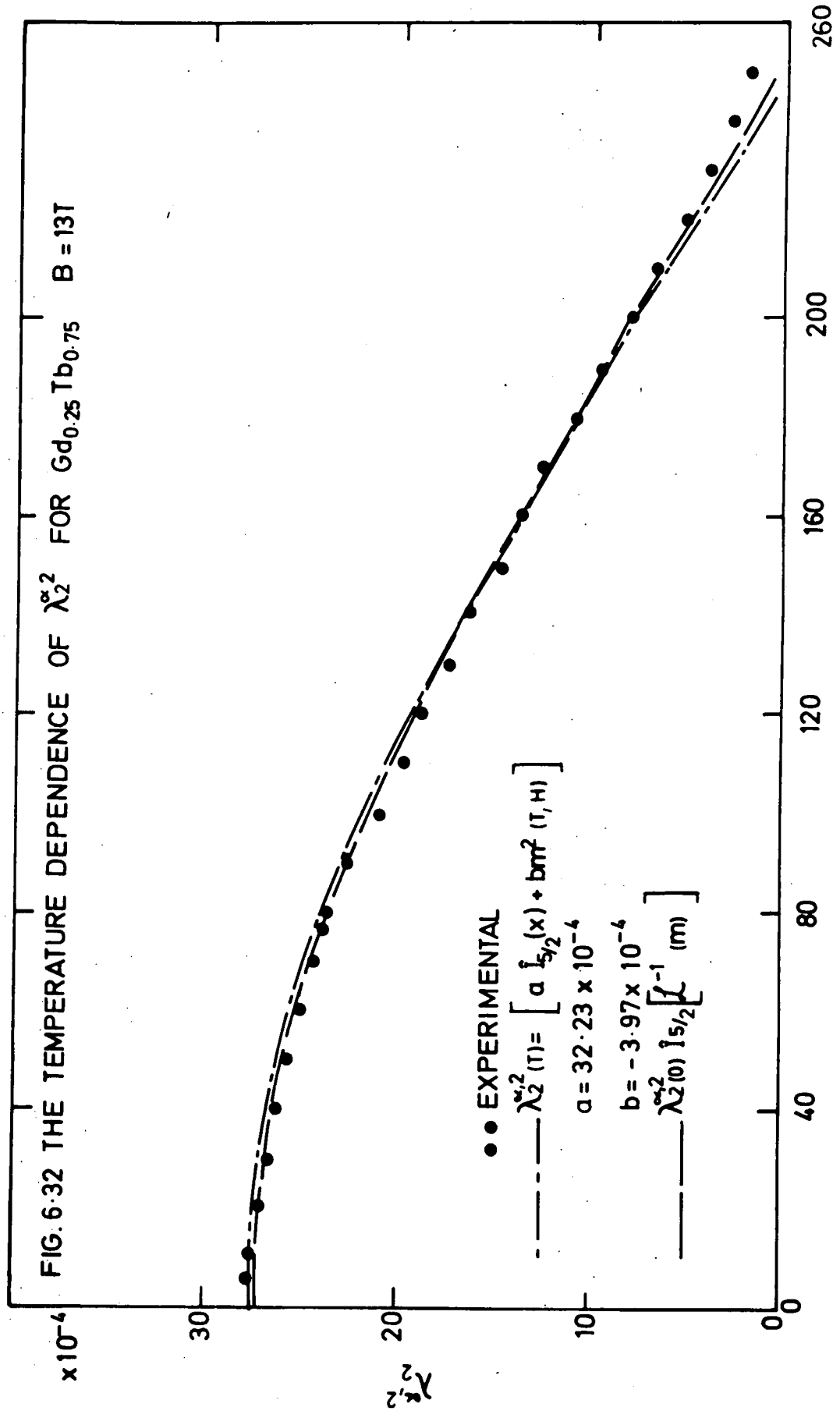
FIG. 6·32 THE TEMPERATURE DEPENDENCE OF $\lambda_2^{\kappa 2}$ FOR $Gd_{0.25}Tb_{0.75}$ B = 13T
$\lambda_2^{\kappa,2}$
x10⁻⁴
30
20
10
0
0
40
80
120
160
200
260
TEMPERATURE (K)
•• EXPERIMENTAL
$\lambda_2^{\kappa,2}(T) = \left[a\, f_{5/2}(x) + bm^2(T,H) \right]$
a = 32·23 x 10⁻⁴
b = - 3·97 x 10⁻⁴
$\lambda_2^{\kappa 2}(0)\, f_{5/2}\left[L^{-1}(m) \right]$

An anomaly can be seen in Fig. (6.28) for the sample containing 20% Terbium. The value of $\lambda_2^{\alpha,2}$ decreases with increasing temperature up to 45 K from 0.48×10^{-4} to 0.37×10^{-4} then shows a sharp rise to a very high value of 0.6×10^{-4} at 60 K above which it decreases again with increasing temperature. The experiment was repeated and the same effect was observed, the maximum and minimum appearing at the same temperatures. The theoretical single-ion curve for this sample was obtained by taking a normalized value of $\lambda_2^{\alpha,2}(0)$ of 0.65×10^{-4} obtained by extrapolation from 60 K to 0 K. This was achieved by fitting the $\hat{I}_{5/2}(x)$ curve to the experimental points at 60 K and then using it as an extrapolation function. The values of $\lambda_2^{\alpha,2}(T)$ calculated using Eq. (6.4) are plotted only between 60 K and 250 K since it is not justifiable to attempt to fit the anomaly in the experimental results. This anomaly cannot be explained by the single-ion mechanism or even by including a term representing a two-ion interaction as in Eq. (6.5). It appears at a composition intermediate between those for which $\lambda_2^{\alpha,2}$ is negative for all temperatures and those for which this coefficient is always positive. It may be associated with a change of mechanism which for a sample with 20% Tb is incomplete at lower temperatures.

The coefficient $\lambda_2^{\alpha,2}$ does not follow the curve appropriate for a single-ion theory for the specimen $Gd_{0.50}Tb_{0.50}$ as may be seen in Fig. (6.30), but agreement is seen to be very good for the sample with 75% Tb in Fig. (6.32). Fig. (6.33) shows on one sheet the experimental values of $\lambda_2^{\alpha,2}$ for the four compositions as functions of temperature. No larger difference is seen between the absolute values of $\lambda_2^{\alpha,2}$ for the samples containing 5%, 20% and 50% of Terbium but further increase of Terbium content to 75% results in a very large increase in the coefficient. On plotting using a log/log scale the values of $\lambda_2^{\alpha,2}$ against $\hat{I}_{5/2}(x)$ for the four samples used, the values for the specimen $Gd_{0.25}Tb_{0.75}$ were found to lie close

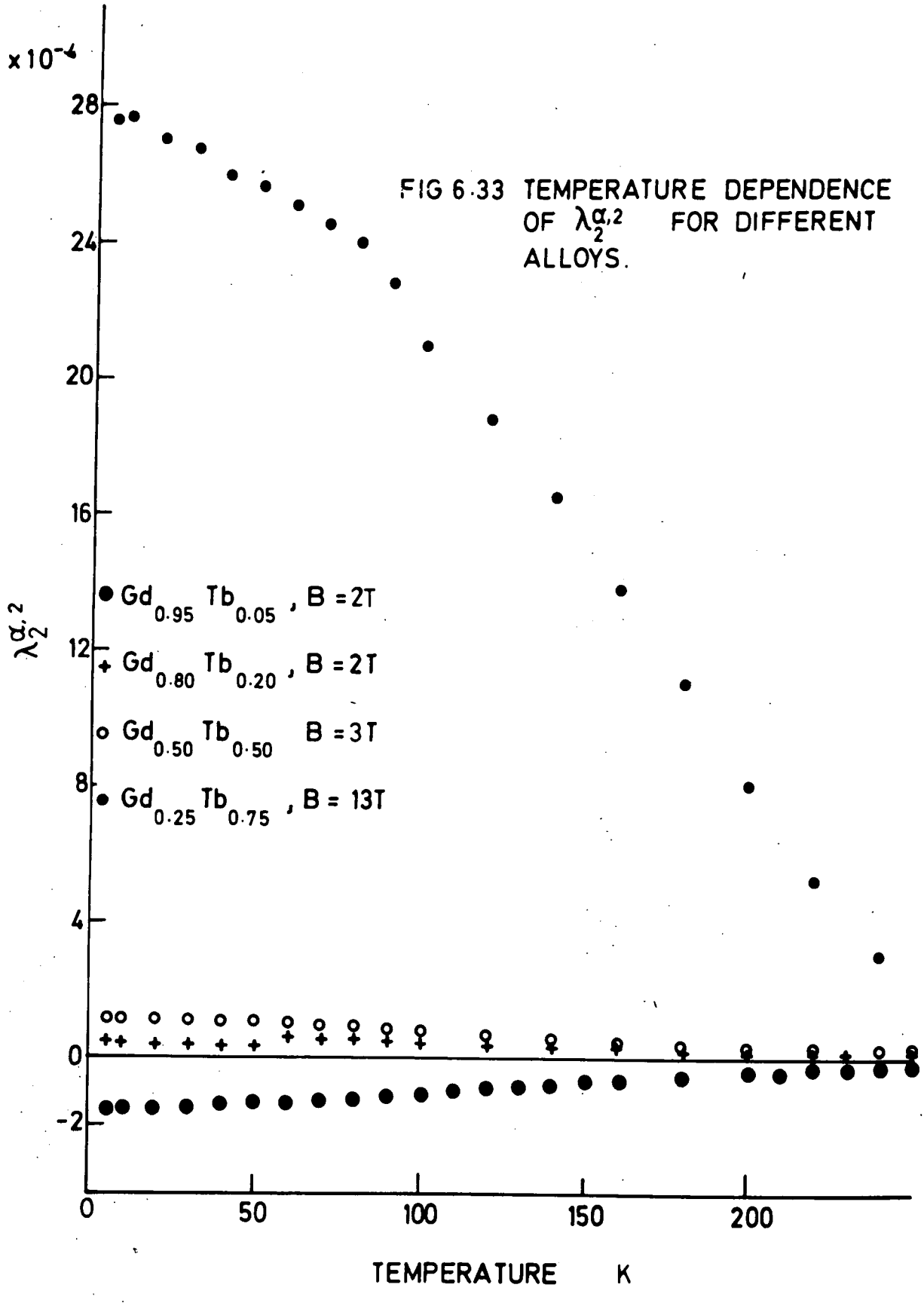

FIG 6.33 TEMPERATURE DEPENDENCE OF $\lambda_2^{\alpha,2}$ FOR DIFFERENT ALLOYS.

to a straight line of slope very close to unity as shown in Fig. (6.34), but at high temperatures a drift was observed similar to the one which was observed for $\lambda^{\gamma,2}$. The values for the other samples are not capable of being represented by a similar straight line.

6.3.3 Temperature Dependence of $\lambda_2^{\alpha,2}$ Using an Expression Containing a Term Representing a Two-ion Mechanism.

Since the single-ion mechanism could not give a reasonable representation of the variation with temperature of the values for $\lambda_2^{\alpha,2}$ for the specimens containing 5%, 20% and 50% of Terbium, an expression of the form given by Eq. (6.5) was used in an attempt to find a better fit to this variation. Curves obtained using the program detailed in Appendix I are shown in Figs. (6.26), (6.28), (6.30), and (6.32) for the samples $Gd_{0.95}Tb_{0.05}$, $Gd_{0.80}Tb_{0.20}$, $Gd_{0.50}Tb_{0.50}$, and $Gd_{0.25}Tb_{0.75}$ respectively. The first sample does not give a satisfactory fitting even on introducing the two-ion interaction coefficient, but it gives a better fitting than the single-ion theory. It was only reasonable to attempt to fit the results for the $Gd_{0.80}Tb_{0.20}$ samples above 60 K due to the anomaly observed and it represents the experimental results fairly well between 60 K and 200 K above which lower values were obtained by Eq. (6.5). The values of the coefficient $\lambda_2^{\alpha,2}$ calculated from Eq. (6.5) for the sample containing 50% Terbium fitted the experimental values better than the single-ion mechanism, but still gave lower values at temperatures above 200 K and slightly highervalues at much lower temperatures. For the sample containing 75% Terbium there was little difference between the values of $\lambda_2^{\alpha,2}$ calculated from the single-ion theory or those using Eq. (6.5). Table (6.3) gives the variation of the two terms a and b with the alloy composition.

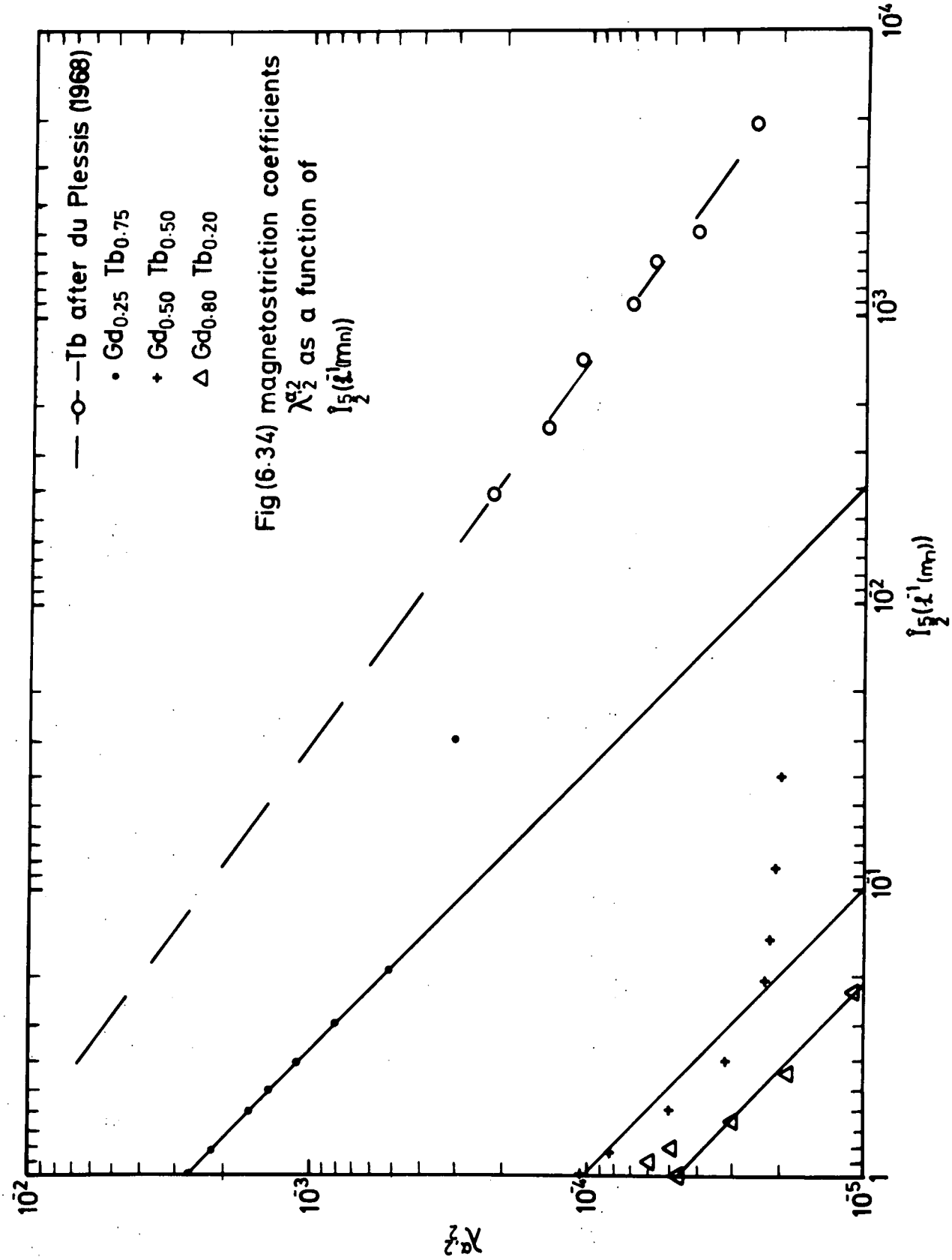

Fig (6·34) magnetostriction coefficients $\lambda_2^{\alpha 2}$ as a function of $f_5(\hat{l}^1 m_l)$

TABLE (6.3): The variation of the terms a and b with the alloy composition for $\lambda_2^{\alpha,2}$

Composition	a x 10^4	b x 10^4
$Gd_{0.95}Tb_{0.05}$	-3.65	2.1
$Gd_{0.80}Tb_{0.20}$	1.50	-0.8
$Gd_{0.50}Tb_{0.50}$	2.4	-1.2
$Gd_{0.25}Tb_{0.75}$	32.2	-4.00

6.3.4 Variation of $\lambda_2^{\alpha,2}$ With Alloy Composition

Fig. (6.35) shows the variation of the normalized saturation magnetostriction coefficient $\lambda_2^{\alpha,2}(0)$ with alloy composition. The value for the sample $Gd_{0.25}Tb_{0.75}$ was obtained by extrapolation of the curve showing the variation of $\lambda_2^{\alpha,2}$ with 1/B given in Fig. (6.36). The results were represented by Eq. (6.8), the two constants A and B having the values,

$$A = 810 \times 10^{-4}$$

$$B = -0.14$$

Fig. (6.35) shows the values to lie on a smooth curve which extrapolates to those given by Mishima for pure Gd and by du Plessis for Tb. This again supports the use of the gauge factors quoted by the makers of the strain gauges.

6.4 The Magnetostriction Coefficient $\lambda_1^{\alpha,2}$

6.4.1. The Field Dependence of the Coefficient $\lambda_1^{\alpha,2}$

The coefficient $\lambda_1^{\alpha,2}$ was obtained by measuring the strain along the b-axis in b-c axis samples and then evaluated from Eq. (3.42). Figs. (6.37) to (6.40) show the magnetostriction against field direction for the $Gd_{0.80}Tb_{0.20}$

Fig(6.35) The normalized saturation magnetostriction coefficient $\lambda^{\alpha}_{2}{}^{,2}$ as a function of alloy composition.

- ⊙ After du Plessis (1968)
- × After Mishima et al (1976)
- —— From the relation $\lambda^{\alpha}{}^{,2}_{2\,(0)} = A\, e^{BC}$

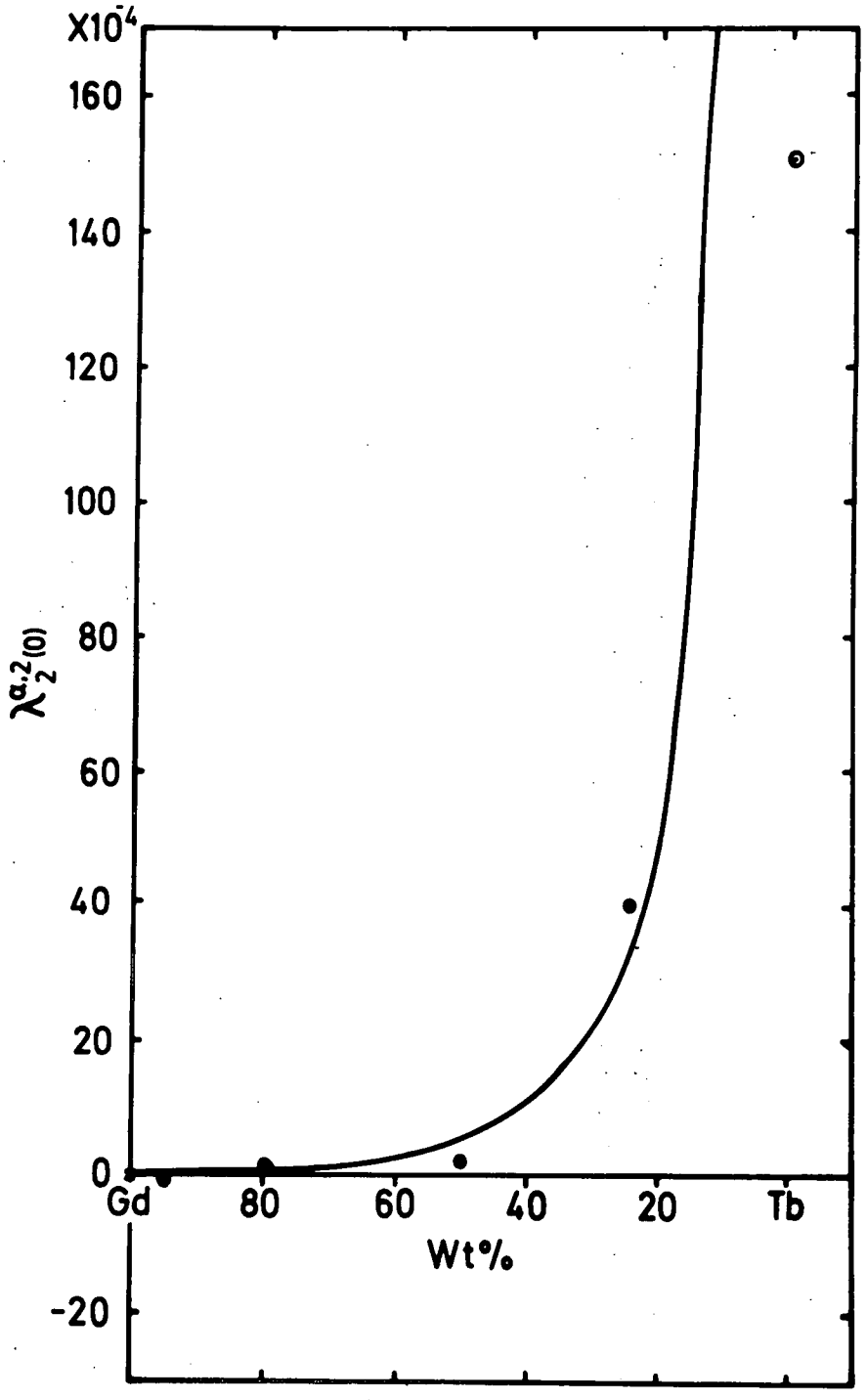

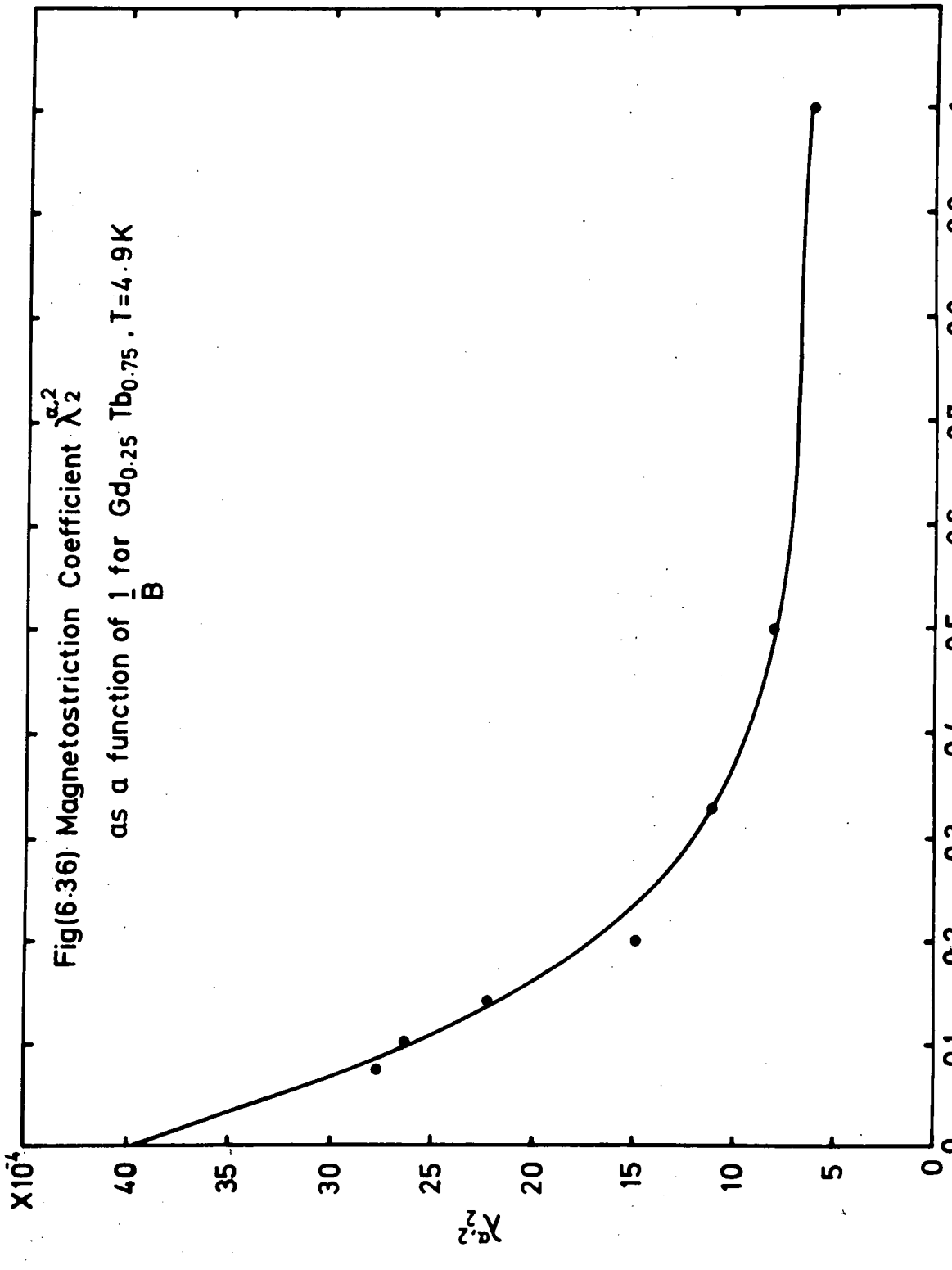
Fig(6.36) Magnetostriction Coefficient $\lambda_2^{\alpha,2}$
as a function of $\frac{1}{B}$ for $Gd_{0.25}$ $Tb_{0.75}$, T=4·9K
$\lambda_{2,2}^{\alpha}$
X10⁻⁴
40
35
30
25
20
15
10
5
0
0
0·1
0·2
0·3
0·4
0·5
0·6
0·7
0·8
0·9
1
1/B (T⁻¹)

specimen as the crystal was rotated in increasing magnetic fields at 4.5 K. An anomaly was observed at lower fields as shown in Fig. (6.37) and (6.38). The splitting of the minimum was smaller than that observed with the gauge attached along the c-axis, but the angles of the inflections were the same. The anomalies disappear as the magnetic field increases and the minimum becomes very sharp. The anomaly did not decrease on raising the temperature, but remained constant and then disappeared completely at (63.5 ± 0.5)K. A typical trace obtained just above this temperature is shown in Fig. (6.41). In the two samples containing 50% and 75% of Terbium no anomalies were observed. No strain was detected for the sample $Gd_{0.95}Tb_{0.05}$ but only a straight line was obtained as a signal. This implies either a zero strain for the system or a very small strain which the apparatus was not capable of measuring. Another strain gauge was fixed along the b-axis after polishing off the first one, but still no signal was obtained even on cooling to 5.3 K.

The magnetostriction coefficients $\lambda_1^{\alpha,2}$ as a function of magnetic field at different temperatures were obtained by taking the amplitude of the changes in length recorded. Results for the specimens $Gd_{0.80}Tb_{0.20}$, $Gd_{0.50}Tb_{0.50}$ and $Gd_{0.25}Tb_{0.75}$ are shown in Figs. (6.42), (6.44), and (6.46) respectively. The sample containing 20% Tb was saturated at about 0.5 Tesla and for all temperature ranges the constants were negative. The sample $Gd_{0.50}Tb_{0.50}$ was saturated at about 1.5 Tesla and negative values were obtained for the coefficient $\lambda_1^{\alpha,2}$ up to 230 K then positive values were obtained. The $Gd_{0.25}Tb_{0.75}$ alloy was saturated at about 2.5 Tesla and positive values were obtained above 200 K.

6.4.2. Temperature Dependence of $\lambda_1^{\alpha,2}$ Using Single-ion Mechanism.

The variation of magnetostriction coefficients $\lambda_1^{\alpha,2}$ with temperature calculated from single-ion theory using Eq. (6.4) are shown with the experimental values in Figs. (6.43), (6.45) and (6.47) for the samples containing 20%, 50% and 75% of Terbium respectively.

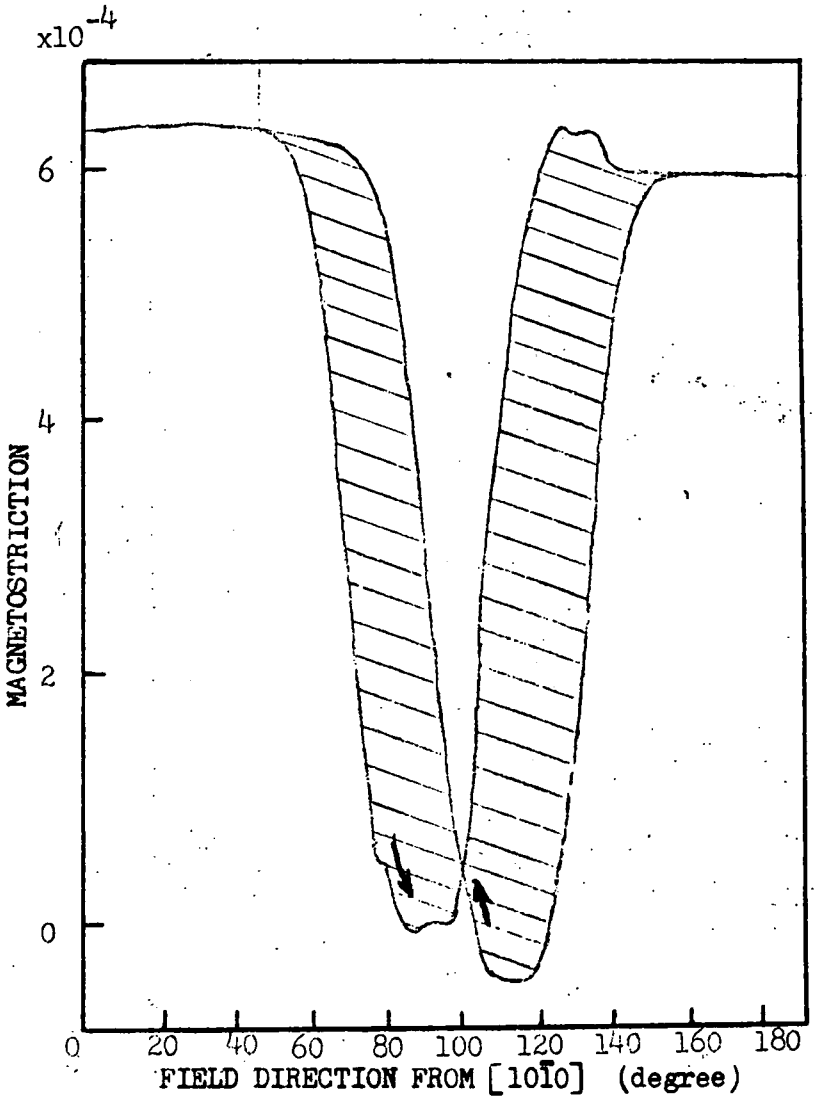

Fig.(6.37) Magnetostriction measured along b-axis in plane containing b and c axes as a function of field direction at 4.5 K and 0.48 Tesla, for $Gd_{0.80}Tb_{0.20}$.

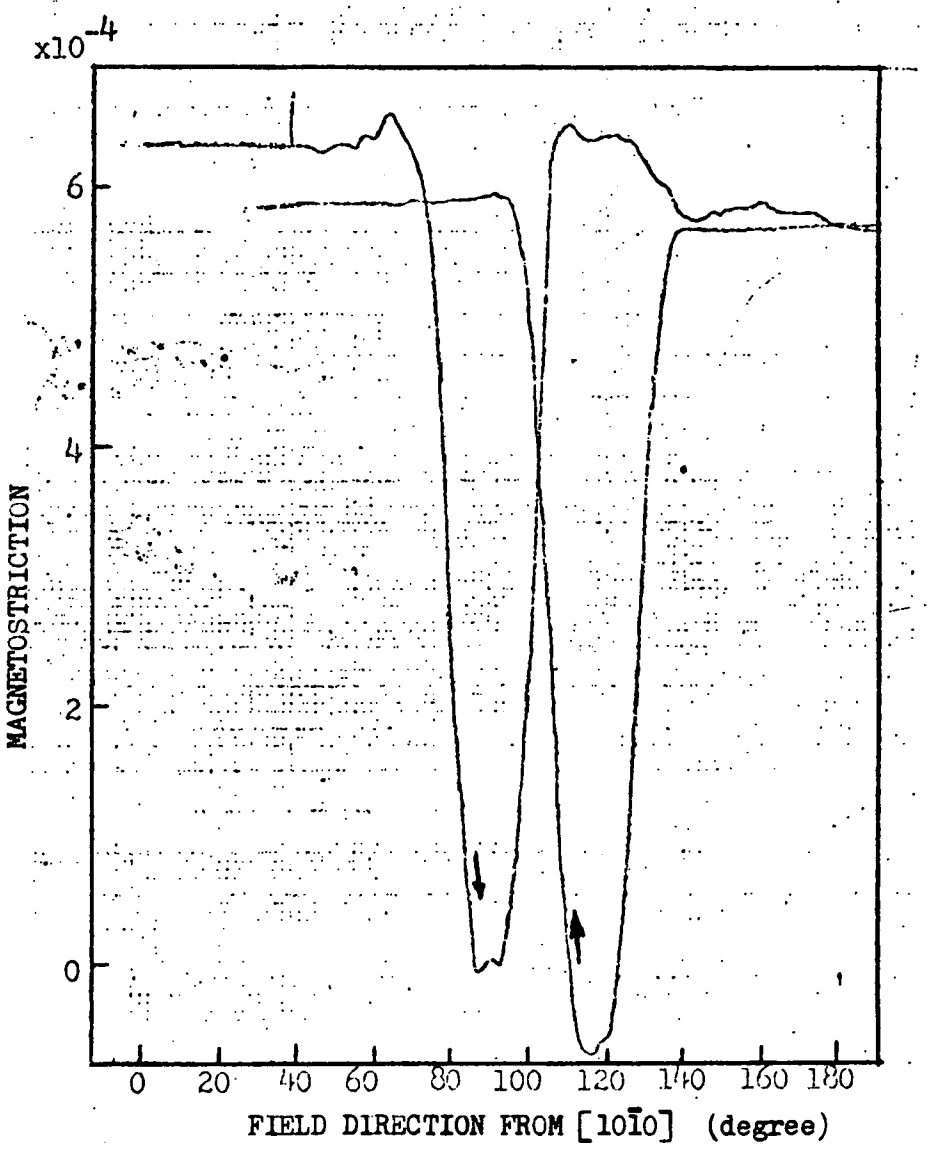

Fig.(6.38) Magnetostriction measured along b-axis in plane containing b and c axes as a function of field direction at 4.5 K and 1 Tesla, for $Gd_{0.80}Tb_{0.20}$.

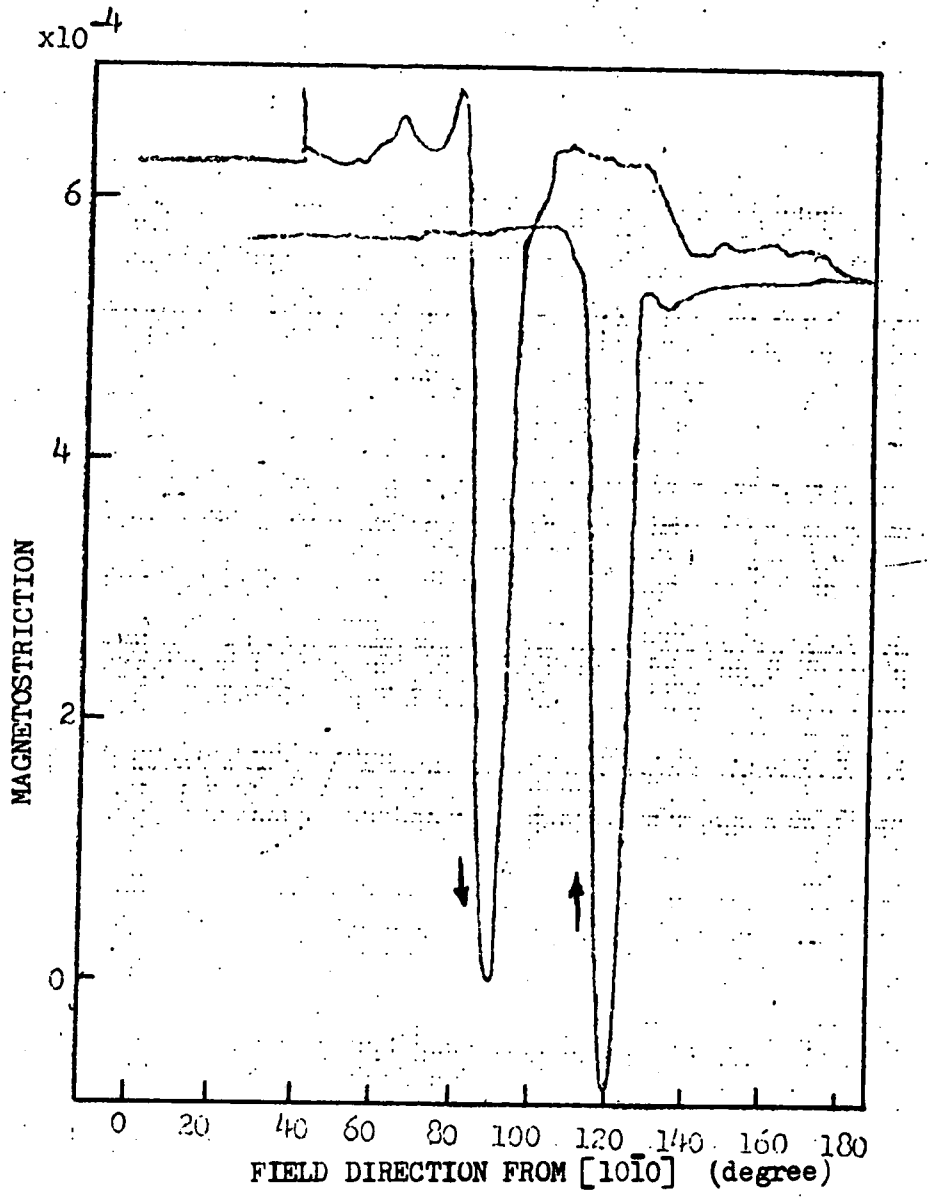

Fig.(6.39) Magnetostriction measured along b-axis in plane containing b and c axes as a function of field direction at 4.5 K and 2 Tesla, for $Gd_{0.80}Tb_{0.20}$.

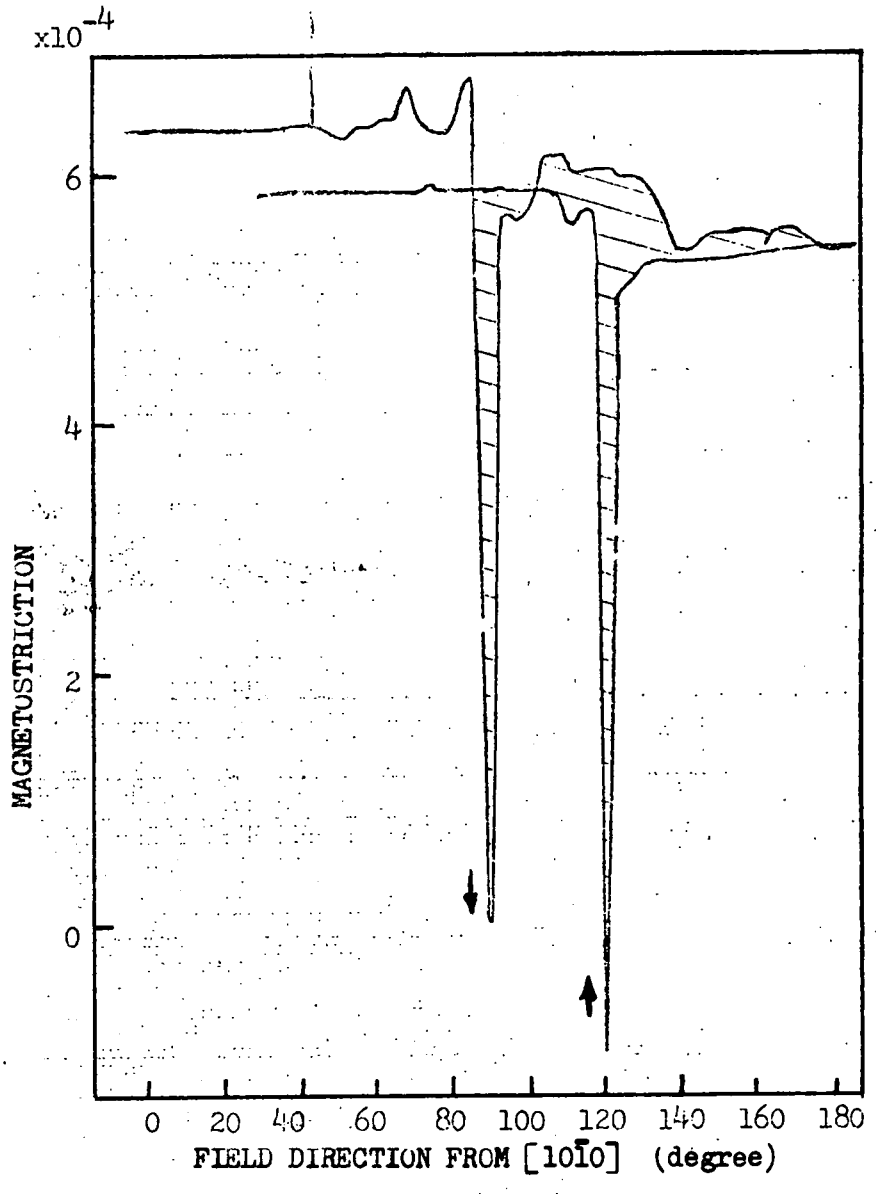

Fig.(6.40) Magnetostriction measured along b-axis in plane containing b and c axes as a function of field direction at 4.5 K and 4 Tesla, for $Gd_{0.80}Tb_{0.20}$.

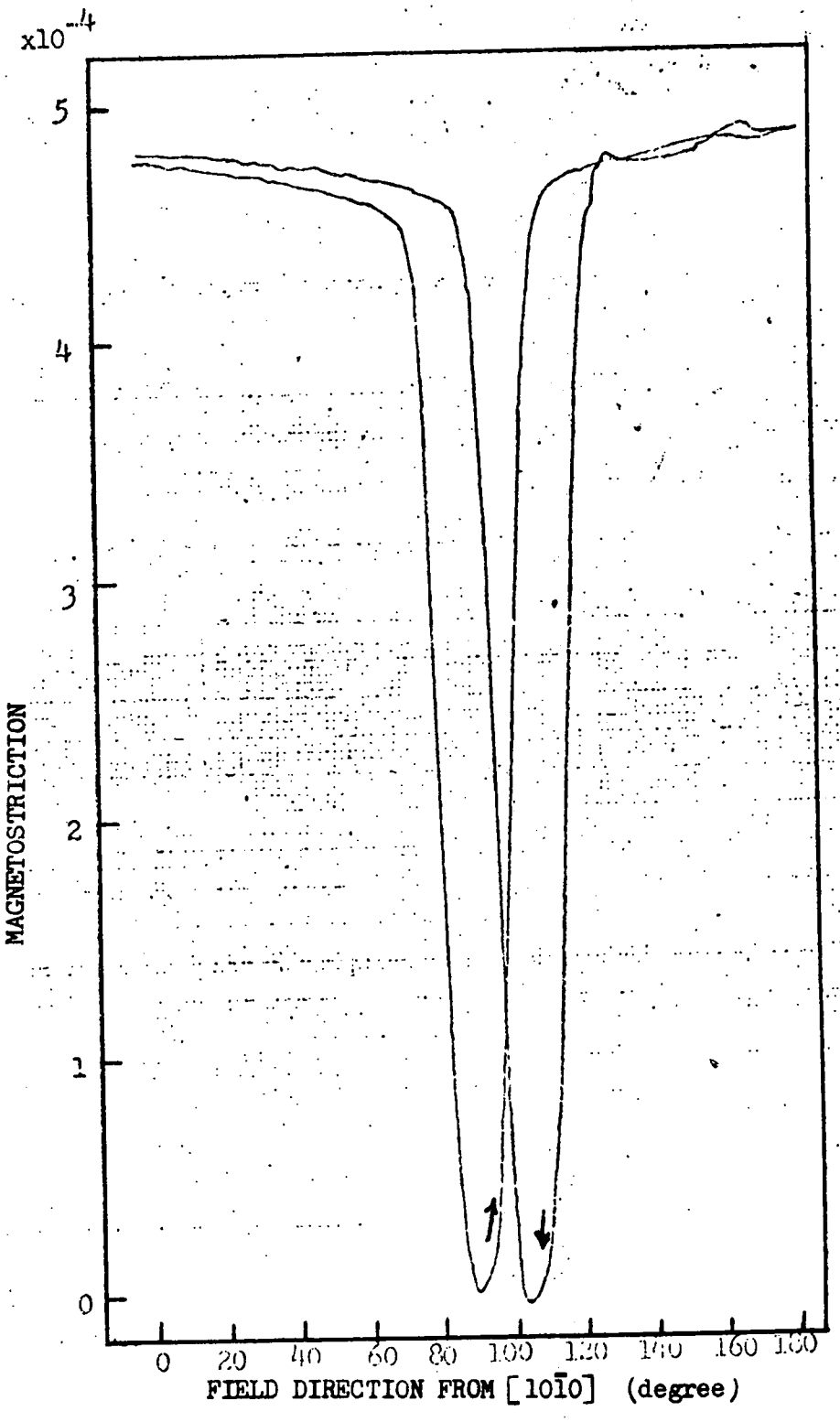

Fig.(6.41) Magnetostriction measured along b-axis in plane containing b and c axes as a function of field direction at 77 K and 1 Tesla, for $Gd_{0.80}Tb_{0.20}$.

Normalized saturation values for the three compositions used were taken as,

$$\lambda_1^{\alpha,2}(0) = (-3.60 \pm 0.4) \times 10^{-4} \quad \text{for } Gd_{0.80}Tb_{0.20}$$

$$\lambda_1^{\alpha,2}(0) = (-10.7 \pm 0.2) \times 10^{-4} \quad \text{for } Gd_{0.50}Tb_{0.50}$$

$$\lambda_1^{\alpha,2}(0) = (-16.6 \pm 1) \times 10^{-4} \quad \text{for } Gd_{0.25}Tb_{0.75}$$

Fig. (6.48) shows the experimental values of $\lambda_1^{\alpha,2}$ for the three compositions used as a function of temperature.

It is clear from the calculated values of magnetostriction coefficient using the single-ion theory that this theory does not give reasonable fitting for the experimental results even for the sample containing 75% of Terbium.

6.4.3. Temperature Dependence of $\lambda_1^{\alpha,2}$ Using an Expression Containing a Term Representing a Two-ion Interaction.

Eq. (6.5) was used along with the computer program in Appendix I in an attempt to fit the temperature variation of the magnetostriction coefficient $\lambda_1^{\alpha,2}$. The resulting curves are shown in Figs. (6.43), (6.45) and (6.47) for samples containing 20%, 50% and 75% Terbium respectively. No appreciable difference was observed for the sample $Gd_{0.80}Tb_{0.20}$ between the values obtained from the single-ion model and those obtained from Eq. (6.5). For the sample $Gd_{0.50}Tb_{0.50}$ the values calculated from Eq. (6.5) fitted the experimental results reasonably well at temperatures between 0 K and 20 K and above 100 K, but between 20 K and 100 K the curve showed values of appreciably greater magnitude than those from the experiment. However, the fit was clearly superior to that given by the $\hat{I}_{5/2}(x)$ function. The results for the specimen $Gd_{0.25}Tb_{0.75}$ were fairly well fitted by Eq. (6.5) up to 200 K, but at temperatures above that at which the sign of $\lambda_1^{\alpha,2}$ changed the calculated values drifted giving lower values than those obtained from the experiment.

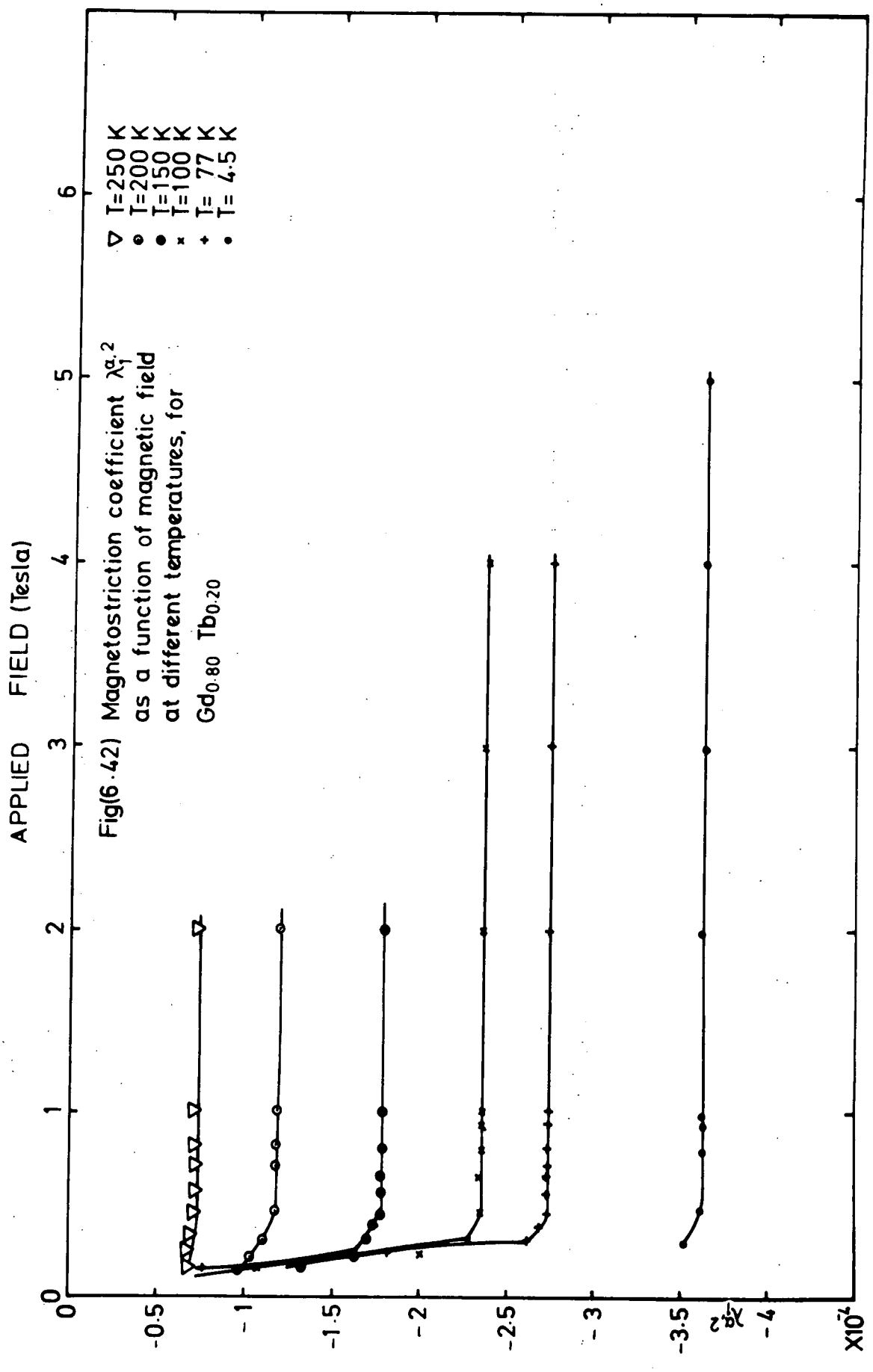

Fig(6.42) Magnetostriction coefficient $\lambda_1^{\alpha,2}$ as a function of magnetic field at different temperatures, for $Gd_{0.80}\ Tb_{0.20}$

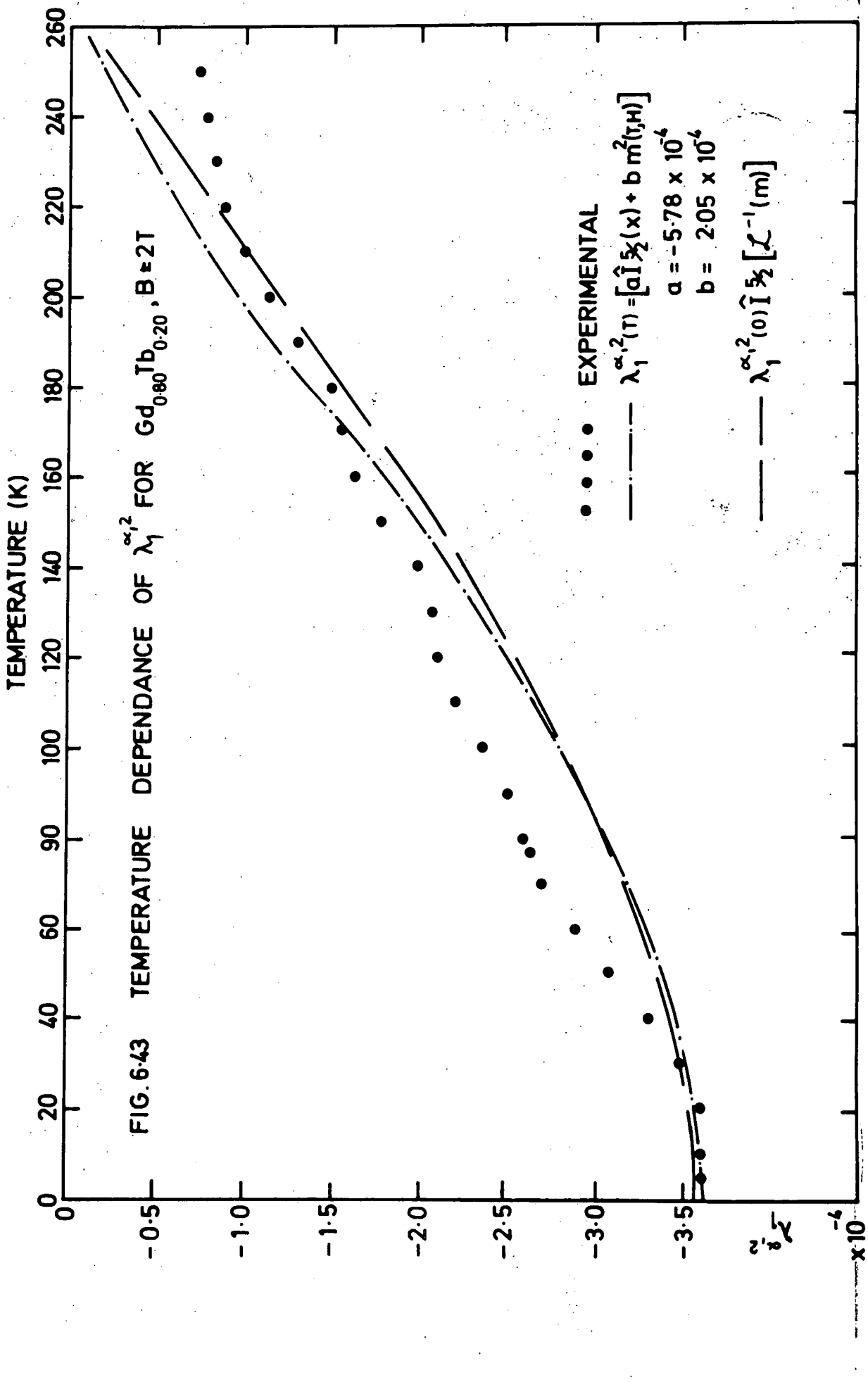
TEMPERATURE (K)
0
20
40
60
90
100
120
140
160
180
200
220
240
260
-0·5
-1·0
-1·5
-2·0
-2·5
-3·0
-3·5
$\frac{\Delta\lambda_1^{\alpha,2}}{\lambda_1^{\alpha,2}}$
$\times 10^{-4}$
FIG. 6·43 TEMPERATURE DEPENDANCE OF $\lambda_1^{\alpha,2}$ FOR $Gd_{0\cdot80}Tb_{0\cdot20}$, B = 2T
EXPERIMENTAL
$\lambda_1^{\alpha,2}(T) = [a\hat{I}^{3/2}(x) + b\,m^2(T,H)]$
a = -5·78 x 10^{-4}
b = 2·05 x 10^{-4}
$\lambda_1^{\alpha,2}(0)\hat{I}^{3/2}[\mathcal{L}^{-1}(m)]$

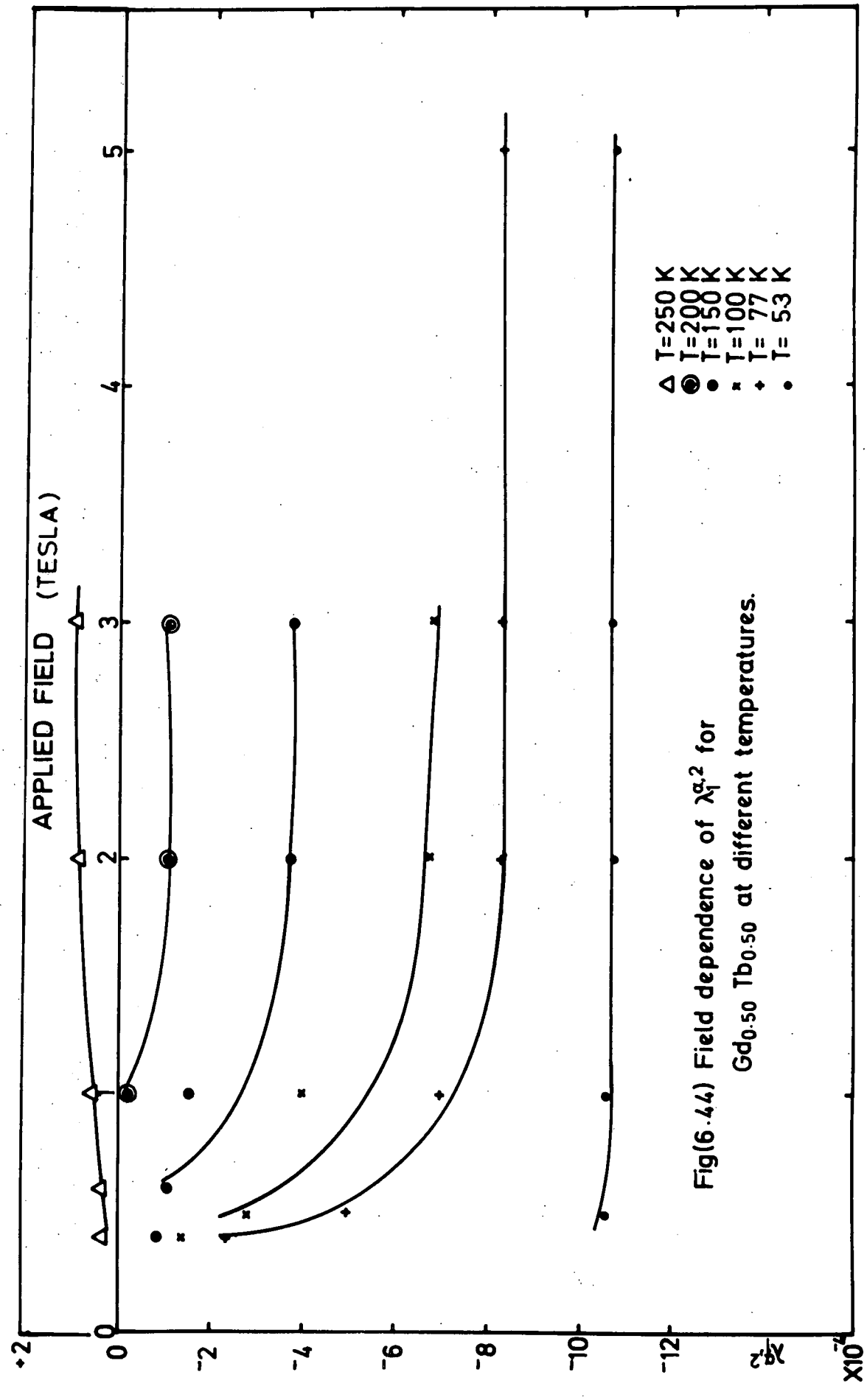

Fig(6.44) Field dependence of $\lambda_1^{a,2}$ for $Gd_{0.50}Tb_{0.50}$ at different temperatures.

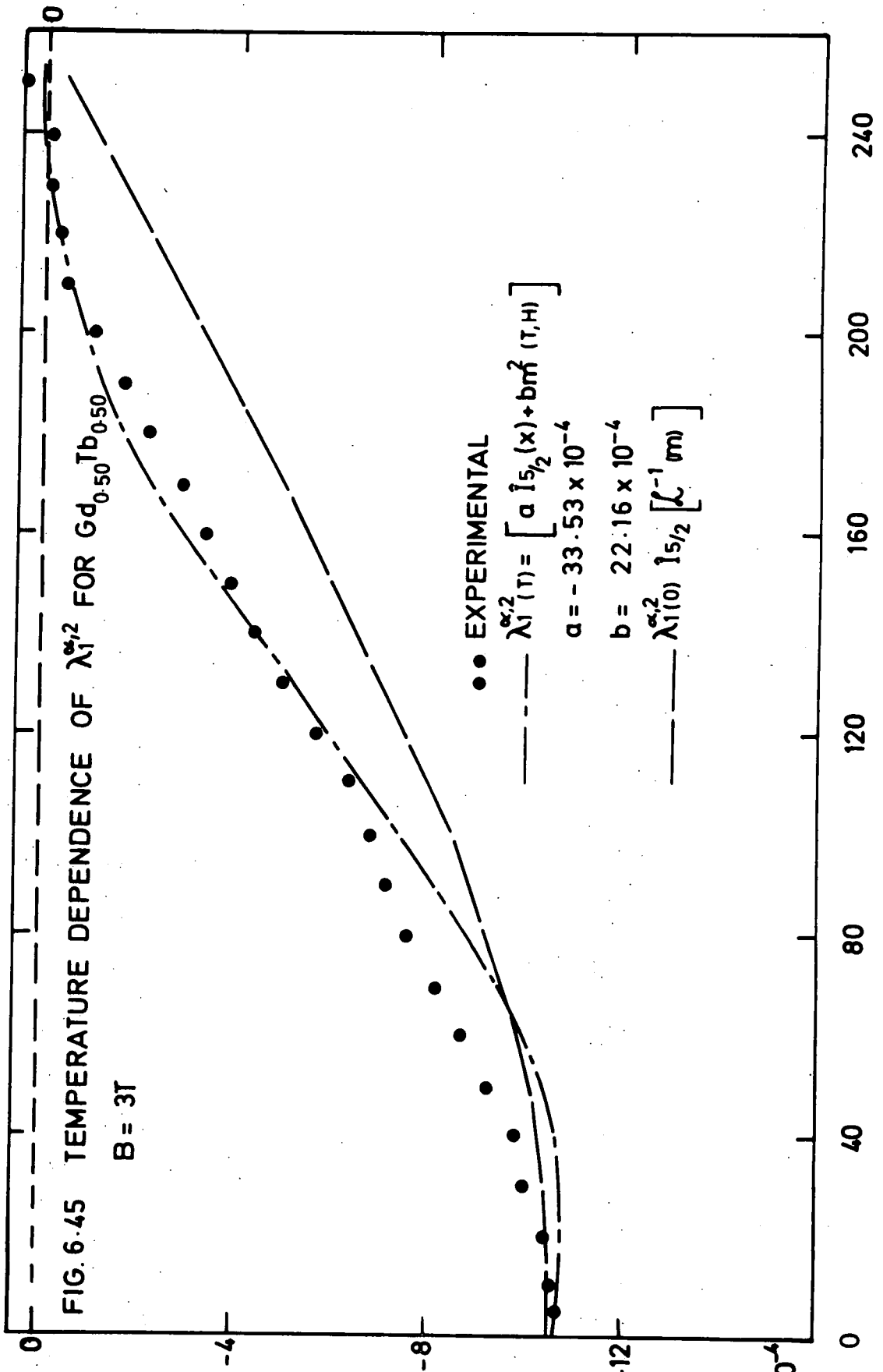
FIG. 6·45 TEMPERATURE DEPENDENCE OF $\lambda_1^{\alpha,2}$ FOR $Gd_{0.50}Tb_{0.50}$
B = 3T
•• EXPERIMENTAL
—— $\lambda_{1(T)}^{\alpha,2} = \left[a\, J_{5/2}(x) + b m^2 (T,H) \right]$
a = - 33·53 x 10^{-4}
b = 22·16 x 10^{-4}
—— $\lambda_{1(0)}^{\alpha,2}\, J_{5/2} \left[\mathcal{L}^{-1} m \right]$
$\lambda_1^{\alpha,2}$
x 10^{-4}
0
-4
-8
-12
0
40
80
120
160
200
240
TEMPERATURE (K)

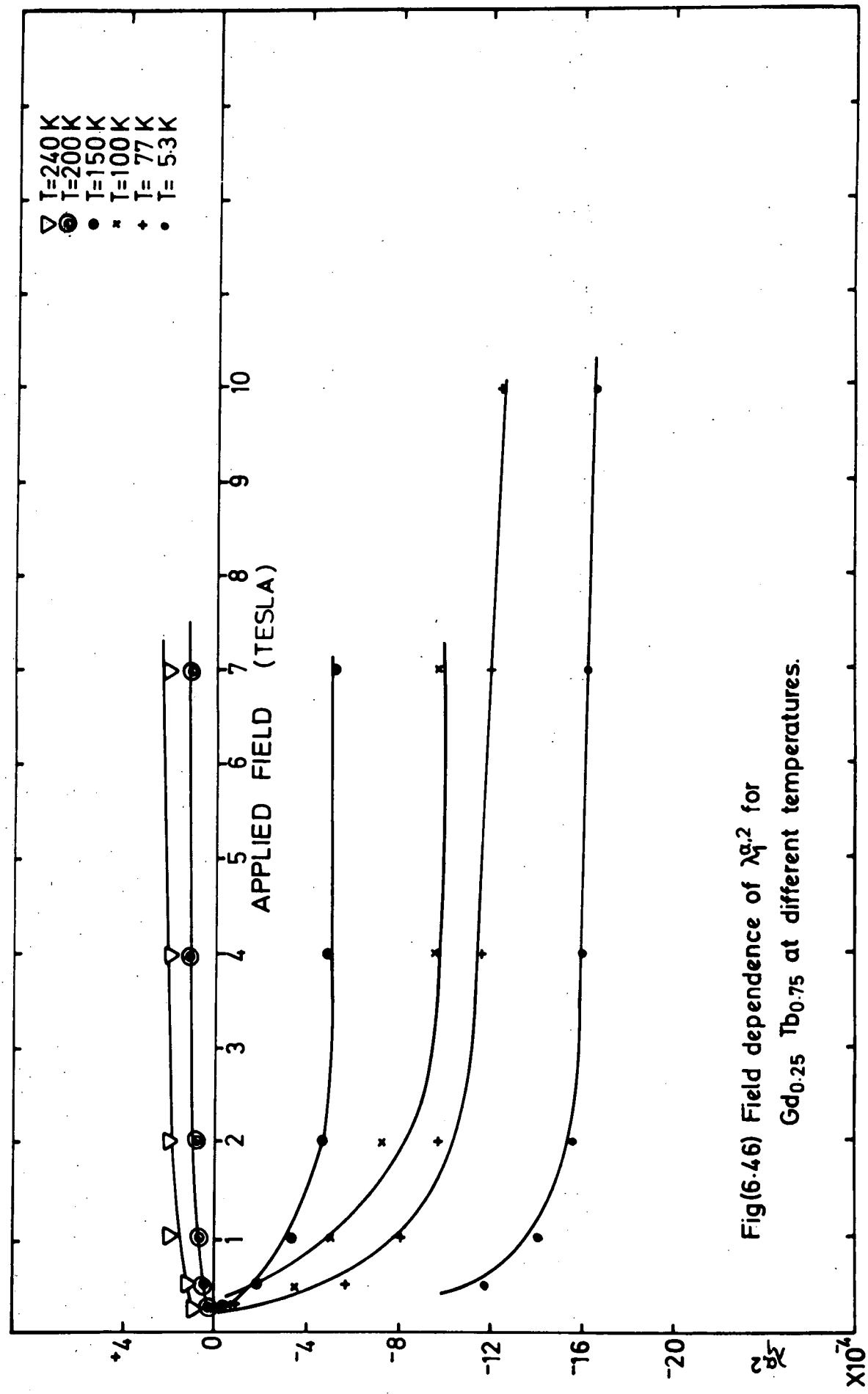

Fig(6.46) Field dependence of $\lambda_q^{2,2}$ for $Gd_{0.25}$ $Tb_{0.75}$ at different temperatures.

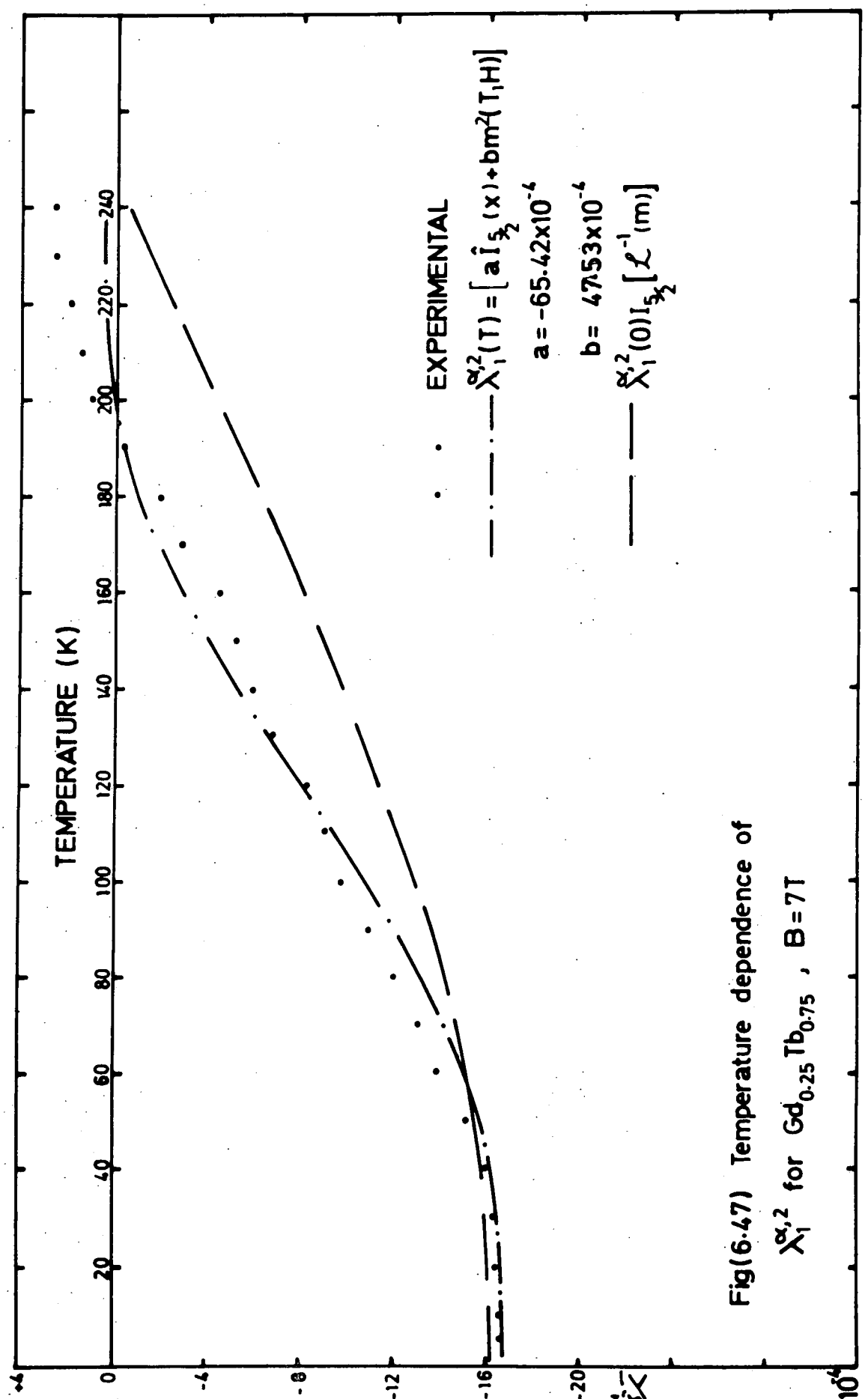

Fig(6.47) Temperature dependence of $\chi_1^{\alpha,2}$ for $Gd_{0.25}Tb_{0.75}$, B = 7T

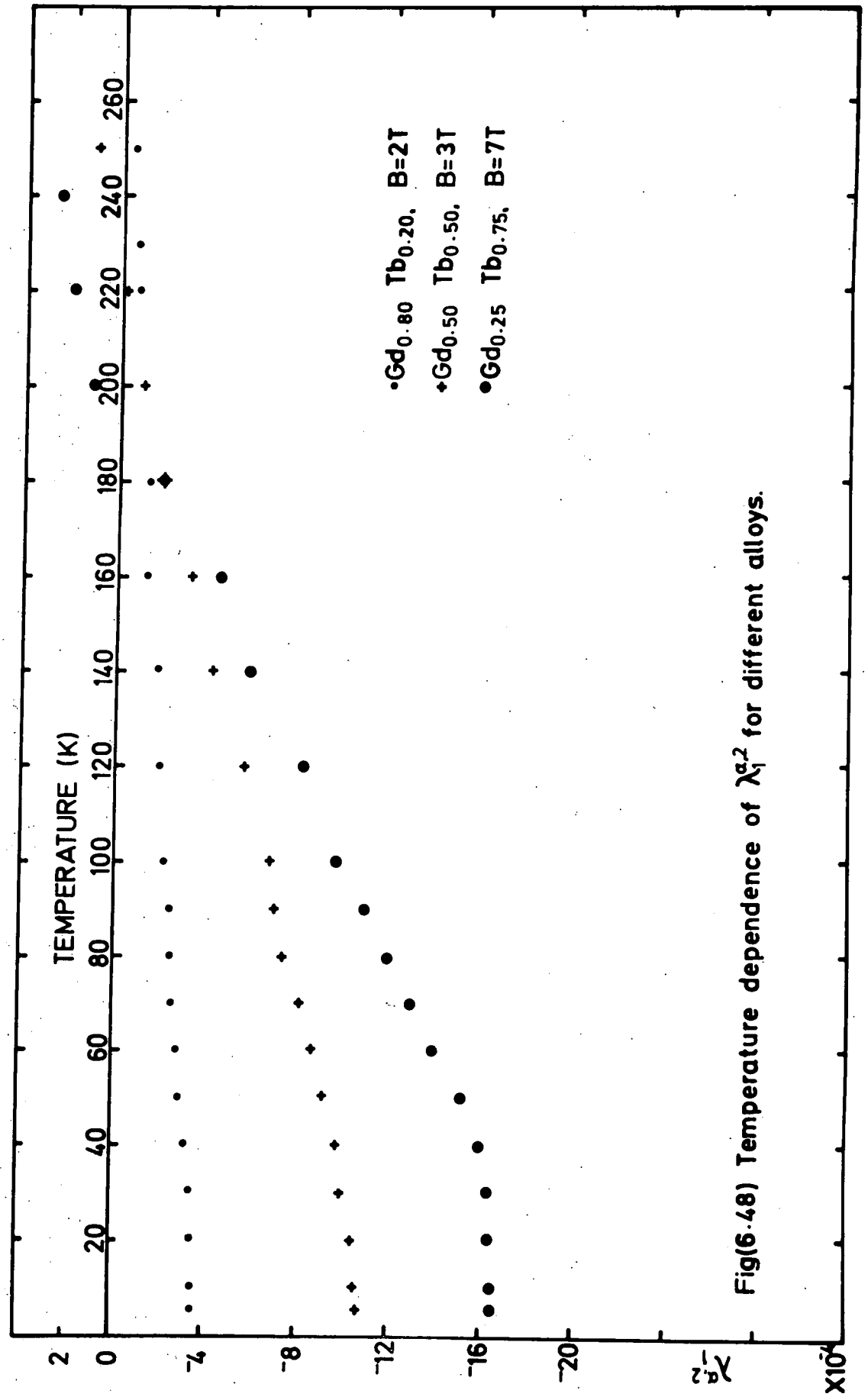

Fig(6.48) Temperature dependence of $\lambda_1^{\alpha,2}$ for different alloys.

Table (6.4) gives the variation of the two coefficients a and b with the alloy compositions.

TABLE (6.4): Variation of the two coefficients a and b with alloy composition for the magnetostriction coefficient $\lambda_1^{\alpha,2}$

Composition	a x 10^4	b x 10^4
$Gd_{0.80}Tb_{0.20}$	-5.78	2.1
$Gd_{0.50}Tb_{0.50}$	-33.5	22.2
$Gd_{0.25}Tb_{0.75}$	-65.4	47.5

6.4.4 Variation of $\lambda_1^{\alpha,2}$ With Alloy Composition.

Fig. (6.49) shows the variation of the normalized saturation values of magnetostriction coefficient $\lambda_1^{\alpha,2}(0)$ with alloy composition. It appears that the coefficient $\lambda_1^{\alpha,2}(0)$ increases linearly with increasing Tb content in the alloy; unlike the other coefficients an exponential relation was not obtained. No value of $\lambda_1^{\alpha,2}(0)$ for pure Terbium has been reported, but the results extrapolated linearly to the value found for Gadolinium by Mishima et al (1976).

6.5 The Magnetostriction Coefficient $\lambda^{\varepsilon,2}$

6.5.1. The Field Dependence of $\lambda^{\varepsilon,2}$

The magnetostriction coefficient $\lambda^{\varepsilon,2}$ was measured by measuring on a disc whose plane contained b and c axes the strain along a direction at 45^o to the c-axis and then evaluating $\lambda^{\varepsilon,2}$ using Eq. (3.50). Some of the experimental curves showing strain versus field direction for $Gd_{0.95}Tb_{0.05}$

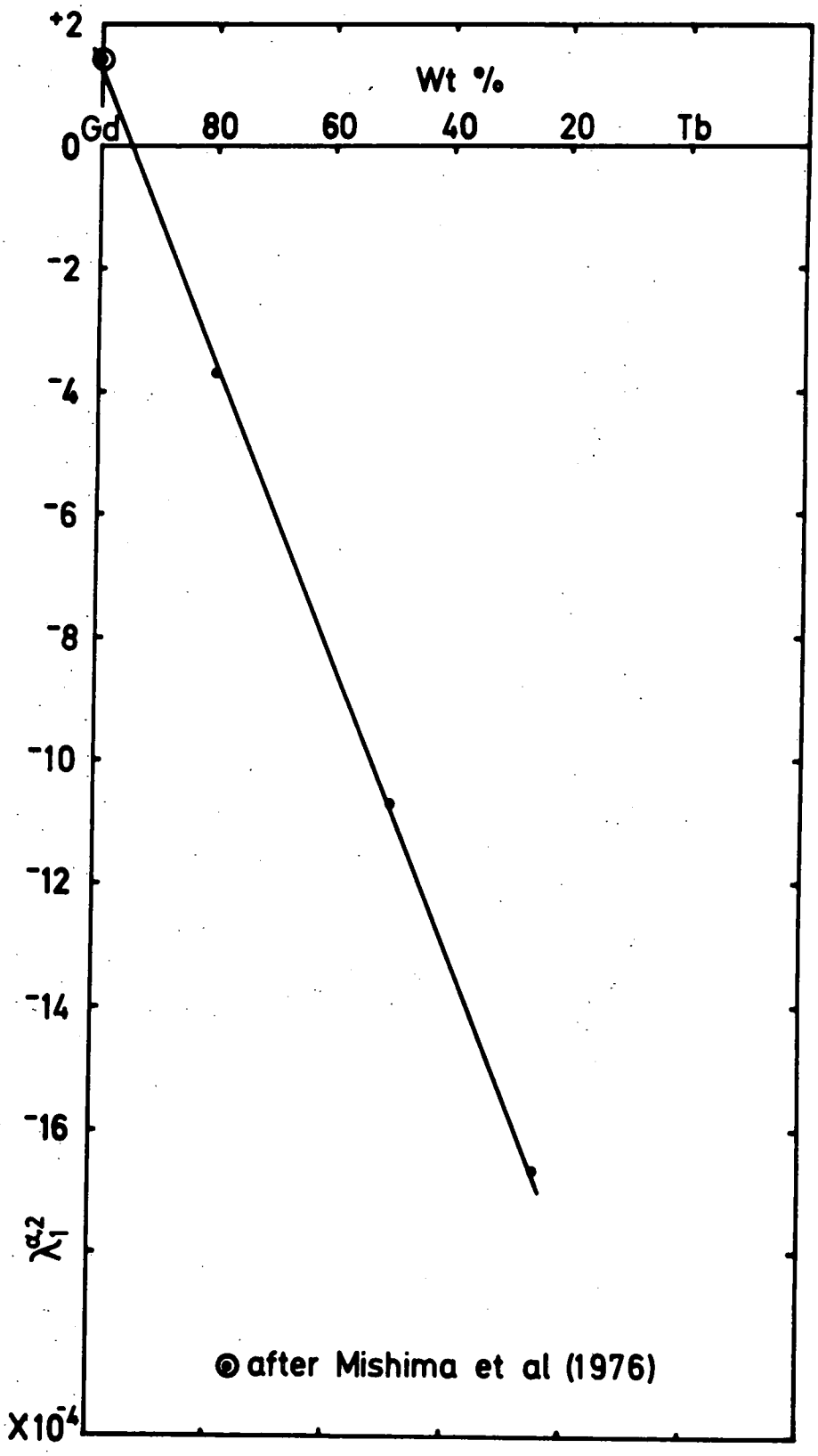

Fig.(6·49)

The normalized saturation magnetostriction coefficient $\lambda_1^{\alpha 2}$ as a function of alloy composition.

are shown from Fig.(6.50) to Fig. (6.53) for a range of temperatures. Other typical traces of strain against field direction are shown in Fig. (6.54) and Fig. (6.55). An anomaly was observed for the sample $Gd_{0.95}Tb_{0.05}$ in a direction of about 90°. This anomaly decreases with increasing temperatures and disappears at (69 ± 1) K. The strain measured at 45° to the c-axis does not repeat after a rotation of 90° as do the measurements already described, but a rotation of 180° is required. The curves for $Gd_{0.80}Tb_{0.20}$ are different from those observed in the sample containing 5% Tb, but on raising the temperature curves of similar form were obtained above 190 K as shown in Fig. (6.55). The low temperature curves for the sample $Gd_{0.50}Tb_{0.50}$ are of the same shape as those observed for the sample $Gd_{0.80}Tb_{0.20}$. The magnetostriction coefficients $\lambda^{\varepsilon,2}$ as a function of magnetic field at different temperatures were obtained by taking the value of the change in length between 0° and 45°. Results for samples containing 5% and 20% of Terbium are shown in Fig. (6.56) and Fig. (6.58) respectively. The first sample became saturated at about 1.5 Tesla and the other one at about 2 Tesla. The measurements for the sample $Gd_{0.50}Tb_{0.50}$ were carried out only at 5.3 K and the magnetostriction versus magnetic field direction result is shown in Fig. (6.60).

6.5.2. Temperature Dependence of $\lambda^{\varepsilon,2}$ Using Single-ion Theory.

The variation of $\lambda^{\varepsilon,2}$ with temperature for the two systems containing 5% and 20% Tb are shown in Fig. (6.57) and Fig. (6.59) respectively. Normalized saturation values of $\lambda^{\varepsilon,2}$ were taken as,

$$\lambda^{\varepsilon,2}(0) = (2.8 \pm 0.7) \times 10^{-4} \qquad \text{for } Gd_{0.95}Tb_{0.05}$$

$$\lambda^{\varepsilon,2}(0) = (6.4 \pm 1) \times 10^{-4} \qquad \text{for } Gd_{0.80}Tb_{0.20}$$

Values obtained using Eq. (6.4) are also shown in the figures. Fig. (6.57) shows that the single-ion theory does not give a reasonable fit to the experimental values, but for the sample containing 20% Tb the $\hat{I}_{5/2}(x)$

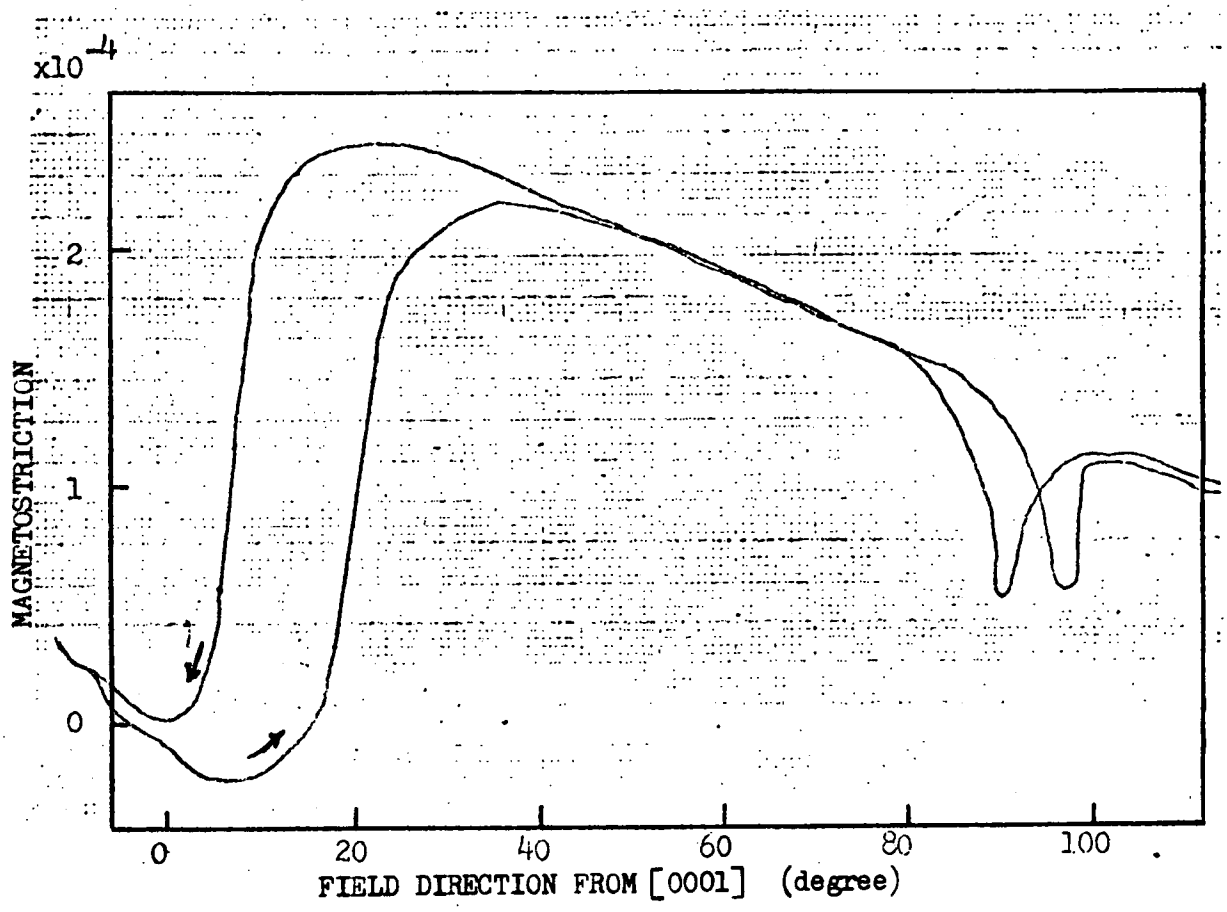

Fig.(6.50) Magnetostriction measured along 45° to c-axis in plane containing b and c axes as a function of field direction at 5.7 K and 4 Tesla, for $Gd_{0.95}Tb_{0.05}$.

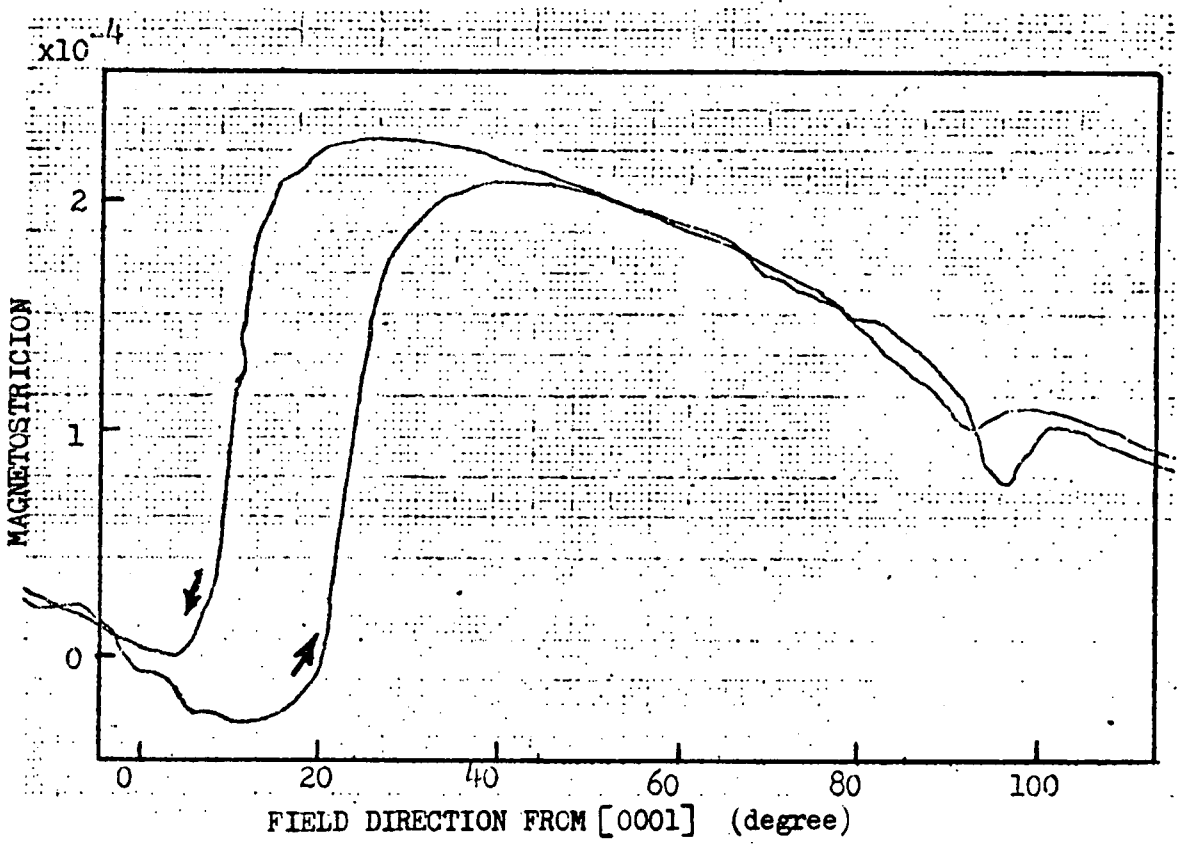

Fig.(6.51) Magnetostriction measured along 45° to c-axis in plane containing b and c axes as a function of field direction at 30 K and 4 Tesla, for $Gd_{0.95}Tb_{0.05}$.

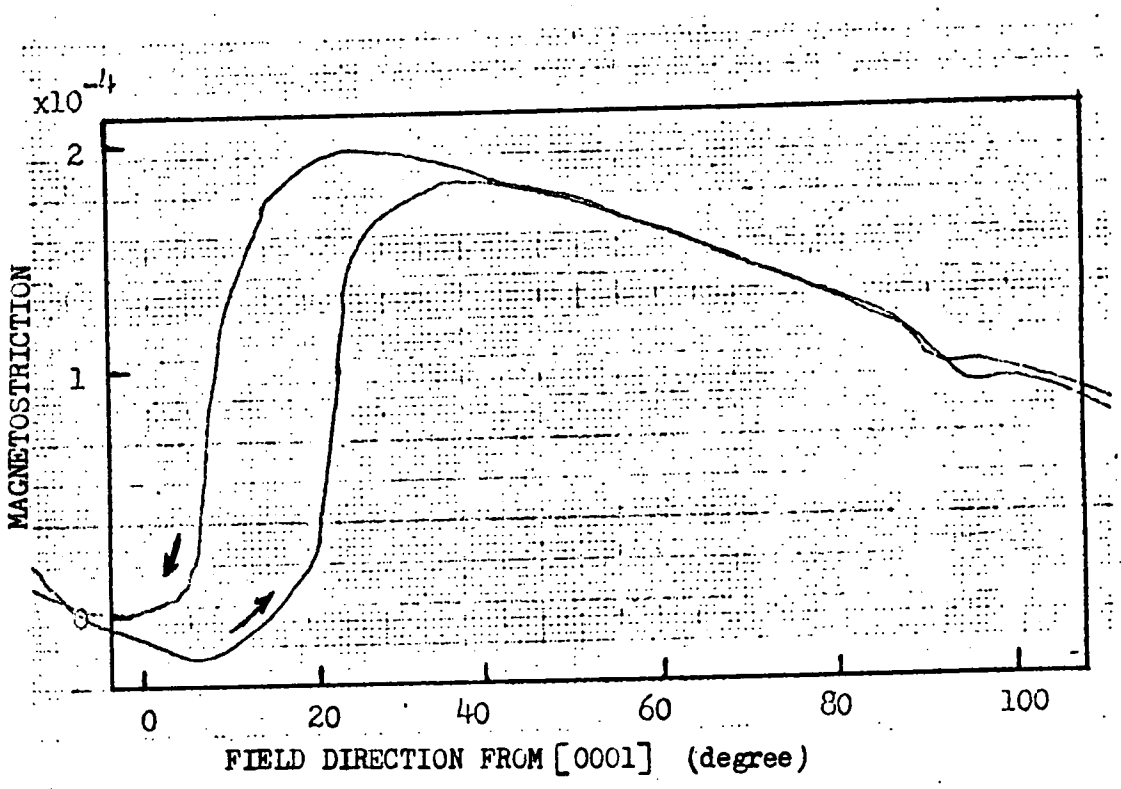

Fig.(6.52) Magnetostriction measured along 45^{o} to c-axis in plane containing b and c axes as a function of field direction at 50 K and 4 Tesla, for $Gd_{0.95}Tb_{0.05}$.

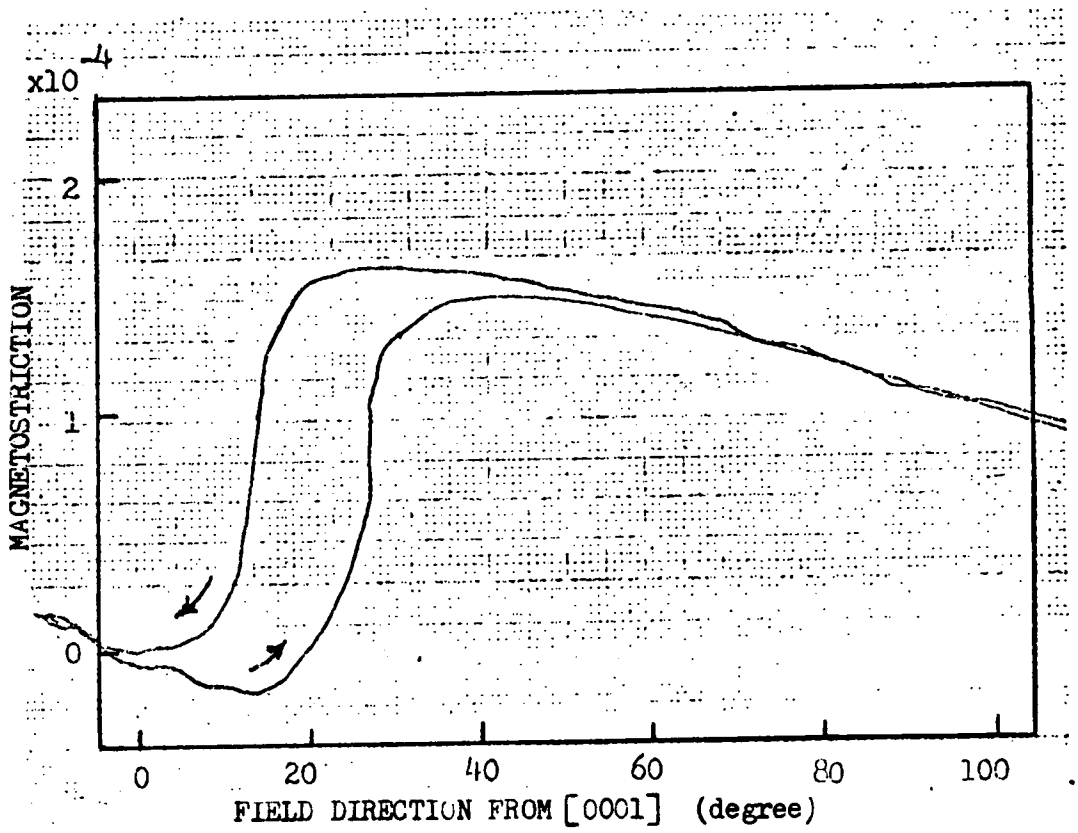

Fig.(6.53) Magnetostriction measured along 45^{o} to c-axis in plane containing b and c axes as a function of field direction at 70 K and 4 Tesla, for $Gd_{0.95}Tb_{0.05}$.

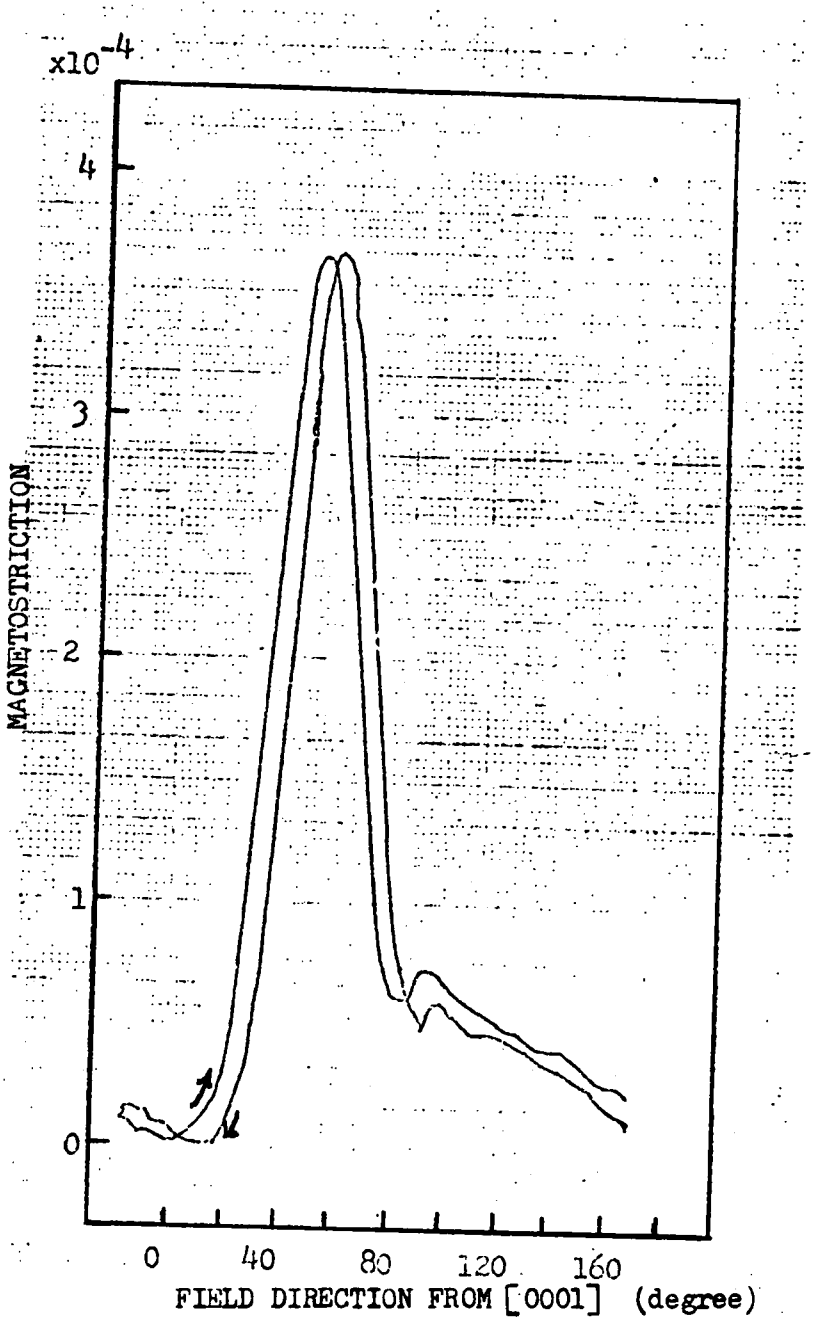

Fig.(6.54) Magnetostriction measured along 45° to c-axis in plane containing b and c axes as a function of field direction at 5.4 K and 0.5 Tesla, for $Gd_{0.80}Tb_{0.20}$.

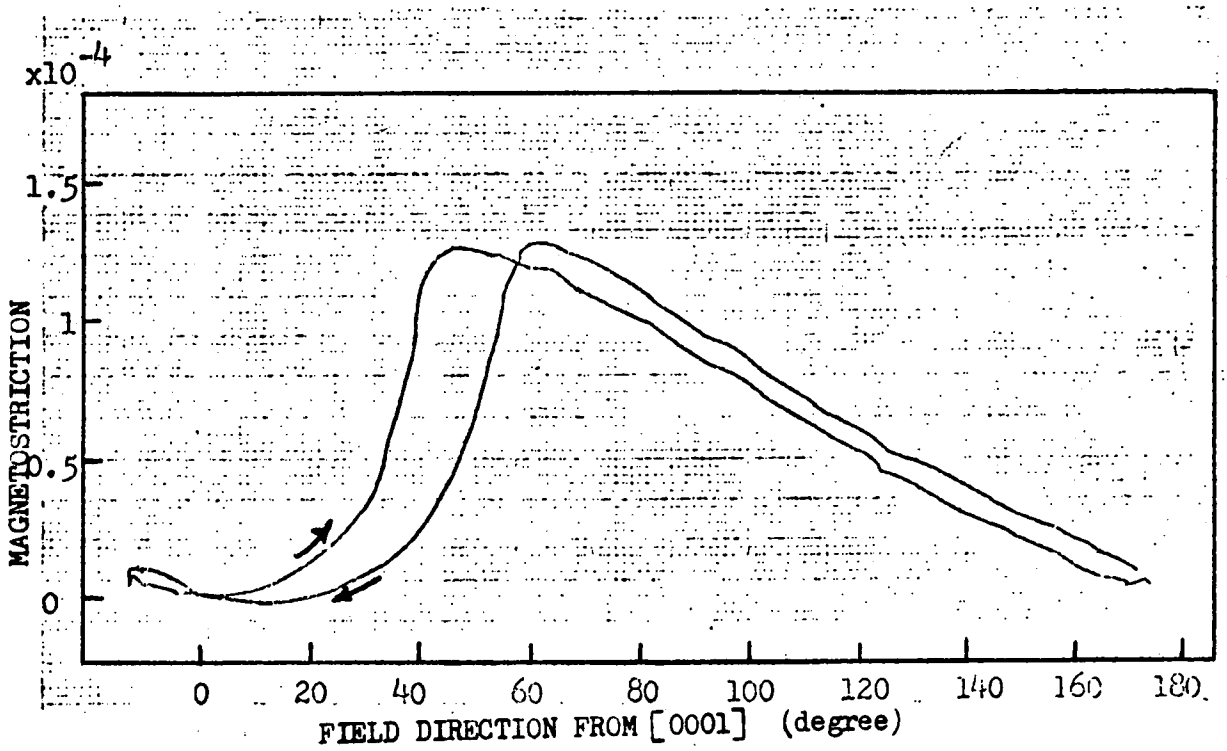

Fig.(6.55) Magnetostriction measured along 45^{o} to c-axis in plane containing b and c axes as a function of field direction at 250 K and 2 Tesla, for $Gd_{0.80}Tb_{0.20}$.

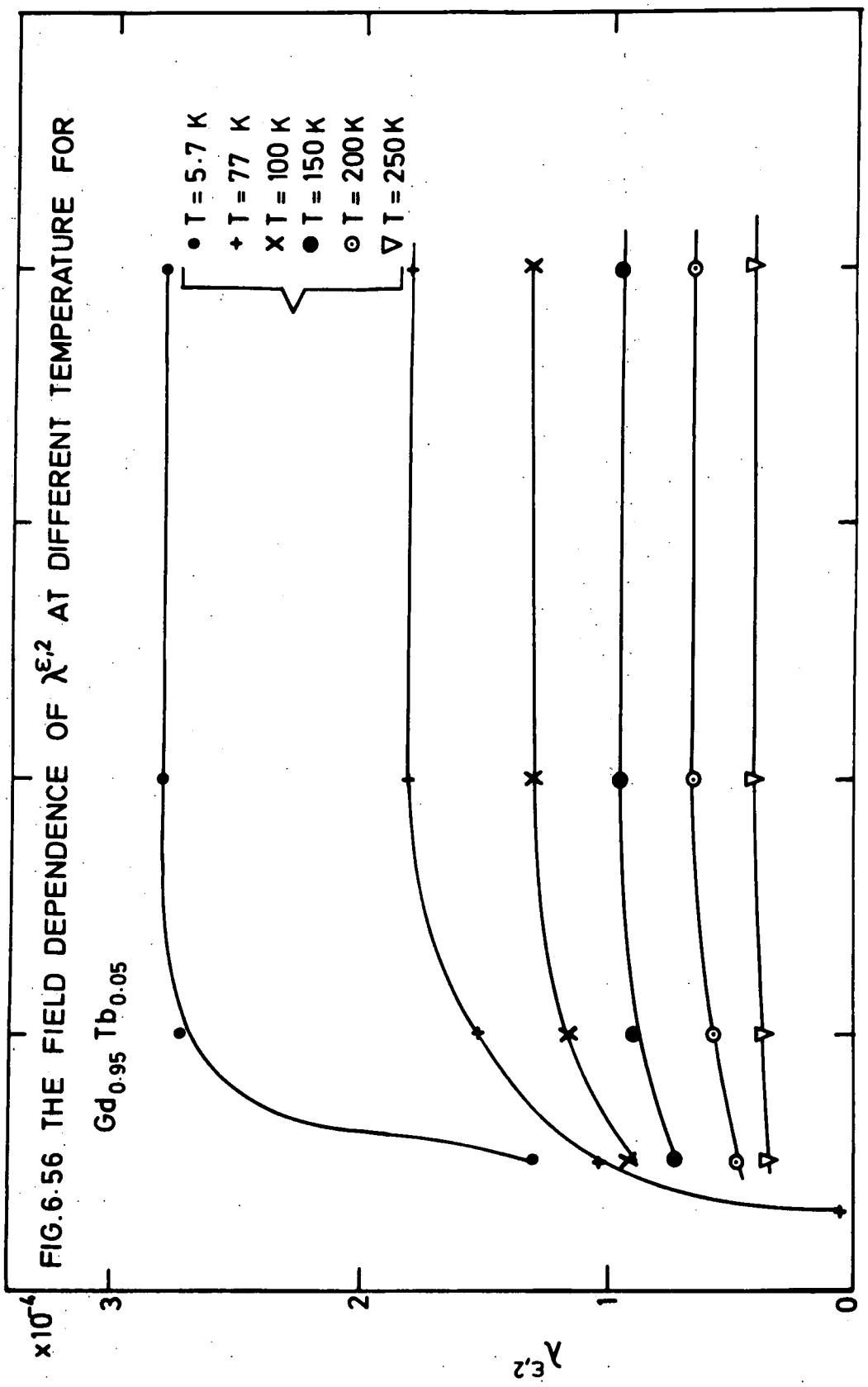
FIG.6.56 THE FIELD DEPENDENCE OF $\chi^{\epsilon,2}$ AT DIFFERENT TEMPERATURE FOR
$Gd_{0.95}Tb_{0.05}$
• T = 5·7 K
+ T = 77 K
× T = 100 K
● T = 150 K
⊙ T = 200 K
▽ T = 250 K
$\chi^{\epsilon,2}$
×10⁻⁴
3
2
1
0
0
2
4
APPLIED FIELD (TESLA)

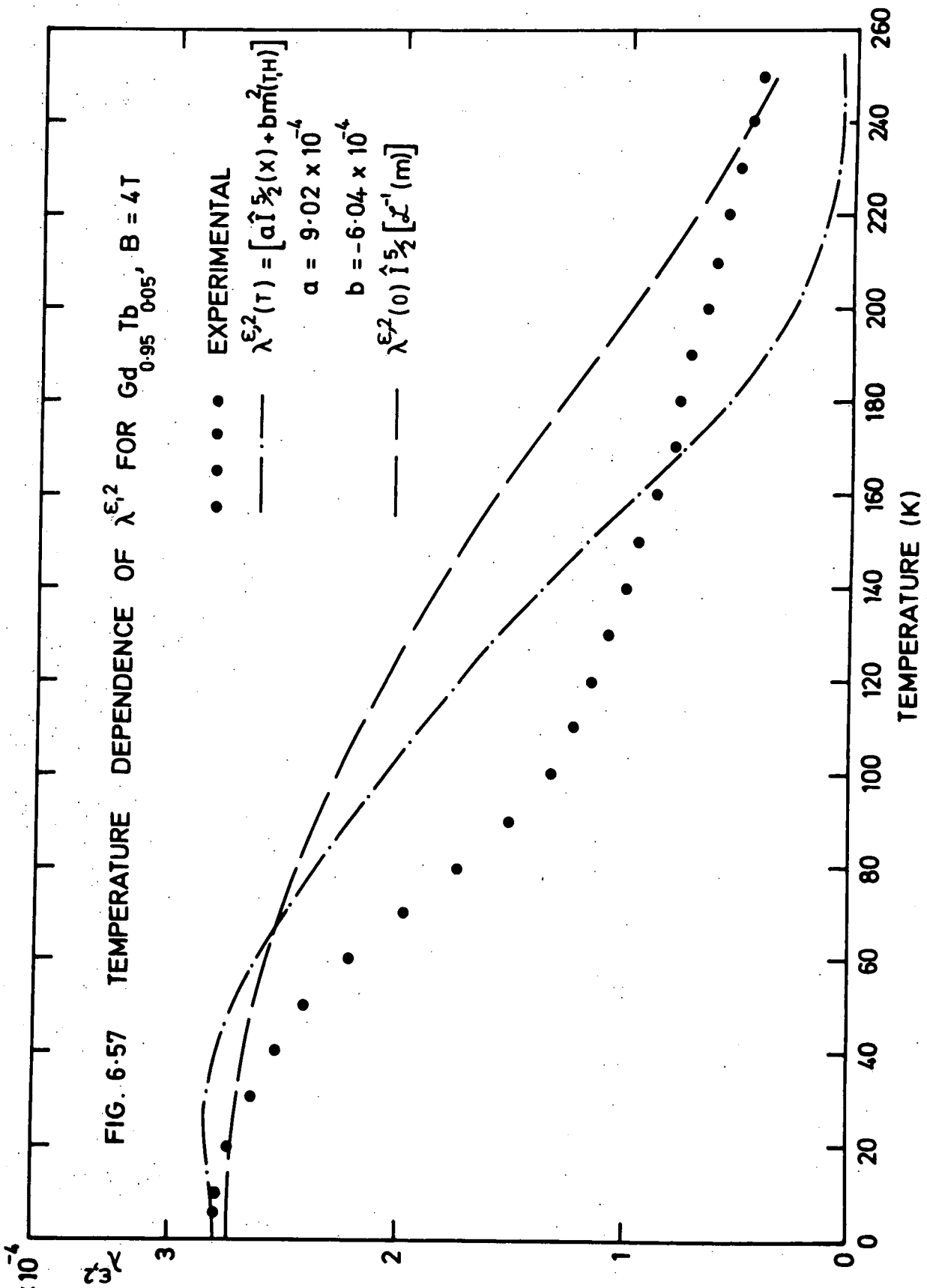
FIG. 6·57 TEMPERATURE DEPENDENCE OF $\lambda^{\varepsilon,2}$ FOR $Gd_{0.95}Tb_{0.05}$, B = 4 T
EXPERIMENTAL
$\lambda^{\varepsilon,2}(T) = [a\hat{I}^{5}_{2}(x) + bm^{2}(T,H)]$
a = 9·02 x 10^{-4}
b = −6·04 x 10^{-4}
$\lambda^{\varepsilon,2}(0)\,\hat{I}^{5}_{2}[\mathcal{L}^{-1}(m)]$
$\zeta_3 \lambda$
x 10^{-4}
3
2
1
0
0
20
40
60
80
100
120
140
160
180
200
220
240
260
TEMPERATURE (K)

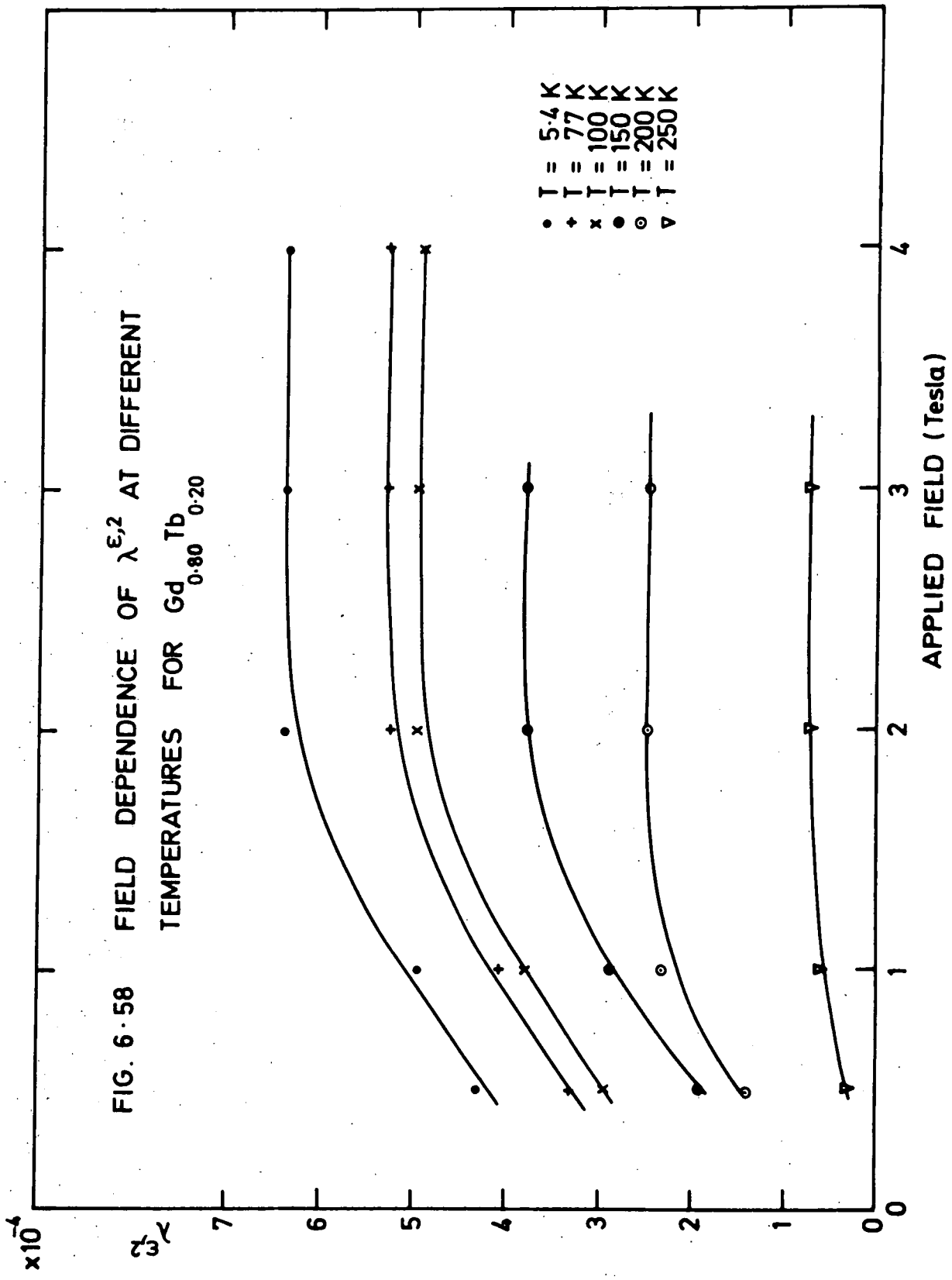

FIG. 6·58 FIELD DEPENDENCE OF $\lambda^{\varepsilon,2}$ AT DIFFERENT TEMPERATURES FOR $Gd_{0.80}Tb_{0.20}$

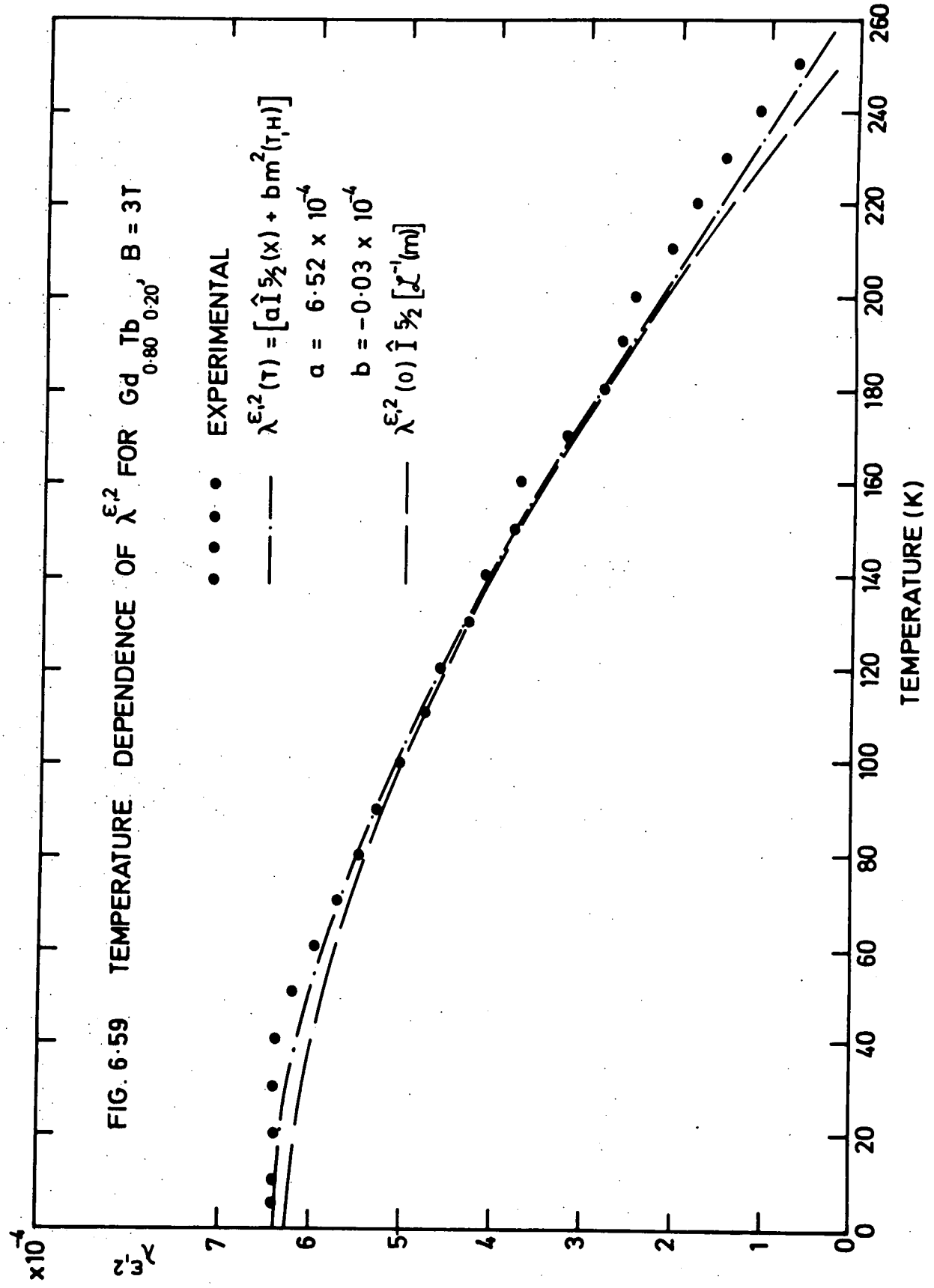
FIG. 6·59 TEMPERATURE DEPENDENCE OF $\lambda^{\varepsilon,2}$ FOR $Gd_{0.80}Tb_{0.20}$, B = 3T
EXPERIMENTAL
$\lambda^{\varepsilon,2}(T) = [a\hat{I}_{5/2}(x) + bm^2(T,H)]$
a = 6·52 x 10^{-4}
b = −0·03 x 10^{-4}
$\lambda^{\varepsilon,2}(0)\,\hat{I}_{5/2}[\mathcal{L}^{-1}(m)]$
$\lambda^{\varepsilon,2}$ x10^{-4}
TEMPERATURE (K)
0
1
2
3
4
5
6
7
0
20
40
60
80
100
120
140
160
180
200
220
240
260

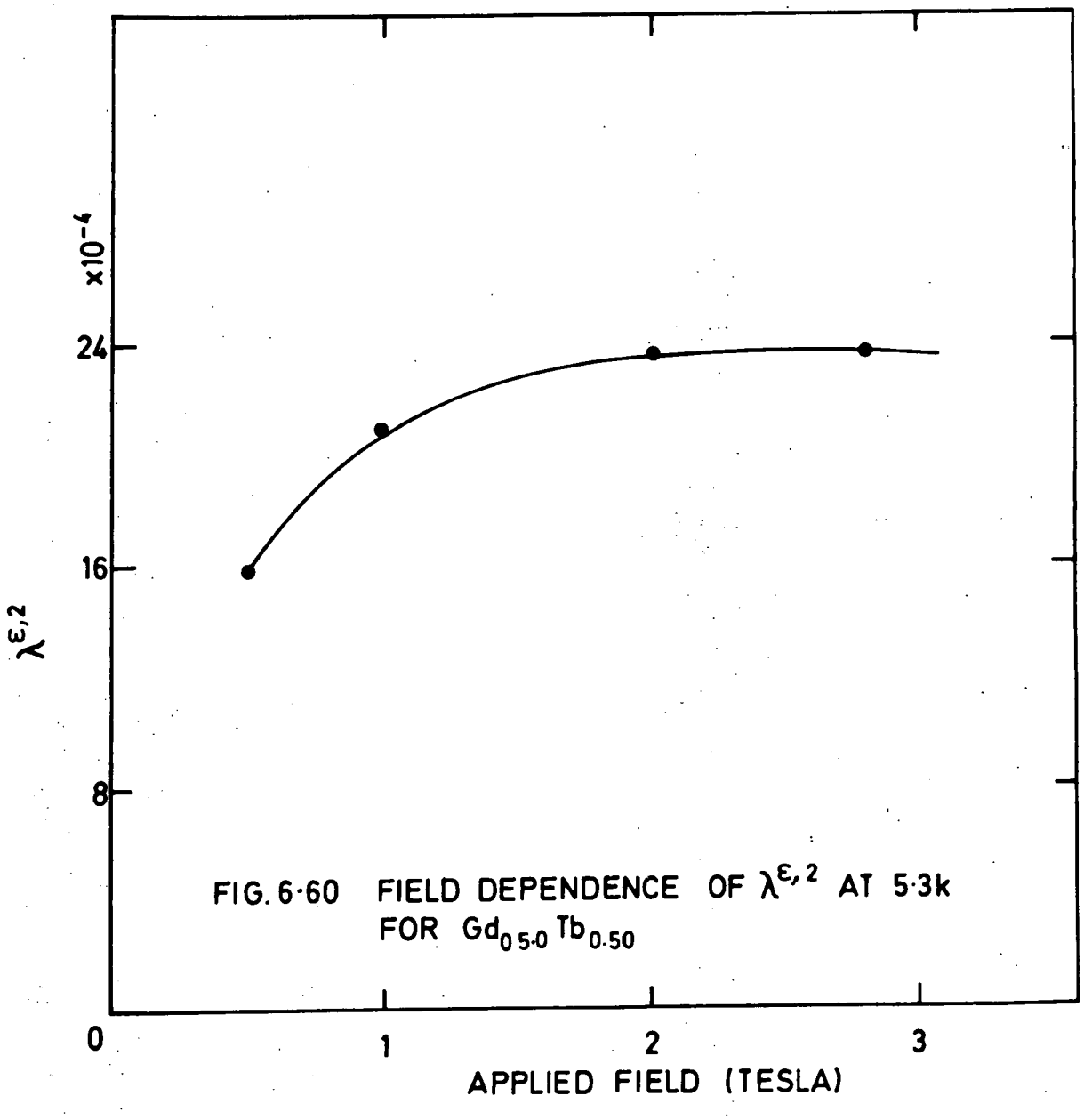

FIG. 6·60 FIELD DEPENDENCE OF $\lambda^{\varepsilon,2}$ AT 5·3k FOR $Gd_{0.5\cdot0}Tb_{0.50}$

function gives a reasonable representation of the temperature variation of the experimental results.

6.5.3. Temperature Dependence of $\lambda^{\varepsilon,2}$ Using an Expression Containing a Term Representing a Two-Ion Interaction

Even by using Eq. (6.5) which includes the two-ion term the temperature variation of the experimental values for the sample containing a low concentration of Terbium could not be fitted with the theoretical results. For the sample $Gd_{0.80}Tb_{0.20}$ not much difference can be seen between the values obtained by the single-ion theory or those obtained by Eq. (6.5) except that at temperatures below 70 K the values obtained by Eq. (6.5) give a better fit with the experimental results than the single-ion theory which gives slightly lower values. The values of the two terms a and b are given in Table (6.5).

TABLE (6.5): Variation of the two terms a and b with alloy composition for the magnetostriction coefficent $\lambda^{\varepsilon,2}$.

Composition	a x 10^4	b x 10^4
$Gd_{0.95}Tb_{0.05}$	9.0	-6.04
$Gd_{0.80}Tb_{0.20}$	6.52	-0.03

6.5.4. Variation of $\lambda^{\varepsilon,2}$ With Alloy Composition

Fig. (6.61) shows the normalized saturation values of $\lambda^{\varepsilon,2}_{(0)}$ against alloy composition. The value of $\lambda^{\varepsilon,2}_{(0)}$ for pure Terbium was obtained from du Plessis (1968) and had been measured in the paramagnetic region because the very large magnetic anisotropy below the Néel point which confines the magnetic moments to the basal plane did not allow him to measure $\lambda^{\varepsilon,2}$ at lower temperatures. However, du Plessis assumed the

Fig(6.61) The variation of the normalized saturation values of $\lambda^{\varepsilon,2}$ with the alloys composition.

⊙ After du Plessis (1968)

× After Mishima et al (1976)

——— From the relation $\lambda^{\varepsilon,2}(0) = A\, e^{BC}$

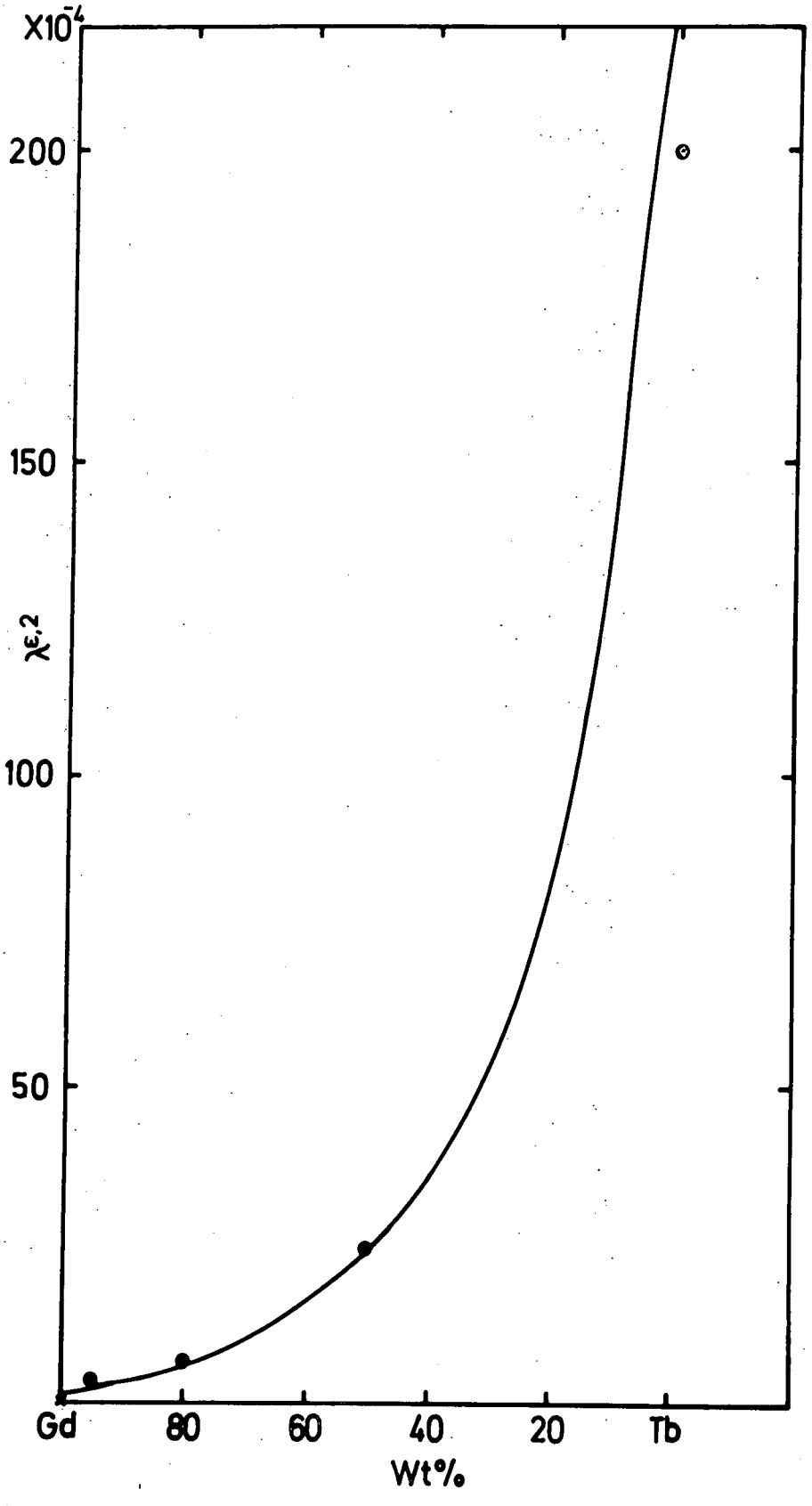

dependence of the classical single-ion theory and extrapolated the value to 0 K. The curve was extrapolated to the values of the pure metals given by Mishima et al (1976) for Gd and du Plessis for Tb. The results can be represented by the exponential relation given by Eq. (6.8) with the two constants A and B having the values,

$A = 232 \times 10^{-4}$

$B = -0.05$

6.5.5. Variation of $\lambda^{\varepsilon,2}(0) / \lambda^{\gamma,2}(0)$ With Alloy Composition

Tsuya et al (1964) have calculated the total theoretical magnetoelastic energies for Dy, $\tilde{B}^{\gamma,2}$ and $\tilde{D}^{\varepsilon,2}$, and the ratio of these coefficients was about 0.6. Clark et al (1965) have suggested that if the single-ion mechanism is the source of magnetostriction in all the ferromagnetic rare earth metals the ratio of $\lambda^{\varepsilon,2}(0) / \lambda^{\gamma,2}(0)$ for these metals should be approximately equal to 0.6. They have measured this ratio for Dy and have indeed found it to be 0.6; also they have calculated the ratio for Gd using the results of Alstad and Legvold (1964) and found it to be 0.65. For Tb du Plessis (1968) has obtained an anomalous value of 2.35. The results of the present investigation have been used to calculate the ratio of $\lambda^{\varepsilon,2}(0) / \lambda^{\gamma,2}(0)$ for the samples $Gd_{0.95}Tb_{0.05}$, $Gd_{0.80}Tb_{0.20}$, and $Gd_{0.50}Tb_{0.50}$, giving the values 0.87, 1.14, and 1.65 respectively. These values are shown in Fig. (6.62) as a function of composition. The curve may be reasonably extrapolated to the values of the pure elements given by Clark et al (1965) and by du Plessis (1968).

6.6 Rotational Hysteresis

When a disc of a magnetic material is turned slowly through 360° in a uniform magnetic field, the energy associated with this rotation is called the rotational hysteresis loss per cycle and is equal to,

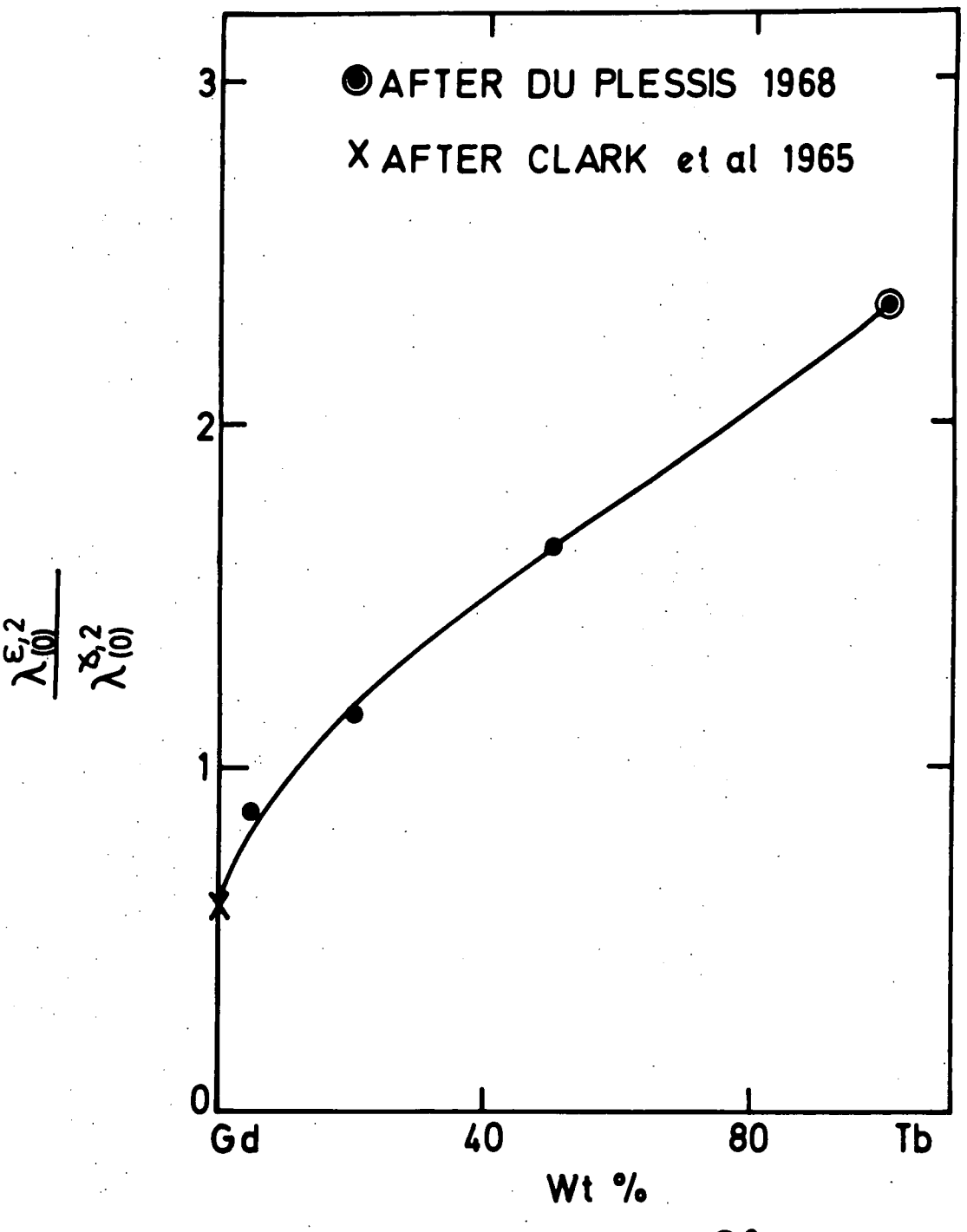

FIG. 6·62 THE VARIATION OF $\frac{\lambda^{\varepsilon,2}_{(0)}}{\lambda^{\gamma,2}_{(0)}}$ WITH ALLOY COMPOSITION.

$$W_r = -\int_0^{2\pi} L \, d\theta$$

.....(6.8)

where L is a torque acting on the disc and is given by,

$$L = - H M_s \sin \theta$$

.....(6.9)

where θ is the angle between the magnetic field H and the magnetization M_s. Determinations of W_r are usually made by measuring L using a torque magnetometer. This method was not feasible with the results of the current series of measurements, but to give a measure of the rotational hysteresis in arbitrary units the area enclosed between the clockwise and anticlockwise rotation b-axis magnetostriction curves for the $Gd_{0.80}Tb_{0.20}$ disc containing the b and c axes was measured for different magnetic fields. The values of these areas are given in Table (6.6) and some of the areas are shown shaded in Fig. (6.37) and (6.40). These areas were plotted against the field and the result is shown in Fig. (6.63), where a very sharp peak was obtained at about 1 Tesla; after this the curve falls rapidly at first and then more slowly above 6 Tesla.

The peak occurs when the sample is just beyond the knee of the magnetisation curve but after this the rotational hysteresis declines towards zero at saturation as found by Bozorth, (1951, p. 515) for a Ni sample.

In an unmagnetized specimen the domains are oriented at a random. When a field is applied domains in which the magnetization is parallel or at a small angle with the field grow at the expense of those where the magnetization is antiparallel. So the boundaries between domains are displaced. This continues on increasing the magnetic field or on turning the sample in a constant magnetic field about a line perpendicular to its axis. When the applied field is reduced or the rotation reversed, there is initially little change in the domain structure, so that the magnetization remains quite high. This gives rise to hysteresis.

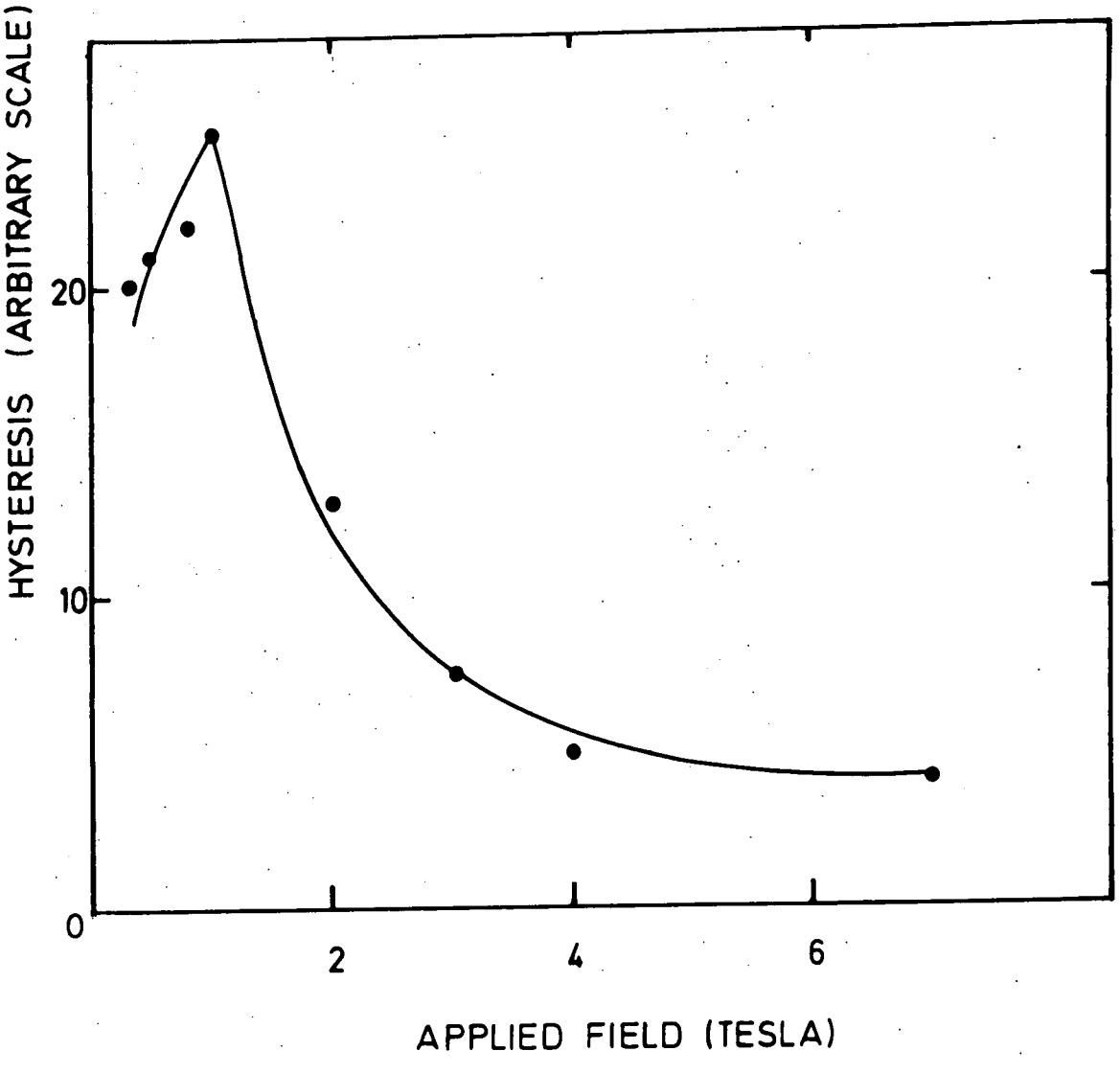

FIG. 6·63 VARIATION OF ROTATIONAL HYSTERESIS WITH APPLIED FIELD FOR $Gd_{0.80}Tb_{0.20}$ AT 4·5 k

TABLE (6.6): Variation of the rotational hysteresis (arbitrary units) with applied field for the sample $Gd_{0.80}Tb_{0.20}$ along b-axis in plane containing b and c axes at 4.5 K.

Applied Field Tesla	Hysteresis (Arbitrary Units)
0.3	20
0.48	21
0.8	22
1	25
2	13.3
3	7.5
4	5.5
7	4

6.7 Conclusion

The aim of the present study was to measure the magnetostriction in Gd-Tb alloys and to attempt to find the best fit between a theory using one of the Callen and Callen equations and the experimental results. The intention was to make a survey along the system Gd-Tb at fairly widely spaced concentrations to attempt to find the important regions of concentration for further investigations. The figures from Fig. (6.64) to Fig. (6.67) show in summary the experimental results for the four magnetostriction coefficients $\lambda^{\gamma,2}$, $\lambda_2^{\alpha,2}$, $\lambda_1^{\alpha,2}$, and $\lambda^{\varepsilon,2}$ studied as a function of temperature. The Tables from Table (6.7) to Table (6.10) give the magnetization values, $\hat{I}_{5/2}(x)$, the experimental results, and the values calculated by Eq. (6.5) for the four compositions studied.

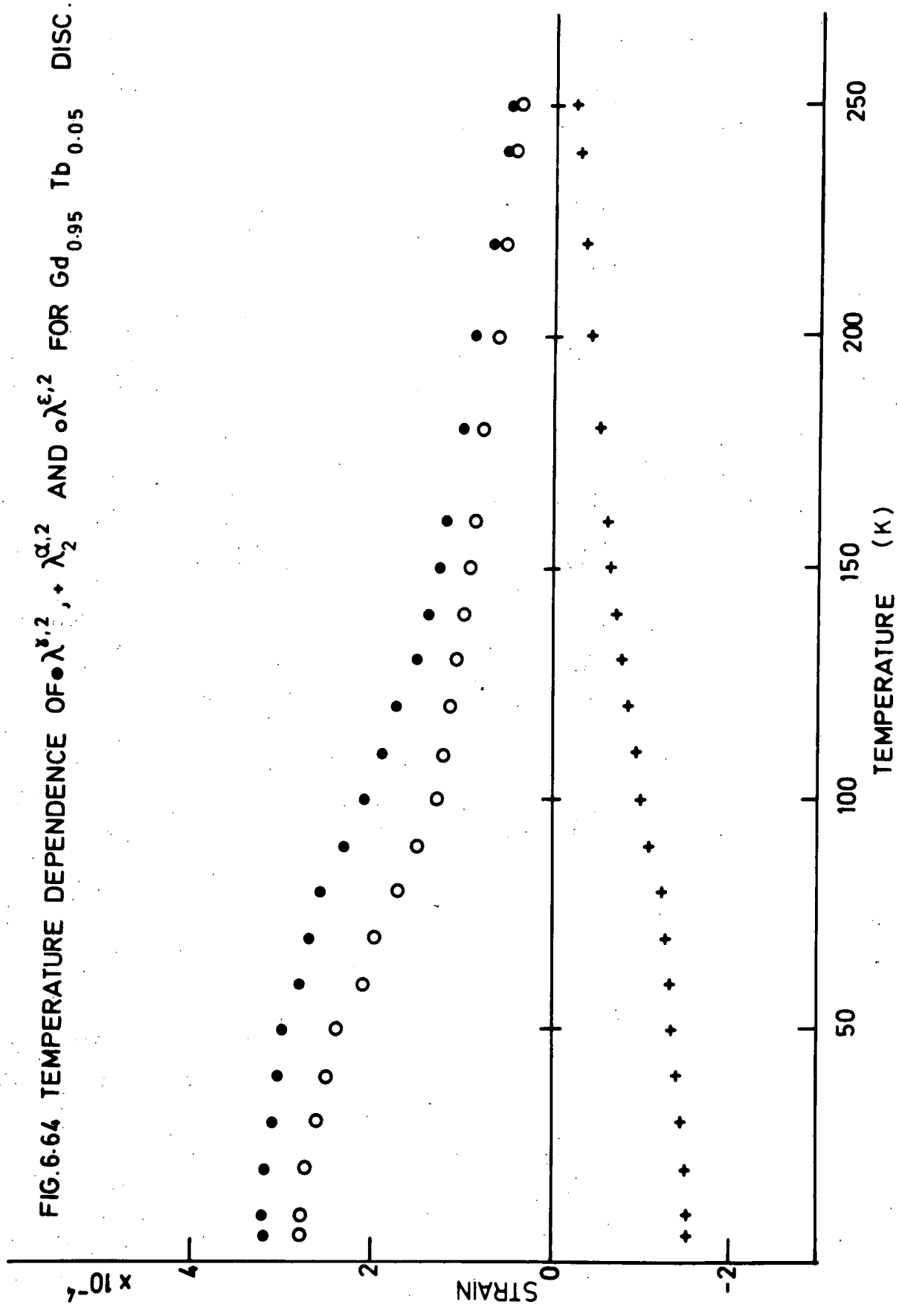

FIG.6.64 TEMPERATURE DEPENDENCE OF $\bullet\lambda^{\gamma,2}$, + $\lambda_2^{\alpha,2}$ AND $\circ\lambda^{\varepsilon,2}$ FOR $Gd_{0.95}$ $Tb_{0.05}$ DISC.

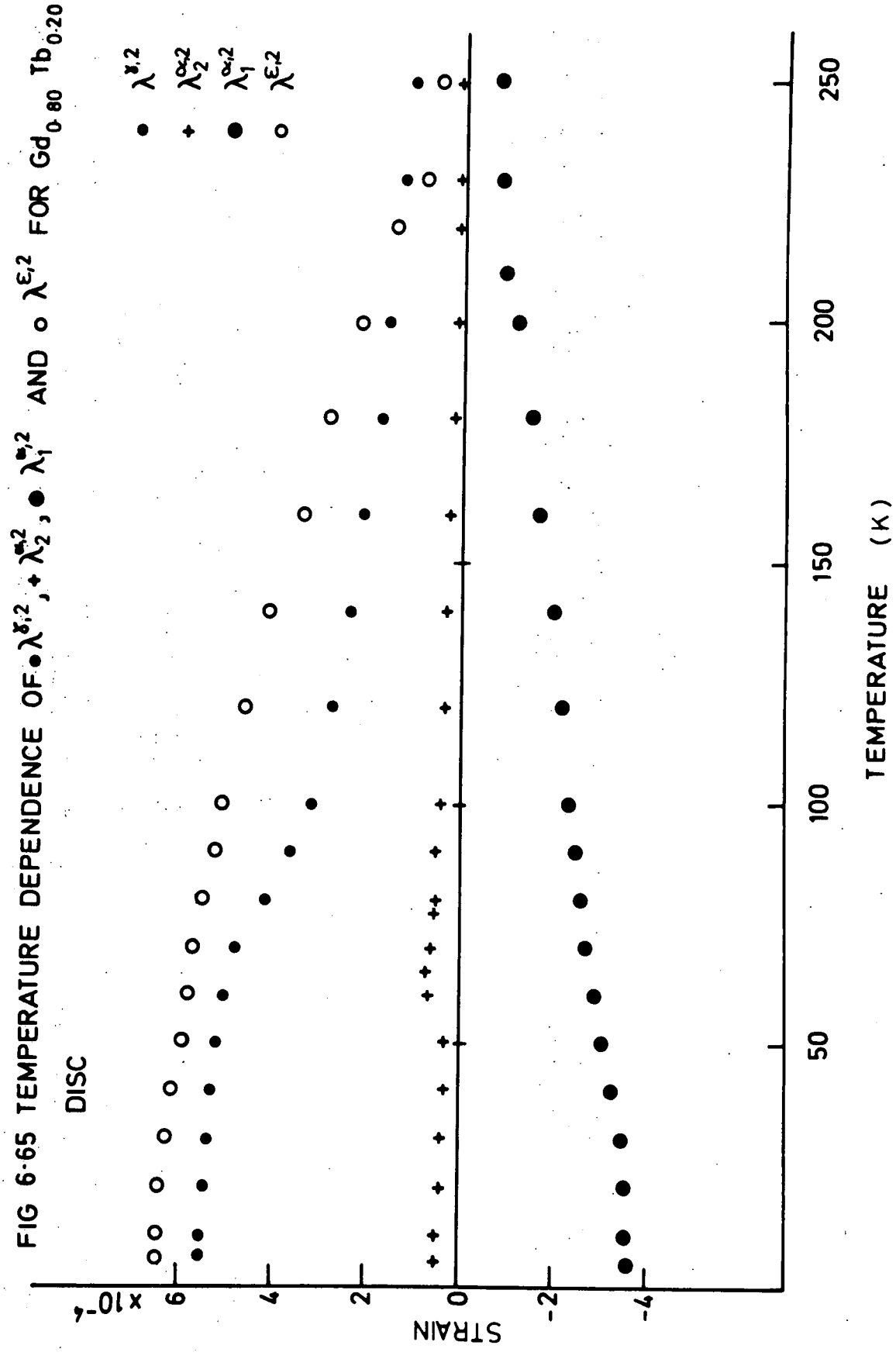
FIG 6·65 TEMPERATURE DEPENDENCE OF • $\lambda^{\gamma,2}$, + $\lambda_2^{\alpha,2}$, ● $\lambda_1^{\alpha,2}$ AND ○ $\lambda^{\varepsilon,2}$ FOR $Gd_{0.80}Tb_{0.20}$
DISC
$\lambda^{\gamma,2}$
$\lambda_2^{\alpha,2}$
$\lambda_1^{\alpha,2}$
$\lambda^{\varepsilon,2}$
STRAIN
x 10⁻⁴
6
4
2
0
-2
-4
50
100
150
200
250
TEMPERATURE (K)

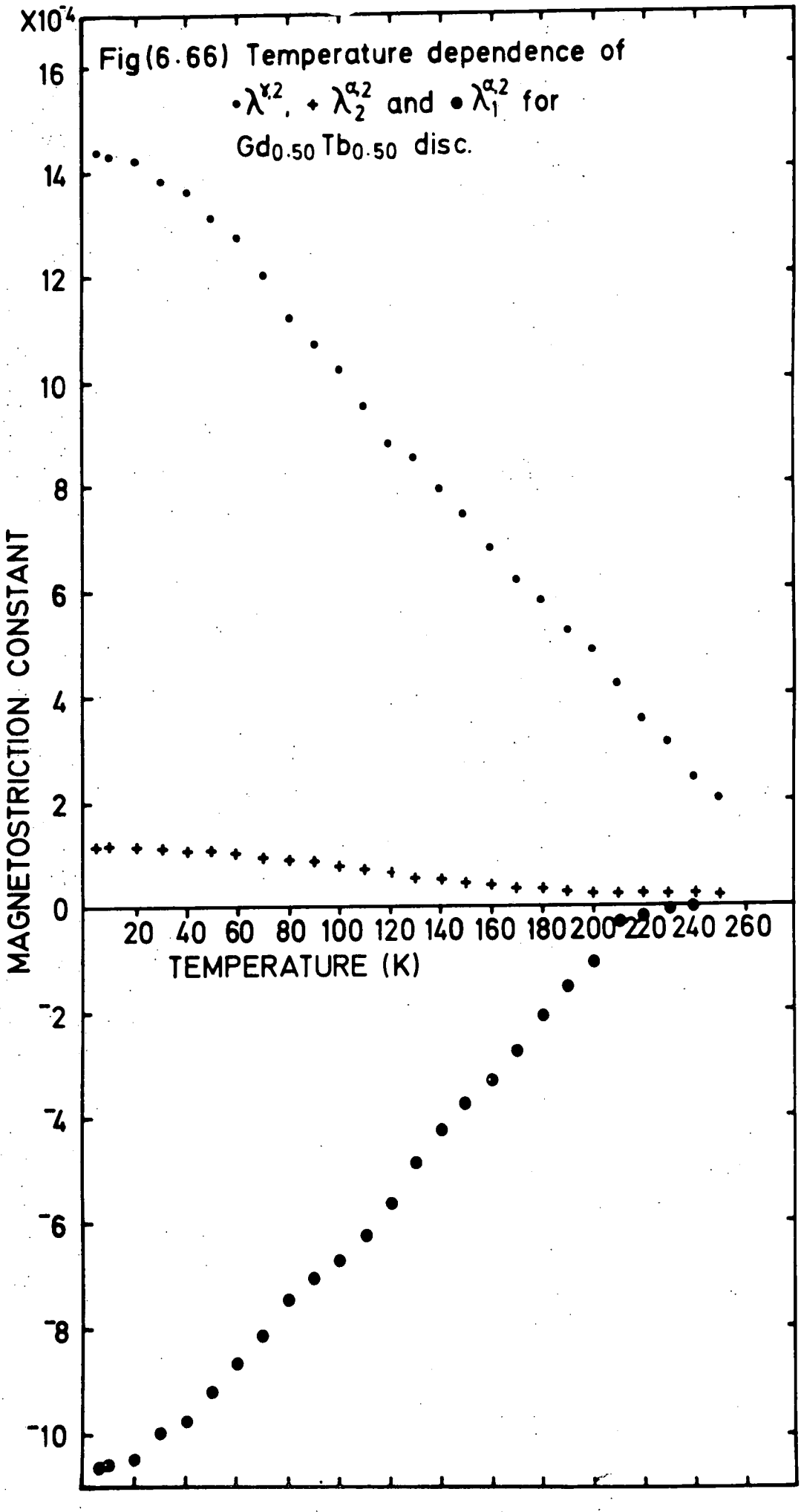

Fig(6.66) Temperature dependence of $\bullet\lambda^{\gamma,2}$, $+\ \lambda_2^{\alpha,2}$ and $\bullet\ \lambda_1^{\alpha,2}$ for $Gd_{0.50}Tb_{0.50}$ disc.

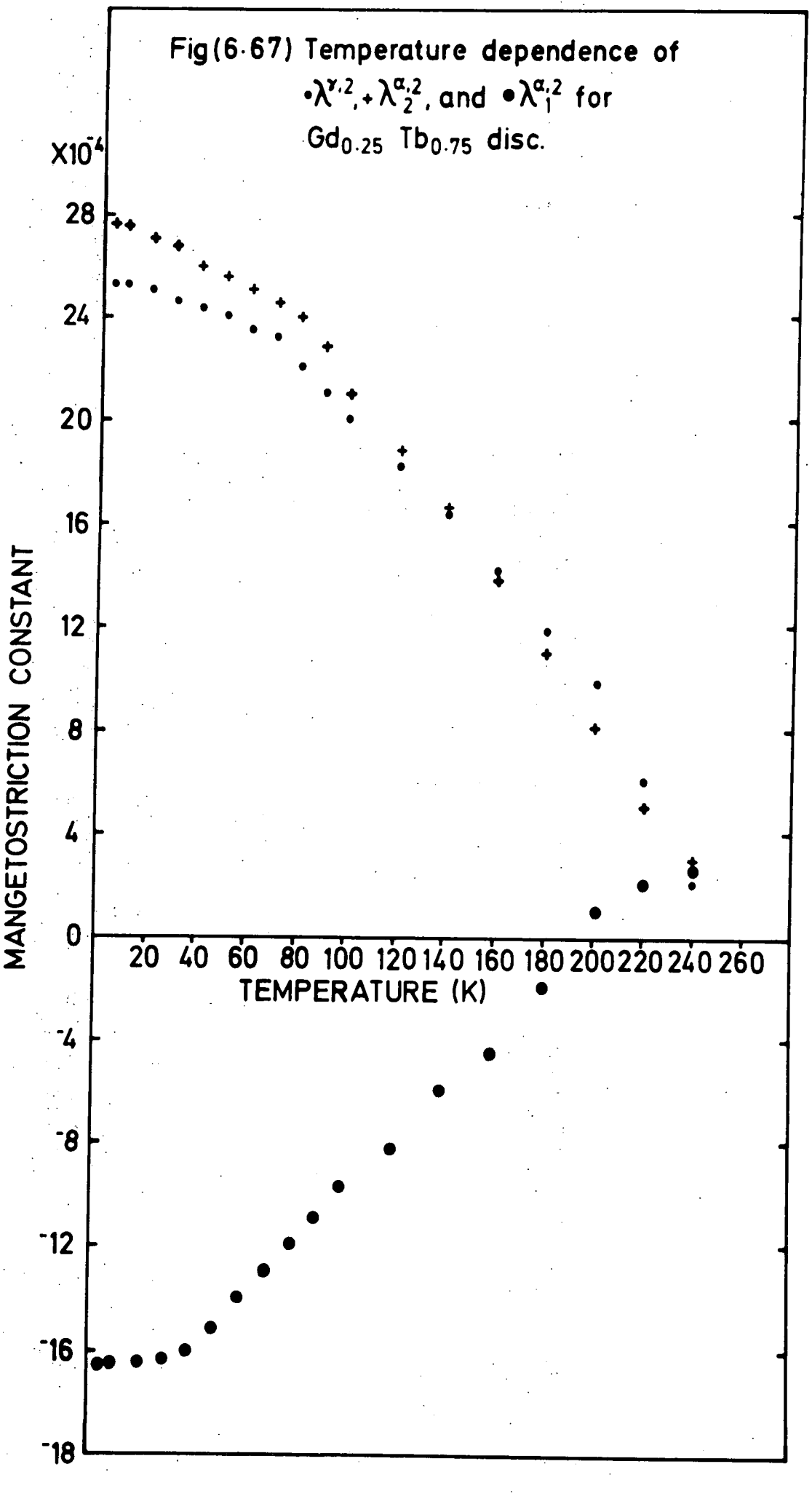
Fig(6·67) Temperature dependence of
•λ^γ,2, +λ^α,2_2, and •λ^α,2_1 for
Gd0.25 Tb0.75 disc.
X10^-4
28
24
20
16
12
8
4
0
-4
-8
-12
-16
-18
MANGETOSTRICTION CONSTANT
20 40 60 80 100 120 140 160 180 200 220 240 260
TEMPERATURE (K)

Along the alloy series the single-ion theory was successful only with the samples containing a high concentration of Terbium. By introducing a term representing a two-ion interaction the experimental results were better fitted than with the single-ion theory, but in most cases the fit was less close than could have been desired. The discrepancy between the experimental results and those calculated either using the single-ion mechanism or by Eq. (6.5) might be due to the uncertainty in the values of the magnetization as a function of temperature. No measurements of this parameter were available for the actual samples used and values obtained by interpolation of the results of Nikitin et al (1977b) had to be employed. Thus measurements of magnetization should be made on these samples over the whole ferromagnetic range. These would form a more satisfactory basis for the calculation of theoretical curves of variation of magnetostriction coefficients with temperature in particular at high temperature near the Curie point. Thus the applicability of theoretical models might be better tested.

While the molecular field-type theory of Callen and Callen for temperature dependence of the macroscopic anisotropy and magnetostriction using single-ion or two-ion models is a very successful theory in many situations it may be still too simple to represent the temperature dependence of the anisotropy and magnetostriction in the rare earths. However, spin-wave theory has received particular attention during the last few years, but the treatment of the anisotropy and magnetostriction is complicated and was not done systematically. The application of the spin-wave theory to calculate the origin of the anisotropy and magnetostriction in rare earths was discussed by J. Jensen in a series of papers, Jensen, (1976 and 1977). Lindgård and Danielsen (1974) have found significant deviations from the classical $\frac{l(l+1)}{2}$ temperature law.

TABLE (6.7) The Experimental and Calculated Values using Eq. (6.5) of $\lambda^{\gamma,2}$, $\lambda_2^{\alpha,2}$, and $\lambda^{\varepsilon,2}$ for $Gd_{0.95}Tb_{0.05}$

T(K)	$I_{\frac{3}{2}}^{m}(x)$	$I_{\frac{5}{2}}(x)$	$\lambda^{\gamma,2}$ x10^4 EXP	$\lambda^{\gamma,2}$ x10^4 CAL	$-\lambda_2^{\alpha,2}$ x10^4 EXP	$-\lambda_2^{\alpha,2}$ x10^4 CAL	$\lambda^{\varepsilon,2}$ x10^4 EXP	$\lambda^{\varepsilon,2}$ x10^4 CAL
0	1	0.98	3.22	3.22	1.53	1.53	2.8	2.8
10	1	0.98	3.22	3.22	1.52	1.53	2.8	2.8
20	1	0.98	3.19	3.25	1.50	1.54	2.75	2.84
30	0.99	0.98	3.1	3.27	1.46	1.55	2.63	2.87
40	0.99	0.97	3.04	3.22	1.40	1.53	2.52	2.82
50	0.98	0.95	3	3.12	1.38	1.48	2.41	2.72
60	0.97	0.92	2.82	2.97	1.35	1.41	2.21	2.57
70	0.97	0.91	2.72	2.92	1.3	1.39	1.98	2.52
80	0.96	0.88	2.6	2.77	1.24	1.32	1.74	2.37
90	0.95	0.84	2.34	2.6	1.13	1.24	1.51	2.19
100	0.94	0.82	2.1	2.51	1	1.20	1.32	2.11
110	0.92	0.78	1.9	2.32	0.94	1.11	1.23	1.92
120	0.91	0.75	1.75	2.18	0.85	1.04	1.18	1.78
130	0.89	0.71	1.54	2.01	0.79	0.97	1.10	1.61
140	0.88	0.67	1.4	1.82	0.72	0.88	1.00	1.42
150	0.85	0.62	1.28	1.61	0.66	0.78	0.95	1.22
160	0.82	0.56	1.2	1.35	0.6	0.66	0.87	0.98
180	0.76	0.46	1.02	0.94	0.52	0.47	0.80	0.58
200	0.69	0.35	0.9	0.59	0.42	0.30	0.66	0.28
210	0.65	0.30	0.8	0.47	0.37	0.24	0.62	0.18
220	0.61	0.26	0.72	0.40	0.34	0.20	0.57	0.15
230	0.56	0.22	0.64	0.28	0.29	0.15	0.50	0.07
240	0.5	0.17	0.56	0.22	0.26	0.12	0.46	0.05
250	0.44	0.14	0.5	0.22	0.2	0.11	0.42	0.10

TABLE (6.8) The Experimental and Calculating Values Using Eq. (6.5) of $\lambda^{\gamma,2}$, $\lambda_2^{\alpha,2}$, $\lambda_1^{\alpha,2}$, and $\lambda^{\varepsilon,2}$ for $Gd_{0.80}\ Tb_{0.20}$

T(K)	$I_{\frac{3}{2}}^{m}(X)$	$I_{\frac{5}{2}}(X)$	$\lambda^{\gamma,2}\times10^4$ EXP	$\lambda^{\gamma,2}\times10^4$ CAL	$\lambda_2^{\alpha,2}\times10^4$ EXP	$\lambda_2^{\alpha,2}\times10^4$ CAL	$-\lambda_1^{\alpha,2}\times10^4$ EXP	$-\lambda_1^{\alpha,2}\times10^4$ CAL	$\lambda^{\varepsilon,2}\times10^4$ EXP	$\lambda^{\varepsilon,2}\times10^4$ CAL
0	1	0.98	5.5	5.5	0.65	-	3.62	3.62	6.36	6.36
10	1	0.98	5.5	5.5	0.47	-	3.62	3.62	6.36	6.36
20	1	0.98	5.45	5.5	0.42	-	3.6	3.62	6.36	6.36
30	0.99	0.96	5.35	5.46	0.4	-	3.5	3.58	6.34	6.25
40	0.98	0.94	5.3	5.29	0.37	-	3.3	3.48	6.32	6.11
50	0.98	0.92	5.2	5.11	0.38	-	3.1	3.38	6.18	5.96
60	0.97	0.90	5	4.98	0.6	0.59	2.9	3.30	5.93	5.84
70	0.96	0.88	4.8	4.82	0.58	0.57	2.7	3.21	5.75	5.71
80	0.94	0.84	4.15	4.54	0.54	0.53	2.6	3.04	5.45	5.47
90	0.93	0.81	3.6	4.29	0.51	0.50	2.5	2.89	5.28	5.23
100	0.92	0.79	3.25	4.14	0.44	0.48	2.35	2.81	4.96	5.11
120	0.90	0.72	2.75	3.70	0.37	0.43	2.1	2.54	4.55	4.70
140	0.86	0.64	2.4	3.10	0.30	0.35	2.0	2.19	4.13	4.16
160	0.81	0.53	2.1	2.29	0.24	0.25	1.65	1.70	3.7	3.42
180	0.76	0.45	1.8	1.83	0.19	0.20	1.5	1.40	2.8	2.89
200	0.69	0.34	1.6	1.19	0.12	0.12	1.15	0.99	2.45	2.21
220	0.59	0.23	1.4	0.75	0.11	0.07	0.9	0.66	1.8	1.53
230	0.45	0.12	1.3	0.28	0.11	0.02	0.85	0.30	1.5	0.80
250	0.36	0.08	1.15	0.22	0.10	0.02	0.75	0.22	0.67	0.55

TABLE (6.9) The Experimental and Calculated Values Using Eq. (6.5) of $\lambda^{\gamma,2}$, $\lambda_2^{\alpha,2}$, and $\lambda_1^{\alpha,2}$ for $Gd_{0.50}Tb_{0.50}$

T(K)	$\frac{m}{2}$ $I_3(X)$	$\frac{I_5(X)}{2}$	$\lambda^{\gamma,2}$ x10^4 EXP	$\lambda^{\gamma,2}$ x10^4 CAL	$\lambda_2^{\alpha,2}$ x10^4 EXP	$\lambda_2^{\alpha,2}$ x10^4 CAL	$-\lambda_1^{\alpha,2}$ x10^4 EXP	$-\lambda_1^{\alpha,2}$ x10^4 CAL
0	1	0.98	14.4	14.4	1.15	1.15	10.7	10.7
10	1	0.98	14.3	14.4	1.15	1.15	10.6	10.7
20	1	0.98	14.2	14.4	1.13	1.16	10.5	10.85
30	0.99	0.98	13.8	14.4	1.09	1.17	10.0	10.89
40	0.99	0.97	13.6	14.3	1.06	1.15	9.8	10.82
50	0.98	0.95	13.1	13.98	1.04	1.12	9.2	10.46
60	0.97	0.92	12.8	13.56	0.99	1.08	8.7	9.94
70	0.96	0.90	12	13.16	0.95	1.03	8.2	9.44
80	0.95	0.87	11.2	12.76	0.91	0.99	7.5	8.95
90	0.94	0.83	10.7	12.22	0.86	0.93	7.1	8.27
100	0.92	0.78	10.2	11.47	0.80	0.85	6.8	7.37
110	0.90	0.74	9.5	10.89	0.72	0.79	6.3	6.71
120	0.89	0.70	8.8	10.33	0.64	0.73	5.7	6.10
130	0.87	0.66	8.5	9.68	0.57	0.67	4.9	5.37
140	0.85	0.61	7.9	8.95	0.51	0.60	4.3	4.58
150	0.82	0.55	7.4	8.13	0.47	0.52	3.8	3.67
160	0.79	0.51	6.8	7.41	0.42	0.45	3.3	2.99
170	0.75	0.44	6.2	6.41	0.36	0.36	2.8	2.05
180	0.72	0.40	5.8	5.82	0.32	0.32	2.1	1.67
190	0.69	0.35	5.2	5.17	0.29	0.27	1.6	1.21
200	0.66	0.32	4.8	4.63	0.26	0.24	1.1	1.06
210	0.61	0.26	4.2	3.77	0.24	0.17	0.4	0.46
220	0.56	0.22	3.5	3.15	0.23	0.14	0.3	0.33
230	0.49	0.16	3.1	2.32	0.22	0.10	0.11	0.10
240	0.37	0.08	2.4	1.24	0.21	0.04	0.05	-0.16
250	0.26	0.04	2	0.59	0.20	0.01	-0.1	-0.18

TABLE (6.10) The Experimental and Calculated Values Using Eq. (6.5) of $\lambda^{\gamma,2}$, $\lambda_2^{\alpha,2}$, and $\lambda_1^{\alpha,2}$ for $Gd_{0.25}Tb_{0.75}$

T(K)	$I_{\frac{3}{2}}^{m}(X)$	$I_{\frac{5}{2}}(X)$	$\lambda^{\gamma,2}$ x10^4 EXP	$\lambda^{\gamma,2}$ x10^4 CAL	$\lambda_2^{\alpha,2}$ x10^4 EXP	$\lambda_2^{\alpha,2}$ x10^4 CAL	$-\lambda_1^{\alpha,2}$ x10^4 EXP	$-\lambda_1^{\alpha,2}$ x10^4 CAL
0	1	0.98	25.3	25.3	27.62	27.62	16.6	16.6
10	1	0.98	25.2	25.2	27.62	27.62	16.6	16.6
20	0.99	0.98	25	25.16	27	27.67	16.4	17.19
30	0.99	0.97	24.6	24.98	26.8	27.45	16.3	16.98
40	0.98	0.95	24.4	24.58	26	26.90	16	16.37
50	0.98	0.94	24	24.19	25.7	26.39	16.2	15.81
60	0.97	0.91	23.6	23.59	25.1	25.58	14	14.88
70	0.96	0.89	23.2	23.22	24.6	25.10	13	14.39
80	0.95	0.87	22	22.64	24	24.31	12	13.49
90	0.94	0.83	21	21.91	22.8	23.36	11	12.49
100	0.92	0.79	20	20.82	21	21.94	9.8	10.98
120	0.89	0.70	18.2	18.95	18.8	19.55	8.3	8.57
140	0.84	0.60	16.4	16.67	16.5	16.65	6	5.68
160	0.80	0.50	14.2	14.27	13.8	13.51	4.6	2.32
180	0.72	0.40	11.8	11.56	11	10.72	2	1.14
200	0.63	0.29	9.8	8.65	8.01	7.77	1	-0.01
220	0.53	0.19	6	5.93	5.3	5.14	-2	-0.64
240	0.22	0.03	2	0.98	3	0.82	-2.5	-0.22

It is clear from the magnetostriction curves that higher order terms are involved, so more advanced analyses using higher order equations will allow the determination of higher order magnetostriction coefficients. This will enable more reliable values of the lower order coefficients to be obtained and permit a more realistic comparison with theory.

The anomaly observed in $\lambda_2^{\alpha,2}$ for the sample containing 20% Tb should be further investigated by filling the gap between 5% and 20% of Terbium with more alloys to find how the coefficient varies with temperature in the region of composition where it is changing sign.

The ratio $\lambda^{\varepsilon,2}(0)/\lambda^{\gamma,2}(0)$ appears to have an anomalously large value compared with that expected for heavy rare earth metals and increases with increasing Tb concentration in the alloy. Another technique for measuring this ratio will give more clarity. An x-ray technique may be applicable.

6.8 Suggestion For Further Work

It is important to measure the magnetization of the Gd-Tb alloy system using the presently available high quality samples. This will give accurate values for the calculation of the theoretical temperature variation using a single-ion model or Eq. (6.5). However, when magnetostriction coefficients are obtained from macroscopic measurements on materials in which magnetization varies sharply with applied field there is always some doubt as to what is the appropriate magnetization value to be used in conjunction with the value of a particular coefficient at a given temperature. The alloys with high Tb content show strong temperature dependence in the region of the Curie point. The values of $\lambda^{\gamma,2}$ obtained by Clark (1980) using the x-ray technique were very well fitted by Eq. (6.5). This suggests that it might be preferable to measure the magnetostriction coefficients at zero field using the x-ray diffraction

technique and also to measure the temperature variation of the reduced magnetization from the intensity of neutron diffraction peaks for Gd-Tb alloy over the whole ferromagnetic range. Domain and other effects which make difficult the achievement of reliable saturation values are avoided entirely. This would allow the comparison of the theoretical models with the temperature variation of the magnetostriction coefficients at zero field.

More measurements of $\lambda_2^{\alpha,2}$ for compositions between 5% and 20% of Tb should be made to investigate the anomalous behaviour of this coefficient. Also values of very low concentration of Gd between the pure Gadolinium metal and 5% of Terbium will give more information about the validity of Eq. (6.5) because Callen and Callen (1965) found that this equation was fitted well by pure Gd. Also it is desirable to repeat the measurements for the metals Gd and Tb using high purity material to check the results of previous workers which have been assumed in the previous discussion.

The computer program could be elaborated by adding more terms to Eq. (6.5) with m raised to higher even numbers. Thus attempts could be made to find an empirical series better able to represent the experimental results. The data could also be subjected to Fourier analysis using a higher order equation than Eq. (3.25) which is of second order only, yeilding values of higher order magnetostriction coefficients.

In parallel of these investigation measurements of magnetocrystalline anisotropy should be made as these too can throw light on the validity of the theoretical models examined in the present work.

REFERENCES

Alberts, L., and du Plessis, P., (1968) — Thermal expansion and forced magnetostriction in a Terbium single crystal. J. Appl. Phys. 39 581

Alstad, J.K., and Legvold, S., (1964) — Saturation Magnetostriction Constants of Gd. J. Appl. Phys. 35 1752

Arajs, S., Keeby, J.R., Rao, K.V., and Rapp, O. (1975) — Magnetic susceptibility of polycrystalline Tb in the neighbourhood of the Néel temperature. J. Low Temp. Phys. 21 91

Barkhausen, H., (1919) — Earth noises and noises due to change of magnetization of Iron. Phys. Zeit 20 401

Behrendt, D.R., Legvold, S. and Spedding, F.H., (1958) — Magnetic properties of Dy single crystals. Phys. Rev. 109 1544

Birss, R.R., (1959) — The saturation magnetostriction of ferromagnetics Advances Phys. 8 252

Bleaney, B.I., and Bleaney, B., (1976) — Electricity and Magnetism Oxford University Press

Bloch, F., (1932) — Theory of the exchange problem and of the residual ferromagnetism. Z. Physik 74 295

Bozorth, R.M., (1951) — Ferromagnetism, Van-Nostrand, Princeton

Bozorth, R.M. (1954) — Magnetostriction and crystal anisotropy of single crystals of hexagonal Cobalt. Phys. Rev. 96 311

Bozorth, R.M., and Van Vleck, J.H. (1960) — Mangetic susceptibility of metallic Eu Phys. Rev. 118 1493

Bozorth, R.M. and Wakiyama, T., (1963) — Magnetostriction and anomalous thermal expansion of single crystals of Gadolinium. J. Phys. Soc. Japan, 18 97

Bozorth, R.M., and Suits, J.C., (1964) — Spiral structure and moments in Gd-Dy alloys. J. Appl. Phys. 35 1039

Bozorth, R.M., and Gambino, R.J., (1966) — Magnetic properties of solid solutions of the Heavy rare earths with each other. Phys. Rev. 147 487

Bozorth, R.M., (1967) — Magnetic properties of compounds and solid solutions of rare earth metals. J. Appl. Phys. 38 1366

Brophy, J.J. (1977) — Basic electronics for Scientists. McGraw-Hill Kogakusha Ltd., London.

Burr, C.R. and Ehara, S., (1966) — High temperature magnetic susceptibility of La and Ce metals. Phys. Rev. 149 551

Cable, J.W., Moon, R.M., Kohler, W.C., and Wollan, E.O., (1964) — Antiferromagnetism of Pr. Phys. Rev. Letts. 12 553

Cable, J.W. and Wollan, E.O., (1968) — Neutron diffraction study of the magnetic behaviour of Gadolinium Phys. Rev. 165 733

Callen, E., and Callen, H.B., (1963) — Static magnetoelastic coupling in cubic crystals. Phys. Rev. 129 578

Callen, E., and Callen, H.B., (1965) — Magnetostriction, forced magnetostriction, and anomalous thermal expansion in ferromagnets Phys. Rev. 139 A455

Callen, H.B., and Callen E., (1966) — The present status of the temperature dependence of magnetocrystalline anisotropy, and the $l(l+1)/2$ power law. J. Phys. Chem. Solids 27 1271

Callen, E., (1968) Magnetostriction
J. Appl. Phys. 39 519

Carey, R., and Isaac, E.D., (1966) Magnetic domains and techniques for their observation
Academic Press, London.

Chatterjee, D., (1972) Ph.D. Thesis, University of Durham.

Chikazumi, S., (1964) Physics of magnetism
J. Wiley and Sons, London.

Child, H.R., Koehler, W.C. Wollan, E.O., and Cable, J.W., (1965) Magnetic properties of heavy rare earths diluted by Yttrium and Lutetium.
Phys. Rev. 138 A1655

Child, H.R. and Koehler, W.C., (1966) Magnetic structure of Tb-Sc alloys.
J. Appl. Phys. 37 1353

Child, H.R. and Cable, J.W., (1969) Magnetic structure properties of Gd-Y and Gd-Sc alloys.
J. Appl. Phys. 40 1003

Clark, A.E. De. Savage, B.F., and Bozorth, R., (1965) Anomalous thermal expansion and magnetostriction of single-crystal Dysprosium
Phys. Rev 138 A216

Clark, G., (1980) Private communication

Coleman, W.E., (1964) Ph.D. Thesis, West Virginia University.

Coleman, W.E., and Pavlovic, A.S., (1965) The forced magnetostriction of single-crystal Gadolinium.
J. Phys. Chem. Solids 26 691

Coqblin, B., (1971) Electronic structure of rare earths and actinides.
Rare Earths and Actinides, Durham
IOP 3 117

Coqblin, B., (1977) — The electronic structure of rare-earth metals and alloys. Academic Press, London.

Corner, W.D., Roe, W.C., and Taylor, K.N.R., (1962) — The magnetocrystalline anisotropy of Gd. Proc. Phys. Soc. (London) 80 927

Corner, W.D., and Tanner, B.K., (1976) — The easy direction of magnetization in Gd J. Phys. C, Solid State Phys. 9 627

Craik, D.J., (1971) — Structure and Properties of Magnetic Materials Pion Ltd., London.

Darby, M.I., and Isaac, E.D., (1974) — Magnetocrystalline anisotropy of ferro and ferrimagnetics. IEEE, Trans. on Mag. 10 259

Darnell, F.J., (1963) — Temperature dependence of lattice parameters for Gd, Dy, and Ho Phys. Rev. 130 1825

Darnell, F.J., (1963) — Lattice parameters of Tb and Er at low temperatures. Phys. Rev. 132 1098

Dietrich, O.V., and Als-Nielsen, J., (1967) — Neutron Diffraction Study of the Magnetic Long-Range Order in Tb. Phys. Rev. 162 315

du Plessis, P., (1968) — Magnetoelastic behaviour of a Terbium single crystal. I - Anisotropic single-ion properties II - Exchange properties Phil. Mag. 18 145/157

Duthie, J.C. and Pettifor, D.G., (1977) — Correlation between d-band and crystal structure in the rare earths. Phys. Rev. Letts. 38 564

Dzyaloshinski, I., (1958) — A thermodynamic theory of "weak" ferromagnetism of antiferromagnetics. J. Phys. Chem. Solids 4 241

Elliot, J.F., Legvold, S. and Spedding F.H., (1953) — Some magnetic properties of Gd metal. Phys. Rev. 91 28

Elliot, R.J. and Stevens, K.W.H., (1953) The magnetic properties of certain rare earth ethyl sulphates. Proc. Roy. Soc. A219 387

Elliot R.J., (1971) Magnetism in rare earth metals - a review. Rare earths and Actinides, Durham. IOP Conf. (London) 3 1

Elliot, R.J., (1972) Magnetic properties of rare earth metals Plenum Press, London

Goldman, J.E., (1947) Strain Gauge Technique for Magnetostriction Phys. Rev. 72 524

Graham, C.D., (1962) Magnetocrystalline anisotropy of Gadolinium. J. Phys. Soc. Japan 17 1310

Graham, C.D., (1964) Field-dependent anisotropy in Gadolinium. Proc. Int. Conf. on Magn. Nottingham England P. 740

Greenough, R.D., and Underhill, C., (1976) Strain Gauges for the Measurement of Magnetostriction in the Range 4 K to 300 K J. Phys. E., Scientific Instruments 9 451

Griffell, M., Skochdopole, R.E., and Spedding, F.H., (1957) Heat capacity of Gd from 15 K to 355 K. Phys. Rev. 93 657

Harris, I.R., Koch, C.C., and Raynor, G.V., (1966) The room temperature lattice spacings of some intra rare earth binary systems. J. Less - Common Metals 11 436

Hegland, D.E., Legvold, S. and Spedding, F.H., (1963) Magnetization and electrical properties of Tb Single crystals. Phys. Rev. 131 158

Heisenberg, W., (1928) Theory of ferromagnetism. Z. Phyzik49 619

Houmann, J.C.G. and Nicklow, R.M., (1970) Lattice Dynamics of Terbium. Phys. Rev. B1 3943

Ito, T., (1973) Magnetic properties of the Gd-Y alloys. J. Sci. Hiroshima Univ. 37 107

Jayaraman, A., and Sherwood, R.C., (1964) — Phase transformation in Sm induced by high pressure and its effect on the antiferromagnetic ordering. Phys. Rev. 134 A691

Jelinek, F.J., Hill, E.D. and Gerstein, B.C., (1965) — Initial susceptibility investigation of magnetic transition in several rare earth metals. J. Phys. Chem. Solids 26 1475

Jennings, L.D., Stanton, R.M., and Spedding, F.H. (1957) — Heat capacity of Tb from 15 K to 250 K. J. Chem. Phys. 27 909

Jensen, J., (1976) — Comment on the two-ion anisotropy in the heavy rare earth metals. Phys. Rev. Letts. 37 951

Jensen, J., (1977) — Two- and Single-ion magnetic anisotropy in the rare earth metals. Physica 86-88 B 32

Johansson, B., (1977) — Structural and elastic properties of f elements. Rare Earths and Actinides 1977, Durham. IOP Conf. 37 39

Johansson, J., Lebech, B., Neilsen, M., Bjerrum-Møller, H., and Machintosh, A.R., (1970) — Crystal fields and magnetic properties of Pr and Nd Phys. Rev. Letters 25 524

Jordan, R.G., (1974) — Electrotransport in Solid Metal Systems. Contemp. Phys. 15 375

Kasuya, T., (1966) — s-d and s-f interaction and rare earth metals. Magnetism vol. IIB p. 215, edited by Rado and Suhl. Academic press, London.

Kittel, C., and Galt., J.K., (1956) — Ferromagnetic domain theory. Solid state physics 3 437

Kittel, C., (1971) — Introduction to solid state physics. J. Wiley and Sons, London.

Koehler, W.D., Child, H.R. Some magnetic structure properties of Tb and Wollen, E.O. and of Tb-Y alloys.
Cable, J.W., (1963) J. Appl. Phys. Suppl. 34 1335

Koehler, W.C., (1965) Magnetic properties of rare earth metals and alloys.
J. Appl. Phys. 36 1078

Koehler, W.C., (1971) Recent development in neutron scattering from rare earths.
Rare earths and actinides, Durham, IOP (London) Conf. 3 25

Landau, L., and Theory of the dispersion of magnetic permeability
Lifshitz, E., (1935) in ferromagnetic bodies.
Phys. Zeits. Sowjetunion 8 153

Lebech, B., and The magnetic structure of Pr and Nd.
Rainford, B.D., (1971) J. de Phys. 32 C1-370

Lifshitz, E., (1944) On the theory of phase transitions of the second order. II-Phase transitions of the second order in alloys.
J. Phys. USSR 8 53

Lindgård, Per-A. and Theory of magnetic properties of heavy rare earth
Danielsen, O., (1974) metals: Temperature dependence of magnetization, anisotropy, and resonance energy.
Phys. Rev. B 11 351

Lock, J.M., (1957) The magnetic susceptibility of La, Ce, Pr, Nd, and Sm.
Proc. Phys. Soc. (London) B70 566

Lounasmaa, O.V. and Specific heat of Gd, Tb, Dy, Ho, and Tm metals
Sundstrom, L.J., (1966) between 3 K and 25 K. Phys. Rev. 150 399

Mason, W.P., (1951) — A phenomenological derivation of the first and second-order magnetostriction and morphic effect for a Nickel crystal. Phys. Rev. 82 715

Mason, W.P., (1954) — Derivation of magnetostriction and anisotropic energies for hexagonal, tetragonal, and orthorhombic crystals. Phys. Rev. 96 302

Mishima, A., Fujii, H., and Okamoto, T., (1976) — Anomalous saturation magnetostriction of Gadolinium single crystal. J. Phys. Soc. Japan 40 962

Moon, R.M., Cable, J.W., and Koehler, W.C., (1964) — Magnetic structure of Nd. J. Appl. Phys. Suppl. 35 104

Mundell, P., (1976) — Ph.D. Thesis, University of Durham.

Néel, L., (1936) — Magnetic properties of the metallic state and energy of interaction between magnetic atoms. Ann. Phys. 5 232

Néel, L., (1944) — Some properties of elementary ferromagnetic domain-walls. Cahiers de Phys. 25 22

Néel, L., (1948) — Magnetic properties of ferrites, ferrimagnetism and antiferromagnetism. Ann. Phys. 3 B137

Nigh, H.E., Legvold, S., and Spedding, F.H., (1963) — Magnetization and electrical properties of Gadolinium single crystals. Phys. Rev. 132 1092

Nigh, H.E., Legvold, S., Spedding, F.H., and Beaudry, B.J., (1964) — Magnetic properties of Gd-Sc alloys. J. Chem. Phys. 41 3799

Nikitin, S.A., Kim, D., and Chistyakov, O.D., (1976) — Magnetostriction and thermal expansion of single crystals of the rare earth Gd-Dy alloys. Sov. Phys. JETP 44 843

Nikitin, S.A., Andreenko, A.S., Posyado, V.P., and Chuprikov, G.E., (1977a) — Magnetostriction and magnetic properties of single crystals of Tb-Y alloys. Sov. Phys. Solid State 19 1045

Nikitin, S.A., Shelndko, N.A., Posyado, V.P., and Chuprikov, G.E., (1977b) — Magnetic, magnetoelastic, and electric Properties of single-crystal Gd-Tb alloys Sov. Phys. JETP 46 530

Nira, K., (1960) — Temperature dependence of the magnetization of Dy metal. Phys. Rev. 117 129

Omar, M.A., (1975) — Elementary Solid State Physics. Addison-Wesley Publishing Co., London.

Osthuizen, C.P. and Alberts, L., (1975) — Magnetization of a Tb single crystal in the antiferromagnetic region, J. Mag & Mag Mat. 1 76

Palmer, S.B., and Lee, E.W., (1972) — The elastic constants of Dy and Ho. Proc. Roy. Soc. (London) A327 519

Palmer, S.B., Lee, E.W., and Islam, M.N., (1974) — The elastic constants of Gd, Tb, and Er. Proc. Roy. Soc. (London) A338 341

Pauthenet, R. (1969) — High magnetic fields and their applications, Nottingham, IOP Cong. 1 85

Polina, R., and Luthi, B. (1968) — Critical attenuation of sound in Gadolinium. Phys. Rev. 167 488

Pollina, R., and Luthi, B., (1969) — Critical scattering of sound in rare earth metals. Phys. Rev. 177 841

Rhyne, J.J., and Legvold, S., (1965) — Magnetostriction of Tb single crystals. Phys. Rev. 138 A507

Rhyne, J.J., Forner, S., McNiff, E., and Doclo, R.J., (1968) — Rare earth metals single crystals. High field properties, Dy, Er, Ho, Tb and Gd. J. Appl. Phys. 39 892

Rhyne, J.J., (1972) Bulk magnetic properties. Magnetic properties of rare earth metals. Edited by Elliot, P.129 Plenum Press, London.

Rodbell, D.S., and Moore, T.W., (1964) Electron spin resonance in Gd metal single crystals. Proc. Int. Conf. on Mag., Nottingham. P. 427

Roeland, L.W., Cock, G.J. and Lindgård, P-A. (1975) High field magnetization of Tb single crystals. J. Phys. C, Solid State Phys. 8 3427

Schieber, M., Foner, S., Doclo, D., and McNiff, E., (1968) Rare earth metal single crystal. II-Magnetic properties of Tm, Eu, Sm and Yb. J. Appl. Phys. 39 885

Smith, R.L., Tanner, B.K., and Corner, W.D., (1977) The effect of nonmagnetic inclusions on the easy direction of Gadolinium. J. Phys. F, Metal Phys. 7 1229

Smith, R.L., Corner, W.D., Tanner, B.K., Jordan,R.G., and Jones, D.W., (1978) The magnetocrystalline anisotropy of high-quality single-crystal Gd. Rare earths and Actinides, IOP (London) Conf. 37 215

Smith, R.J. (1971) Circuits devices and systems. J. Wiley and Sons, London.

Spedding, F.H., Legvold, S. Daane, A.H., and Jennings, L.D., (1957) Some physical properties of the rare earth metals. Prog. in Low. Temp. Phys. 2 368

Spedding, F.H., Jordan,R.G. and Williams R.W., (1969) Magnetic properties of Tb-Ho single crystal alloys. I-Magnetization measurements. J. Chem. Phys. 51 509

Spedding, F.H., Ito, T., and Jordan, R.G., (1970) Magnetic properties of Tb-Ho single crystal alloys. II-Neutron diffraction studies. J. Chem. Phys. 53 1455

Stevens, K.W.H., (1952) Matrix elements and operator equivalents connected with the magnetic properties of rare earth ions. Proc. Phys. Soc. (London) A65 209

Strandburg, D.L., Legvold, S., and Spedding, F.H., (1962) Electrical and magnetic properties of Holmium single crystals. Phys. Rev. 127 2046

Tajima, K. and Chikazumi, S., (1967) Magnetocrystalline anisotropy of Gd-Tb and Gd-Dy alloys. J. Phys. Soc. Japan 23 1175

Taylor, K.N.R., and Darby, M.I., (1972) Physics of rare earth solids. Chapman and Hall Ltd., London.

Thorburn, W.C., Legvold, S. and Spedding, F.H., (1958) Magnetic properties of the Gd-Lu and Gd-Y alloys. Phys. Rev. 110 1298

Tonegawa, T., (1964) Exchange of strictions of the single crystal of Gadolinium. J. Phys. Soc. Japan 19 1168

Trombe, F., (1937) Magnetic Properties of rare earth metals. Ann. Phys. 7 385

Tsuya, N., Clark, A.E., and Bozorth, R.M., (1964) Magnetostriction in heavy rare earth metals. Proc. Int. Conf. on Mag. Nottingham, P. 250

Unvala, B.A., and Green, A.K., (1974) An inexpensive voltage-stabilized power supply for strain-gauge applications. J. Strain Analysis 9 88

Unvala, B.A., Green, A.K., and Ivory, J.C., (1976) An inexpensive system for precision strain gauge monitoring. J. Phys. E. Scientific Insturments 9 368

Van Vleck, J.H., (1937) On the anisotropy of cubic ferromagnetic crystals. Phys. Rev. 52 1178

Villian, J., (1959) The structure of magnetic substances. Phys. Chem. Solids 11 303

Vorobev, V.V., Belovol, V.S., and Finkel, V.A., (1977) X-ray diffraction study of magnetostriction and phase transitions in a magnetic field in rare earth metals and some alloys. Phys. Stat. Sol. 82 213

Weinstein, S., Craig, R.S., and Wallace, W.E., (1963) Structural and magnetic characteristics of Dy-Y solid solutions. J. Appl. Phys. 34 1354

Weiss, P., (1907) Hypothesis of the molecular field and ferromagnetism. J. de Phys. 6 661

Welford, J., (1975) Ph.D. Thesis, University of Durham

Wilkinson, M.K., Child, H.R., MacHargue, C.J., Koehler, W.C., and Wollen, E.O., (1961) Neutron diffraction investigations of metallic Ce at low temperature. Phys. Rev. 122 1409

Williams, H.J., Bozorth, R.M., and Shockley, W., (1949) Magnetic domain patterns on single crystals of Silicon-Iron. Phys. Rev. 75 155

Wolf, W.P., (1957) Effect of crystalline electric field on ferromagnetic anisotropy. Phys. Rev. 108 1152

Yafet, Y., and Kittel, C., (1952) Antiferromagnetic arrangements in ferrites. Phys. Rev. 87 290

Yoshimori, A., (1959) A new type of antiferromagnetic structure in the rutile type crystal. J. Phys. Soc. Japan 14 807

Yosida, K., and Watabe, A., (1962) Fermi surfaces and spin structures in heavy rare earth metals. Prog. Theor. Phys. 28 361

Yosida, K., (1968) The status of the theories of magnetic anisotropy. J. Appl. Phys. 39 511

Zener, C., (1954) Classical theory of the temperature dependence of magnetic anisotropy energy. Phys. Rev. 96 1335

APPENDIX I

A computer program for calculating the values of the four magnetostriction coefficients from Eq. (6.5) using the least square technique.

```
      ∇FIT[⎕1] ∇
[1]   ABDEV←⍳6
[2]   LOSTORE←⍳6
[3]   'MAG*2 TERM, +1  ZERO  OR ¯1 '
[4]   B←⎕
[5]   AVALS←⍳6
[6]   DEV←0
[7]   BESTLO←0
[8]   'PRECISION IN A'
[9]   ACC←⎕
[10]  'START VALUE FOR I(5/2) TERM'
[11]  A←⎕
[12]  'INCREMENT SIZE FOR I(5/2) COEFF'
[13]  INT←⎕
[14] OUT1:C2←0
[15] OUT2:C2←C2+1
[16]  A←A+INT
[17]  FIT2
[18]  ABDEV[C2]←DEV
[19]  AVALS[C2]←A
[20]  LOSTORE[C2]←BESTLO
[21]  →(C2≤5.9)/OUT2
[22]  AVALS
[23]  D2←⍋(ABDEV)
[24]  LOWDEV←D2[1]
[25]  A←AVALS[LOWDEV]-INT
[26]  INT←INT÷2.5
[27]  A←A-INT
[28]  →(INT>ACC)/OUT1
[29]  BESTLO←LOSTORE[LOWDEV]
[30]  ICOEFF←BESTLO×AVALS[LOWDEV]
[31]  MCOEFF←BESTLO×B
[32]  CALCL←(ICOEFF×I)+(MCOEFF×M*2)
[33]  'COEFFICIENT OF THE I TERM';ICOEFF
[34]  'COEFFICIENT OF THE MAGNETISATION TERM';MCOEFF
[35]  'CALCULATED VALUES';CALCL
[36]  'ROOT OF SUM OF THE SQURED DEVIATIONS ÷ NUMBER OF VALUES     ';((
      ABDEV[LOWDEV]*0.5)÷⍴M)
SI DAMAGE


      ∇FIT2[⎕1] ∇
[1]   X1←(A×I)+(B×M*2)
[2]   N←⍴L
[3]   XLSUM←+/(X1×L)
[4]   XSUM←+/(X1)
[5]   LSUM←+/L
[6]   XSQSUM←+/(X1*2)
[7]   BESTLO←L[1]÷X1[1]
[8]   CONST←(LSUM-BESTLO×XSUM)÷N
[9]   DEV←(+/(L-(BESTLO×X1))*2)
```

```
      ∇GRAPH[□1] ∇
[1]   EDGE←70⍴'-'
[2]   'INPUT SCALING FACTOR'
[3]   W←□
[4]   EDGE
[5]   P←1
[6]   Q←⍴L
[7]   LINE←80⍴' '
[8]   LINE[1]←'|'
[9]   PRINT:LINE[⌊CAL CL[P]×W]←'C'
[10]  LINE[⌊L[P]×W]←'L'
[11]  LINE[1]←'|'
[12]  LINE
[13]  LINE←80⍴' '
[14]  P←P+1
[15]  →(P≤Q)/PRINT
```

APPENDIX II

Reduced hyperbolic Bessel functions of x from 0 to 150, adapted from Welford (1975).

x	ORDER			
	3/2	5/2	9/2	13/2
0.05	0.016663	0.000166	0.000000	0.000000
0.10	0.033311	0.000666	0.000000	0.000000
0.15	0.049925	0.001496	0.000000	0.000000
0.20	0.066489	0.002656	0.000001	0.000000
0.25	0.082988	0.004142	0.000004	0.000000
0.30	0.099405	0.005949	0.000008	0.000000
0.34	0.115724	0.008072	0.000015	0.000000
0.39	0.131932	0.010506	0.000025	0.000000
0.44	0.148013	0.013244	0.000042	0.000000
0.49	0.163953	0.016279	0.000064	0.000000
0.54	0.179735	0.019602	0.000093	0.000000
0.59	0.195358	0.023205	0.000131	0.000000
0.64	0.210799	0.027079	0.000179	0.000000
0.69	0.226050	0.031213	0.000239	0.000000
0.74	0.241100	0.035597	0.000313	0.000001
0.79	0.255940	0.040222	0.000401	0.000001
0.84	0.270561	0.045075	0.000507	0.000002
0.89	0.284956	0.050146	0.000631	0.000003
0.94	0.299116	0.055422	0.000775	0.000004
0.99	0.313035	0.060894	0.000942	0.000006
1.05	0.326708	0.066548	0.001132	0.000008
1.10	0.340129	0.072373	0.001347	0.000011
1.14	0.353296	0.078357	0.001590	0.000014
1.19	0.366204	0.084489	0.001861	0.000018
1.24	0.378850	0.090757	0.002163	0.000023
1.29	0.391234	0.097150	0.002496	0.000028
1.34	0.403354	0.103657	0.002863	0.000035
1.39	0.415208	0.110266	0.003265	0.000043
1.44	0.426798	0.116967	0.003702	0.000053
1.49	0.438124	0.123750	0.004177	0.000063
1.54	0.449187	0.130604	0.004689	0.000076
1.59	0.459988	0.137521	0.005241	0.000091
1.64	0.470530	0.144489	0.005834	0.000107
1.69	0.480815	0.151501	0.006468	0.000126
1.74	0.490846	0.158548	0.007143	0.000147
1.79	0.500627	0.165621	0.007861	0.000171
1.84	0.510160	0.172713	0.008623	0.000198
1.89	0.519449	0.179816	0.009428	0.000228
1.94	0.528499	0.186923	0.010277	0.000261
1.99	0.537314	0.194027	0.011170	0.000298
2.04	0.545899	0.201123	0.012108	0.000338
2.09	0.554257	0.208203	0.013091	0.000383
2.14	0.562394	0.215264	0.014119	0.000432
2.19	0.570314	0.222298	0.015192	0.000485
2.24	0.578023	0.229302	0.016309	0.000544
2.29	0.585525	0.236271	0.017471	0.000607
2.34	0.592825	0.243201	0.018677	0.000676
2.39	0.599929	0.250088	0.019927	0.000750
2.44	0.606841	0.256928	0.021221	0.000830
2.49	0.613567	0.263719	0.022558	0.000917

X	ORDER			
	3/2	5/2	9/2	13/2
2.59	0.626478	0.277139	0.025360	0.001108
2.69	0.638703	0.290329	0.028328	0.001328
2.79	0.650280	0.303271	0.031459	0.001576
2.89	0.661245	0.315952	0.034745	0.001856
2.99	0.671636	0.328363	0.038180	0.002169
3.09	0.681486	0.340496	0.041759	0.002517
3.19	0.690828	0.352348	0.045475	0.002901
3.29	0.699694	0.363914	0.049320	0.003324
3.39	0.708112	0.375194	0.053287	0.003786
3.49	0.716111	0.386190	0.057369	0.004289
3.59	0.723716	0.396902	0.061559	0.004834
3.69	0.730952	0.407335	0.065849	0.005422
3.79	0.737843	0.417491	0.070233	0.006055
3.89	0.744409	0.427377	0.074702	0.006732
3.99	0.750671	0.436996	0.079252	0.007455
4.09	0.756647	0.446355	0.083874	0.008225
4.19	0.762354	0.455461	0.088562	0.009041
4.29	0.767810	0.464318	0.093310	0.009905
4.39	0.773028	0.472934	0.098112	0.010816
4.49	0.778024	0.481316	0.102962	0.011775
4.59	0.782810	0.489471	0.107854	0.012781
4.69	0.787399	0.497404	0.112783	0.013835
4.79	0.791802	0.505123	0.117744	0.014937
4.89	0.796029	0.512635	0.122731	0.016085
4.99	0.800090	0.519945	0.127742	0.017281
5.09	0.803995	0.527061	0.132770	0.018523
5.19	0.807753	0.533988	0.137811	0.019811
5.29	0.811370	0.540733	0.142863	0.021145
5.39	0.814855	0.547302	0.147921	0.022523
5.49	0.818215	0.553700	0.152981	0.023946
5.59	0.821455	0.559934	0.158041	0.025412
5.69	0.824583	0.566008	0.163097	0.026921
5.79	0.827604	0.571928	0.168146	0.028472
5.89	0.830523	0.577699	0.173186	0.030065
5.99	0.833345	0.583327	0.178214	0.031697
6.09	0.836075	0.588815	0.183228	0.033369
6.19	0.838717	0.594168	0.188225	0.035079
6.29	0.841276	0.599392	0.193204	0.036827
6.39	0.843755	0.604489	0.198163	0.038611
6.49	0.846158	0.609465	0.203100	0.040431
6.59	0.848488	0.614323	0.209013	0.042285
6.69	0.850749	0.619067	0.212901	0.044172
6.79	0.852943	0.623701	0.217763	0.046092
6.89	0.855074	0.628228	0.222597	0.048044
6.99	0.857144	0.632652	0.227402	0.050026
7.09	0.859156	0.636976	0.232177	0.052037
7.19	0.861112	0.641203	0.236921	0.054077
7.29	0.863014	0.645336	0.241634	0.056145
7.39	0.864865	0.649378	0.246314	0.058239
7.49	0.866667	0.653333	0.250961	0.060357

X	ORDER			
	3/2	5/2	9/2	13/2
7.64	0.[illegible]281	0.659105	0.257869	0.063581
7.79	0.[illegible]795	0.664694	0.264698	0.066857
7.94	0.[illegible]214	0.670107	0.271449	0.070181
8.09	0.[illegible]543	0.675354	0.278118	0.073550
8.24	0.[illegible]788	0.680440	0.284707	0.076961
8.39	0.[illegible]952	0.685374	0.291214	0.080412
8.54	0.[illegible]041	0.690161	0.297638	0.083899
8.69	0.[illegible]057	0.694807	0.303980	0.087418
8.84	0.[illegible]005	0.699320	0.310239	0.090969
8.99	0.[illegible]888	0.703703	0.316415	0.094548
9.14	0.[illegible]710	0.707963	0.322508	0.098152
9.29	0.[illegible]473	0.712105	0.328519	0.101780
9.44	0.[illegible]179	0.716133	0.334449	0.105428
9.59	0.[illegible]833	0.720052	0.340297	0.109094
9.74	0.[illegible]435	0.723865	0.346065	0.112776
9.89	0.[illegible]989	0.727578	0.351752	0.116473
10.04	0.900497	0.731194	0.357360	0.120182
10.19	0.901960	0.734717	0.362890	0.123901
10.34	0.903381	0.738150	0.368342	0.127628
10.49	0.904761	0.741496	0.373717	0.131362
10.64	0.906103	0.744759	0.379017	0.135101
10.79	0.907407	0.747942	0.384241	0.138844
10.94	0.908675	0.751047	0.389392	0.142588
11.09	0.909909	0.754078	0.394470	0.146332
11.24	0.911111	0.757037	0.399476	0.150076
11.39	0.912280	0.759926	0.404412	0.153817
11.54	0.913419	0.762748	0.409277	0.157555
11.69	0.914529	0.765505	0.414074	0.161289
11.84	0.915611	0.768199	0.418803	0.165016
11.99	0.916666	0.770833	0.423466	0.168737
12.14	0.917695	0.773408	0.428063	0.172450
12.29	0.918699	0.775927	0.432595	0.176154
12.44	0.919678	0.778390	0.437065	0.179849
12.59	0.920634	0.780801	0.441471	0.183533
12.74	0.921568	0.783160	0.445816	0.187206
12.89	0.922480	0.785469	0.450101	0.190867
13.04	0.923371	0.787730	0.454327	0.194516
13.19	0.924242	0.789944	0.458494	0.198151
13.34	0.925093	0.792113	0.462604	0.201773
13.49	0.925925	0.794238	0.466657	0.205380
13.64	0.926739	0.796320	0.470655	0.208972
13.79	0.927536	0.798361	0.474599	0.212549
13.94	0.928315	0.800362	0.478489	0.216109
14.09	0.929078	0.802323	0.482326	0.219654
14.24	0.929824	0.804247	0.486112	0.223181
14.39	0.930555	0.806134	0.489847	0.226692
14.54	0.931271	0.807985	0.493532	0.230185
14.69	0.931972	0.809801	0.497166	0.233660
14.84	0.932659	0.811583	0.500755	0.237118
14.99	0.933333	0.813333	0.504296	0.240557

X	ORDER			
	3/2	5/2	9/2	13/2
15.19	0.934210	0.815616	0.508944	0.245113
15.39	0.935064	0.817944	0.513512	0.249636
15.59	0.935897	0.820019	0.518000	0.254125
15.79	0.936708	0.822143	0.522412	0.258579
15.99	0.937500	0.824218	0.526748	0.262999
16.19	0.938271	0.826245	0.531011	0.267384
16.39	0.939024	0.828227	0.535202	0.271733
16.59	0.939759	0.830164	0.539322	0.276047
16.79	0.940476	0.832057	0.543374	0.280326
16.99	0.941176	0.833910	0.547359	0.284569
17.19	0.941860	0.835722	0.551278	0.288776
17.39	0.942528	0.837495	0.555133	0.292947
17.59	0.943181	0.839230	0.558926	0.297083
17.79	0.943820	0.840929	0.562657	0.301182
17.99	0.944444	0.842592	0.566329	0.305245
18.19	0.945054	0.844221	0.569942	0.309275
18.39	0.945652	0.845817	0.573498	0.313267
18.59	0.946236	0.847381	0.576998	0.317224
18.79	0.946808	0.848913	0.580443	0.321146
18.99	0.947368	0.850415	0.583835	0.325033
19.19	0.947916	0.851888	0.587174	0.328885
19.39	0.948453	0.853331	0.590462	0.332701
19.59	0.948979	0.854746	0.593701	0.336494
19.79	0.949494	0.856137	0.596890	0.340231
19.99	0.950000	0.857499	0.600031	0.343945
20.19	0.950495	0.858857	0.603125	0.347624
20.39	0.950980	0.860149	0.606173	0.351270
20.59	0.951456	0.861438	0.609176	0.354882
20.79	0.951923	0.862703	0.612136	0.358461
20.99	0.952380	0.863945	0.615052	0.362007
21.19	0.952830	0.865165	0.617926	0.365520
21.39	0.953271	0.866363	0.620758	0.369001
21.59	0.953703	0.867541	0.623550	0.372449
21.79	0.954128	0.868697	0.626303	0.375866
21.99	0.954545	0.869834	0.629016	0.379251
22.19	0.954954	0.870952	0.631692	0.382605
22.39	0.955357	0.872050	0.634330	0.385928
22.59	0.955752	0.873130	0.636932	0.389220
22.79	0.956140	0.874192	0.639498	0.392481
22.99	0.956521	0.875236	0.642028	0.395712
23.19	0.956896	0.876263	0.644525	0.398914
23.39	0.957264	0.877273	0.646987	0.402086
23.59	0.957627	0.878267	0.649417	0.405229
23.79	0.957983	0.879245	0.651814	0.408342
23.99	0.958333	0.880208	0.654179	0.411427
24.19	0.958677	0.881155	0.656513	0.414484
24.39	0.959016	0.882088	0.658816	0.417513
24.59	0.959349	0.883006	0.661089	0.420514
24.79	0.959677	0.883909	0.663333	0.423487
24.99	0.960000	0.884799	0.665548	0.426434

X	ORDER			
	3/2	5/2	9/2	13/2
25.24	0.960396	0.885893	0.668277	0.430079
25.49	0.960784	0.886966	0.670963	0.433682
25.74	0.961165	0.888019	0.673606	0.437245
25.99	0.961538	0.889053	0.676208	0.440768
26.24	0.961904	0.890068	0.678769	0.444251
26.49	0.962264	0.891064	0.681291	0.447694
26.74	0.962616	0.892042	0.683775	0.451099
26.99	0.962962	0.893004	0.686221	0.454466
27.24	0.963302	0.893948	0.688629	0.457796
27.49	0.963636	0.894876	0.691002	0.461088
27.74	0.963963	0.895787	0.693339	0.464344
27.99	0.964285	0.896683	0.695642	0.467563
28.24	0.964601	0.897564	0.697911	0.470748
28.49	0.964912	0.898430	0.700147	0.473897
28.74	0.965217	0.899281	0.702351	0.477012
28.99	0.965517	0.900118	0.704523	0.480093
29.24	0.965811	0.900942	0.706664	0.483140
29.49	0.966101	0.901752	0.708774	0.486155
29.74	0.966386	0.902549	0.710855	0.489136
29.99	0.966666	0.903333	0.712907	0.492086
30.24	0.966942	0.904104	0.714930	0.495004
30.49	0.967213	0.904864	0.716925	0.497891
30.74	0.967479	0.905611	0.718893	0.500747
30.99	0.967741	0.906347	0.720834	0.503573
31.24	0.967999	0.907071	0.722749	0.506369
31.49	0.968253	0.907785	0.724638	0.509135
31.74	0.968503	0.908487	0.726502	0.511873
31.99	0.968749	0.909179	0.728341	0.514581
32.24	0.968992	0.909861	0.730155	0.517262
32.49	0.969230	0.910532	0.731946	0.519915
32.74	0.969465	0.911193	0.733714	0.522540
32.99	0.969696	0.911845	0.735458	0.525139
33.24	0.969924	0.912487	0.737180	0.527710
33.49	0.970149	0.913120	0.738881	0.530256
33.74	0.970370	0.913744	0.740559	0.532775
33.99	0.970588	0.914359	0.742216	0.535269
34.24	0.970802	0.914966	0.743853	0.537738
34.49	0.971014	0.915563	0.745469	0.540182
34.74	0.971223	0.916153	0.747065	0.542601
34.99	0.971428	0.916734	0.748641	0.544997
35.24	0.971631	0.917307	0.750198	0.547368
35.49	0.971830	0.917873	0.751735	0.549716
35.74	0.972027	0.918431	0.753255	0.552041
35.99	0.972222	0.918981	0.754756	0.554343
36.24	0.972413	0.919524	0.756239	0.556622
36.49	0.972602	0.920060	0.757704	0.558880
36.74	0.972789	0.920588	0.759152	0.561115
36.99	0.972972	0.921110	0.760583	0.563329
37.24	0.973154	0.921625	0.761997	0.565521
37.49	0.973333	0.922133	0.763395	0.567692

X	ORDER			
	3/2	5/2	9/2	13/2
37.79	0.973544	0.922734	0.765051	0.570271
38.09	0.973753	0.923326	0.766684	0.572819
38.39	0.973958	0.923909	0.768294	0.575339
38.69	0.974160	0.924483	0.769883	0.577831
38.99	0.974358	0.925049	0.771450	0.580294
39.29	0.974554	0.925606	0.772997	0.582730
39.59	0.974747	0.926155	0.774522	0.585139
39.89	0.974937	0.926696	0.776028	0.587521
40.19	0.975124	0.927229	0.777513	0.589876
40.49	0.975308	0.927754	0.778979	0.592206
40.79	0.975490	0.928272	0.780426	0.594511
41.09	0.975669	0.928783	0.781855	0.596790
41.39	0.975845	0.929286	0.783265	0.599044
41.69	0.976019	0.929782	0.784657	0.601275
41.99	0.976190	0.930272	0.786031	0.603481
42.29	0.976359	0.930754	0.787388	0.605664
42.59	0.976525	0.931230	0.788728	0.607824
42.89	0.976689	0.931700	0.790051	0.609960
43.19	0.976851	0.932163	0.791358	0.612075
43.49	0.977011	0.932619	0.792649	0.614167
43.79	0.977168	0.933070	0.793924	0.616237
44.09	0.977324	0.933515	0.795184	0.618286
44.39	0.977477	0.933954	0.796429	0.620314
44.69	0.977628	0.934387	0.797658	0.622320
44.99	0.977777	0.934814	0.798873	0.624307
45.29	0.977924	0.935236	0.800073	0.626273
45.59	0.978070	0.935653	0.801259	0.628219
45.89	0.978213	0.936064	0.802432	0.630145
46.19	0.978354	0.936470	0.803590	0.632052
46.49	0.978494	0.936871	0.804736	0.633940
46.79	0.978632	0.937267	0.805868	0.635809
47.09	0.978768	0.937659	0.806987	0.637659
47.39	0.978902	0.938044	0.808093	0.639492
47.69	0.979035	0.938425	0.809186	0.641306
47.99	0.979166	0.938802	0.810268	0.643102
48.29	0.979296	0.939174	0.811337	0.644881
48.59	0.979423	0.939541	0.812394	0.646643
48.89	0.979550	0.939904	0.813440	0.648388
49.19	0.979674	0.940263	0.814474	0.650115
49.49	0.979797	0.940618	0.815497	0.651827
49.79	0.979919	0.940968	0.816508	0.653522
50.09	0.980039	0.941314	0.817509	0.655201
50.39	0.980158	0.941657	0.818498	0.656864
50.69	0.980276	0.941995	0.819477	0.658511
50.99	0.980392	0.942329	0.820446	0.660143
51.29	0.980506	0.942660	0.821404	0.661760
51.59	0.980620	0.942987	0.822353	0.663362
51.89	0.980732	0.943310	0.823291	0.664949
52.19	0.980842	0.943629	0.824219	0.666521
52.49	0.980952	0.943945	0.825138	0.668079

X	ORDER			
	3/2	5/2	9/2	13/2
52.84	0.981078	0.944309	0.826198	0.669878
53.19	0.981203	0.944669	0.827245	0.671659
53.54	0.981325	0.945023	0.828280	0.673421
53.89	0.981447	0.945374	0.829302	0.675164
54.24	0.981566	0.945719	0.830312	0.676889
54.59	0.981684	0.946061	0.831311	0.678596
54.94	0.981801	0.946398	0.832298	0.680286
55.29	0.981916	0.946731	0.833273	0.681958
55.64	0.982030	0.947060	0.834237	0.683613
55.99	0.982142	0.947385	0.835190	0.685251
56.34	0.982253	0.947706	0.836133	0.686872
56.69	0.982363	0.948023	0.837064	0.688478
57.04	0.982471	0.948336	0.837985	0.690067
57.39	0.982578	0.948645	0.838896	0.691640
57.74	0.982683	0.948951	0.839797	0.693197
58.09	0.982788	0.949253	0.840687	0.694739
58.44	0.982891	0.949552	0.841568	0.696266
58.79	0.982993	0.949847	0.842439	0.697778
59.14	0.983093	0.950138	0.843301	0.699275
59.49	0.983193	0.950427	0.844153	0.700758
59.84	0.983291	0.950712	0.844996	0.702226
60.19	0.983388	0.950993	0.845830	0.703680
60.54	0.983484	0.951272	0.846656	0.705120
60.89	0.983579	0.951547	0.847472	0.706547
61.24	0.983673	0.951820	0.848280	0.707959
61.59	0.983766	0.952089	0.849079	0.709359
61.94	0.983857	0.952355	0.849870	0.710745
62.29	0.983948	0.952619	0.850653	0.712119
62.64	0.984038	0.952879	0.851427	0.713479
62.99	0.984126	0.953136	0.852194	0.714827
63.34	0.984214	0.953391	0.852953	0.716162
63.69	0.984301	0.953643	0.853704	0.717485
64.04	0.984387	0.953892	0.854447	0.718796
64.39	0.984472	0.954139	0.855183	0.720095
64.74	0.984555	0.954383	0.855912	0.721382
65.09	0.984639	0.954624	0.856633	0.722658
65.44	0.984721	0.954863	0.857347	0.723922
65.79	0.984802	0.955100	0.858054	0.725174
66.14	0.984882	0.955334	0.858754	0.726416
66.49	0.984962	0.955565	0.859448	0.727646
66.84	0.985041	0.955794	0.860134	0.728866
67.19	0.985119	0.956021	0.860814	0.730075
67.54	0.985196	0.956245	0.861487	0.731273
67.89	0.985272	0.956468	0.862154	0.732460
68.24	0.985347	0.956688	0.862815	0.733638
68.59	0.985422	0.956905	0.863469	0.734805
68.94	0.985496	0.957121	0.864117	0.735962
69.29	0.985569	0.957334	0.864759	0.737109
69.64	0.985642	0.957545	0.865394	0.738246
69.99	0.985714	0.957755	0.866024	0.739374

X	ORDER			
	3/2	5/2	9/2	13/2
70.39	0.985795	0.957991	0.866737	0.740651
70.79	0.985875	0.958225	0.867442	0.741915
71.19	0.985955	0.958456	0.868140	0.743168
71.59	0.986033	0.958685	0.868830	0.744409
71.99	0.986111	0.958912	0.869514	0.745637
72.39	0.986187	0.959135	0.870190	0.746854
72.79	0.986263	0.959357	0.870859	0.748059
73.19	0.986338	0.959576	0.871522	0.749253
73.59	0.986413	0.959792	0.872177	0.750436
73.99	0.986486	0.960007	0.872826	0.751608
74.39	0.986559	0.960219	0.873469	0.752770
74.79	0.986631	0.960429	0.874105	0.753920
75.19	0.986702	0.960636	0.874735	0.755060
75.59	0.986772	0.960842	0.875358	0.756189
75.99	0.986842	0.961045	0.875975	0.757308
76.39	0.986910	0.961246	0.876587	0.758417
76.79	0.986979	0.961446	0.877192	0.759516
77.19	0.987046	0.961643	0.877791	0.760605
77.59	0.987113	0.961838	0.878385	0.761685
77.99	0.987179	0.962031	0.878972	0.762754
78.39	0.987244	0.962222	0.879555	0.763815
78.79	0.987309	0.962412	0.880131	0.764866
79.19	0.987373	0.962595	0.880702	0.765907
79.59	0.987437	0.962785	0.881268	0.766940
79.99	0.987500	0.962968	0.881828	0.767963
80.39	0.987562	0.963150	0.882383	0.768978
80.79	0.987623	0.963330	0.882933	0.769984
81.19	0.987684	0.963509	0.883478	0.770981
81.59	0.987745	0.963685	0.884018	0.771970
81.99	0.987804	0.963860	0.884553	0.772950
82.39	0.987864	0.964034	0.885083	0.773922
82.79	0.987922	0.964205	0.885608	0.774885
83.19	0.987980	0.964375	0.886128	0.775841
83.59	0.988038	0.964544	0.886643	0.776788
83.99	0.988095	0.964710	0.887154	0.777728
84.39	0.988151	0.964876	0.887661	0.778660
84.79	0.988207	0.965039	0.888163	0.779584
85.19	0.988262	0.965202	0.888660	0.780500
85.59	0.988317	0.965362	0.889153	0.781409
85.99	0.988372	0.965521	0.889642	0.782310
86.39	0.988425	0.965679	0.890126	0.783204
86.79	0.988479	0.965835	0.890606	0.784091
87.19	0.988532	0.965990	0.891082	0.784971
87.59	0.988584	0.966144	0.891554	0.785843
87.99	0.988636	0.966296	0.892022	0.786709
88.39	0.988687	0.966447	0.892486	0.787567
88.79	0.988738	0.966596	0.892945	0.788419
89.19	0.988789	0.966744	0.893401	0.789264
89.59	0.988839	0.966891	0.893853	0.790102
89.99	0.988888	0.967037	0.894302	0.790934

X	ORDER			
	3/2	5/2	9/2	13/2
90.44	0.988944	0.967199	0.894801	0.791862
90.89	0.988998	0.967359	0.895256	0.792781
91.34	0.989053	0.967518	0.895787	0.793693
91.79	0.989106	0.967676	0.896273	0.794597
92.24	0.989159	0.967832	0.896754	0.795493
92.69	0.989212	0.967986	0.897231	0.796381
93.14	0.989264	0.968139	0.897703	0.797261
93.59	0.989316	0.968291	0.898172	0.798134
94.04	0.989367	0.968441	0.898636	0.799000
94.49	0.989417	0.968589	0.899095	0.799858
94.94	0.989468	0.968737	0.899551	0.800709
95.39	0.989517	0.968883	0.900002	0.801552
95.84	0.989567	0.969027	0.900450	0.802389
96.29	0.989615	0.969170	0.900893	0.803218
96.74	0.989664	0.969312	0.901333	0.804041
97.19	0.989711	0.969453	0.901769	0.804857
97.64	0.989759	0.969592	0.902201	0.805666
98.09	0.989806	0.969730	0.902629	0.806469
98.54	0.989852	0.969867	0.903053	0.807265
98.99	0.989898	0.970003	0.903474	0.808054
99.44	0.989944	0.970137	0.903891	0.808837
99.89	0.989989	0.970270	0.904304	0.809614
100.34	0.990034	0.970402	0.904714	0.810384
100.79	0.990079	0.970533	0.905121	0.811149
101.24	0.990123	0.970663	0.905523	0.811907
101.69	0.990167	0.970791	0.905923	0.812659
102.14	0.990210	0.970918	0.906319	0.813405
102.59	0.990253	0.971045	0.906712	0.814145
103.04	0.990295	0.971170	0.907102	0.814880
103.49	0.990338	0.971294	0.907488	0.815609
103.94	0.990379	0.971417	0.907871	0.816332
104.39	0.990421	0.971539	0.908251	0.817049
104.84	0.990462	0.971660	0.908628	0.817761
105.29	0.990503	0.971780	0.909002	0.818467
105.74	0.990543	0.971899	0.909373	0.819168
106.19	0.990583	0.972017	0.909741	0.819863
106.64	0.990623	0.972134	0.910105	0.820554
107.09	0.990662	0.972250	0.910467	0.821239
107.54	0.990701	0.972365	0.910826	0.821918
107.99	0.990740	0.972479	0.911182	0.822593
108.44	0.990779	0.972592	0.911536	0.823263
108.89	0.990817	0.972704	0.911886	0.823927
109.34	0.990855	0.972816	0.912234	0.824587
109.79	0.990892	0.972926	0.912579	0.825241
110.24	0.990929	0.973035	0.912921	0.825891
110.69	0.990966	0.973144	0.913261	0.826536
111.14	0.991003	0.973252	0.913598	0.827177
111.59	0.991039	0.973359	0.913932	0.827812
112.04	0.991075	0.973465	0.914264	0.828443
112.49	0.991111	0.973570	0.914593	0.829069

X	ORDER			
	3/2	5/2	9/2	13/2
112.99	C.991150	0.973686	0.914956	0.829760
113.49	C.991189	0.973801	0.915316	0.830445
113.99	C.991228	0.973915	C.915673	0.831125
114.49	C.991266	0.974027	0.916026	0.831799
114.99	C.991304	0.974139	C.916377	0.832466
115.49	C.991341	0.974250	C.916725	0.833131
115.99	0.991379	0.974360	0.917070	0.833790
116.49	C.991416	0.974469	C.917412	C.834443
116.99	C.991452	C.974578	0.917752	0.835091
117.49	C.991489	0.974685	0.918088	0.835734
117.99	C.991525	0.974791	C.918422	0.836372
118.49	0.991561	0.974897	0.918753	0.837005
118.99	C.991596	0.975001	C.919082	C.837634
119.49	C.991631	0.975105	C.919408	C.838257
119.99	C.991666	0.975208	C.919731	C.838876
120.49	0.991701	0.975310	C.920052	0.839490
120.99	C.991735	C.975411	C.920370	C.840099
121.49	0.991769	0.975511	C.920685	0.840704
121.99	0.991803	0.975611	C.920998	0.841305
122.49	C.991836	0.975710	C.921309	0.841900
122.99	0.991869	0.975808	0.921617	0.842492
123.49	0.991902	0.975905	C.921923	0.843079
123.99	C.991935	C.976001	C.922226	0.843661
124.49	0.991967	0.976097	0.922527	C.844239
124.99	0.992000	C.976191	C.922826	C.844813
125.49	C.992031	0.976286	0.923123	0.845383
125.99	0.992063	0.976379	0.923417	0.845949
126.49	C.992094	0.976472	C.923709	0.846510
126.99	0.992125	0.976563	0.923998	0.847068
127.49	0.992156	0.976655	0.924286	0.847621
127.99	C.992187	0.976745	C.924571	C.848171
128.49	0.992217	0.976835	0.924855	0.848716
128.99	C.992248	0.976924	C.925136	0.849258
129.49	C.992277	C.977012	C.925415	0.849796
129.99	C.992307	0.977100	C.925692	0.850330
130.49	C.992337	0.977187	C.925967	C.850860
130.99	0.992366	0.977274	0.926239	0.851387
131.49	C.992395	0.977359	0.926510	C.851909
131.99	C.992424	0.977444	0.926779	0.852428
132.49	C.992452	0.977529	0.927046	0.852944
132.99	0.992481	0.977613	C.927311	0.853456
133.49	C.992509	0.977696	C.927574	0.853964
133.99	C.992537	0.977779	0.927835	C.854469
134.49	C.992565	0.977861	0.928095	0.854970
134.99	C.992592	0.977942	0.928352	C.855468
135.49	0.992619	0.978023	C.928608	0.855963
135.99	C.992647	0.978103	C.928862	C.856454
136.49	0.992673	0.978182	C.929114	0.856942
136.99	0.992700	C.978262	C.929364	C.857427
137.49	C.992727	0.978340	0.929612	0.857908

X	CRDER			
	3/2	5/2	9/2	13/2
138.04	0.992756	0.978426	0.929884	0.858434
138.59	0.992784	0.978511	0.930153	0.858956
139.14	0.992813	0.978595	0.930420	0.859474
139.69	0.992841	0.978679	0.930685	0.859988
140.24	0.992869	0.978762	0.930948	0.860498
140.79	0.992897	0.978844	0.931209	0.861005
141.34	0.992925	0.978926	0.931468	0.861508
141.89	0.992952	0.979007	0.931726	0.862008
142.44	0.992979	0.979087	0.931981	0.862504
142.99	0.993006	0.979167	0.932234	0.862996
143.54	0.993033	0.979246	0.932486	0.863485
144.09	0.993060	0.979325	0.932735	0.863970
144.64	0.993086	0.979403	0.932983	0.864452
145.19	0.993112	0.979481	0.933229	0.864931
145.74	0.993138	0.979558	0.933474	0.865406
146.29	0.993164	0.979634	0.933716	0.865876
146.84	0.993190	0.979710	0.933957	0.866347
147.39	0.993215	0.979785	0.934196	0.866812
147.94	0.993240	0.979859	0.934433	0.867274
148.49	0.993265	0.979934	0.934668	0.867733
149.04	0.993290	0.980007	0.934902	0.868189
149.59	0.993315	0.980080	0.935134	0.868641
150.14	0.993339	0.980153	0.935365	0.869091